INFRARED AND RAMAN SPECTROSCOPIC STUDIES OF MATRIX ISOLATED AMINES

by

Colin James Purnell

A thesis submitted to the
University of Salford
for the degree of
Doctor of Philosophy

November 1974

Declaration

This thesis is a record of research work carried out by me in the Department of Chemistry and Applied Chemistry of the University of Salford during the period 1970 - 1974 and has not, to my knowledge, been currently submitted in part or in total in candidature for any other degree of this or any other University.

Signed: C.J. Pownall

Signature of Supervisor: D.J. Dall
W.J. Wilkie-Thomas

Date: 19th November 1974

Acknowledgements

The work described in this thesis is the outcome of a scheme of research suggested by Professor W. J. Orville-Thomas and Dr. D. F. Ball to whom I would like to express my gratitude for their constant encouragement and advice. I am also grateful to Dr. A. J. Barnes for devoting considerable time to discussing this work and for his many helpful suggestions.

My thanks go also to:- Dr. S. Suzuki for the use of certain computer programs and advice on the force constant calculations of chapter 5; Mr. R. Whitehead for many stimulating discussions of the group theoretical considerations presented in chapter 7; Mr. J. C. Bignall for his interest and assistance during the development of the Raman matrix isolation system and for running many of the spectra.

I am also grateful to:- Mr. P. J. Walkden and the technical staff at the University of Salford; to the Science Research Council for the provision of a grant for the period 1970-1974; and finally to Mrs. A. Foster for the typing of this thesis.

SUMMARY

This thesis describes the infrared and Raman spectroscopic studies on ammonia, methylamine and ethylamine in low temperature argon and nitrogen matrices.

The initial aim was to classify qualitatively and quantitatively the matrix isolated spectra of these molecules and subsequently to evaluate whether the method would prove sufficiently sensitive for the subsequent analysis of these malodorous substances in polluted atmospheres, and to compare the results with those already available from gas liquid chromatography and mass spectrometry. These results are discussed in chapter 8.

In practice anomalous intensity variations were discovered in the spectrum of methylamine (chapter 4) which complicated the quantitative work. No such intensity variations were observed for ethylamine or ammonia (chapters 6 and 7). The abnormalities justified a thorough infrared and Raman spectroscopic analysis of the three molecules.

Chapter 1 gives an outline of the project and introduces the matrix isolation technique.

Chapters 2 and 3 deal with the experimental techniques employed for the infrared and Raman spectroscopic studies along with additional data analysing techniques.

Chapter 4 presents the results and a complete spectral assignment for methylamine and methylamine-d_2. These results are used in a normal coordinate analysis (chapter 5). The resulting force field is used to predict the spectrum of the methylamine-d_1 molecule, enabling a more positive assignment to be made for the previously unobserved NH_2 and ND_2 twisting frequencies.

In chapter 6 information concerning the conformational isomerism of ethylamine is obtained. Although there is some conflict between the infrared and Raman results for the CCN symmetric stretching vibration, the evidence is generally in favour of both conformers being present in argon and only the more stable trans conformer in nitrogen.

The spectroscopic studies of ammonia in argon and nitrogen matrices are presented in chapter 7. Agreement is obtained with previous work for the argon matrix in the infrared, namely that the temperature dependence of the bands could be explained as being due to the rotational freedom of the molecule in the substitutional site. However, the Raman results are completely incompatible with the theory that relatively free rotation in the matrix site is occurring. Using a group theoretical treatment the results are explained, at least qualitatively, as due to a constrained orientational motion rather than a rotational one.

Further information was obtained concerning the dimer species of ammonia in the matrices. The evidence leads to the conclusion that the open chain dimer predominates in the argon matrix but that both open chain and cyclic dimers are present in reasonable quantities in the nitrogen matrix. A detailed assignment of the open chain dimer frequencies is presented.

TABLE OF CONTENTS

CHAPTER 1

INTRODUCTION

1.1 Aim of project

The original purpose of the investigation described in this thesis was to examine the feasibility of using matrix isolation infrared spectroscopy to analyse quantitatively mixtures of aliphatic amines. If this proved successful, it was then to be applied to determining atmospheric concentrations of these malodorous substances in polluted areas. During the course of the quantitative study (described in chapter 8) unusual intensity variations were discovered in the spectrum of methylamine. A thorough spectroscopic investigation of methylamine in argon and nitrogen matrices was consequently undertaken, which is discussed in chapters 4 and 5. The nearest members of the aliphatic amine homologous series - ammonia and ethylamine - were also examined to determine whether the effect observed for methylamine also occurred for these molecules. These studies provided new information concerning the rotation of ammonia in argon matrices (chapter 7) and the conformational isomerism of ethylamine (chapter 6).

1.2 Matrix isolation method

Matrix isolation is a technique for trapping molecular species in an inert solid (matrix) at low temperatures to study their spectroscopic properties. An ideal matrix, at the experimental temperature, must be a solid which is chemically inert, rigid (to prevent molecular diffusion), of low volatility and

transparent in the spectral region of interest.

The type of matrix material employed must have a high vapour pressure at room temperature and hence is usually a gas although high vapour pressure liquids are occasionally used. The cryogenic liquids which are employed as refrigerants are nitrogen, hydrogen and helium with boiling points of 77, 20 and 4 K respectively. Nitrogen is not normally used as a refrigerant by itself since materials that can be used for matrices at 77 K usually have complex infrared or Raman spectra. However, most materials with the exception of hydrogen and helium will form rigid matrices at 4 and 20 K. The increasing availability of commercial open cycle and closed cycle miniature cryostats has facilitated the increasing use of the matrix isolation technique. The rare gases and nitrogen are the most commonly used matrix materials for infrared and Raman work.

The production and trapping of free radicals at low temperatures was first applied by Lewis et al {1,2} in the early 1940's. The early development of matrix isolation was directed principally to the study of unstable species. Norman and Porter {3} and independently Whittle et al {4} proposed what is now called the matrix isolation method for studying free radicals or highly reactive molecules. Pimentel and his coworkers {4,5} developed the matrix isolation technique into its present form in order to investigate unstable molecules and radicals by infrared spectroscopy.

Since then the scope of the matrix isolation technique has grown and it has been applied with great advantage to the spectroscopy of stable molecules. The isolation of monomeric solute molecules in an inert environment reduces intermolecular

interactions, resulting in sharpening and simplification of solute absorptions. Matrix isolation has been successfully applied to many problems including molecular association, molecular rotation, vibrational analysis, gas mixture analysis, high temperature molecular species and noble gas compounds.

Recent developments in laser-Raman spectroscopy have resulted in this technique taking its place alongside infrared spectroscopy as a complementary way of observing vibrational spectra, although Raman matrix isolation investigations are unlikely to become as routine as infrared matrix isolation studies.

1.3 Experimental technique

In matrix isolation experiments, the temperature required depends upon the matrix being used. The matrix must be condensed at a sufficiently low temperature to prevent diffusion of molecular species. Provided these two criteria have been fulfilled matrix formulation is as follows:
The absorbing species (A) is mixed with a large excess of matrix material (M) in a known molar ratio (M/A). This gas mixture is then allowed to condense onto a cold target. Two methods are available for deposition.

(i) Slow spray on (S.S.O.)

This technique involves the flow of the gaseous mixture through a controlled leak. The gas flow characteristics depend on the orifice size which is usually variable with the aid of a needle valve.

(ii) Pulsed matrix isolation (P.M.I.)

Originally developed by Rochkind {6} for gas analysis, this technique involves the deposition of a matrix mixture in

discrete pulses.

Whichever technique is used there are several factors which influence the spectra. For a solute molecule to be isolated it has to be completely surrounded by the host material in order to minimise solute-solute interactions or to stabilise reactive molecular species. Although true isolation, as seen from Table 1.1, is only achieved at high M/A ratio, successful matrix isolation experiments may be performed at M/A ratios of 500-1,000. The actual M/A ratio required for complete isolation will depend upon the type of molecular species present.

The higher the M/A ratio the greater the amount of material which may need to be deposited to obtain a solute spectrum. However, a thick layer of matrix material will often cause appreciable light scattering. Highly scattering matrices limit the amount of energy passing through the sample for detection in the infrared technique and increase the amount of background scattering in the Raman matrix isolation technique. These losses will therefore limit the total thickness of matrix which may be deposited and hence set an upper limit to the M/A ratio.

The cooling capacity of the refrigerator has to be adequate to remove the heat released by the condensing gas. The matrix must be at the temperature of the refrigerant and so thermal conduction between the condensing surface and the refrigerant is critical. As the thickness of the matrix increases conduction of heat from fresh matrix condensing must be removed and unless the thermal conductivity of the matrix is good, local heating will occur resulting in loss of isolation. The rate of deposition will therefore depend on the thermal conductivity of the matrix material and the cooling capacity of the refrigerator.

Table 1.1

Percentage of completely isolated molecules for a given M/A ratio for various crystal lattices {7}

M/A ratio	Percentage isolation		
	Simple cubic lattice	Body centred cubic lattice	Face centred cubic lattice
10,000	99.8	99.9	99.8
5,000	99.6	99.7	99.6
2,000	99.1	99.3	99.1
1,000	98.2	98.6	98.2
500	96.5	97.2	96.5
200	91.4	93.2	91.4
100	83.5	86.9	83.5
50	69.5	75.4	69.5
20	39.7	48.8	39.7
10	15.0	22.9	15.0

1.4 General applications of the matrix isolation technique

The generation and isolation of reactive species received a large amount of attention in early work. One of the first polyatomic free radicals to be stabilised in the matrix in sufficient quantity for direct observation by infrared spectroscopy was HCO produced by the photolysis of a mixture of HI and CO in argon {8}.

Generation of these reactive species and radical systems may be achieved by a variety of methods {9,10,11}. These fall into two main groups:

(i) generation in situ, e.g. photolysis of matrix-isolated parent molecules.

(ii) generation at ambient or high temperatures in the gas phase followed by rapid quenching with excess inert gas.

Photolysis continues to be the favourite method for producing free radicals, although the pyrolysis method has been successfully used by many workers, including Snelson {12} in stabilising CH_3 from the thermal decomposition of CH_3I and $(CH_3)_2Hg$, and Current and Burdett {13} in producing CCl_3 by pyrolysis of CCl_3Br.

The reactive species are normally produced by photolysis, in situ, of a single molecule. The first such species to be characterised was HNO, produced by the photolysis of nitromethane in argon {14}.

Photolysis of an isolated molecule may be followed by reaction with adjacent molecules, or with the matrix itself when a reactive matrix is employed, to produce a new species, for example, HCO from the photolysis of HI, HBr, or H_2S in a CO matrix {15,16}. Photolysis of HI or HBr and O_2 in an argon matrix

produced HO_2 {17,18}.

Andrews and Pimentel {19} developed a technique for the codeposition of a beam of alkali-metal atoms produced in a Knudsen furnace, with a suitable molecule, at high dilution in a rare gas matrix. Using this technique species such as CH_3 {20}, CCl_3 {21}, OF {22}, and ClO {23}, have been produced by halide extraction. However, the alkali-metal halide molecule necessarily produced may perturb the radical and so complicate the observed vibrational spectrum; such is the case apparently with CH_3.

The above technique has been utilised to trap simple molecular derivatives of metals, the alkali metal oxide systems MO_2 and MO_2M (M = Li, Na, K or Rb), binary derivatives of molecular nitrogen, LiN_2 and N_2LiN_2, $Ni(N_2)x$, and $Cr(N_2)x$, etc.,{24}. Andrews and Carver have produced trichloromethyl {20} and tribromomethyl {25} radicals as the primary products of the matrix reaction of lithium atoms with the appropriate carbon tetrahalide using this technique.

Although a Knudsen cell is most commonly favoured as the source of the metal atoms, Shirk and Bass {26} used microwave-discharged gases to "sputter" metal atoms, e.g., Cu, Fe or Ag, from filaments into Ar, Kr, and Xe matrices. CuO molecules were successfully isolated by the action of a microwave-discharged $Xe-O_2$ mixture on a copper target.

Milligan and Jacox {27} combined both the photolytic and alkali-metal atom techniques to provide a photoelectron source within a matrix and succeeded in stabilising negative ion, rather than free radicals, in an inert non-ionic environment, e.g. NO_2^- from a $Ar-NO_2$ sample codeposited with an alkali-metal atom beam.

Linevsky {28} adapted the matrix technique to the difficult

problem of measuring the infrared spectra of metal oxides and halides. A molecular beam of the gaseous species produced by the vapourisation of a refractory solid at high temperatures (1,000-2,700 K), is allowed to diffuse from a Knudsen cell into a vacuum and is then simultaneously condensed with a stream of matrix gas (noble gas or nitrogen) onto a cold window. The first systems examined were the vapour species of naturally occurring {29} and isotopically enriched lithium halides {30}. Other studies {31,32} include the halides of Zn, Cd, Hg and the iron chloride system {33}.

The small bandwidths obtained in low temperature matrices make matrix isolation useful in investigating such problems as conformational isomerism. A study of ethanol {34} and ethanethiol {35} in an argon matrix provides a good example in this respect. For ethanol there are two distinguisable conformers with the OH group trans or gauche with respect to the methyl group. A comprehensive study of ethanol in its various phases as well as in inert solutions failed to establish conclusively the presence of both conformers, suggested by a slight asymmetry of the absorption of the OH stretching frequency. However, the small splitting of 4.6 cm^{-1} and the similar intensity of the two OH stretching frequencies for ethanol in an argon matrix at 20 K explains the controversy. Since the sample is rapidly cooled to 20 K, the relative intensity of the bands reflects the proportion of the two conformers in the vapour phase at approximately room temperature.

Ethanethiol has also been successfully analysed and evidence found for the existence of the trans and gauche conformers. From the results the ratio of the trans and gauche in the vapour phase at room temperature was estimated to be 0.8:1 for ethanethiol

and 2:1 for ethanol.

Quantitative analysis of multicomponent mixtures was carried out by Rochkind {36-39}. His method, although basically the same as the standard technique, replaces continuous flow deposition with condensation of the sample mixture at 20 K in a nitrogen matrix by controlled-pulse deposition. Rochkind was able to apply the technique to the quantitative analysis of a mixture of (1,1), cis (1,2), and trans (1,2) isomers of deuterated ethylenes {39}. In this respect the technique has superiority over conventional gas chromatography.

The matrix isolation technique has been increasingly applied to the vibrational analysis of stable molecules. The general principle is that molecules in an inert matrix at very low temperatures have a simpler spectrum than in other phases. Using this method the vibrational spectrum of the species is obtained from which the band frequencies can be identified with a particular vibrational motion and from this knowledge structural data and force constants for the species or molecule can be obtained. The small bandwidths at the low temperatures employed give a better chance of resolving bands close in frequency and the symmetry of the environmental interactions often cause the degeneracy of some bands to be lifted. However, since the spectra of a particular molecule or molecular species may not have previously been known it is important to know the various possible effects the matrix host environment may have on the guest species.

1.5 Environmental effects

1.5.1 Matrix shifts

In order to explain vibrational frequency shifts in liquid

media several theories have been put forward, one of the most successful being the Kirkwood-Bauer-Magat {40,41} relationship relating the vibrational shift $\Delta\nu$ to the dielectric constant of the medium for both polar and non-polar systems {42,43} . Analogous to the solvent shift in room temperature solution spectra is the matrix shift of matrix isolated molecules. The frequency shift in this case, measured relative to the accepted gas phase value may be related to the intermolecular interactions (I.M.I.) between the vibrating molecule and the surrounding lattice cage.

Many attempts have been made to give quantitative descriptions of matrix induced frequency shifts, especially for the two body problem, as a function of the polar properties of the guest and host molecules and the nature of the matrix. The matrix-induced shift is an overall sum of dielectric effects, dispersive forces and specific solute-matrix interactions. However, in solid solution repulsive forces can play an important part and must be taken into consideration. Intermolecular potential energy may therefore be expressed as a summation over energy terms arising from dispersive, inductive, electrostatic, repulsive and dynamic forces. The frequency shift is given by

$$\Delta\nu = \nu \text{ matrix} - \nu \text{ gas} = \Delta\nu \text{ dis} + \Delta\nu \text{ ind} + \Delta\nu \text{ elec} + \Delta\nu \text{ rep} + \Delta\nu \text{ dyn}$$

The individual contributions may be calculated separately using a number of models. The dispersive and repulsive forces are usually calculated using the semi-empirical Lennard-Jones potential {44}. The electrostatic term represents the interaction between the permanent charge distribution of the solute and matrix

molecules. For the noble gases it is zero. The dynamic contribution arises from the constrained translational motion of the solute molecule; it is small and relatively unimportant.

The inductive forces can be explained by either (i) point polarisable model (p.p.a.) {45} which assumes the interaction as being between a point non-polarisable dipole and a point polarisable atom, or (ii) cavity model {46} which assumes that the change in potential energy of the oscillator is attributable to the potential of a point dipole moment in its own reaction field.

However, both models suffer from oversimplification of the interaction. The p.p.a. model underestimates short range interactions with nearest neighbours actually in contact with the solute molecules and the latter model overestimates them.

Calculations have been made using both models {47-50} and although calculated and experimental rarely agree the theory does seem to be able to predict the general trend.

As described above, in a dilute matrix in which all solute-solute interactions have been eliminated, the guest molecule is only subjected to solute-matrix interactions. These interactions will perturb the solute's vibrational energy levels and will be reflected in the frequency shift $\Delta\nu$. It is generally found that the shift tends to become more positive as the frequencies decrease. Pimentel and Charles {51} gave a qualitative discussion of the factors which influence vibrational shifts of polyatomic solute molecules in matrices. They argue that a matrix isolated molecule in a site will be expected to adopt the lowest energy position which has to be a compromise between the optimum positions for each of the points of contact between the molecule and the matrix environmental cage. There is a tendency for the lattice to

distort the matrix isolated molecule to fit the available site. The extent to which a given coordinate will distort is a function of the force constant associated with that coordinate. Thus low force constant coordinates are more likely to be in a tight environment than high force constant coordinates and hence the former are likely to be more perturbed in a matrix site than the lattice.

The stretching vibrations usually exhibit shifts to lower frequency than the gas phase values, while low frequency bending modes are shifted to higher frequency {51}. The shift will depend on the polar nature of the molecules and the type of site occupied.

1.5.2 Rotational effects

In general most matrix isolated molecules will be so tightly held in the matrix cage as to prevent rotation and at the low temperatures attained the vibrational modes will appear as very sharp absorptions. However, where the matrix cavity is sufficiently large and the molecule is small enough (but not small enough to diffuse out) the isolated molecule is comparatively unperturbed by neighbouring molecules. It is anticipated that the rotational energy levels of the small guest molecule would only be slightly perturbed and thus rotation be relatively unhindered.

At the low temperatures employed in matrix isolation experiments (4-20 K) only the lowest rotational levels will be appreciably populated. The characteristic of rotational structure on an absorption band is that it exhibits reversible intensity changes on temperature cycling due to Boltzmann population and depopulation of the low-lying rotational energy levels of the

matrix isolated molecules.

A number of small molecules have been reported to rotate in inert gas matrices; these include HX (X = F, Cl, Br or I), {47,52,53}, H_2O {54-58}, NH_3 {58-65}, NH_2 {66}, NO_2, SO_2, CH_4 and CH_3. However, the spectra of ammonia are complicated by inversion effects, and those of water and methane by nuclear spin species conversion. If indeed rotation does occur in matrices, in addition to vibration - rotational structure pure rotational transitions should also be observable in both the infrared and Raman - although the selection rules must of course be considered.

Although rotational motion has been observed in matrix environments other than those of the rare gas systems no molecule has been shown to rotate in nitrogen. The general conclusion is that small molecules may rotate in matrices offering spherical sites whilst rotation does not occur for molecules in unsymmetrical sites.

Numerous attempts have been made to provide a quantitative description of the rotational energy level perturbations of a diatomic solute molecule in inert gas matrices. Two approaches have been discussed in the literature and the models employed have involved either (i) rotational motion limited by a potential energy barrier - crystal field model {71}, or (ii) perturbation of the rotational motions by the constrained translational motion of the rotating molecule in the lattice site, - R.T.C. model {44}.

Although the crystal field hindered rotor model is successful in predicting the general trend of rotational spacings in noble gas matrices and the splitting of the J = 2 level, it fails

to predict that the spacing for DX should decrease less from gas to matrix than those for HX. The rotational-translational coupling model neglects any effect due to the anisotropy of the crystal field but removes the constraint of rotation about a fixed point, and gives much closer agreement with the observed spectral effects for HCl and DCl in the noble gas matrices. However, it is not consistent with the matrix shifts found for HF and DF, which with other anomalous features, are better served by considerations of the anisotropies in the rotational potential function. That the J = 1 level of HCl appears to be split by 0.8 cm^{-1} when the molecule is isolated in argon at 4 K has been explained by the fact that the noble gas atoms may adopt an h.c.p. structure, instead of their normal b.c.c. structure, in the neighbourhood of the HCl impurity. A recent study {72} has extended the scope of theoretical treatment to take account of a tetrahedral guest molecule, the vibration-rotation states having been determined for ν_3 and ν_4 of CH_4 entrapped in a noble gas matrix to give results in good agreement with experimental findings.

An extension of the crystal field model has been put forward by Miller and Decius {73} in which the necessary group theory has been developed and applied to molecules of any symmetry, matrix isolated at a site in a crystal field of any symmetry. As the potential barrier to rotation of the molecule relative to the host crystal is increased, certain symmetry operations become decreasingly feasible. Correlation methods are used to determine the symmetry species of the rotational states from the free rotation limit to any of the possible vibrational limits.

1.5.3 Aggregation

For isolation of a solute molecule to be complete very high M/A ratios are required usually greater than 1,000. The limit of the M/A ratio for complete isolation will depend on the size and nature of the guest molecule and to a certain extent upon the type of matrix gas used as the host. The degree of isolation is therefore dependent on the M/A ratio. At low M/A ratios molecular aggregates are formed and trapped in the matrix in addition to monomers, giving rise to solute-solute interactions. These interactions result in the appearance of new absorptions in the spectrum attributable to dimer, trimer and higher multimer molecular species. Molecular association will be greatest for solutes capable of forming hydrogen bonds. These multiple features due to association are usually readily identified from their M/A dependence and from controlled warm up experiments in which monomers diffuse to form the multimer species.

By plotting relative optical densities of bands as a function of M/A ratio it is possible to show which bands arise from a particular species i.e. monomer, dimer, trimer or higher multimer. Diffusion experiments, where possible, can be used to aid the assignment of multimer species.

1.5.4 Multiple trapping sites

The effects associated with the more intimate properties of the matrix enclosing the guest species can cause complications in the spectra. Thus the observation of a multiplet where only a single spectroscopic feature is anticipated is commonly attributed to variations in the matrix environment experienced

by the guest. The most commonly used matrix materials, the noble gases, have spherical atoms and in the solid state adhere generally to the principle of closest packing. Three types of trapping sites are possible in these matrices; interstitial, dislocation and substitutional sites. Interstitial sites between layers of close packed spheres are of two kinds, tetrahedral and octahedral. Tetrahedral sites are too small but octahedral sites may possibly accommodate the smaller diatomic molecules not polyatomics, which leaves dislocation and substitutional sites to be considered.

The variations in the matrix environment reflect (i) different orientations of the guest within a particular matrix cage, (ii) population of more than one type of cage because of the opportunities offered by substitutional, multiple substitutional and dislocation sites within the host lattice and (iii) occupation of cages which include guest, as well as host molecules as nearest or next nearest neighbours; this is the so-called aggregation site effect. The intermolecular forces between the solute species and its environment will differ slightly for each site and hence will cause different perturbations of the energy levels which may generate discernable multiplet structure in the spectra of the guest.

The spectra of matrix isolated molecules are generally reproducible from one experiment to another indicating that the guest molecules are all in similar sites. This would suggest that the most likely sites are substitutional sites which are large enough to accommodate a normal size diatomic guest. Multiple sites may also occur due to the fact that two or more matrix atoms or molecules may be removed to form the substitutional site

in more than one way. Altering of the symmetry of the site occurs and hence the perturbations of the isolated molecule. Adjacent vacancies may also alter the site symmetry and lattice dislocations may provide further trapping sites but these would be expected to be nonreproducible.

Large guest molecules would be expected to occur in sites in which two or more lattice molecules have been displaced. Leach {74} supposes that for molecular solids, in which the intermolecular forces are weak, the presence of extrinsic impurities e.g. solute molecules can induce particular and varied forms of short range or long range order in the surrounding matrix. This can lead to a number of metastable minima of free energy and so to the coexistence of a number of different local structures in the matrix. In some cases, the different structures may simply reflect the existence of misoriented solute or solvent molecules. Annealing experiments would tend to modify the number of these structures present in the matrix and so cause variations in the number of multiplet bands observed and their relative intensities. The persistence of multiple sites after thorough annealing of the solid solution would indicate either that the potential barrier to the conversion of the different structures with the most stable one is very high or the various minima of free energy have substantially the same value. Finally the stabilisation of a particular site would depend on the relative disorder in the surrounding matrix, the more host molecules around a particular solute molecule in a given site the greater the opportunity for the strain caused by the solute molecule to be taken up. It would therefore be expected that the number of multiplet structures should increase with increasing M/A ratio.

As previously described multiple bands can arise from other effects viz. rotation and aggregation. However, bands due to multiple sites, unlike those due to rotation, do not show a reversible temperature dependence and providing temperature cycling is carried out at temperatures which preclude diffusion mechanisms, the matrix can be annealed so that the multiple site bands disappear.

Multiple site effects have been observed in other matrices viz. N_2, CO_2 and CO offering unsymmetrical sites {49},

CHAPTER 2

EXPERIMENTAL PROCEDURES

2.1 Introduction

The aim in a matrix isolation experiment is the deposition of a gas mixture onto a refrigerated support for sufficient time to study the spectroscopic properties at ease. The fundamental problems in achieving this aim are outlined below.

A cryostat must be capable of generating sufficient refrigeration at a temperature low enough to condense the sample mixture and to prevent sample diffusion. The temperature required will depend on the matrix gas involved. The sample must be protected by an evacuated shroud (or vacuum cell) at a low enough pressure (10^{-5} torr*) to act as a radiation shield to minimise heat losses and to prevent atmospheric contamination of the matrix. A means of introduction of the gas mixture; usually an injection needle is required to direct the gas stream onto the cooled support within the cell. The outer windows of the cell will depend on the type of spectroscopic instrument being used to study the matrix sample.

Since both infrared and Raman studies were undertaken, this chapter will be divided into two sections based on these two techniques.

---

* Since all the vacuum pressure and sample measuring devices were calibrated in units of torr it was reasonable to use these units in the text in describing vacuum pressure noting that 1 torr = 133.3 Nm^{-2}.

SECTION 1

2.2 Infrared matrix isolation system

2.2.1 The spectrometer

The infrared spectra in this work were recorded on a Perkin Elmer model 225 infrared spectrophotometer. This instrument is an automatic recording double beam grating spectrophotometer with a drum recorder and using the optical null system. The model 225 has two monochromators which cover the whole spectral range of 5000-200 cm^{-1}. A resolution of better than 0.5 cm^{-1} at all wavenumbers is specified.

Ordinate presentation is transmittance on a linear scale with a reproducibility within noise level. Abscissa presentation of the spectrum is linear in wavenumber with facilities for scale expansion. The accuracy of the abscissa scale is ±0.02% with a reproducibility better than accuracy. The wavenumber calibration was made for all ranges using standard calibration gases and the I.U.P.A.C. values {75}. From a paper tape output of the calibration gas spectra from the spectrophotometer data logger (see chapter 3) SRCH 2A computer program was used to aid the calibration.

Fifteen slit programs are available, simultaneous indication of the geometric slit width and dispersion allows for rapid determination of the spectral slit width.

2.2.2 Vacuum system

When designing a vacuum system suitable for sample preparation and shroud evacuation several points must be considered. To reduce the length of cooldown times due to a heat leak from

the surroundings the cell must be evacuated to a pressure of $< 10^{-4}$ torr at room temperature. Once the cryostat cold finger reaches cryogenic temperature any remaining gas in the cell is condensed onto it and the pressure will drop to $< 10^{-5}$ torr.

To enable high pumping speeds to be attained, wide bore glass tubing was used wherever possible in both sample and cell evacuation lines. Large bore taps were therefore required; these were of the greased type in the main manifold lines to the cryostat and sample preparation system.

The sample preparation system (Fig. 2.1) consists of a manifold onto which are connected large bulbs to enable storage of the matrix mixture once prepared. Each sample line has its own pressure measuring device, a condensing finger, and an exit point for the introduction of gas mixture to the cryostat cell via the injection port. Two sample preparation systems were available as a precaution against vacuum failure in one system. One system could be used while the other was being repaired and cleaned so as not to interrupt experimentation.

Since it was sometimes necessary to attach additional apparatus, (such as sample bulbs, drying tubes, cold traps, etc.) outlets ending in cones and sockets were included in the system. Taps were included in line for isolation purposes. The sample and cryostat manifold lines both have an oil rotary pump acting as fore pumps for water cooled mercury diffusion pumps. Both systems have an ultimate vacuum of 10^{-6} torr. Liquid nitrogen cold traps were used on each side of the mercury pumps to prevent back diffusion of vapours into the vacuum system and to hold any pumped off samples.

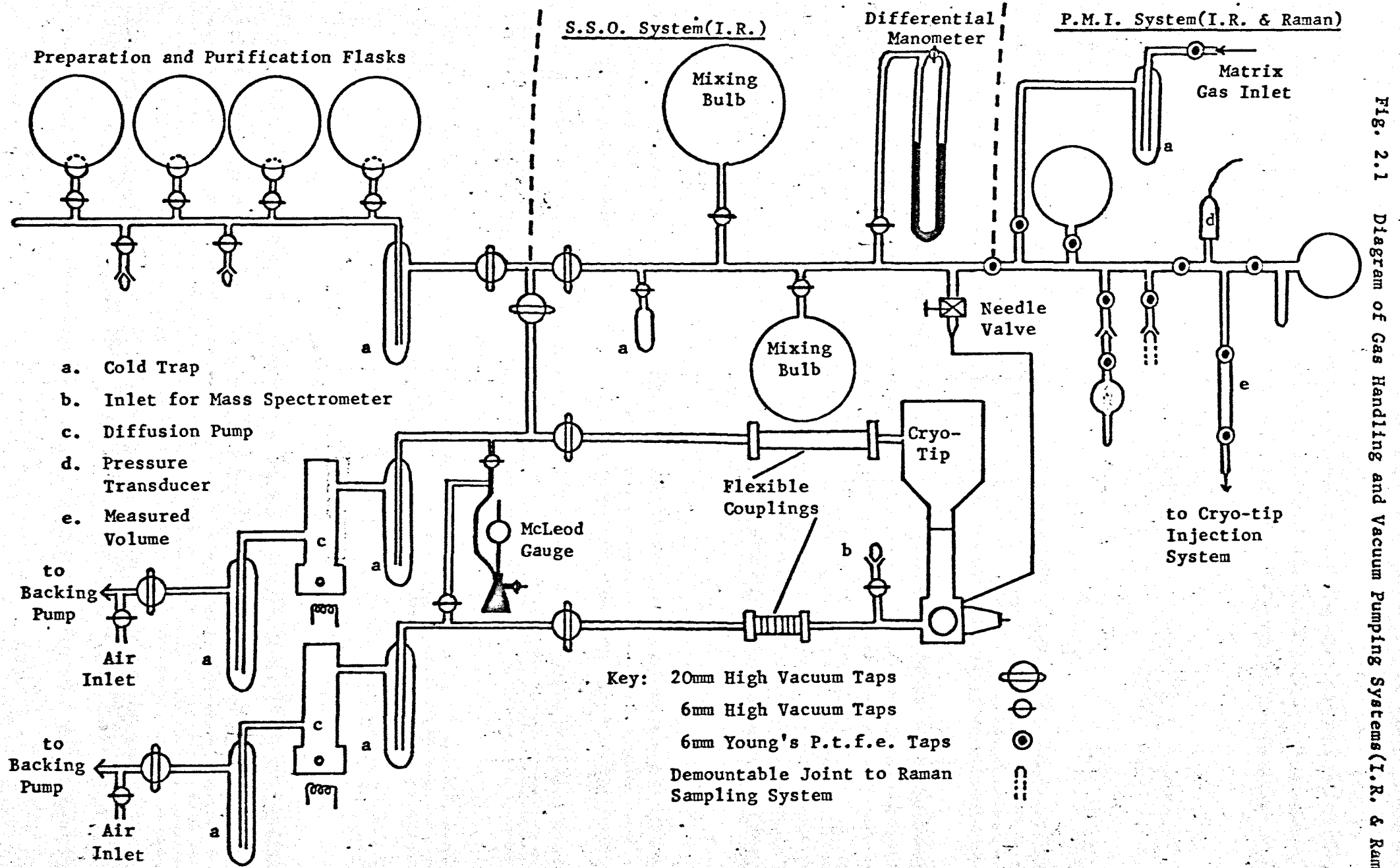

Fig. 2.1 Diagram of Gas Handling and Vacuum Pumping Systems(I.R. & Raman).

2.2.3 Pressure measurement

Pressure measurements in the range 2 torr - 760 torr on the gas mixing manifold were determined with a differential mercury manometer; variations in the mercury levels were measured using a cathetometer.

The most convenient way of measuring absolute pressure was the McLeod gauge. One was built into the system to check the ultimate vacuum which was calibrated down to 10^{-5} torr.

The disadvantages of a McLeod gauge are that mercury has an appreciable vapour pressure at room temperature and that although the McLeod gauge is capable of measuring a standing vacuum it is not capable of seeing changing pressures over short periods of time. To overcome these problems Penning gauges were installed in both the infrared and Raman systems and situated directly on the evacuation cell of each cryostat. Two different makes of gauge were employed although they each had the same principle of operation.

These gauges were calibrated for nitrogen or air prior to use. Their response to pressure changes within the system was immediate.

2.2.4 Temperature measurement

Temperature measurement for the infrared cryogenic system was a chromel vs constantin thermocouple. A reference of 273.2 K was used and the output in millivolts was measured using a potentiometer. During experimentation the mV readings were converted directly to temperature by the use of a calibration graph supplied by the manufacturers.

2.2.5 AC - 3L - 110 Cryo-tip

This is a three-stage Joule-Thomson open cycle cooler for operation at liquid helium or liquid hydrogen temperatures. High pressure helium and hydrogen gases are used with liquid nitrogen as the precoolant. The unit operates in the range 3.6 to 70 K giving from 500 mW at 4.4 K to 4 W at 20 K, temperature stability is ±0.1 K to ±0.5 K depending on the temperature of usage. The basic components are a sample support window, which is connected to a heat exchanger, a radiation shield around the sample area, a vacuum shroud around the whole and injection ports for introducing the gaseous sample mixture. A schematic diagram of the system used is shown in Fig. 2.2.

(i) Heat exchanger

The heat exchanger (Fig. 2.3) providing the refrigeration has two separate gas circuits, one for hydrogen and one for helium. It also contains a liquid nitrogen reservoir in which the cold trap coils for both gas circuits are located.

Refrigeration, which is obtained by the Joule-Thomson cycle, occurs when a non-ideal gas expands without doing work (isenthalpic expansion). Before Joule-Thomson cooling will occur, however, the gas must be cooled below its inversion temperature. The main purpose of the liquid nitrogen reservoir is to cool the hydrogen below its inversion point, which is 160 K, precooling of the helium gas in the helium circuit also occurs to some extent. The liquid hydrogen produced by Joule-Thomson expansion cools the helium below its inversion point (40 K).

Each gas circuit consists of a coil of paired tubing. The

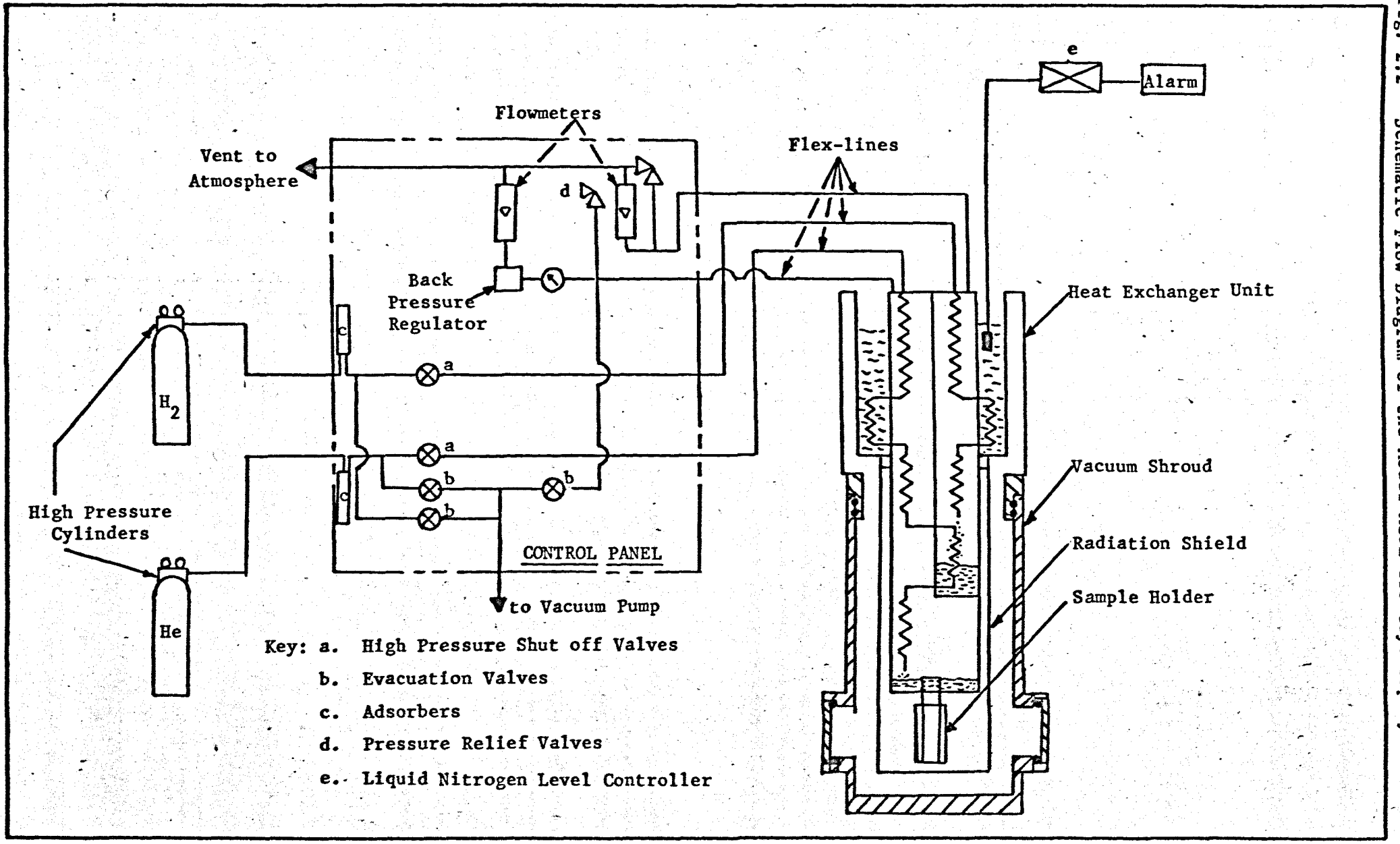

Fig. 2.2 Schematic Flow Diagram of the Model AC3L-110 Cryo-tip System.

Fig. 2.3 Heat Exchanger Assembly.

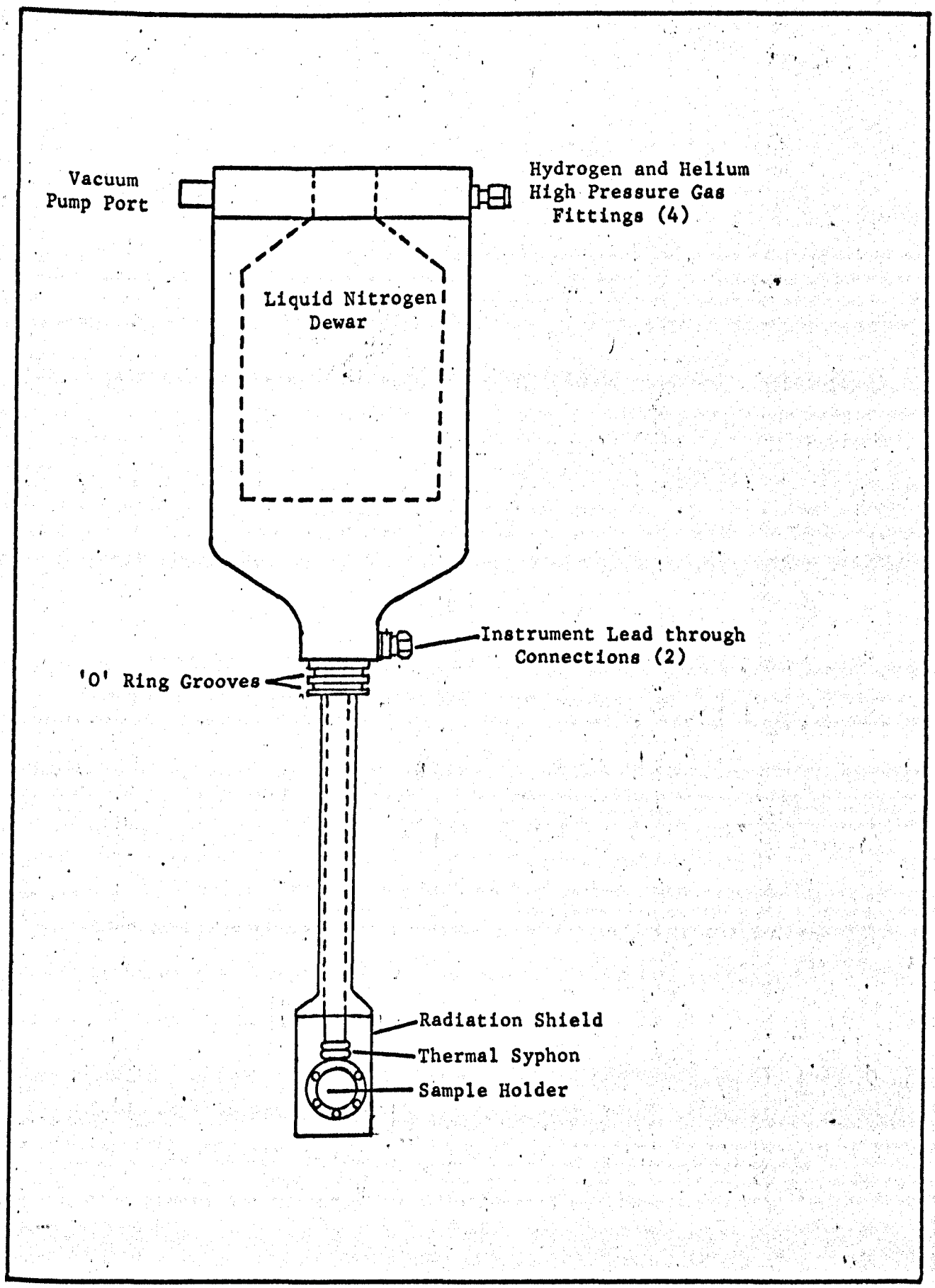

colder heat exchange circuits consist of coiled finned tubing wound around a mandrel to form efficient counter-current heat exchangers. Because of the recuperative effect from the heat exchangers, all gas lines leading to and from the heat exchanger are essentially at room temperature.

The copper tip, into which the sample holder is fastened, is the only part of the heat exchanger which is at liquid helium temperatures. A radiation shield, attached to the liquid nitrogen reservoir, surrounding the sample holder, greatly reduces the heat leak. It was found, however, that although this shield was effective in reducing radiation losses it also reduced the incident radiation falling on the sample from the spectrometer. To overcome this a new radiation shield was made to allow greater transmission of incident radiation through the cell without any obvious deterioration in heat shielding.

The exact temperature of the tip and sample holder will depend on the boiling point of the tip reservoir at the bottom of the heat exchanger. It is possible to vary this temperature since this is a function of the gas (i.e. the helium or hydrogen). This gas pressure is referred to as the back pressure. Since the liquid refrigerant is normally boiling at atmospheric pressure, it is required that the back pressure is increased above or lowered below atmospheric pressure to raise or lower the boiling point of the liquid. The various operational modes for the different temperature ranges are shown in Fig. 2.4.

(ii) Control panel

The ancillary equipment for handling and controlling the high pressure gases consists of a control panel, gas clean up

Fig. 2.4 Cryostat Mode of Operation for Various Temperature Ranges.

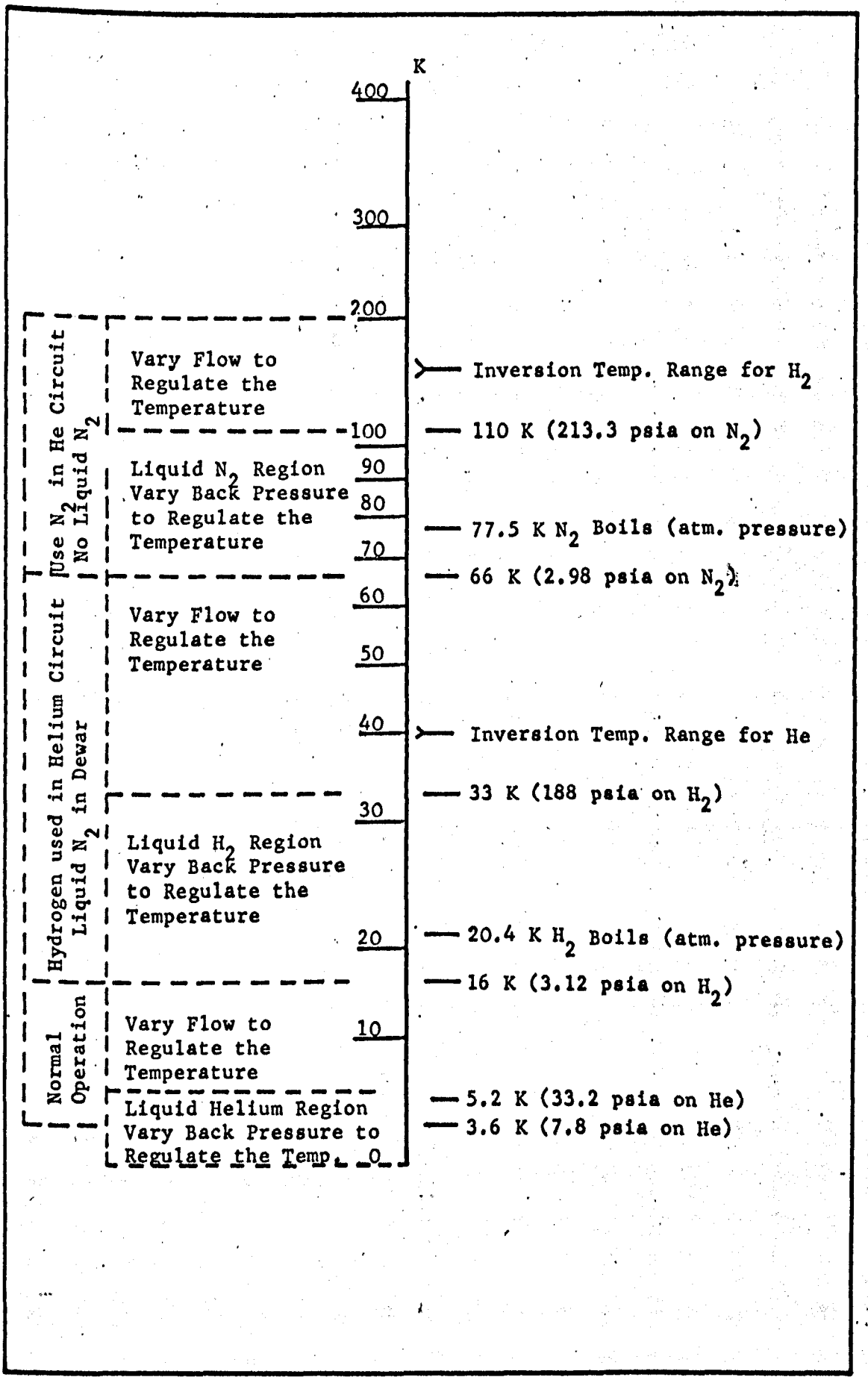

units, to protect the heat exchanger, and flex lines for the gases (Fig. 2.2).

The heat exchanger is connected to the cylinder gas supplies through valves and high pressure tubing mounted on a control panel onto which are built the pressure regulators for hydrogen and helium and flowmeters for monitoring the flow.

The high pressure flex lines, which carry the gases to the exchanger, are of the bronze metal bellows type with a woven cable reinforcement. For safety purposes these have been strapped down as far as possible to avoid any dangerous lashing of the lines should a fitting fail. The outgoing gases are vented out of the laboratory where rapid diffusion of the gas with the atmosphere takes place.

The gas clean up units contain molecular sieve at ambient temperature to remove water and carbon dioxide from the gases, an additional cold trap has been added to the hydrogen line to remove nitrogen impurity to avoid blocking of the cryostat Joule-Thomson nozzles.

(iii) Vacuum shroud

The vacuum shroud (Fig. 2.5) has four ports, two of which are required for the infrared beam, one contains a Penning gauge for pressure monitoring and the fourth is connected to the vacuum system pumping line for evacuation of the cell. There are two injection ports at 45° to the infrared beam ports. The relative orientation of these can be changed since the top half of the heat exchanger can rotate.

Two pumping lines are used to evacuate the cryostat vacuum shroud, each utilising a mercury diffusion pump backed by

Fig. 2.5 Vacuum Shroud and Sample Compartment.

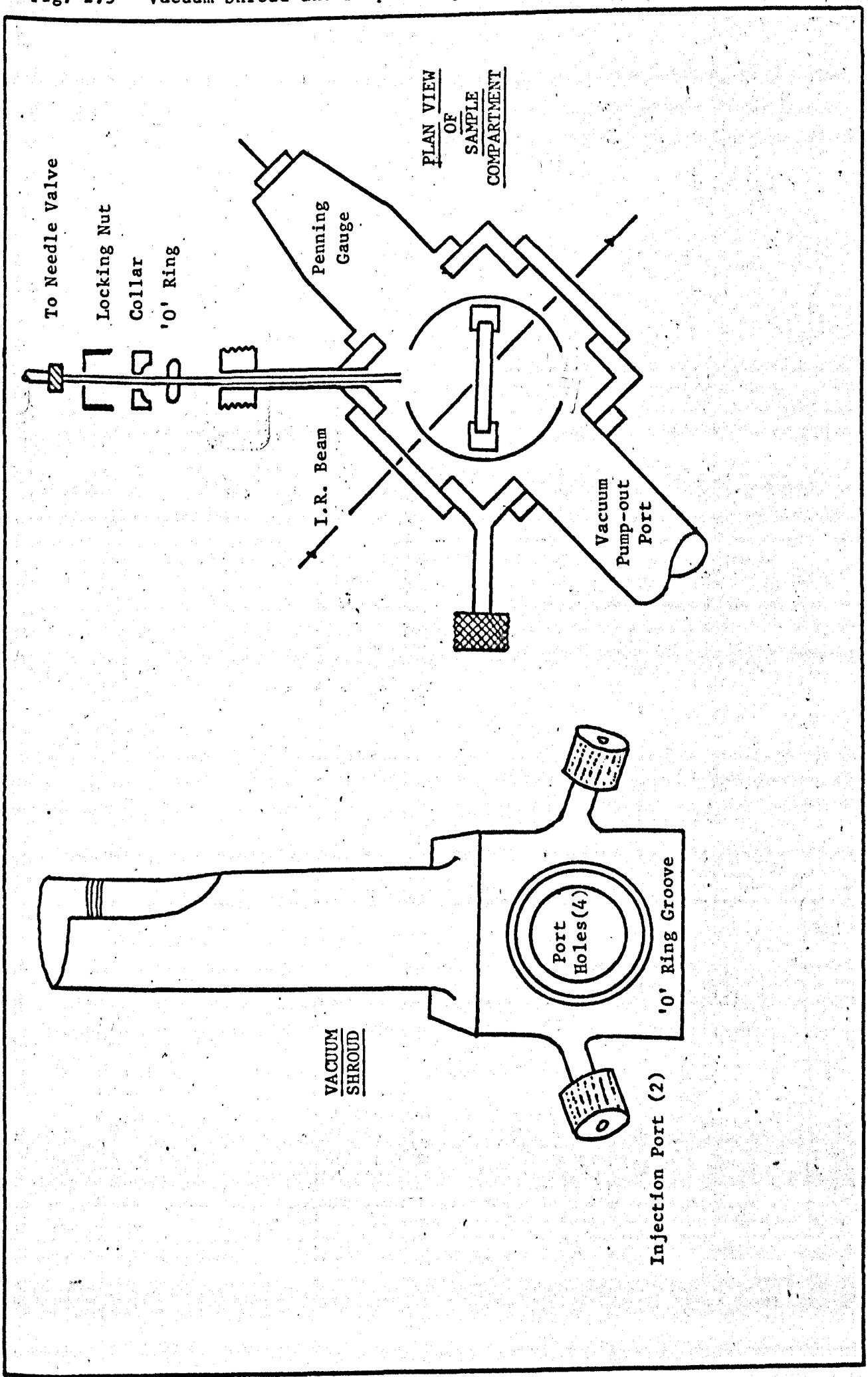

a mechanical rotary pump. One pumps the top outlet, whilst the other pumps from the bottom shroud port.

2.2.6 Positioning of the Cryo-tip

The Cryo-tip was mounted on a rigid aluminium arm bolted at one end to the framework housing the vacuum equipment . The upper part of the Cryo-tip was fitted to a shaped moulding and held in position by a curved metal band to lend stability to the structure and to allow for rotation of the heat exchanger. The base of the Cryo-tip fitted into a small well on the metal bar to prevent the possibility of dislodging it from the supporting bar.

This arrangement of the Cryo-tip allowed the spectrometer, which was mounted on a trolley, to slide easily into position so that the sample beam was in line with the Cryo-tip windows. The maximum transmission through the cell was then achieved by ensuring that the deposition and shroud windows were parallel, the spectrometer being manoeuvred so that the sample beam was perpendicular to these windows. A small jack was then placed between the remote end of the bar and the spectrometer to raise the bar slightly to give maximum transmission. It also acted as an anchor to prevent any movement of the Cryo-tip relative to the spectrometer during operation. Maximum transmission values of 80% could be achieved with an empty cell. With a matrix deposited, cell transmission depended on the matrix thickness, diluent gas, deposition technique and deposition temperature. It was normal to attenuate the reference beam to give a value of between 60-80% transmission while recording a spectrum.

2.2.7 Dismantling and cleaning procedures

It is necessary to dismantle the cryocooler and gauges occasionally to clean the sample deposition surfaces, replace worn "O" ring seals and polish the optical windows.

To clean the AC-3L-110 Cryo-tip the following procedure was adopted. The Cryo-tip was isolated from the vacuum system and the injection needles and optical windows removed. The flex-lines and flexible couplings to the vacuum system are dismantled. After loosening the restraining strap the Cryo-tip may be completely removed from its mount and dismantled.

The sample window (KBr or CsI) is removed for cleaning or replacement, and refitted with fresh indium wire gaskets in the grooves provided in each half of the sample holder. After tightening the five screws holding together the two parts of the sample holder it had to be left for at least 24 hours and then retightened to ensure good thermal contact. This was because the indium tended to "flow" under pressure. The Cryo-tip could then be reassembled, the "O" ring grooves being cleaned of old grease and the "O" rings either cleaned or replaced as necessary. A light smearing of Apierzon "N" grease (vapour pressure $< 10^{-6}$ torr at room temperature) was used on the "O" rings to give a good vacuum seal. The spectroscopic windows were polished and replaced on the "O" rings and held there while the Cryo-tip shroud was pumped out. Once this had been achieved atmospheric pressure held the windows in place and the windows could be centralised by carefully moving them on the "O" rings while under vacuum. The whole system was pumped out with the backing pump for at least 24 hours before use to outgas water vapour from the metallic sides of the vacuum shroud. If after this time, when using the

diffusion pumps on the top and bottom of the Cryo-tip shroud, a pressure of 10^{-4} torr was not achieved then there was likely to be a leak.

2.2.8 Vacuum testing

Leak testing was achieved by the modification of a V.G. Micromass ½ portable mass spectrometer as a helium leak detector. A flexible lead was connected from the mass spectrometer to the lower pump-out pipe through a 12 mm greased tap provided. The Cryo-tip was isolated from the pumping line and helium gas was sprayed round each joint and "O" ring seal in turn. The mass spectrometer was tuned to helium (mass range 4). If helium was leaking in, a corresponding increase in the reading of the mass spectrometer could be seen and the leak isolated to a particular part of the Cryo-tip shroud or couplings.

2.2.9 Manufacture of samples

The basic aim was to prepare a diluted sample of sample gas and transfer this to the low temperature cell. The partial pressures of the sample and diluent gas must be known accurately and the mixture must be free of any impurities, since the slightest trace of impurity in the gas sample could give rise to induced bands in the matrix. After ample time has been allowed for mixing, the gas mixture is then deposited onto the cold window for subsequent spectroscopic analysis.

Two methods of deposition are available, (i) Slow Spray On (S.S.O.), (ii) Pulsed Matrix Isolation (P.M.I.).

In the first technique, the gas mixture is slowly leaked onto the cold window. The rate of deposition is controlled by

means of a needle valve which allows the rate of flow of sample mixture to the cryostat cell to be varied accurately as required. The normal method of calibrating is to assume a constant pressure head behind the needle valve. Hence for a known volume of gas the drop in pressure can be related to the flow through the needle valve and therefore the amount of matrix material deposited on the cold window. The volume of sample mixture preparation system had to be kept large (3 l) to avoid a drastic fall off in pressure of the mixture supply as the sample is used. This would cause a concomitant fall off in deposition rate for a given needle valve setting. The volumes of the sample mixing bulbs were calibrated with water and the manifold volumes found by gas expansion technique at constant temperature. The sample size in terms of reagent is calculated directly.

The lead off from the needle valve to the cell was originally made of copper pipe. An epoxy resin adhesive "Araldite" was used to bond the injection needle and control valve connection to the copper pipe. One disadvantage to this was that the copper pipe was not very flexible and if strained occasionally caused a leak. An alternative method was sought for transferring the gas mixture to the cryostat cell. Polytetrafluorethylene (p.t.f.e.) tubing was used, this is light, extremely flexible and non-porous (slightly porous to helium).

However under normal circumstances there is no adequate adhesion of any material (including "Araldite") to such fluorocarbons as p.t.f.e. this characteristic is inherent in the chemical nature of the fluorocarbon. The use of a chemical etchant such as "Bondaid" treats the fluorocarbon so that a carbonaceous film is created on the surface. This film is now

the anchor for any applicable adhesive. Full details of surface pretreatment and use of epoxy resins are given in Appendix 1.

A considerable amount of the sprayed sample (mainly diluent gas) will bounce off the cold window and either condense onto the other cold surfaces or be pumped away. Too high a flow rate may therefore raise the pressure in the cryostat, indicated by the Penning gauge, sufficiently to cause an appreciable heat leak causing a temperature rise of the deposition window with a consequent warming of the matrix. Too high a flow rate will also cause badly scattering matrices and a possible increase in aggregation of solute species, too low a flow rate also results in badly scattering matrices. It was found that a flow rate of between 6-10 mmol/hr corresponding to a deposition pressure of between 8×10^{-5} torr and 2×10^{-4} torr gave satisfactory matrices using this method.

However, despite keeping the M/A ratio, initial pressure head of sample, and needle valve settings constant for different experiments of the same sample, consistent results could not be achieved in terms of quantitative estimates of the amount of solute deposited in relation to spectroscopic absorbance of a particular solute band. Furthermore, whenever it was necessary to let the manifold system up to atmospheric pressure to regrease the taps a strong odour of amines was apparent from the grease residues. It was believed therefore that a certain unknown percentage of the solute (amine) was being removed from the sample mixture.

Although the S.S.O. technique afforded itself well for qualitative spectroscopic work, the problem of the amine absorption on the grease in the system necessitated its rebuilding and at

the same time an alternative method of deposition was sought for the quantitative work envisaged.

2.2.9.1 Pulsed matrix isolation system

Rochkind {36} has shown that good matrices can be obtained by depositing the gas phase mixture in discrete pulses at 20 K. Rochkind used nitrogen gas as the support matrix. This avoided the possible complication of absorbance measurements due to the appearance of rotational fine structure for small trapped molecules since no molecules have been found to rotate in nitrogen. However, if rotation is not a problem then there is no reason why other matrix gases cannot be used.

The apparatus (Fig. 2.1) consists of a measured volume between two stopcocks connected to a reservoir bulb (containing the mixture to be analysed) and a pressure measuring device. The measured volume is pressurised with gas and deposited on the cold window by manual control of the stopcocks. Since the pressure, volume, temperature and M/A ratio are known, an accurate estimate of the number of molecules of solute gas being condensed on the window can be calculated. Moreover because the pressure of gas is measured directly before deposition, the concomitant fall of the pressure is of no consequence and the total volume of the sample preparation system can be made 1/10 th that of the S.S.O. system and hence less solute need be required for sample preparation.

Rochkind reported that although the substrate temperature does appear to rise during deposition of each pulse the temperature attained is not sufficiently high to cause diffusion and hence aggregation of the solute species. This annealing has the

effect of reducing the possibility for solutes to be isolated in alternative trapping sites and also provides matrices which do not scatter the infrared radiation significantly.

It was therefore decided to add onto the existing pumping line a pulse matrix isolation system with its own sample preparation manifold(Fig. 2.1). The taps were of the greaseless type namely 6 m.m. Young's p.t.f.e. taps and a pressure transducer was used instead of a differential mercury manometer. The greaseless taps required no maintenance other than occasional replacement of the "O" ring seals. The pressure transducer (Appendix 2) converted the gas pressures experienced by the diaphragm of the instrument to a controlled strain in an excited Wheatstone bridge of strain gauge winding in which all four arms were active. The thermal and mechanical symmetry of the unit and precise construction ensured that the output was a linear function of the pressure applied to the diaphragm of the instrument.

The transducer circuit was excited by a stabilised voltage of 10 volts and the output measured by a potentiometer and monitored on a digital volt meter (D.V.M.).

Connection to the vacuum system was facilitated by means of a compressed "O" ring fitted onto a length of 5 mm glass tubing. (Care was taken to ensure that the tubing did not touch the delicate diaphragm.) The connection was helium leak tested and supported a vacuum of 10^{-6} torr.

The transducer was calibrated and found to be linear over the range required for experimentation (0-1 atmosphere). Specifications are given in Appendix 2 and calibration graph given in Fig. 2.6.

Fig. 2.6 Calibration Graph for Transducer Type 4-366-0002-01. Serial No. L48797.

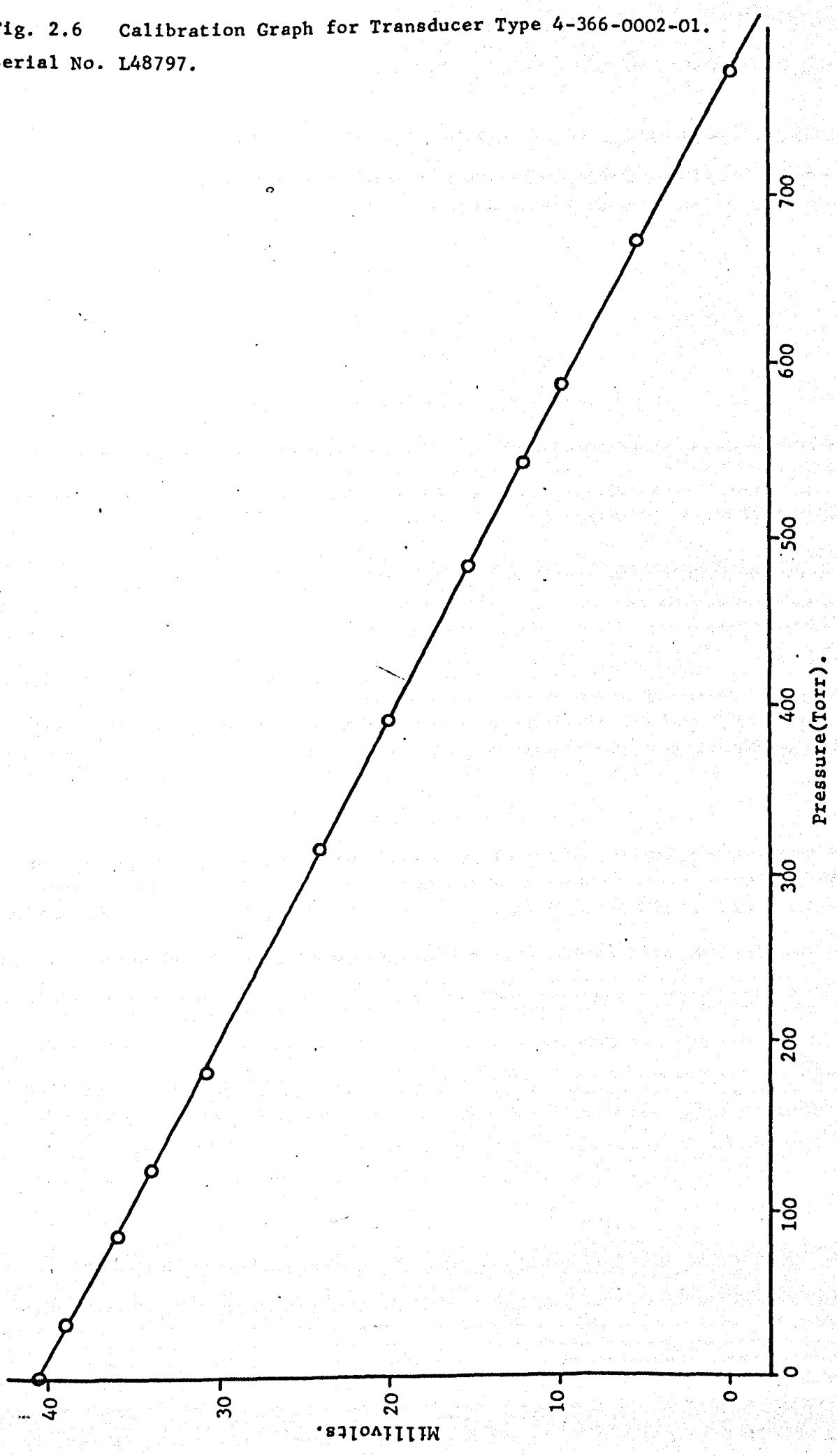

A measured volume of 15 ml was used and was calibrated with mercury (all traces of mercury were removed after calibration), the reservoir bulbs were calibrated with water prior to glass-blowing to the manifold, the volume of which was kept as small as possible. The manifold was subsequently calibrated by gas expansion technique and pressures read by the transducer.

Experimentation was carried out to decide the best pulse pressure and a pressure of 300-400 torr was found to give satisfactory results (chapter 8). After each pulse the temperature drops to its original value before the next pulse is allowed to condense on the cold window, approximately 15 secs for a 400 torr pulse, pulsing being carried out at one minute intervals.

2.2.10 Experimental procedure

The experimental technique has been described in reasonable detail to emphasize the precautions necessary during the operation of the equipment for satisfactory results to be obtained. This section will briefly describe the procedure followed in this work.

With the backing pump operative only, a small storage bulb containing the sample gas to be used in the experiment was attached to the sample preparation manifold, Apiezon "W" was used to seal the ground glass joint and the volume in the joint pumped out. A cylinder containing the matrix gas to be used was attached to the low pressure inlet line. The pressure transducer exciting unit was switched on, the potentiometer and D.V.M. were attached to the output from the transducer. The inlet line was pumped out and flushed once or twice with matrix gas to

remove any air and finally pressurised to slightly above atmospheric pressure up to the tap of the cold trap. This ensured no air leaks could enter the flexible line to the sample preparation manifold.

The system was then pumped down using the diffusion pump and the vacuum checked on the McLeod gauge before continuing, the lowest reading on the scale was 10^{-5} torr and since the mercury usually filled the bulb completely the vacuum used in this work was estimated at $< 10^{-5}$ torr.

The output of the pressure transducer at vacuum was measured with the potentiometer, atmospheric pressure was measured with a barometer and a calibration graph constructed. (The output of the transducer at atmospheric pressure did not vary from experiment to experiment and was taken as constant.)

The pumping system was isolated from the sample preparation manifold by closing the teflon tap, sample gas was then carefully admitted to the sample manifold only until the required mV reading appeared on the D.V.M. this reading was then read using the potentiometer. The manifold tap to the sample bulb was closed and the sample gas allowed to expand into the mixing bulb. A liquid nitrogen Dewar was placed under the cold trap in the matrix gas inlet line. The matrix gas was allowed into the sample mixing bulb to the required mV reading and the tap to the bulb closed. This voltage was then measured on the potentiometer. The matrix gas cylinder was turned off and liquid nitrogen Dewar removed and the pressure released by opening the tap to atmosphere. Care has to be taken to allow any liquified matrix gas to boil off before closing this tap again to avoid dangerous build up of pressure in the line.

The partial pressure of the two gases in the mixing bulb was known so the M/A ratio could be calculated. The error in the M/A ratio was estimated as ±1%.

The sample was allowed to stand for at least 12 hours to permit natural mixing of the sample and diluent gas in the mixing bulb.

2.2.11 Operation of the AC-3L-110 Cryo-tip

Prior to any series of experiments very thorough checks were carried out on all parts of the apparatus.

The Cryostat vacuum shroud was pumped on at the top and bottom vacuum connections to approximately 10^{-4} torr or better, pumping was continued throughout the experiment.

Cylinders of hydrogen and helium, previously attached to the gas-handling manifold were tested for leaks. All valves on the control panel were closed except the valves on the flow-meters which were always kept open. With the helium and hydrogen shut off valves closed the helium and hydrogen evacuate valves were opened and evacuated for a few minutes to remove air from the lines. (A mechanical pump was permanently attached to the vacuum pump connection for this purpose.) Once evacuation was completed the evacuate valves were closed.

The high pressure gas lines were now checked for leaks. The manifold gas regulation valves were closed and one cylinder opened carefully thus pressurising the section of line to full cylinder pressure. All joints were then tested for leaks by brushing soap solution over the couplings to the cylinders and looking for bubbles. If bubbles occurred the connections were retightened and tested again. The pressure in the other lines

was slowly increased to the maximum working pressure 7.0 MNm^{-2} (1,000 psi) and the connections checked as before. If no leaks were found the cylinders were closed until required, the gases were allowed to bleed off and all valves (including the high pressure inlet valves on the control panel) were closed.

The sequence of operations was then as follows. The high pressure inlet lines were pressurised to 1.7 MNm^{-2} (250 psi)up to the inlet valves. These valves were then opened, the indicators on the control panel flowmeters read (in arbitrary units) 0.5 and 2.0 for hydrogen and helium respectively. The small thermal syphon tube was purged out with dry nitrogen gas to avoid moisture freezing in the tube causing long cooldown times. The lines were purged for at least half an hour prior to cooldown.

After this time the reservoir in the heat exchanger was filled with liquid nitrogen after which the purging of the syphon tube was terminated by carefully removing the neoprene tubing attached to the top of the steel tube.

The hydrogen pre-purifier unit was filled with liquid nitrogen and about five minutes after this the hydrogen pressure was raised to 7.0 MNm^{-2} (1,000 psi), the flow read 1.5 on the flowmeter, and the vacuum was now usually 5×10^{-5} torr or less. It normally required forty minutes from this point for liquid hydrogen to be formed, when the hydrogen flow read 4.3. The hydrogen pressure was now turned down to 5.5MNm^{-2} (800 psi) corresponding to a flow of 3.7.

The helium pressure was now increased to 4.1 MNm^{-2} (600 psi) (flow reading 4.0) and required a further twenty minutes for liquid helium to be formed. The temperature was checked using the potentiometer before reducing the helium pressure to

2.8 MNm^{-2} (400 psi) the flowmeters usually registered 4.0 and 6.5 for hydrogen and helium respectively and the pressure in the cell was less than 5×10^{-6} torr. Cooldown time was dependent on mass load, for a tip mass of 40 g the time taken to reach 4 K was usually 60 mins.

Table 2.1

Refrigeration load	He pressure	H_2 pressure
Very light	7.0×10^2 kNm^{-2} (100 psi)	3.5 MNm^{-2} (500 psi)
Light (100 mW)	2.1 MNm^{-2} (300 psi)	5.6 MNm^{-2} (800 psi)
Medium (200 mW)	2.8 MNm^{-2} (400 psi)	6.3 MNm^{-2} (900 psi)
Heavy (500 mW)	3.5 MNm^{-2} (500 psi)	7.0 MNm^{-2} (1,000 psi)

The sample deposition plate was rotated 45^{o} to the direction of the infrared beam. This put the face of the sample plate at right angles to the injection needle. However, depending on the technique used and the rate of deposition of gaseous mixture it was sometimes necessary to increase the refrigeration by increasing the helium pressure to 5.5 MNm^{-2} (800 psi) to ensure adequate temperature control. This was reduced once deposition was completed. The sample plate was then rotated back and spectroscopic information of the matrix sample recorded.

The only maintenance during operation was the occasional replenishing of the liquid nitrogen reservoir. A temperature sensitive resistor, kept in the reservoir, was connected to a relay which operated an audio alarm. When the level of liquid nitrogen dropped below the sensor it activated the alarm and the reservoir was filled manually. Only one cylinder of each circuit was connected to the Cryo-tip at a time to enable quick isolation

of the gas supplies should a fitting fail. As the cylinders ran down new ones were switched on in their place.

After running the spectrum the temperature of the cell was raised up so that all the condensed gas could evaporate off. The gas supply from both the hydrogen and helium cylinders was shut off (all other valves were left open), the liquid nitrogen Dewar in the hydrogen line was removed. When the pressure had fallen to one atmosphere all valves were closed including the high pressure hydrogen and helium valves on the control panel. The temperature in the cell slowly rose, the sample normally evaporated off the sample deposition window in about thirty minutes and was pumped away. The warm up was speeded up by blowing the liquid nitrogen out of the reservoir. The easiest way was to use a rubber bung with a copper tube through it pushed onto the reservoir opening, this forced the liquid nitrogen out of the reservoir in about two minutes.

Once warm up had taken place the diffusion pumps were switched off and the vapour traps removed, the cell continuing to be evacuated by the backing pump until the next experiment.

If temperatures no lower than 15 K were desired it was a simple matter to operate the AC-3L-110 with liquid nitrogen and gaseous hydrogen only.

The hydrogen gas was piped through its normal circuit except that the high pressure hydrogen was connected to the helium inlet on the exchanger which was the tip circuit. The system was purged as previously described. After the liquid nitrogen reservoir had been filled the hydrogen pressure was raised to 7.0 MNm^{-2} (1,000 psi) (3.8 on the flowmeter). The hydrogen flow usually stepped > 10 after approximately twenty minutes and the

pressure throttled back to 1.7 MNm^{-2} (250 psi) (5.0 on the flowmeter). This mode of operation produced about 2 W of net refrigeration at 20 K with an inlet pressure of 1.7 MNm^{-2} (250 psi).

It was sometimes desirable to run the spectrum with the matrix sample at a higher temperature than that of the boiling point of the particular refrigerant used in the tip circuit. This was done by carefully raising the helium or hydrogen back pressure above the level of the boiling refrigerant to raise its boiling point and hence the temperature of the sample.

A back pressure of 1.2 MNm^{-2} (180 psi) produced a temperature of approximately 13 K and 30 K for helium and hydrogen respectively, the exact temperature was measured by the thermocouple.

A pressure release valve fitted at the back of the control panel limited the maximum pressure to 1.4 MNm^{-2} (200 psi).

2.2.12 Diffusion operation

For successful diffusion of sample molecules through the matrix to be obtainable it was often necessary to raise the temperature of the matrix above that attainable by back pressure increase. This was carried out by reducing the flow of gas through the tip circuit so that the temperature slowly rose. The spectrometer was used to monitor a monomer band and the Penning gauge used to monitor the pressure in the cell. As the temperature rose the matrix vapour pressure rose, the maximum temperature that can be used without total loss of matrix being about 40 K. The temperature was kept constant by controlling the flow of refrigerant gas. When the monomer band had halved its original absorbance, (taking account of any temperature dependence or spectral shift of the monomer band), the temperature of the

matrix was then lowered back to its original value and the spectrum was rerun.

SECTION 2

2.3 Raman cryogenic system

2.3.1 Introduction

There are considerable practical difficulties in Raman spectroscopy of matrix isolated species but although the field of Raman studies is growing rapidly there is limited published work dealing with experimental detail. However, from the available literature {76-89} several experimental points were noted.

(i) The weakness of the Raman effect (approximately 10^{-6} of the intensity of the Rayleigh scattering) necessitates the use of matrix to absorber ratios of 500-100 : 1 and sample deposits of approximately 10 times those for the corresponding infrared investigations.

(ii) The necessity for clear matrices, since frosty matrices tended to give high background scattering.

(iii) The prevention of diffusion pump vapours (such as mercury and oil) from condensing on the sample support causing fluorescent problems.

(iv) The necessity of working at reduced laser power, large enough to obtain a useful signal but low enough to prevent local heating of the matrix and a subsequent rise in temperature

to a point when unwanted diffusion may occur.

(v) To achieve an acceptable signal to noise ratio greater spectral slit widths than those generally used in infrared spectroscopy were sometimes necessary, and hence high resolution will invariably be difficult to achieve.

2.3.2 The spectrometer

The Raman spectra in this work were recorded on a Cary 82 laser Raman spectrophotometer. The model 82 incorporates a triple monochromator laser filter system and pulse rate detection system.

A Coherent Radiation Model 52 B argon ion laser with a maximum output of 1.4 W at 488 nm is used as the excitation source.

The laser beam passes through the laser filter system which eliminates non lasing plasma lines. This system is actually a premonochromator with Brewster's angle prism which is adjustable for use with the different laser excitation lines of the argon ion laser. The triple monochromator has three 1,800 lines/mm gratings, six parabolic collimators and curved invariant slits. The radiation passing through the monochromators is detected by a cooled I.T.T. FW 130 photomultiplier with extended S 20 response.

The ordinate presentation is linear between 10^5-50 counts/sec, the full scale of which is variable on the chart paper. The abscissa presentation is linear in wavenumber which is achieved by a cosecant grating mechanism driving a precision lead screw. Wavenumber accuracy is 0.3 cm^{-1} with a reproducibility of 0.1 cm^{-1} or better. Variable scale expansion is provided by interchangeable

gears on the chart paper drive mechanism.

The Cary 82 monochromator slits may be programmed to function in a constant slitwidth or constant spectral bandwidth mode.

Polarization measurements may be easily carried out by means of the polarization analyser comprised of a Polaroid analyser and a calcite wedge scrambler.

2.3.3 Vacuum system

The same vacuum integrity as in the infrared system was aimed for in designing the Raman matrix isolation system.

Owing to the lack of space around the spectrometer and its many other research commitments a permanent vacuum rig could not be built. It was therefore decided to purchase a commercial vacuum pumping system which was compact and could be easily moved should the need arise.

The portable pumping unit (Fig. 2.7) for evacuating the Cryodyne evacuation cell took the form of a watercooled three stage fractionating oil diffusion pump backed by a mechanical rotary pump, fully interconnected by "Vac Lok" coupled copper pipework and four manually operated valves for sequencing of the pumping operation. The diffusion pump was surmounted by a liquid nitrogen vapour trap above which was the baffle/isolation valve. Connection to the Cryodyne shroud sample compartment was facilitated by means of a flexible metal coupling, isolation of the pumping system from the shroud was by means of an in line 25 mm Sanderson valve. The original "veeco" valve at the top of the shroud was kept permanently closed and sealed off under vacuum. All electrical components of the pump were wired to a central

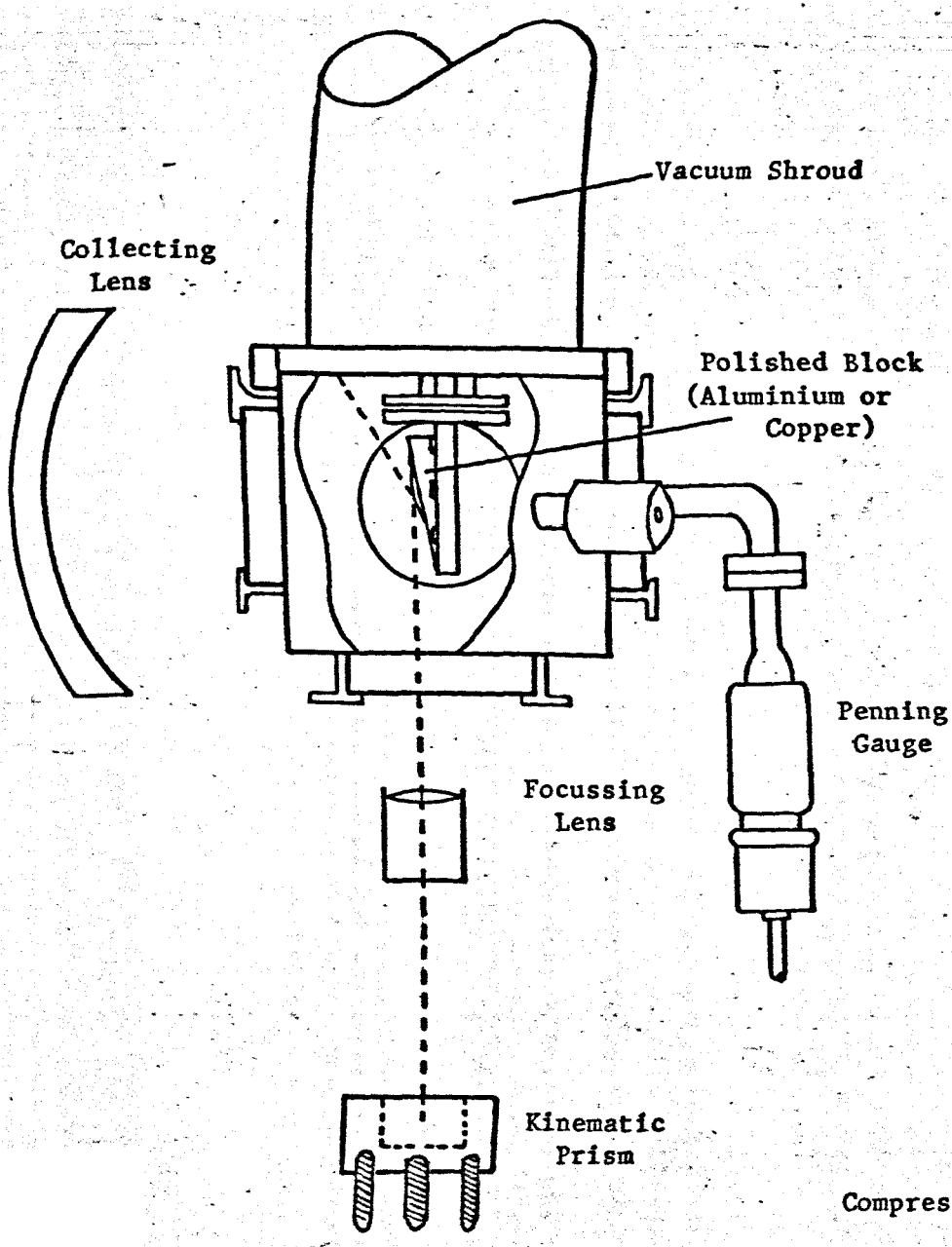

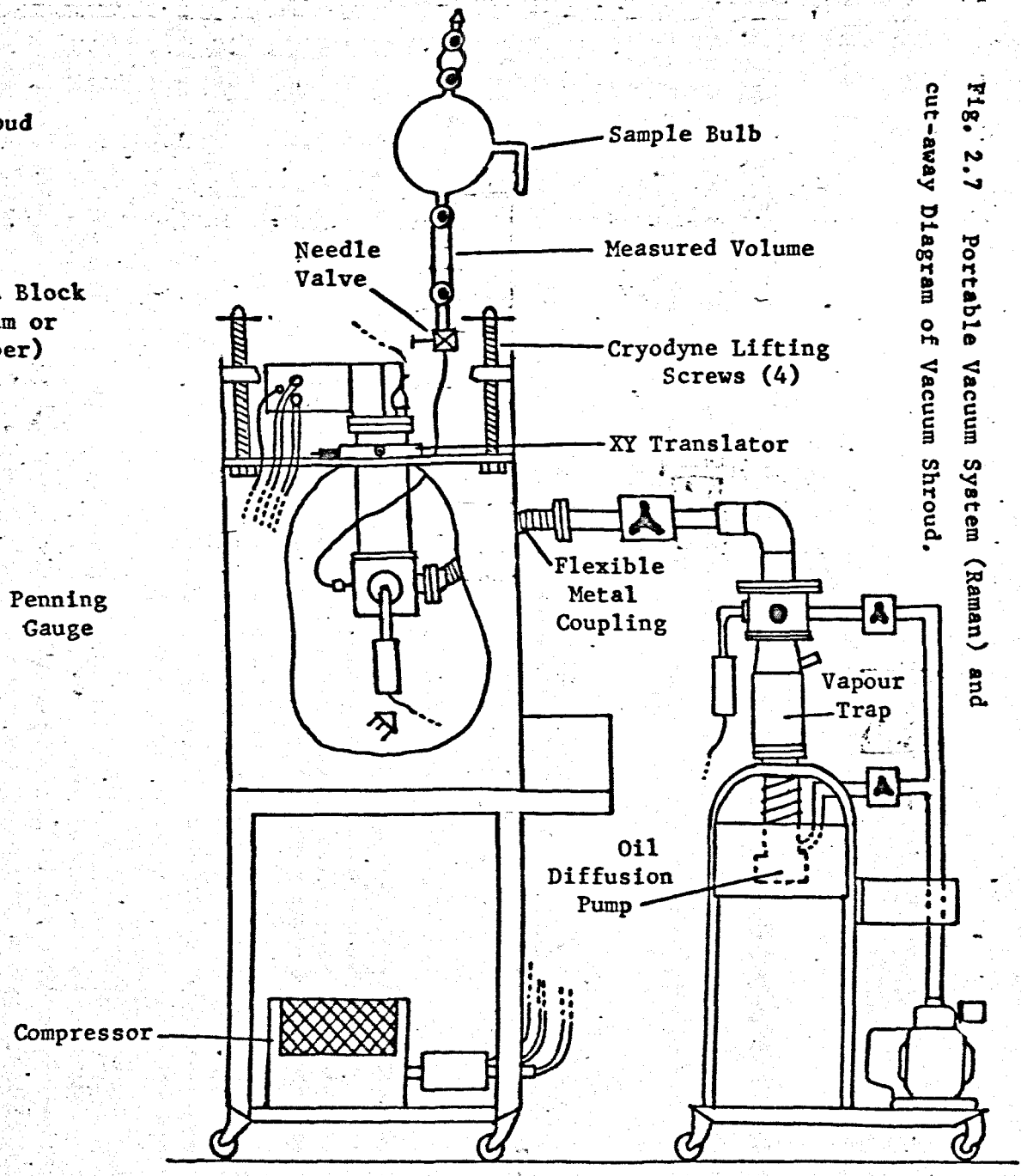

Fig. 2.7 Portable Vacuum System (Raman) and cut-away Diagram of Vacuum Shroud.

control box.

The diffusion pump was filled with "Santavac 5" diffusion pump oil, this had very low "creep" properties and a vapour pressure of 10^{-11} torr at room temperature. All the "O" rings of the high vacuum side were greased with Apiezon "L" grease, vapour pressure 10^{-11} torr at room temperature.

2.3.4 Positioning of the Cryodyne

The Cryodyne unit was clamped into an XY translator which was supplied with the unit for this purpose. The translator with the Cryodyne unit was bolted to a 6 mm thick aluminium plate with a hole through which the Cryodyne unit passed. This aluminium plate could be raised or lowered by means of four bolts which were screwed into the spectrometer sample compartment. Once the Cryodyne unit was in position the sample compartment of the Cryodyne could be attached and evacuated. Lines to the vacuum gauge and injection ports were allowed to leave the spectrometer compartment through another hole in the aluminium plate. When the Cryodyne sample block had been positioned level with the collecting lens of the spectrometer final adjustment was made by use of the XY translator micrometer screws. Rotation of the Cryodyne unit could easily be performed by slackening the translator clamping screws and bodily rotating the unit, once rotation had been achieved, the clamp being retightened. The flexible metal coupling allows rotation of the Cryodyne unit without causing any strain on any part of the system.

2.3.5 Model 21 Cryodyne

The model 21 Cryodyne (Fig. 2.8) is an extremely efficient

Fig.2.8 Cut-away Diagram of Cryodyne Unit.

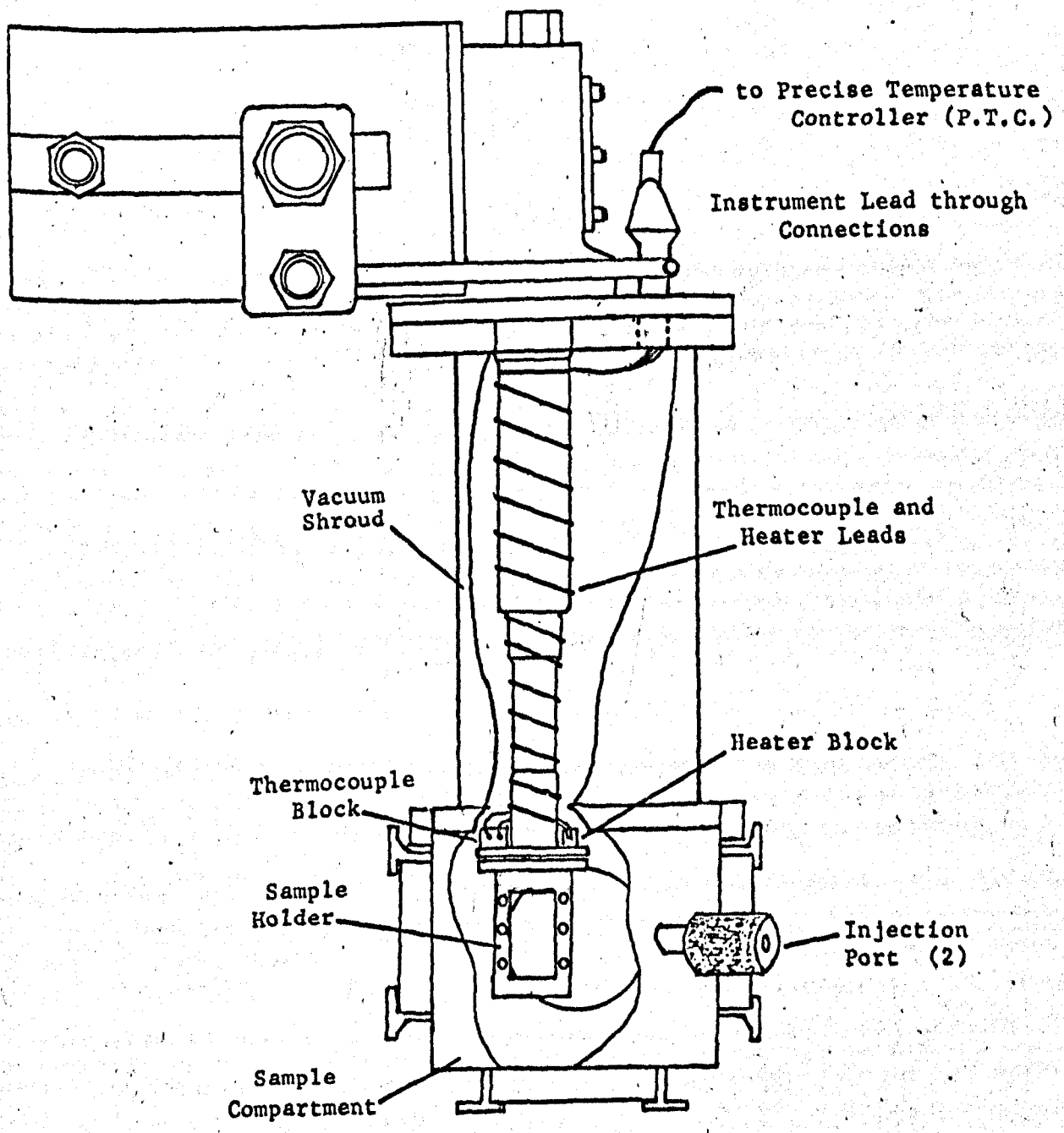

refrigerator, helium gas is used as the refrigerant, the only consumable is electrical power so the running costs are much lower than for the open cycle systems.

The C.T.I. Cryodyne cryocooler is designed to provide reliable refrigeration without maintenance or adjustment for long continuous periods. The principal components of the system are a cold head, a compressor unit, an absorber and interconnecting piping (Fig. 2.9).

The compressor unit has three functions; it supplies helium gas to the cold head at the required pressure and flow rates, secondly it removes from the helium gas both the entrained heat (the small amount of heat from the load being cooled) and the heat of compression, thirdly it removes oil from the helium stream by passing it through an oil separator.

The helium stream leaving the oil separator which is essentially free of oil drops is passed through an absorber to remove the hydrocarbon vapours still present in the helium gas. This adsorber is replaced after each 3,000 hours of operation. The helium gas then flows to the cold head. The function of the cold head is to produce continuous refrigeration at temperatures depending on the heat load in the range 12-300 K.

The model 21 utilises the Gifford-McMahon cycle - a modified Stirling refrigeration cycle. The out-of-phase operation of two pistons causes the refrigeration gas to pass to and fro between a number of interconnecting sections.

The cycle begins with compression of the helium gas at ambient temperature, the gas being transferred through a cooler, (which dissipates the heat of compression) to the regenerator (which cools the gas nearly to the refrigerating temperature)

Fig. 2.9 Schematic Diagram of Cryodyne, Compressor and Precise Temperature Controller

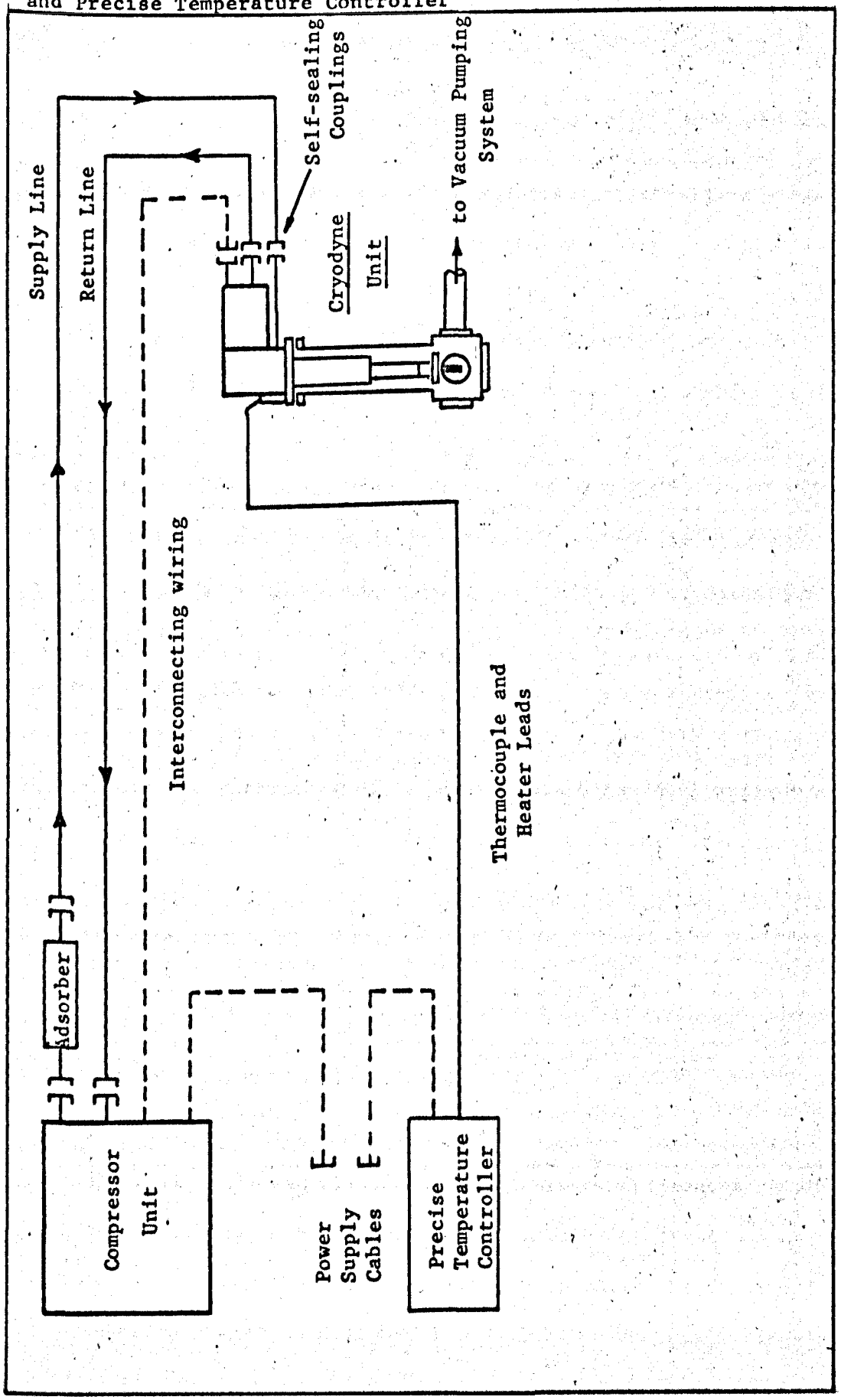

where heat is temporarily stored as the gas moves on to the freezer. This gas then expands into the first stage expansion space hence becoming still colder as a result of work done against a pair of expansion pistons. The upper piston is pushed back mechanically, moving the gas to a second stage expansion chamber where it does work against the lower expansion piston. This piston is not mechanically driven, being returned by the gas expanding at the first stage. The returning cold gas on passing through the freezer absorbs heat from the system being cooled (i.e. heat load) and as it passes through the regenerator it picks up the previously stored heat and is returned to the ambient temperature for the commencement of a new cycle.

Onto the lower cold station of the Cryodyne cold finger is attached the sample mount with an angled copper or aluminium deposition block. Good thermal contact is achieved by the use of indium gaskets compressed between the separate components. The cold finger is surrounded by a vacuum shroud, the lower half of which is rotatable. This vacuum shroud has four ports two of which are required for the incident and scattered laser radiation, one contains a Penning gauge for pressure monitoring and the fourth is connected to the vacuum system. There are two injection ports on either side of an inspection window and at an angle to it.

2.3.6 Temperature control and measurement

For obtaining the temperature of a localised area in a small cell, enclosed within a vacuum, with sufficient accuracy, sensitivity and speed of response thermocouples are the most suitable devices. Negligible heat losses occur through the long thin wires and rapid response is obtained to changes in local

temperature. However, they produce a slightly non-linear millivolt output directly increasing according to the difference between the temperature of the measuring junction and that of the reference junction. The precise temperature controller (P.T.C.) (Fig. 2.9)used in conjunction with the Cryodyne overcomes the problem of non-linearity over the whole working range of temperature i.e. 300-12 K.

The instrument is designed for closed-loop control of temperature and at the same time is able to provide linearised read out of the measurement values in real physical units, in this case Kelvin. These features are achieved primarily by comparing the incoming measured value immediately with a precise linearised set point voltage, so that subsequent amplification is of an error signal only.

The thermocouple provides a voltage that is non-linear with the actual measurement units (K). However, characterisation of the set point voltage or measurement produces an immediate improvement. This characterisation consists of altering the shape of the temperature setting/mV relationship in a number of segments, in this case three are quite adequate.

The thermocouple used in the Cryodyne unit is an iron/0.07% gold vs chromel, the characteristics of which were measured against a Cryogenic Linear Temperature Sensor (C.L.T.S.) device, accurate to 0.01 K, by Oxford Instruments. The P.T.C. segments were then matched up with these calibration figures.

The thermocouple is referenced at 293.2 K. To avoid the inconvenience of a 293.2 K reference bath, a device is used to generate a reference voltage for this temperature. The device is fed with a highly stable constant current and the voltage

generated acts as a reference junction of 293.2 K. The effect of room temperature variations on this cold junction is compensated by a correction introduced by a temperature sensitive diode which is located in the device.

Although the P.T.C. had been matched up to the Cryodyne thermocouple calibration at the manufacturers, it was decided that an independent check would have to be made since the P.T.C. was the only indication of the temperature. The most suitable check that was found was the Raman spectrum of solid α-nitrogen. Two bands at 32 cm^{-1} and 36.5 cm^{-1} were extremely temperature dependent. Cahill and Leroi {90} have published data concerning this temperature dependence and from our results it appeared that the actual temperature of our solid α-nitrogen sample was approximately 13 K higher than that indicated by the P.T.C. To check this the thermocouple was immersed in liquid nitrogen and the read out of the P.T.C. was 88.6 K.

The P.T.C. was recalibrated on the figures supplied by the manufacturers. The thermocouple was again immersed in liquid nitrogen and a reading on the P.T.C. was 77.5 K.

As a final check a sample of solid nitrogen was prepared at 14 K and the Stokes and anti-Stokes bands obtained for the transitions at 32 cm^{-1} and the intensities in counts/sec. The temperature was calculated using eqn. 2.1 below:

$$\frac{I_s}{I_{as}} = \left(\frac{\nu_o - \nu_m}{\nu_o + \nu_m}\right)^4 e^{h\nu_m/kT} \qquad (2.1)$$

where k is the Boltzmann constant

h is Planck's constant

ν_o is the Raman excitation frequency

ν_m is the frequency of the vibrational transition

T is the temperature (K).

The temperature was found to be 15 K but since there is some error (approximately 1 K) involved in the calculation of the temperature the P.T.C. was taken to be reading correctly.

2.3.7 Cleaning procedures for the Cryodyne

The same cleaning methods of "O" rings are applied to the Raman system as the infrared cryocooler. The copper or aluminium block, depending which is to be used, is polished to a mirror finish by using a polishing cloth (a metal polish should not be used as this may lead to contamination of the block). Two thicknesses of 0.05 mm indium gasket are used between the block and the sample holder, the six screws are tightened, left for a few hours and then retightened to ensure good thermal contact.

On reassembly of the vacuum shroud the whole unit was pumped to outgas water vapour prior to cooldown.

2.3.8 Experimental technique

From the experience gained in the use of the infrared system it was decided to adopt P.M.I. as the deposition procedure, since the method tended to give clearer matrices than S.S.O.. Only a simple sample deposition system(Fig. 2.7)was needed, namely a one litre bulb (containing the matrix mixture), a measured volume between two p.t.f.e. taps, connected to a length of flexible p.t.f.e. 4 mm tubing with an injection needle. The only parameters needed for calculation of deposited material were

the initial pulse pressure of the bulb, temperature of the gaseous mixture and the M/A ratio.

The samples were made up in the same way as previously described in section 1. The sampling system was then disconnected from the infrared sample preparation system and transferred to the Cryodyne unit for connection into the cell. This had the advantage of being able to run both infrared and Raman spectra of the same sample. The volumes of the bulb and volume between the taps were accurately calibrated.

The method of calculation of deposited sample was as follows:

Let P_o be the pressure of gas in the bulb of volume V_1 and let V_2 be the measured volume between the taps.

When the gas in V_1 is allowed to expand into the measured volume the pressure will drop to $\frac{P_o \cdot V_1}{(V_1 + V_2)}$.

Let $x = \frac{V_1}{V_1 + V_2}$

$\therefore$ New pressure, $P_1 = P_o \cdot x$ (2.2)

The tap from the bulb is closed and the pulse is allowed to deposit onto the refrigerated support. When the bulb tap is again opened to fill the measured volume the pressure will be

$$P_2 = P_1 \cdot x \quad (2.3)$$

$$\therefore \quad P_2 = P_o x^2 \quad (2.4)$$

$\therefore$ The final pulse pressure after n pulses will be

$$P_n = P_o \cdot x^n$$

Since relatively large amounts of sample were deposited the error in this method is small. A small computer program was

written to calculate the total amount of deposited material and the size of each pulse (Appendix 3).

From the work carried out on solid α-nitrogen it was immediately apparent that several modifications in the technique would have to be made.

The samples were deposited using the pulse technique onto the polished surface of a copper block with the injection needle ≈ 20 mm away from the block. When the first pulse was admitted, rings were seen to move out from the centre of the block surface (observed in monochromatic laser light). If the evacuation cell was rotated the centre of the solid sample could be placed in the centre of the block. However, this effect could only be seen on the first pulse and only lasted about 10 seconds.

There was no apparent increase in temperature during deposition and the temperature could be maintained to ±0.2 K provided the base temperature was at least 2 K below the deposition temperature.

Because the α-nitrogen was completely transparent the reflected laser beam hit the top of the collecting lens and a piece of black tape had to be used to prevent this. According to Nibler and Coe {80} variation of the tip angle was desirable (10-30°). The original block had an angle of 35° so a new one was made, this time out of aluminium. This had an angle of 20° and was polished to a mirror finish before installation. The laser beam was now reflected up into the shroud of the Cryodyne out of the way.

In the first experiments with a sample gas, nitrogen was used as the matrix gas at an M/A ratio of 100. After the first 4 or 5 pulses had been deposited serious cracking of the matrix

occurred. The condition of the matrix deteriorated as more pulses were deposited. Under the same conditions no cracking occurred with pure nitrogen, so the cracking effect was believed due to the addition of the sample molecule causing distortion of the nitrogen lattice (borne out by the broadening of the phonon band of α-nitrogen). The thermal conductivity of the condensed matrix mixture was considered. Upon condensation of the gas, the heat is removed from the sample area (via the copper or aluminium block). Initial thermal conductivity through the matrix is good, since the matrix is thin, however, as the layer of matrix material gets thicker, conduction of the heat being supplied by the fresh condensing gas must take place through this layer. A temperature gradient will be formed but although not sufficient to cause loss of isolation, is sufficient to strain the matrix layer as it is quickly cooled down hence cause cracking.

To overcome this effect in subsequent experiments a needle valve was put in the injection line. For each pulse the setting on the needle valve was slowly altered to let the gas mixture deposit on the block, then opened wider, the actual shroud deposition being held constant until all the pulse had been deposited. This had the desired effect and perfectly clear matrices were obtained with only limited cracking patterns for around 100 μmol of sample gas.

Several other points appeared to affect the quality of the matrices.

(i) Distance of needle from block.

(ii) Initial pulse pressure of the bulb.

(iii) Matrix host gas used.

(iv) Temperature of deposition.

The best position of the needle was ≈ 20 mm from the block, initial pulse pressures above 500 torr tended to cause serious cracking, 400 torr was found to be the most satisfactory. Of the two matrix gases used argon gave the worst matrices. A deposition temperature of between 17 and 20 K was found to give the clearest matrices for both gases, above 20 K gave very frosty matrices and below 17 K resulted in very serious cracking and on several occasions the matrix actually dropped off the block.

Once the matrix had been deposited, provided that only temperature changes at a rate of < 1 K/min were carried out no deterioration of the matrix occurred. However, a rate of temperature change of 4 K/min caused excessive shattering of the matrix.

Since deposition was carried out using the P.T.C. to control the depositing temperature, it was found important to have the deposition temperature at least 2 K above base temperature. This was because if base temperature varied, a change in temperature occurred more rapidly than the P.T.C. could react and a corresponding rise or fall in temperature would result in cracking the matrix. The best conditions were found to be a deposition temperature ≈ 2 K above base temperature, and using the P.T.C. on "auto" controller set to a fast response to any sudden changes in refrigeration.

2.3.9 Operation of the Raman system

The sample bulb containing the gas mixture to be analysed was connected to the sampling system prior to cooldown. The Cryodyne vacuum shroud and the connection between needle valve

and sample bulb were evacuated to a vacuum better than 10^{-4} torr registered on the Penning gauge.

Prior to start up, it was ensured that the charge pressure was $9.3 \times 10^2 \pm 34$ KNm^{-2} (135 ±5 psi) on the suction pressure gauge and that the oil level was correct. The P.T.C. was switched on and the thermocouple and heater leads checked. The controller was switched to "manual", a "set" value of 300 was fixed and on switching to "measure" room temperature was displayed.

The system on-off switch was act u ated and cooling began immediately.

Pumping was continued during cooldown until the temperature reached approximately 40 K when cryopumping began. At this stage the vacuum shroud was isolated from the pumping system by means of the 25 mm Sanderson valve. This prevented the possibility of the cryopumping and subsequent deposition of any vacuum pump oil on the cold surface of the block.

Immediately after cooldown the base temperature monitored by the P.T.C. should be less than 14 K, the Cryodyne was left for 30 minutes to stabilise at a base temperature of less than 13 K. (The actual base temperature of 12 K takes approximately one hour.)

The actual cooldown time depended on the heat load i.e. for a mass of 8 g cooldown time was 45 mins with an average cooldown rate of 6.5 K/min, for a mass of 40 g cooldown time was 50 mins with an average cooldown rate of 5.9 K/min.

It should be noted that although cooldown time is dependent on mass load, base temperature is not, thus a small vacuum leak will result in higher than normal operating temperatures and a gradual increase in temperature. A larger leak may prevent

system cooldown. If the final pressure immediately after cooldown to base temperature (12-14 K) is not 10^{-5} torr or less a leak should be suspected. Leak testing was carried out using the V.G. micromass ½ as previously described in section 1.

Temperature control of the model 21 was achieved either manually or automatically by off setting the capacity of the refrigeration with an electrical resistance heater mounted on the second cold station directly above the block. For a particular set value of temperature, the heater power was adjusted by means of the feed-back controller. As the cold head tried to cool below the set point of the controller, the power to the heater was automatically increased, thus maintaining constant temperature. This automatic control was available over the entire range of the model 21 i.e. 12-300 K.

After cooldown the sample mixture was transferred to the Cryodyne via the injection system as previously described. Deposition time varied depending on the M/A ratio used but between 60-100 μmol of sample gas had to be deposited in the Raman work to obtain a spectrum.

Once deposition was completed, the Cryodyne unit was rotated, lowered and the block aligned with the collecting lens. To facilitate initial sample alignment for the most efficient energy collection, a built-in tungsten lamp operated by the panel switch on the spectrometer, provided a well defined slit image at the sample point. This slit image was projected out onto the matrix and the laser beam carefully aligned with the image. A suitable band was chosen in the spectrum to allow final "peaking up" to obtain maximum signal from the matrix. This was done by careful adjustment of the kinematic prism and the XY translator

until maximum signal had been obtained. Usually a low laser power of between 300-400 mW was used which corresponded to 150-200 mW at the sample. Occasional "peaking up" was necessary to check whether maximum signal was still being obtained. The slightest movement of the Cryodyne can cause complete loss of signal and care should be taken to avoid any unnecessary vibration or movement during the running of the spectrum.

Upon completion of the experiment the Cryodyne can be switched off. Warm up to room temperature can be speeded up by use of the auto controller to heat up the matrix and the block. Once the pressure inside the vacuum shroud had increased to approximately 10^{-3} torr the 25 mm Sanderson valve was opened to the pumping system and the sample gases pumped off. Warm up using the auto controller set at room temperature takes approximately 15 minutes.

2.4 Miscellaneous topics

2.4.1 Cooling gases for air products AC-3L-110 Cryo-tip

(i) Helium

Helium was supplied by Gardener Cryogenic Ltd., at a purity of 99.998% having less than 3 ppm of water and 6 ppm of nitrogen. Each cylinder contained normally 9.1 m^3 of gas at an initial pressure of 20 MNm^{-2}. Three cylinders gave approximately twelve hours of operation before renewal was required.

(ii) Hydrogen

Hydrogen was supplied by B.O.C.Ltd., as white spot grade with a purity of 99.99%. This gas contained less than 10 ppm of water and 1 ppm of nitrogen. Each cylinder contained normally 6.9 m^3 of gas at an initial pressure of 17.5 MNm^{-2}. Five cylinders

gave approximately 10.5 hours of operation at 20 K and 16.5 hours at 4 K.

2.4.2 Working gas for C.T.I. model 21 Cryodyne

Helium is supplied by Matheson Gas Products at a purity of 99.9999%. Impurities are quoted as < 0.1 ppm for argon, nitrogen, oxygen, neon, hydrogen, carbon dioxide and hydrocarbon (as CH_4).

2.4.3 Matrix gases

The matrix gases were all supplied by B.O.C. Ltd.. Grade X nitrogen was used as supplied without further purification. High purity grade argon and white spot nitrogen were both passed through a liquid nitrogen trap before use.

2.4.4 Window materials

(i) AC-3L-110 Cryotip

The outer windows of the Cryo-tip remained at room temperature during all stages of operation and 5 x 45 mm KBr or CsI windows were used. The deposition window was CsI, 3 x 25 mm. CsI was used rather than KBr since the latter tended to shatter at low temperature and required frequent replacement.

(ii) Model 21 Cryodyne

The outer windows of the Cryodyne remained at room temperature during all stages of operation and 3 x 50 mm glass windows were used.

2.4.5 Purification of sample gases

The methylamine and ethylamine were supplied in gas

cylinders by B.D.H. Ltd., at a purity of ≈ 98%.

The ammonia used was supplied in a cylinder by Matheson Gas Products.

The methylamine-d_2 was supplied by Merck and was used without further purification.

The ammonia gas was introduced into the vacuum system from the cylinder, condensed over sodium metal to remove any water that might be present and then vacuum distilled into a storage bulb.

The methylamine and ethylamine which were known to contain impurities were purified in the following manner:

A sample of each gas was taken from the cylinder for subsequent chromatographic analysis. A Pye Series 104 chromatograph with a flame ionization detector head was used for the analysis. A suitable column was prepared which consisted of a 4 m x 5 mm id stainless steel column which was packed with 15 per cent diglycerol, 5 per cent tetraethylenepentamine and 2 per cent polyethylenimine, (the latter to act as an "antitailing" agent) on 60-80 Chromosorb "W". The column was operated at 313.2 K with a nitrogen carrier gas flow of 20 ml min^{-1}.

From the analysis of methylamine it appeared that approximately 0.5% ammonia and a small amount of methanol was present. The ethylamine contained approximately 0.5% ammonia. Water could not be detected with a flame ionization detector.

Methylamine was dried by passing it through freshly prepared potassium hydroxide/calcium oxide under vacuum. The gas was then liquified at 223 K and distilled under vacuum at this temperature. The first portion of the distillate was discarded as containing ammonia and only the middle fraction was

collected in a storage bulb. This was repeated until the ammonia and methanol peaks had been eliminated from any subsequent chromatographic analysis.

The same method was adopted in the purification of ethylamine.

CHAPTER 3

DATA ANALYSIS

3.1 Introduction

This chapter has been divided into two sections. Section 1 deals with the acquisition of data from the Perkin Elmer 225 spectrophotometer by means of a digital data recorder and subsequent computational analysis. Section 2 deals with the increase of the signal to noise ratio and resolution for weak bands in the Raman spectrum of matrix isolated molecules using an automatically controlled time averaging computer.

SECTION 1

3.2 Infrared digital data analysis

3.2.1 Introduction

A large amount of information is obtainable from a spectrum, much of which is never utilised due to the tediousness of its extraction. A calculation such as an integrated band intensity is usually performed very inaccurately simply as a result of insufficient data collection. The availability of digital computers nowadays enable vast quantities of data to be handled at high speeds.

Two requirements are necessary for data analysis.

(i) The data must be in a convenient form for inputting

into the computer, namely on paper tape.

(ii) The data must be transformed by a computer program into a meaningful result.

An Elliot 903 computer was used which in its basic configuration has an internal memory of only 8,192 words. Programming in 903 Algol immediately consumed 4,573 words of the store space due to the Algol interpreter. This leaves approximately 3,500 words for the program and data handling space. However, this was not regarded as being a significant problem in the analysis of matrix bands which are generally sharp and symmetric having half bandwidths of $< 4\ cm^{-1}$, a properly digitised matrix band would contain upto 100 data points which was regarded as sufficient for the type of analysis problem envisaged.

3.2.2 The data recorder

The Perkin Elmer DDR-1C digital data recorder produces a computer compatable paper tape record of data generated by single brush absolute position shaft encoders directly coupled to the 225 spectrophotometer. Up to sixteen characters can be punched in one data word and the DDR-1C is capable of recording data at a rate up to 50 characters per second. Commands to record data may be generated manually by the operator using the "record" push button or automatically by the trigger commutator, mounted on the shaft of the wavenumber data source, this automatically generates 100 record commands per revolution of this shaft, a rate switch controls the actual recording rate (i.e. 1, 2, 5, 10, 20, 50 or 100 commands per revolution). The data characters are transmitted to a patchboard which allows the format of the data word to be compatable with the input requirements of the

Elliot 903 computer. A keyboard allows manual entry of information onto the punched tape.

A P.E. 345/1,000 shaft encoder consists of a 1,000 count disc that resolves the 1,000 counts in a 345° rotation of the encoder shaft, it is coupled to the optical attenuator cam and provides the photometric information. The wavenumber information is provided by a P.E. 1/100 T.C. shaft encoder which resolves 100 counts per revolution with a trigger commutator generating 100 record commands per revolution. This encoder is directly coupled to the Littrow cam drive of the spectrophotometer.

The purpose of the encoders is to transmit changes in positional information which basically set and reset flip flops in the encoder registers which store the positional information. This information is transferred to a data tape every time a record signal is generated, the rate switch selects these record commands at intervals from the trigger commutator.

Each time a record command is generated an eleven character data word is punched on a tape consisting of two parts.

(i) Wavenumber word

The up-down counter in conjuction with the 100 count encoder provides a five digit data number proportional to the abscissa reading on the spectrometer. The 100 count encoder provides the two least significant data digits, the up-down counter counts the number of revolutions of the 100 count encoder, provides the three most significant digits. Logic circuits monitor the output signals of the 100 count encoder register and generates a count pulse every time the encoder changes from 99 to 00 or 00 to 99 and also supplies the direction of rotation information.

With the instrument linked to the spectrometer and the

power turned on, the up-down counter modules have to be preset corresponding to a calibration wavenumber reading of the spectrometer. For the model 225 this value is 4 000 cm^{-1} corresponding to a reset value of 927 for the up-down counter. The last two digits being supplied by the angular position of the 100 count encoder making a total of five digits for the wavenumber data word.

(ii) Transmittance word

The 1,000 count encoder provides a three digit data number proportional to the ordinate reading on the spectrophotometer.

Both data numbers are punched on a record command, each data number having its own terminator so that it is accepted separately into the computer for decoding.

3.2.3 Calibration of the DDR-1C

Difficulty was initially experienced in obtaining a consistent reset value for the calibration at 4 000 cm^{-1}. This was eventually traced to the fact that the 100 count encoder was slipping on the Lithrow cam drive shaft. The screws were tightened and consistent readings for the reset value obtained.

Calibration of the wavenumber and transmission encoders were made using the following procedure:

The power switches of the spectrophotometer and the DDR-1C were turned on. The spectrophotometer was scanned to about 4 008 cm^{-1} then scanned slowly forward (to take up any backlash in the gears) to exactly 4 000.0 cm^{-1}. The punch was turned on followed by the "data" button. The reset button mounted on the spectrophotometer facia was pushed, this forced digits of 9, 2 and 7 into the up-down counter modules. With the

DDR-1C switched to "manual" the "record" button was pushed and a reading of 92752 punched for the wavenumber part of the data word. The rate switch was then set to 100 and with the DDR-1C set to "auto" the spectrometer was slowly scanned forward. The first wavenumber data word punched was 92699 corresponding to a wavenumber reading on the spectrometer of 3992.4 cm^{-1}.

"Manual" readouts were obtained at the exact beginning and end of each range and at one third intervals of each range. These are given in Table 3.1. It can be seen that there are 21,000 figures in each range and 4,200 figures per transitional range.

Data points were obtained at 0%,50% and 100% transmission values on the chart paper. Although the encoder is off set at 0%, the number of encoder counts from midscale to 100% equals that from midscale to 0% within a tolerance of a few counts. This was taken into account in the computer software for processing transmittance data. A calibration graph is given in Fig. 3.1. Once the calibration of abscissa and ordinate scales had been affected, only resetting at 4 000 cm^{-1} was necessary in subsequent experiments. Provided that (i) the link between the spectrophotometer and the DDR-1C is not interrupted, and (ii) the spectrophotometer is not scanned forward over the transition between the end of range 4 and the beginning of range 1, calibration will be correct over all the ranges for repeated scans. If (i) or (ii) occurs the DDR-1C will have to be reset at 4000 cm^{-1} again.

Data will be punched during forward scan only provided a punch rate of 50 characters per second is not exceeded. Maximum scanning speed will therefore depend on the rate switch setting.

Table 3.1

Calibration figures for the DDR-1C

Range	Drum reading (cm^{-1})	Wavenumber Encoder Figure	Wavenumber (cm^{-1}) interval at rate 100
1	5000.0	99752	1/7
	4000.0	92752	
	3000.0	85752	
	2000.0	78752	
2	2500.0	74552	1/14
	2000.0	67552	
	1500.0	60552	
	1000.0	53552	
3	1000.0	49352	1/35
	800.0	42352	
	600.0	35352	
	400.0	28352	
4	500.0	24152	1/70
	400.0	17152	
	300.0	10152	
	200.0	3152	

Fig. 3.1 Calibration Graph for the DDR-1C Transmission Encoder.

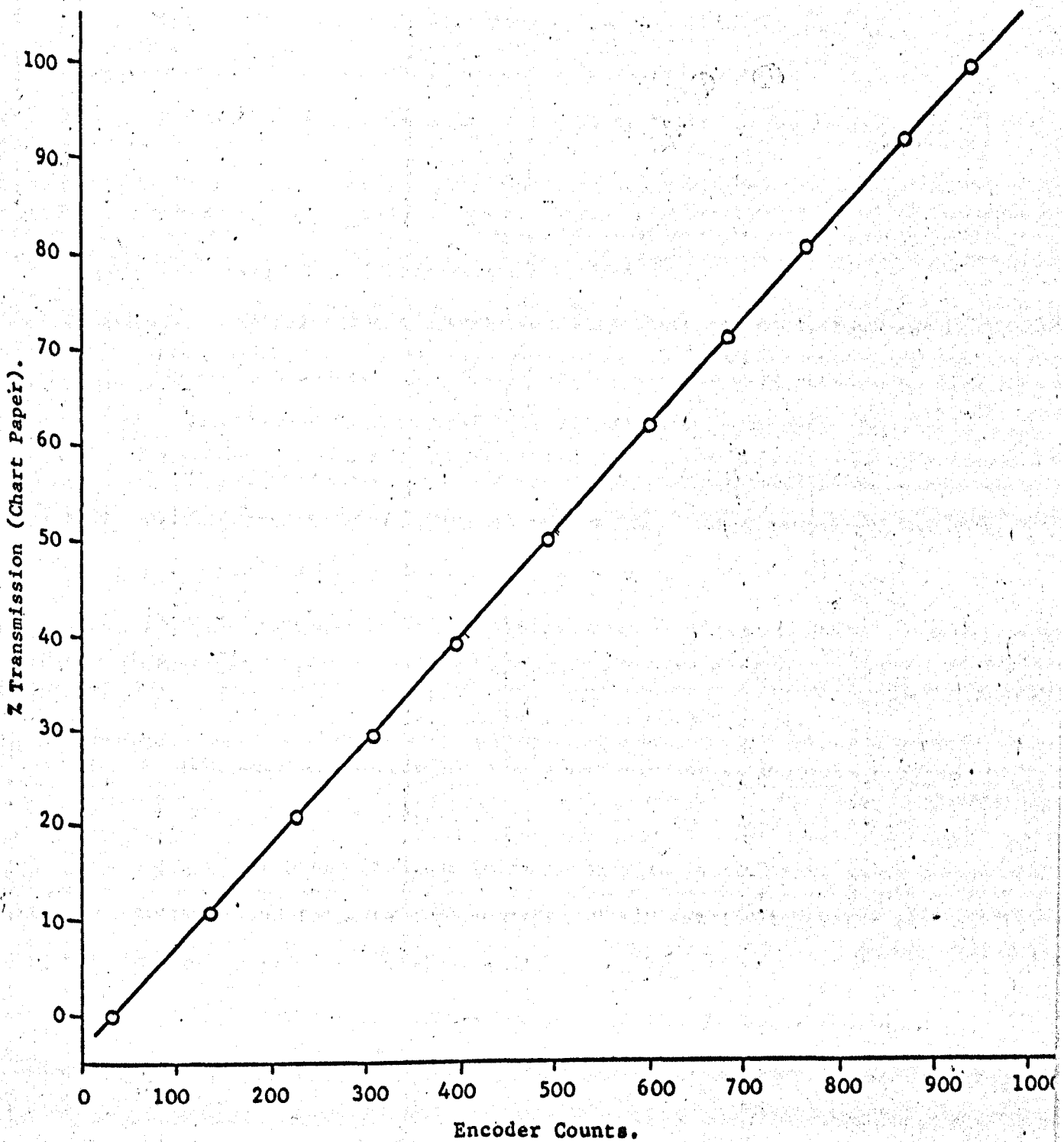

In order for the computer to decode the encoder counts it requires:

(i) the transmission calibration

(ii) the encoder figure and the starting wavenumber for the beginning of each range and its corresponding wavenumber interval at rate 100 between encoder figures. These are given in Table 3.1.

A computer procedure was written in 903 Algol code to decode the encoder figures for any range. This is given in Appendix 4. This procedure may be included in any subsequent program. A schematic diagram of the system is given in Fig. 3.2.

3.2.4 Development of computer programs

(i) Band Search Program SRCH 2A

Matrix bands are generally very sharp and close together requiring expansion on the chart paper for the band structure to be obtained in reasonable detail for subsequent analysis. However, although the chart paper may be accurately marked, slight stretching often occurs on the drum. When scanning over a few hundred wavenumbers using the whole length of the chart paper this slight stretching will therefore result in a progressive error from the beginning to the end of the paper.

To overcome this problem a program was developed (Appendix 5) to give accurate values for peak centres. Included in the program was an approximate definition of a band. The approximate values of the band peaks from the chart paper were entered into the computer and the data tape searched within set limits either side of the search value until a band was found.

To ensure that a band had in fact been found, a section

Fig. 3.2 Schematic Diagram for (a) Raman Signal Averaging and (b) Infrared Digital Data Recording Systems.

(a).

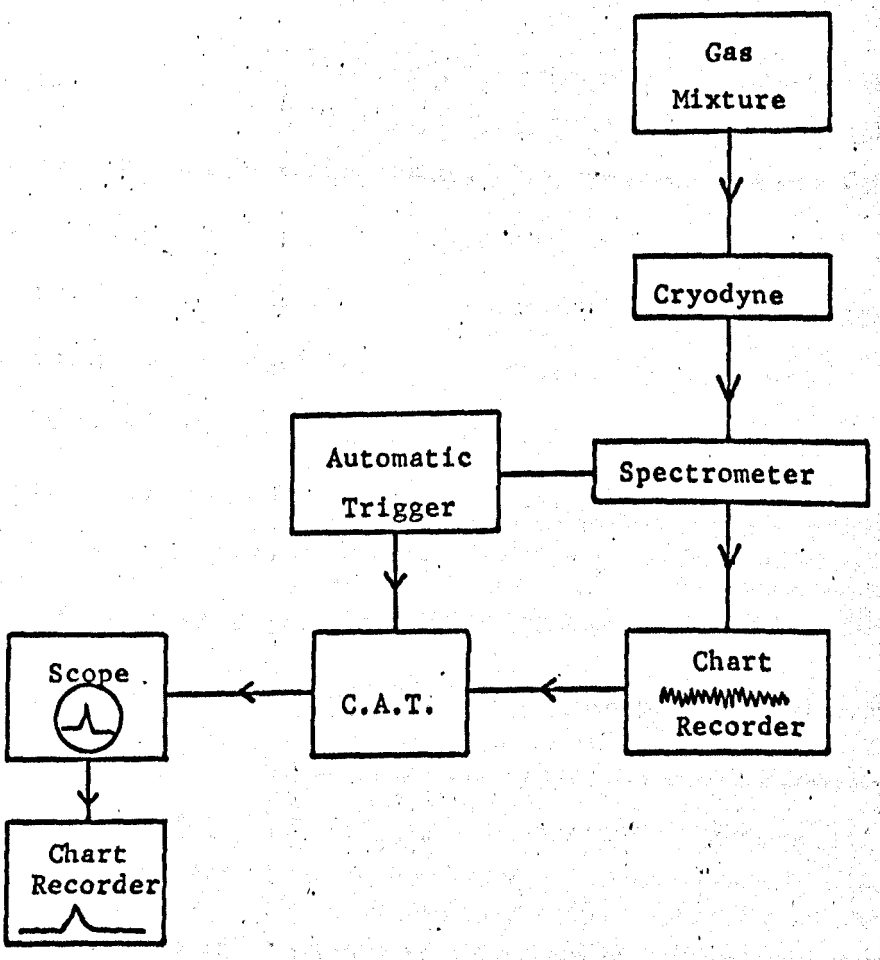

(b).

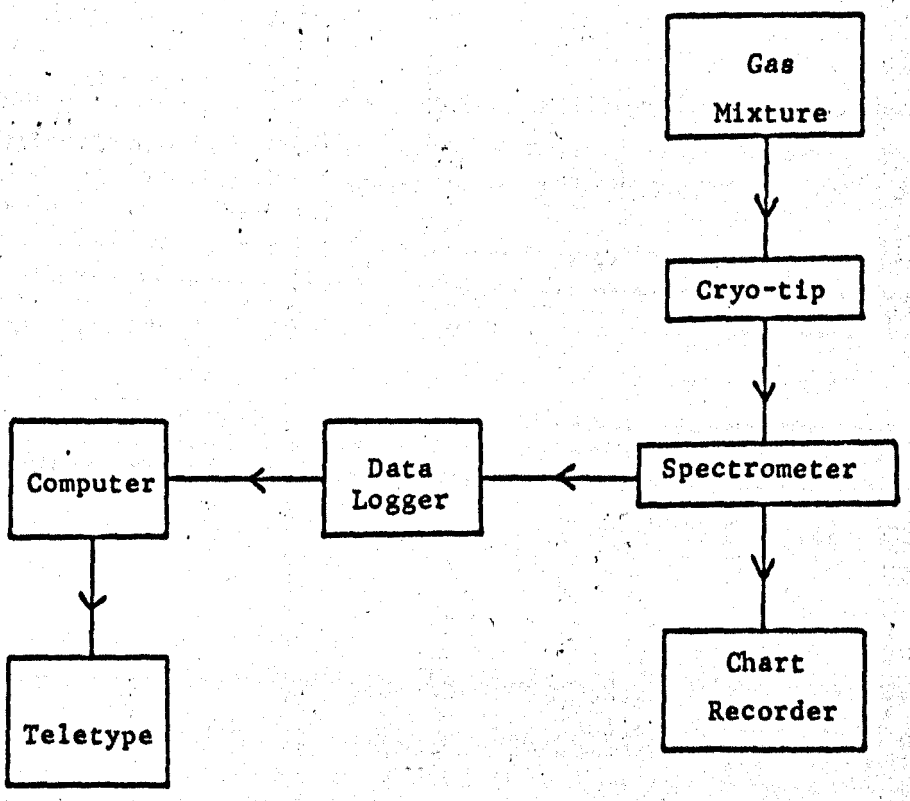

of the band was plotted. The output was a span of wavenumbers containing the actual band centre, each wavenumber having its corresponding point plotted. Scaling was automatic. Providing the search value was reasonable a span of twenty points was sufficient to obtain the band peak. Where there were several adjacent bands the span had to be sufficiently small to prevent inclusion of neighbouring peaks. The more points considered in a span the greater the time taken to search the data tape. Using this program the band peak for a particular matrix band at a particular temperature from one data tape to another was reproducible to within ± 0.1 cm^{-1}. Shifts of < 1 cm^{-1} could be accurately measured for matrix bands during temperature cycling experiments. A typical output is given in Fig. 3.3.

(ii) Band Integration Program COL 1B

The second program COL 1B was developed, Appendix 6, for integration of matrix bands to check that relative "peak" absorbance was a good enough approximation to relative "integrated" absorbance.

Two parts of the program were already available in this laboratory for use with another instrument {92}, these were a convolution technique and a transposition of background data technique, and were rewritten in procedure form. All the above procedures were designed to operate on arrays. Owing to the limitations of the storage space in the computer up to 400 points may be integrated.

The program was designed to be flexible, the various procedures could be called to analyse the data in a number of different ways.

Fig. 3.3

(a) Typical Output from SRCH 2A

```
BAND AT 796.000WAVENUMBER.
SEARCH VALUE = 796.100WAVENUMBER.
 796.714                                                        *
 796.571                                                *
 796.429                                        *
 796.286                                *
 796.143                        *
 796.000*
 795.857 *
 795.714         *
 795.571                 *
 795.429                         *
 795.286                                 *
 795.143

BAND AT 789.571WAVENUMBER.
SEARCH VALUE = 789.700WAVENUMBER.
 790.286                                        *
 790.143                                *
 790.000                                *
 789.857                 *
 789.714 *
 789.571*
 789.429         *
 789.286                 *
 789.113                                 *
 789.000                                         *
 788.857                                                 *
 788.714                                                                *
```

(b) Typical Output from COL 1B

```
BAND POINTS UNSMOOTHED.
BASELINE POINTS UNSMOOTHED.
INTERVAL BETWEEN POINTS= .285714
START OF INTEGRATION= 826.000CM-1
  END OF INTEGRATION= 806.000CM-1
NUMBER OF POINTS TO BE INTEGRATED=      71
INTEGRATED PEAK ABSORPTION FROM 826.000CM-1 TO  806.000CM-1= .906688
BAND AT 816.000WAVENUMBER.
PEAK HEIGHT ABSORPTION AT 816.000CM-1= .468640
```

3.2.5 Method of operation

A background tape was obtained for each region of the spectrum to the analysed prior to any experiment. The desired regions of the matrix isolated sample spectrum were run and a data tape output was obtained. The sampling rate was usually set to give at least thirty points for each matrix band which was regarded as sufficient for successful integration. The initial parameters were typed into the computer via the teletype. The data tape output from the spectrometer was then fed into the computer.

Any region of the spectrum may be selected for integration, smoothing and transposition may be performed if required. The program starts and ends an integration at specified wavenumber limits initially set by the operator. Once one integration has been completed the computer then searches for the starting wavenumber of the next integration to be carried out. The program automatically decodes the raw data from the data logger as each point is read into the computer using the decode procedure. A typical output for COL 1B is given in Fig. 3.3.

It should be pointed out that the integration is only of an area of absorbance and was not intended to be regarded as an absolute value of intensity, since absolute intensities cannot be measured for matrix isolated molecules.

SECTION 2

3.3 Raman data analysis

3.3.1 Introduction

In chapter 2 reference was made to the weakness of the Raman effect and to the necessity of working at low laser power. High resolution was invariably difficult to achieve for the matrix isolated samples. Large spectral slit widths were often necessary and a resultant sacrifice of resolution had to be made in an effort to achieve an acceptable signal to noise ratio from the matrix signal. In some cases the Raman effect was so weak that only with high sample concentrations and maximum sensitivity could some bands be observed and then the spectral bandwidth was too large to resolve close bands. Often in this application, relatively weak signals from the dilute sample of interest are measured with large amounts of background scatter from the matrix material; under these conditions the signal to noise ratio becomes the limiting factor. The criterion for high resolution is invariably related to the quality of the matrix, the light scattering properties of the matrix sample molecules and the degree of sophistication of the Raman detection system.

A method was therefore sought for increasing the signal to noise ratio for analysis of these weak bands of the matrix isolated molecules.

3.3.2 Signal averaging computer

A Varian Model C-1024, time averaging computer was used in conjunction with the Cary 82 spectrophotometer to increase the signal to noise ratio. This was accomplished by sweeping

through the spectrum of interest many times and adding information into the ferrite-core memory of the computer.

When a spectrum of interest was swept repeatedly, signal information was added into the memory channels in direct proportion to the number of sweeps {93}. The information stored in the memory may be displayed on the front panel oscilloscope, or read out through a recorder. The computer sweep of the memory channels may be triggered internally by the operator or externally by the Cary 82 (see later). There are a maximum of 1,024 memory locations. It is equipped to accept analog signals of 1, 3, 10 or 30 volts and pass the signal through an analog-to-digital converter and store the signal in its memory. The sweep time can be varied over a variety of time intervals from 0.025 to 1,000 seconds.

The ordinate spectral information is supplied by a very linear ten turn potentiometer directly coupled to the pen servo motor shaft. This potentiometer is supplied with a stabilised 10 volts power supply and gives a 0 to 10 volts output directly proportional to the signal incident on the detector. Fig. 3.4 illustrates how this system provided an improvement to final spectral results and a schematic diagram is given in Fig. 3.2.

3.3.3 Operation of the Time Averaging System

The spectrum was scanned repeatedly over a fixed number of wavenumbers from a fixed wavenumber starting point. The speed of scanning over the spectral region depended on the pen period, spectral bandwidth and the sweep time of the computer. Once these parameters had been fixed they were not altered. The computer was triggered manually for sweeping to begin at the same

Fig. 3.4 Improvement of Signal to Noise Ratio by use of the Time Averaging Computer for Matrix Isolated Molecules

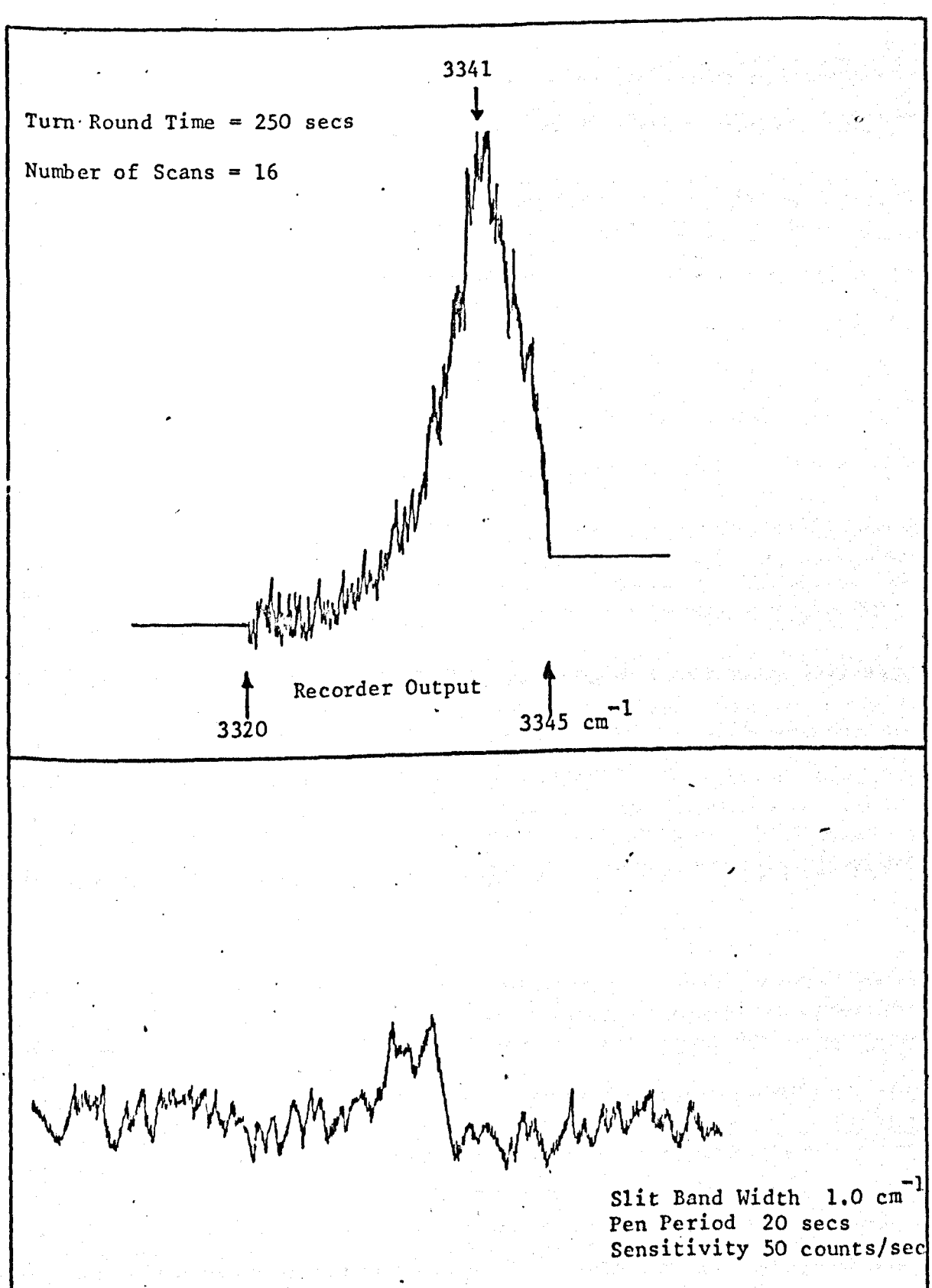

time as the forward scan was manually switched. At the end of each sweep the spectrometer was reversed scanned passed the sweep starting wavenumber. Alteration of the scan speed was not possible since this would cause an error in the wavenumber sweep of the computer. The spectrometer was then scanned slowly forward to the starting wavenumber ready for triggering of the next sweeping operation of the computer.

The above operations required a certain amount of coordination of movement as well as being tedious and requiring constant attention for long periods of time. Thus although results were obtainable modification was necessary.

The system was therefore automated by means of microswitches which were triggered by the movement of the cosecant drive mechanism of the Cary 82 spectrophotometer. The microswitches energised relays to control the operating modes of the spectrometer. Accurate alignment of these microswitches enabled any spectral region > 10 cm^{-1} to be repeatedly scanned. The computer was triggered by one of the microswitches to within an accuracy of ± 0.1 cm^{-1} each scan.

CHAPTER 4

METHYLAMINE IN ARGON AND NITROGEN MATRICES

4.1 Introduction

Durig et al {94} studied the infrared spectra of methylamine and its deuterated analogues (CH_3ND_2, CD_3NH_2 and CD_3ND_2) in argon matrices. They present or assign most of the monomer fundamentals of each isotopic species on the basis of the matrix and condensed phase infrared and Raman spectra. Recently Hirakawa et al {95} have carried out a detailed force constant analysis of methylamine using their own spectra of methylamine and $CH_3{}^{15}NH_2$ in the gas phase and Gray and Lord's gas phase data {96} for the deuterated species. There are a number of disagreements between these assignments and those of Durig et al. Wolff et al {97-102} have examined the Raman spectra of CH_3NH_2, CH_3NHD and CH_3ND_2 in the gas, liquid and solid phase. They observe the NHD twisting mode of CH_3NHD at 878.0 cm^{-1} in the gas phase which is at a considerably lower frequency than previous assignments.

In order to resolve these disagreements, and as a necessary precursor to carrying out quantitative studies of the amines (discussed in chapter 8), infrared and Raman matrix studies of methylamine, methylamine-d_1 and methylamine-d_2 were undertaken in this work. The first and last isotopic species belong to the point group, Cs, consequently, the normal vibrations divide into only two symmetry species, symmetric to the plane A′ and antisymmetric to the plane A″. Of a total of fifteen normal modes for the monomer species, nine are of species A′ and six are of species A″, all are infrared and Raman active. However,

depending on the isolation of the molecules in a matrix, the type of matrix used, the temperature and M/A ratio, additional absorptions due to multimer species and molecules trapped in different sites affected the complexity of the spectra. Careful experimentation and comparison of results obtained in both the infrared and Raman for argon and nitrogen matrices of the methylamines was necessary to aid the frequency assignments of the monomer species in each fundamental region. In general, frequencies for the monomeric species were taken from the infrared results since these frequencies are more accurate because of the higher resolution used in obtaining the infrared spectra than for the Raman. Multimer species were apparent in the infrared spectra at low M/A ratios but although multimer species were observable in the Raman results they did not appear to be strong scatterers. Clearer spectra free of multimer frequencies were obtained at lower M/A ratios than would normally be used in the infrared. The effects of M/A ratio changes, temperature and diffusion are discussed where applicable in each fundamental region. Unless otherwise stated all matrix samples were deposited at 20 K.

Experimentation carried out for the molecules described in this chapter is given in Table 4.1.

4.2 Monomer assignments

4.2.1 NH_2 stretching region

The NH stretching frequencies of methylamine were extremely weak in the infrared and were only observable at low M/A ratios where spectral assignment of the monomer bands was hindered by the overlapping bands due to multimer absorptions. Attempts

Table 4.1

Experimentation carried out for methylamine and methylamine-d_2

I N F R A R E D

Molecule	Matrix	M/A	Technique	Temperature (K)	Amount of sample deposited (μmol)
CH_3NH_2	Nitrogen	100	S.S.O.	20	60.0
	"	100	"	"	20.0
	"	200	"	"	20.0
	"	500	"	"	20.0
	"	1040	"	"	10.0
	"	2140	"	"	10.0
	"	530	"	4	10.0
	"	1040	"	"	20.0
	"	1080	"	"	3.5
	"	100	P.M.I.	20	18.0
	"	100	"	"	13.0
	"	100	"	"	13.0
	"	200	"	"	12.0
	"	220	"	"	15.0
	"	400	"	"	5.0
	"	450	"	"	5.0
	"	510	"	"	15.0
	"	970	"	"	6.5
	"	1650	"	"	1.0
	Argon	180	S.S.O.	20	31.0
	"	490	"	"	10.0
	"	1000	"	"	10.0
	"	50	P.M.I.	20	13.0
	"	100	"	"	42.0
	"	120	"	"	7.5
	"	180	"	"	30.0
	"	200	"	"	4.2
	"	250	"	"	7.1
	"	550	"	"	7.1
	"	1050	"	"	7.0
	"	2050	"	"	7.1

Table 4.1 (contd.)

Molecule	Matrix	M/A	Technique	Temperature (K)	Amount of sample deposited (μmol)
CH_3NH_2	Argon	200	P.M.I.	4	15.4
	"	200	"	"	9.9
	"	540	"	"	13.4
CH_3NH_2/H_2O	Nitrogen	200	"	20	21.0
" "	Argon	500	"	20	10.1
CH_3NH_2/N_2	Argon	540	"	20	7.5
CH_3ND_2	Nitrogen	90	"	"	14.0
	"	100	"	"	26.5
	"	300	"	"	6.0
	"	850	"	"	4.0
	"	1500	"	"	10.0
	Argon	110	"	"	18.0
	"	240	"	"	14.0
	"	580	"	"	7.0
	"	860	"	"	7.0
	"	1030	"	"	7.0
	"	1040	"	"	10.0
CH_3NH_2/CH_3ND_2	Nitrogen	1000	"	"	10.0
CH_3NH_2/CH_3ND_2	Argon	1000	"	"	10.0

R A M A N

CH_3NH_2	Nitrogen	55	P.M.I.	20	100
	"	100	"	"	81
	"	100	"	12	60
	"	100	"	17	89
	"	100	"	20	76
	"	200	"	"	52
	"	520	"	"	10
	Argon	50	"	"	120
	"	100	"	"	100
	"	200	"	"	50
CH_3ND_2	Nitrogen	100	"	"	90
	Argon	100	"	"	86
CH_3NH_2/CH_3ND_2	Nitrogen	100	"	"	90
CH_3NH_2/CH_3ND_2	Argon	100	"	"	82

Fig. 4.1 Raman Spectrum of the NH_2 Stretching Region of CH_3NH_2 in a Nitrogen Matrix.

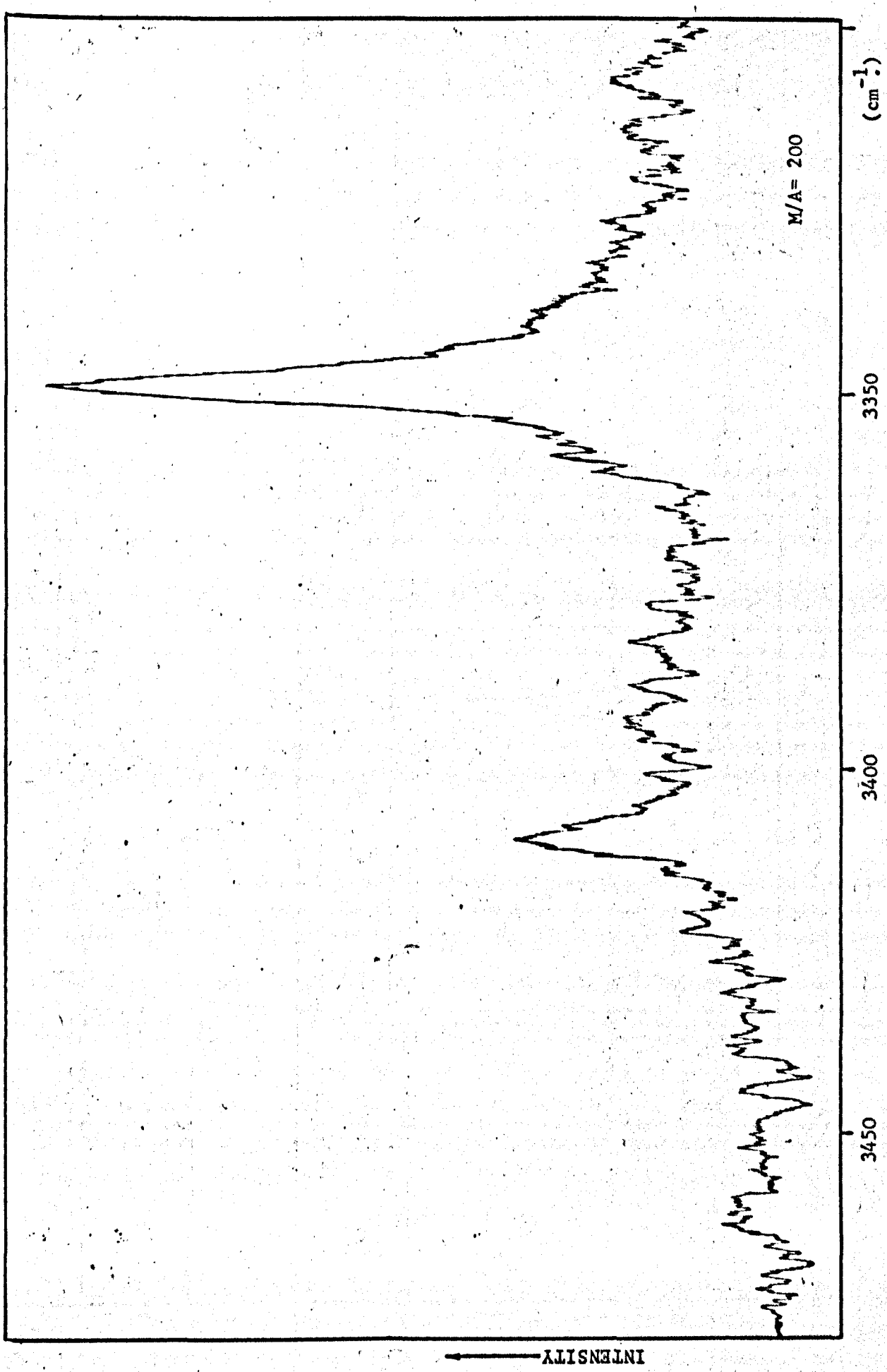

Fig. 4.2 Infrared and Raman Spectra of the ND_2 Stretching Region of CH_3ND_2 in a Nitrogen Matrix.

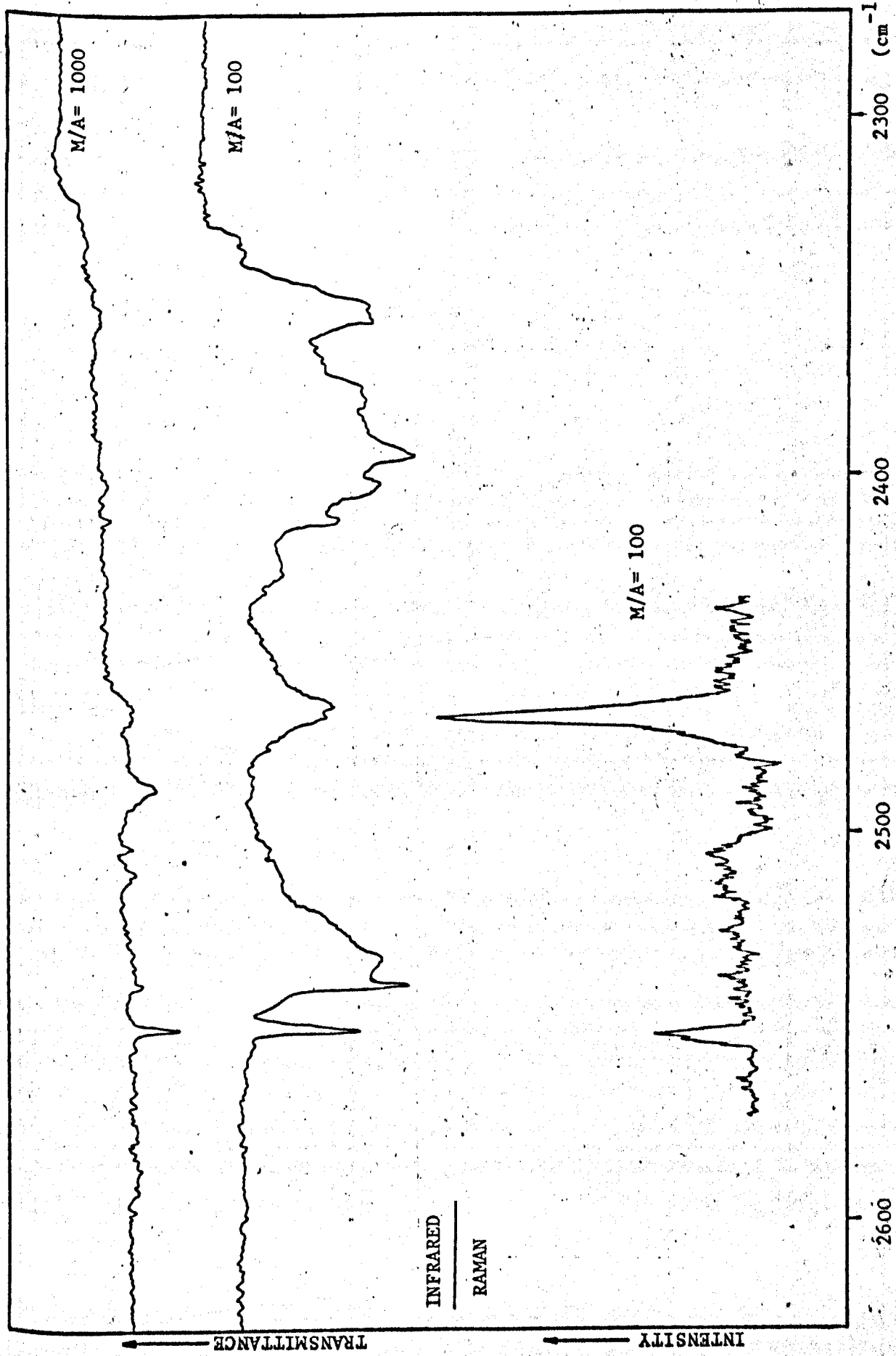

Fig. 4.3 Infrared and Raman Spectra of the CH_3 Stretching Region of CH_3NH_2 in a Nitrogen Matrix.

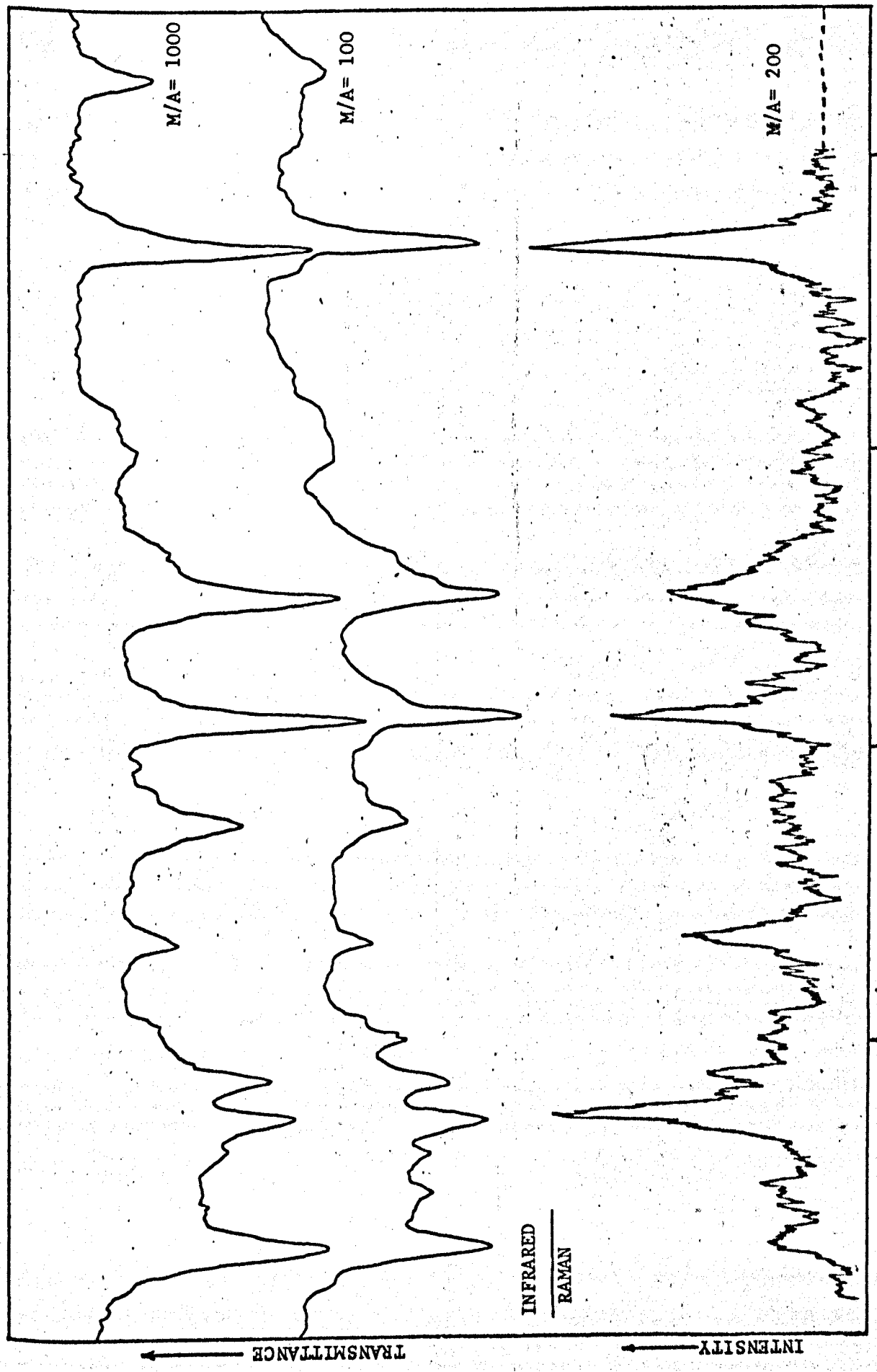

Fig. 4.4 Infrared and Raman Spectra of the CH_3 Stretching Region of CH_3ND_2 in a Nitrogen Matrix.

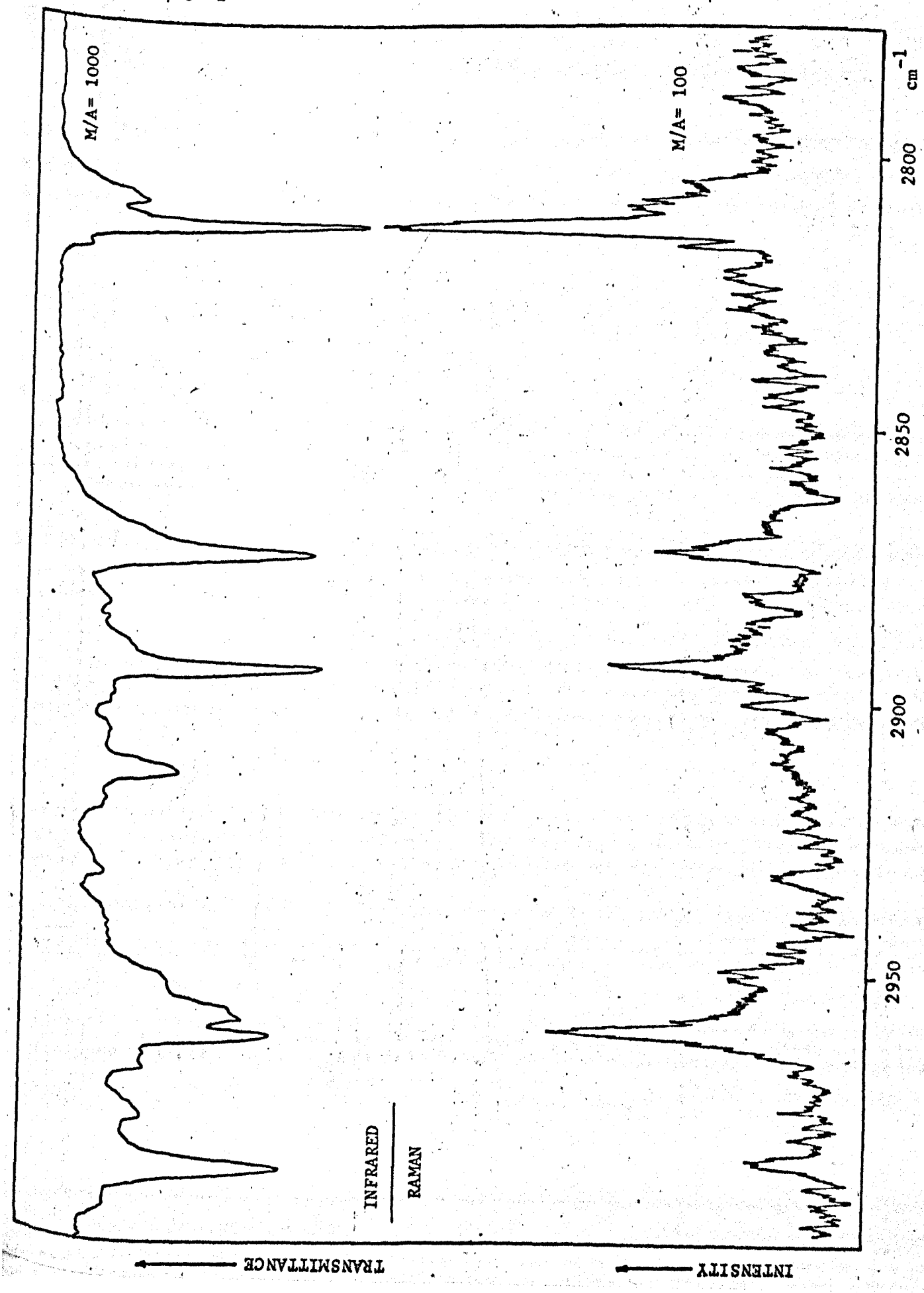

Fig. 4.5 Infrared and Raman Spectra of the CH_3 Deformation Region of CH_3NH_2 in a Nitrogen Matrix.

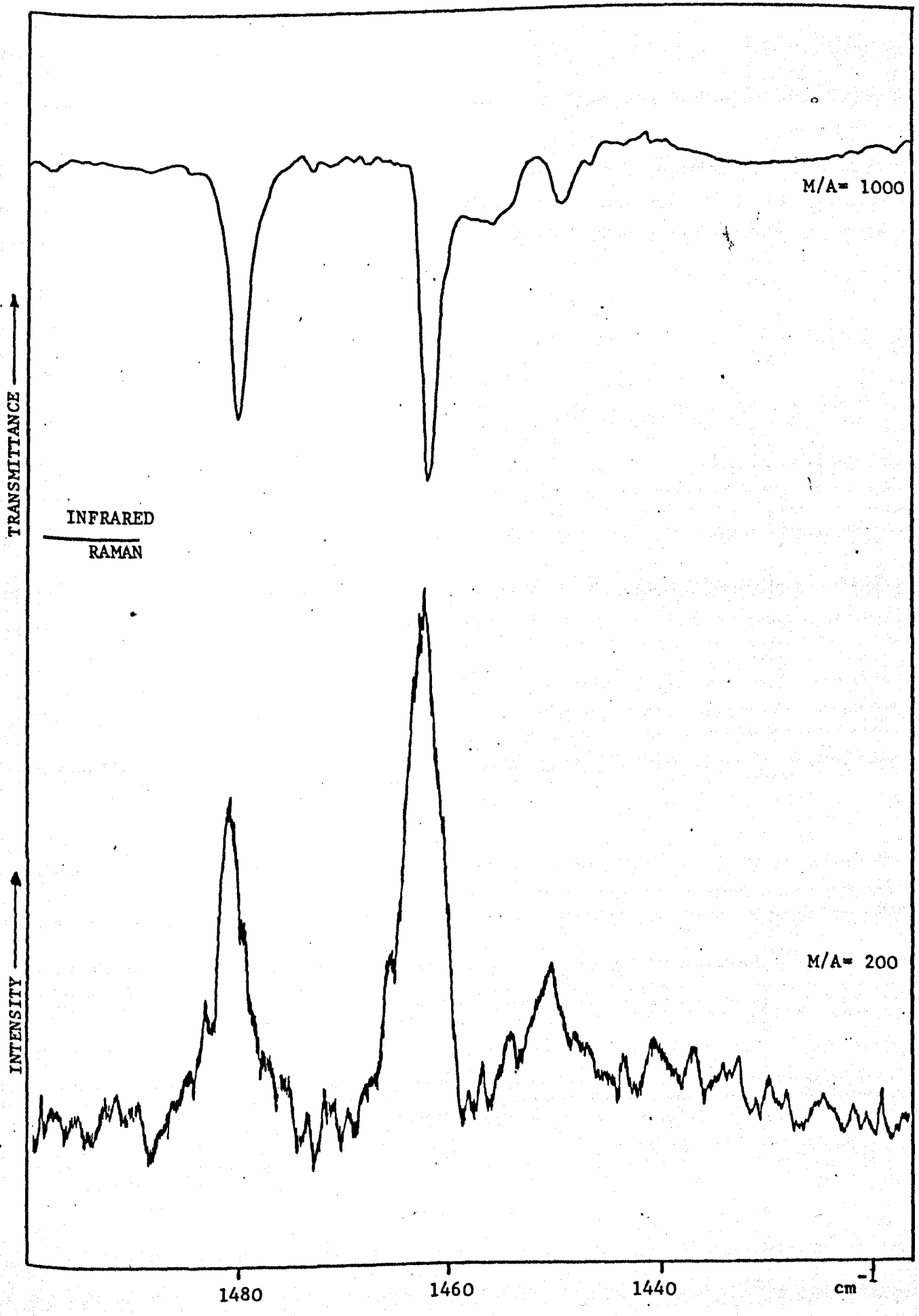

Fig. 4.6 Infrared and Raman Spectra of the CH_3 Rocking and CN Stretching Regions of CH_3NH_2 in a Nitrogen Matrix.

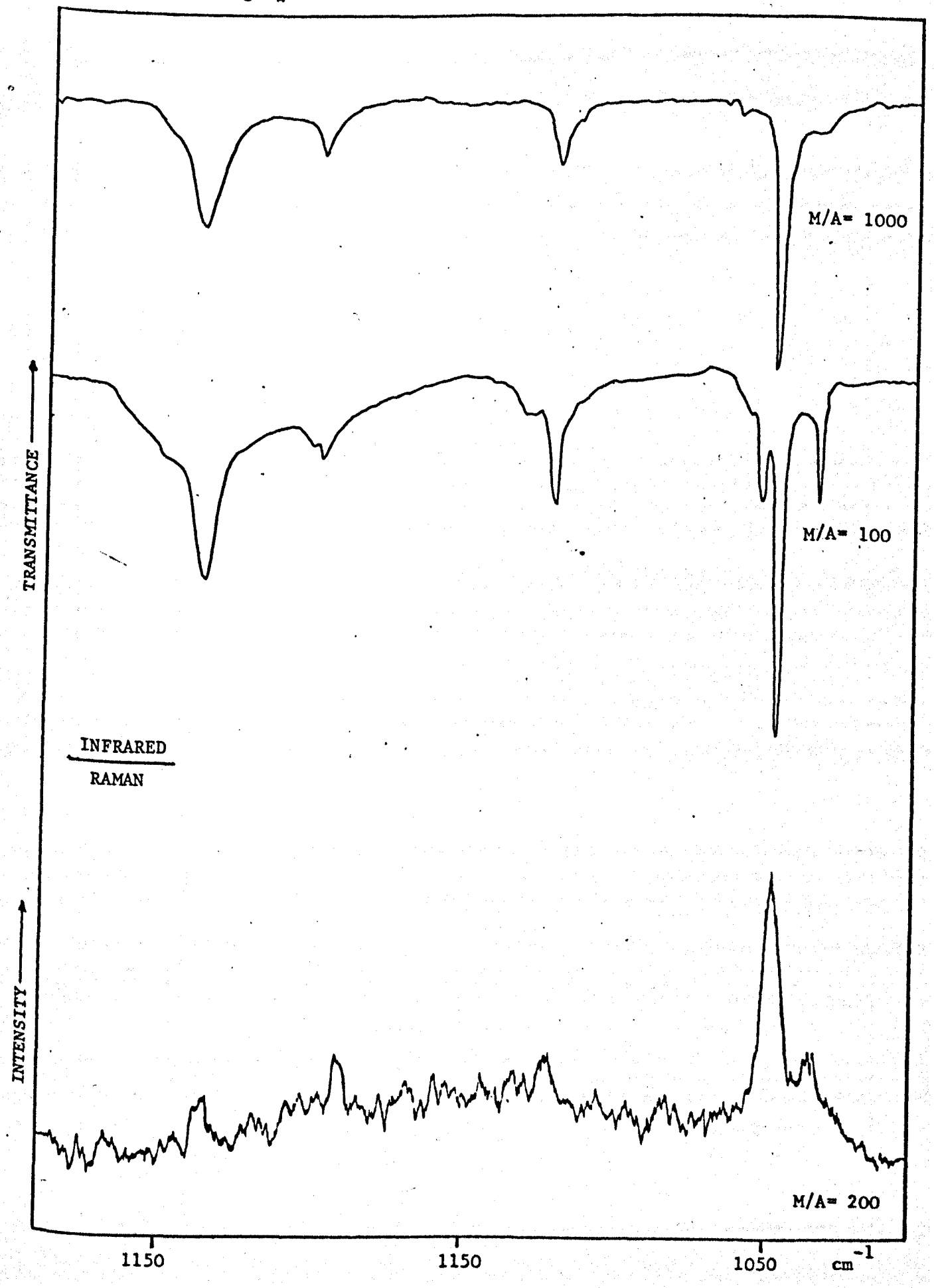

Fig. 4.7 Infrared Spectrum of the NH_2,NHD,ND_2 Wagging Mode of a CH_3NH_2/CH_3ND_2 Mixture in a Nitrogen Matrix, showing NHD Twist.

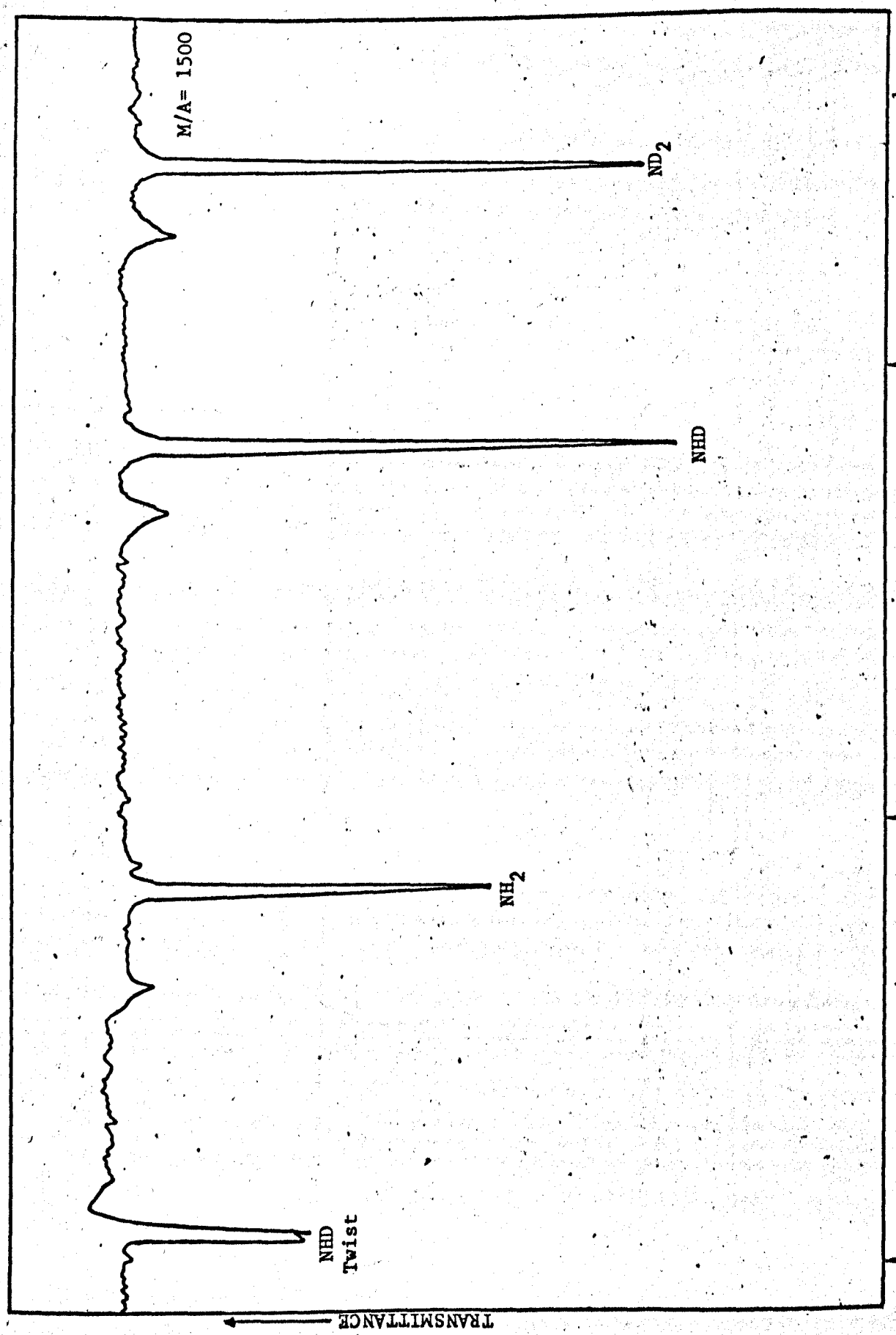

Fig. 4.8 Infrared Spectra of the NH_2 Wagging Region of CH_3NH_2 in an Argon Matrix deposited and recorded at 20K showing diffusion effects.

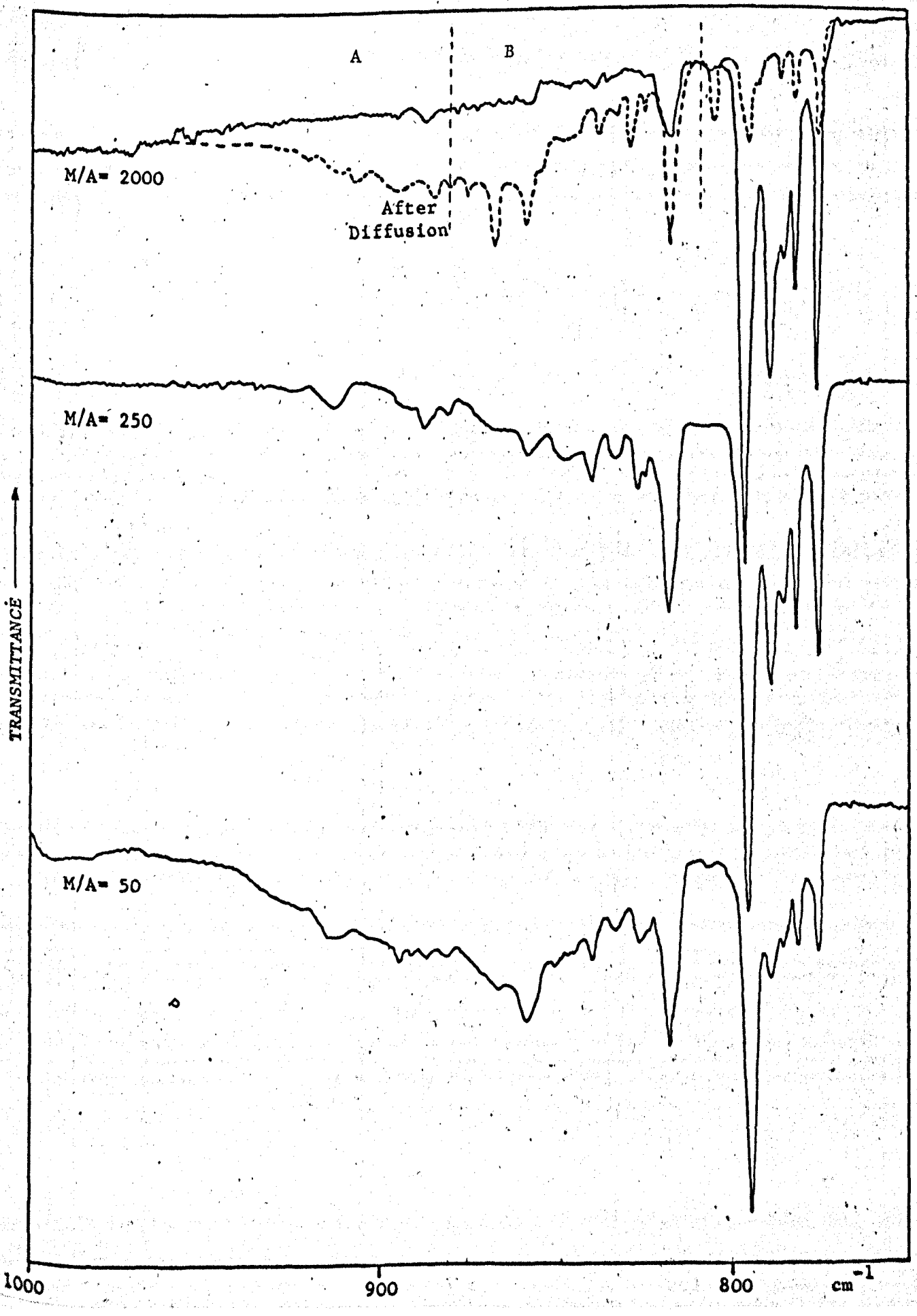

Fig. 4.9 Infrared Spectra of the NH_2 Wagging Region of CH_3NH_2 in a Nitrogen Matrix.

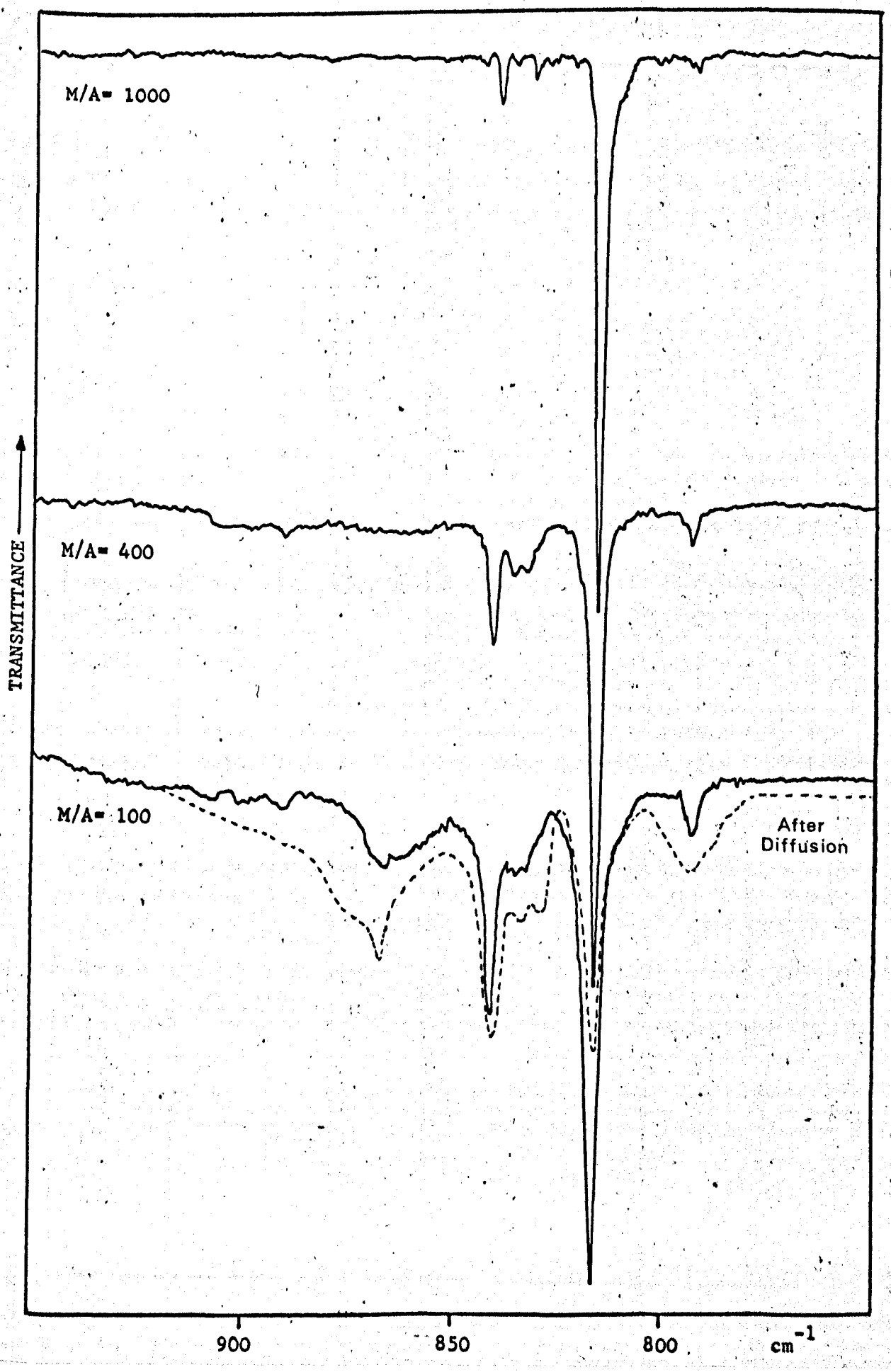

Table 4.2

Infrared and Raman bands observed for CH_3NH_2 in an argon matrix

Frequency cm^{-1}		Species	Assignment
Infrared	Raman		
∿3410	3414.8	MONOMER	NH_2 asym. stretching (A")
∿3389		dimer	
∿3346	3352.2	MONOMER	NH_2 sym. stretching (A')
∿3300		multimer	
∿3282			
∿3256			
∿3236			
∿3199			
∿3180			
2990.8	∿2988	MONOMER	CH_3 asym. stretching (A")
2982.8		multimer	
2978.2		multimer	
2967.1	2967.4	MONOMER	CH_3 asym. stretching (A')
2959.8	2962.6	Monomer	2 x 1480.8 = 2961.6 (A')
2954.8	-	multimer	
2934.1	2932.0	Monomer	1480.8 + 1463.8 = 2944.6 (A")
2916.6	2914.6	Monomer	2 x 1463.8 = 2927.6 (A')
2901.5	2902.8	Monomer	1463.8 + 1449.8 = 2913.6 (A')
2893.5	∿2894	multimer	
2878.8	2877.2	Monomer	2 x 1449.8 = 2899.6 (A')
2870.6	∿2873	multimer	
2819.3	2819.0	MONOMER	CH_3 sym. stretching (A')
2815,0		multimer	
2797.3	2714.7	dimer	
2792.8		dimer	
2784.8	∿2790	multimer	
2779.4		multimer	
1636		multimer	
1630		multimer	NH_2 scissors (A')
1623.0		MONOMER	
1480.8	1482.2	MONOMER	CH_3 asym. deformation (A")

Table 4.2 (contd.)

Frequency cm^{-1}		Species	Assignment
Infrared	Raman		
1478.9		multimer	
1465.3		multimer	
1463.8	1465.3	MONOMER	CH_3 asym. deformation (A')
1456.5		multimer	
1449.8	1451.5	MONOMER	CH_3 sym. deformation (A')
1429.8		multimer	
1423.1			
1395.8			
1376.8			
1368.0			
∿1148		multimer	
1139.7	-	MONOMER	CH_3 rocking (A')
∿1130		multimer	
1117.4	-	MONOMER	CH_3 rocking (A")
1086		multimer	
1082		dimer	
1053.8		multimer	
1052.2	1053.1	MONOMER	CN stretching (A')
1045.8	∿1045	multimer	
1041.8		site	
1039.2	∿1040	monomer	
1034		multimer	
∿ 972		MONOMER	NH_2 twisting (A")
926		multimer	
915			
∿ 896			
∿ 888			
868.7			
859.2			

Table 4.2 (contd.)

Frequency cm^{-1}		Species	Assignment
Infrared	Raman		
840.4		multimer	
833.1			
827.3			
824.7			
818.6		dimer	
(806)	-	(N_2 induced)	
796.1	-	MONOMER	NH_2 wagging (A')
789.7		monomer	site bands
786.4		monomer	
782.4		monomer	
776.2		monomer	
766.8		monomer(SSO)	
764.2		monomer(SSO)	
~ 370	-	dimer	

Table 4.3

Infrared and Raman bands observed for CH_3NH_2 in a nitrogen matrix

Frequency cm^{-1}		Species	Assignments
Infrared	Raman		
∿3410	3411.0	MONOMER	NH_2 asym. stretching (A")
∿3392	-	multimer	
∿3350	3349.2	MONOMER	NH_2 sym. stretching (A')
∿3340	-	multimer	
∿3283	∿3305	multimer	
∿3200	-	multimer	
2991.3	-	multimer	CH_3 asym. stretching (A")
2985.3	2985.0	MONOMER	
2976.1	2976.3	multimer	
2969.8	2966.0	multimer	
2963.1	2963.2	MONOMER	CH_3 asym. stretching (A')
2956.8	2956.9	Monomer	2 x 1480.5 = 2961.0 (A')
2950.1	2950.5	multimer	
2933.6	2933.2	Monomer	1480.5 + 1462.5 = 2943.0 (A")
2912.6	∿2914	Monomer	2 x 1462.5 = 2925.0 (A')
2895.1	2895.8	Monomer	1462.5 + 1449.6 = 2912.1 (A')
2874.6	2874.8	Monomer	2 x 1449.6 = 2899.2 (A')
∿2866	2864.3	multimer	
∿2849	2851.5	multimer	
2819	2821	multimer	
2816.0	2815.8	MONOMER	CH_3 sym. stretching (A')
∿2797	2812.8	multimer	
∿2785	2787.3	multimer	
∿1655	-	multimer	NH_2 scissors (A')
1642.0	-	MONOMER	
1480.5	1481.2	MONOMER	CH_3 asym. deformation (A")
1471.7	-	multimer	
1462.5	1463.2	MONOMER	CH_3 asym. deformation (A')
1456.3	-	multimer	
1449.6	1451.0	MONOMER	CH_3 sym. deformation (A')

Table 4.3 (contd.)

Frequency cm^{-1}		Species	Assignment
Infrared	Raman		
1433.6	-	multimer	
1152.0		multimer	
1144.0	1143	MONOMER	CH_3 rocking (A')
1126.6		multimer	
1125.0	1121	MONOMER	CH_3 rocking (A")
∿1090		multimer	
1085.8		dimer	
1055.7	1061.6	dimer	
1052.0		monomer?	site band
1049.5	1049.5	MONOMER	CN stretching (A')
1043.0	1043.5	monomer	
∿ 966		multimer	
∿ 945			
∿ 907			
∿ 885			
868			
840.4		dimer	
836.4		multimer	
832.0		multimer	
816.0	-	MONOMER	NH_2 wagging (A')
795.2		multimer	
792.8		multimer	
-	365.5	dimer	

Table 4.4

Infrared and Raman bands observed for CH_3ND_2 in an argon matrix

Frequency cm^{-1}		Species	Assignment
Infrared	Raman		
∿2995		multimer	
2991.1	∿2991	MONOMER	CH_3 asym. stretching (A")
2985.0	2983.0	multimer	
2969.8	-	monomer	site band
2966.0	2966.0	MONOMER	CH_3 asym. stretching (A')
2962.4	2960.5	Monomer	2 x 1479.3 = 2958.6 (A')
∿2957	-	multimer	
∿2943	-	multimer	
2933.0	-	Monomer	1479.3 + 1462.2 = 2941.5 (A")
2917.3	2916.5	Monomer	2 x 1462.2 = 2924.4 (A')
2909.3	-	multimer	
2899.1	2902.5	Monomer	1462.2 = 2924.4 (A')
2892.8	-	multimer	
2877.8	2880.5	Monomer	2 x 1456.0 = 2912.0 (A')
2870.7	-	multimer	
2818.7	∿2819.0	MONOMER	CH_3 sym. stretching (A')
2811.8	-	multimer	
2809.3	-	multimer	
∿2554	-	multimer	
2548	2548.0	MONOMER	ND_2 asym. stretching (A")
2545	-	multimer	
2534	-		
2527.8	-		
2518	-		
2478	-		
∿2462	2461.0	MONOMER	ND_2 sym. stretching (A')
2456.5	-	multimer	
2432	-		
2416	-		
∿2390	-		
∿2340	-		

Table 4.4 (contd.)

Frequency cm^{-1}		Species	Assignment
Infrared	Raman		
1487.6		multimer	
1479.3	1479.0	MONOMER	CH_3 asym. deformation (A")
~1476	-	multimer	
1462.2	1462.0	MONOMER	CH_3 asym. deformation (A')
1456.0	1456.0	MONOMER	CH_3 sym. deformation (A')
1245		multimer	
~1225		multimer	
1218.6		multimer	
1207.6		dimer	
1203.0	~1200	MONOMER	ND_2 scissors
1189	-	MONOMER	CH_3 rocking (A')
~1134		multimer	
1125.5	-	MONOMER	CH_3 rocking (A")
1120.5		multimer	
~1035		dimer	
1011.1		multimer	
1006.1	1006.0	MONOMER	CN stretching (A')
1001.1	~1000	multimer	
994.9		site monomer	
~ 758	-	MONOMER	ND_2 twisting (A")
683.4		multimer	
668.6		multimer	
663.0		multimer	
659.6		multimer	
656.6		dimer	
654.2		dimer	
(644.8)		(N_2 induced)	
638.6	-	MONOMER	ND_2 wagging
634.2		monomer	site bands
632.2		monomer	site bands
630.4		monomer	site bands

Table 4.5

Infrared and Raman bands observed for $CH_3 ND_2$ in a nitrogen matrix

Frequency cm^{-1}		Species	Assignment
Infrared	Raman		
2993.4	-	multimer	
2987.2	∿2987	MONOMER	CH_3 asym. stretching (A")
2976.6	-	multimer	
2965.3	-	multimer	
2962.2	2962.8	MONOMER	CH_3 asym. stretching (A')
2959.7	-	Monomer	2 x 1479.6 = 2959.2 (A')
2950.6	2950.8	multimer	
2932.6	2933.0	Monomer	1479.6 + 1462.2 = 2941.8 (A")
2919.0	-	multimer	
2913.3	-	Monomer	2 x 1462.6 = 2925.2 (A')
2907.0	-	multimer	
2898.8	2901.4	multimer	
2894.6	2894.8	Monomer	1462.2 + 1456.0 = 2918.2 (A')
2889.7	-	multimer	
2882.6	∿2882	multimer	
2873.8	2874.0	Monomer	2 x 1456.0 = 2912.0 (A')
2869.7	-	multimer	
2818.3	-	multimer	
2814.5	2814.7	MONOMER	CH_3 sym. stretching (A')
2809.7	2810.2	multimer	
2545.8	2545.8	MONOMER	ND_2 asym. stretching (A")
2532	-	dimer	
2524	-	multimer	
2476	-	monomer?	
∿2456	2458.1	MONOMER	ND_2 sym. stretching (A')
∿2453	-	multimer	
∿2416	-		
2402	-		
∿2385	-		
∿2344	-		
1479.6	1480.5	MONOMER	CH_3 asym. deformation (A")
1476.4	-	multimer	

Table 4.5 (contd.)

Frequency cm^{-1}		Species	Assignment
Infrared	Raman		
1471.7	-	multimer	
1466.9	∿1466	multimer	
1462.6	1462.6	MONOMER	CH_3 asym. deformation (A')
1456.0	∿1456	MONOMER	CH_3 sym. deformation (A')
1226.3	-	multimer	
1222.4	-	dimer	
1218.2	-	dimer	
1211	-	-	
1207.1	∿1208	MONOMER	ND_2 scissors (A')
1128.0	-	MONOMER	CH_3 rocking (A")
∿1035	1039.7	dimer	
1007.3	1008.5	multimer	
1004.1	1005.0	MONOMER	CN stretching (A')
999.0	999.5	multimer	
∿ 700	-	multimer	
691.6	-		
690.6	-		
687.6	-		
684.2	-		
670.2	-	dimer	
668.0	-	multimer	
663.4	-	multimer	
653.6	∿ 654	MONOMER	ND_2 wagging (A')

were made to obtain spectra at high dilution but the large amounts of matrix material which were required to obtain a spectrum caused excessive scattering of the incident radiation from the infrared source. No satisfactory spectra were obtained to enable an accurate frequency assignment of the bands. However, in contrast, as shown in Fig. 4.1 in the Raman the monomer NH stretches were much stronger and therefore easily identified. The two groups of bands in this region for methylamine showed the presence of multimer bands which disappeared as the M/A ratio was increased. The monomer NH stretches consist of two bands. The strong band at 3352.3 cm^{-1} in argon and 3349.2 cm^{-1} in nitrogen corresponding to the 3360 cm^{-1} band in the infrared gas phase is clearly the symmetric NH stretch and the weaker band at 3414.8 cm^{-1} in argon and 3411.0 cm^{-1} in nitrogen is assigned to the antisymmetric stretch. On deuteration the ND stretches are slightly stronger in the infrared but again are more easily identified in the Raman spectra. For methylamine-d_2 (Fig. 4.2) the ND symmetric stretch is at 2461 cm^{-1} in argon and 2458.1 cm^{-1} in nitrogen and the ND antisymmetric stretch is at 2548 cm^{-1} and 2545.8 cm^{-1} for argon and nitrogen matrices respectively. In the Raman spectra of a mixture of methylamine and methylamine-d_2 the stretching frequencies of the CH_3NHD molecule have been recognised. The NH and ND oscillators in this molecule are essentially independent and the NH and ND stretching frequencies have been identified at 3382 cm^{-1} and 2498 cm^{-1} respectively in argon and 3373.7 cm^{-1} and 2495.5 cm^{-1} in nitrogen.

4.2.2 CH stretching region

A complex series of strong and medium intensity bands occurs

in the CH stretching region of methylamine in argon or nitrogen for both the infrared and Raman (Fig 4.3). The effect of changing the M/A ratio for both matrices only slightly affected the spectral features in this region. A sharpening of the main bands was observed with increasing M/A ratio as a result of a decreasing in the intensity of the shoulders on these bands. These shoulders are due to multimer species having frequencies very close to those of the monomer bands.

Comparison of the infrared and Raman monomer spectra in the CH stretching region allowed positive assignments for the CH stretching fundamentals to be made for each of the isotopic species studied.

The Raman spectra of methylamine show clearly that the strongest feature is the CH_3A' symmetric stretch at 2819.3 cm^{-1} in argon and 2816.0 cm^{-1} in nitrogen corresponding with 2820 cm^{-1} found in the infrared and Raman gas phase. The CH_3 A'' antisymmetric stretch will be expected to be weaker in the Raman than the infrared and hence leads to the assignment of the band at 2990.8 cm^{-1} in argon and 2985.3 cm^{-1} in nitrogen to this fundamental (Fig. 4.3). The CH_3A' antisymmetric stretch corresponds to 2967.1 cm^{-1} in argon and 2963.1 cm^{-1} in nitrogen. The remaining monomer bands are due to overtones and combinations of the CH_3 deformation modes intensified by Fermi resonance with the A' fundamentals. Tentative assignments are given in Tables 4.2 and 4.3.

The spectrum of methylamine-d_2 is very similar (Fig. 4.4) the CH_3 fundamentals of the molecule being essentially unshifted. The assignments are given in Tables 4.4 and 4.5.

4.2.3 CH_3 deformations region

There are three methyl deformations, again multimer absorptions overlap or appear as shoulders on the monomer bands. These shoulders disappear with increasing M/A ratio. The monomer CH_3 deformation region of methylamine in argon comprises bands at 1480.8 cm^{-1}, 1463.8 cm^{-1} and 1449.5 cm^{-1} in both the infrared and Raman (Fig. 4.5). The very weak band at 1450 cm^{-1} corresponds to the symmetric deformation which is considerably shifted from the apparent gas phase value of 1430.6 cm^{-1} {96}. A band was observed at 1428 cm^{-1} in the matrix but the symmetric deformation would not be expected to shift appreciably for the methylamine-d_2 molecule. This is the case the band at 1456 cm^{-1} being assigned to this mode. Confirmation that any shift on deuteration is small is provided by the CH_3 stretching region since the overtone and combination bands are not shifted appreciably from the values for CH_3NH_2.

The A′ and A″ CH_3 antisymmetric deformations are assigned in agreement with the gas phase assignment and have frequencies of 1463.8 cm^{-1} and 1480.8 cm^{-1} corresponding to the gas phase values of 1473.6 cm^{-1} and 1485.1 cm^{-1} {96}. These frequencies along with those obtained for these molecules isolated in a nitrogen matrix are given in Tables 4.2, 4.3, 4.4 and 4.5. Again the shifts from argon to nitrogen are slight.

4.2.4 $NH_2(ND_2)$ bending modes (scissors)

For the CH_3NH_2 molecule the assignment is the same as that of previous workers {96}, but due to the presence of atmospheric water vapour in the infrared spectrometer housing arising from the absence of adequate dry air flushing equipment the amount of

energy available in this region was limited. Only two bands were observed in the infrared. The main spectral feature (a broad band at 1623 cm^{-1}), present at high M/A ratios, was taken as being due to monomer and agrees well with the gas phase value also of 1623 cm^{-1}. This band shifts up to 1642 cm^{-1} for CH_3NH_2 in a nitrogen matrix. No Raman band could be obtained in this region for CH_3NH_2 in argon or nitrogen matrices even at the lowest M/A ratio, largest amounts of matrix deposited and highest spectral bandwidths practicable. Although "C.A.T." facilities were available for the Raman work, it was not envisaged that additional data over the results already obtained in the infrared would be gained by using this method.

In CH_3ND_2 the ND_2 bending mode moves down to 1203 cm^{-1} in argon and 1207.1 cm^{-1} in nitrogen. On the basis of the above frequency assignment, the corresponding band for CH_3NHD would be expected to be around 1440 cm^{-1} but no band was detected in either the infrared or Raman in either matrix. Since this is the region of the CH_3 deformation modes, the NHD bending mode may overlap with one of these bands.

4.2.5 CH_3 rocking modes

These modes were very weak in both the infrared and the Raman (Fig. 4.6). Durig et al {94} assign both the A′ and A″ CH_3 rock to a band they observed at 1140 cm^{-1} for CH_3NH_2 and 1128 cm^{-1} for CH_3ND_2 in an argon matrix. In the gas phase of CH_3NH_2 Gray and Lord {96} observe the A′ component at 1130 cm^{-1} and assign the antisymmetric A″ CH_3 wagging vibration to an assumed value of 1195 cm^{-1}, although they did not observe a band in this region. Hirakawa {95} calculates this vibration and

gives it a value of 1120 cm^{-1}.

In this work in the infrared two bands appear to be due to monomeric absorptions they are 1139.7 cm^{-1} and 1117.4 cm^{-1} for CH_3NH_2 in argon, but owing to the weakness of these bands the M/A ratio dependence is not clear. However, they are still present at high dilution at which multimer species have disappeared from the spectra. Confirmation of these bands in the Raman was not possible for the argon matrix, but good agreement was obtained between the infrared and Raman spectra of CH_3NH_2 isolated in a nitrogen matrix (nitrogen gives clearer matrices than argon). Bands at 1144 cm^{-1} and 1125 cm^{-1} in the infrared corresponding to 1143 cm^{-1} and 1121 cm^{-1} in the Raman were assigned to the A' CH_3 rock and A'' CH_3 rock respectively.

For CH_3ND_2 in argon the CH_3 A' and A'' modes were found at 1125.5 cm^{-1} and 1189 cm^{-1} no corresponding bands were able to be found in the Raman and only the CH_3 A' mode was found in the nitrogen matrix at 1128 cm^{-1}.

4.2.6 CN stretching region

The CN stretching mode has a strong absorption in the infrared for all the isotopic species studied in argon and nitrogen matrices (Figs. 4.6 and 4.7). The structure of the CN stretching absorption is complex for each isotopic species there are several bands in this region exhibiting different concentration dependence. Additional monomer bands appear to be present at higher M/A ratios and disappear on annealing the matrix at a temperature which makes diffusion unlikely. These absorptions have therefore been assigned to monomer occupying alternative trapping sites. The disappearance of the bands on annealing parallels similar

intensity changes in the NH_2 wagging region - both regions appear to be sensitive to the environment. A fuller discussion of these effects will be given later in this chapter. The CN stretch of CH_3NH_2 and CH_3ND_2 in argon was found to be 1052.3 cm^{-1} and 1006.1 cm^{-1} respectively. The identification of the CN stretch at 1042.0 cm^{-1} for CH_3NHD in argon was made possible by using 50:50 mixtures of CH_3ND_2 and CH_3NH_2 and allowing isotopic exchange to take place (Fig. 4.7). The values for the CN stretch for the molecules isolated in a nitrogen matrix are given in Tables 4.3 and 4.5.

4.2.7 NH_2 wagging mode

The NH_2 wag is the strongest absorption in the spectrum of the methylamines in the infrared in both argon and nitrogen matrices, Figs. 4.7, 4.8 and 4.9, but was too weak to be observed in the Raman.

The structure of the NH_2 wag monomer absorption in CH_3NH_2 in argon is complex due to the presence of alternative trapping sites (see later). The strongest absorption (796.1 cm^{-1}) at high M/A ratio that changed least in intensity after annealing was taken as the monomer band in the most stable site.

The corresponding absorption for this mode for CH_3ND_2 is identified at 639.0 cm^{-1} in argon. Mixtures of CH_3NH_2 and CH_3ND_2 isolated in an argon matrix produced an additional series of bands of which an absorption at 702.0 cm^{-1} is assigned to the NHD wag.

Methylamine in a nitrogen matrix shows less complex spectral features at high M/A, and the monomer species is more easily identifiable at 816 cm^{-1}. Assignments for CH_3NH_2 and CH_3ND_2

are given in Tables 4.2, 4.3, 4.4 and 4.5.

4.2.8 NH_2 twist

The frequency for the NH_2 twist has been under dispute {94,95,96,102,103}. Lord and Gray observed a band in the gas phase spectra of methyl-d_3 amine at 1416 cm^{-1} which they assigned to the NH_2 twist for this molecule, and calculations showed that the NH_2 twist of CH_3NH_2 should be at 1455 cm^{-1}. Crawford {103} calculated the NH_2 twisting motion as being 977 cm^{-1} and 744 cm^{-1} for CH_3NH_2 and CH_3ND_2 respectively. Later Hirakawa {95} in his calculations took the NH_2 twisting frequency for CH_3NH_2 to be at 1419 cm^{-1} but found that his force constant calculations gave no information as to the frequency of this mode. Durig et al {94} report that the NH_2 twist is absent from the matrix isolated but is present in the solid spectra.

In this work in the infrared spectra of matrix isolated CH_3NH_2 and CH_3ND_2 in argon weak bands were observed at 972 cm^{-1} and 758 cm^{-1} respectively but they are too weak for the M/A dependence to be studied in detail. However, the spectra of CH_3NH_2 and CH_3ND_2 mixtures in argon and nitrogen (Fig. 4.7) show bands at 885.7 cm^{-1} and 892 cm^{-1} respectively which parallel the absorption of the NHD wagging mode even at high M/A ratio. Since it is present at M/A ratios where multimer species have disappeared from the spectra this band must be assigned to monomer and hence to the NHD twisting vibration in agreement with Wolff's {97} gas phase Raman observation. The apparent intensification of this vibration relative to NH_2 and ND_2 is due to its close proximity to the very strong NHD wagging. In the case of the NH_2 and ND_2 species the twisting and wagging

vibrations are still close together, but interaction cannot take place because one vibration is A'' and the other A'. In the case of CH_3NHD, which has no symmetry, the interaction is allowed.

4.2.9 Torsion

Gray and Lord {96} assigned the torsion in the gas phase for methylamine at 263.4 cm^{-1}. Durig et al {94} claimed to have observed this fundamental at 370 cm^{-1} for methylamine isolated in an argon matrix. However, although a band is observed at this frequency in this work it only appears at low M/A ratio and is not present at high M/A ratio. Therefore it is reasonably assigned to the torsion mode of a multimer, most probably dimer. The torsion would not be expected to shift a great deal from the gas phase value and certainly not 100 cm^{-1}. No band was found for the torsion in either nitrogen or argon in the infrared for the experimental frequency range (down to 250 cm^{-1}) and no band was observable in the Raman spectra.

A comparison of the gas and matrix CH_3NH_2 and CH_3ND_2 fundamentals in the infrared and Raman is given in Table 4.6.

4.3 Product rule ratios

The monomer frequencies for the isotopic species of methylamine in an argon matrix are summarised and compared with the corresponding gas phase frequencies in Table 4.7.

In order to check that these assignments were reasonable the Teller-Redlich product rule was applied. The general formula for any molecule is:

$$\prod \frac{w^i}{w} = \left[\left(\frac{m_1}{m_1^i}\right)^{\alpha}\left(\frac{m_2}{m_2^i}\right)^{\beta}\ldots\ldots\left(\frac{M^i}{M}\right)^{t}\left(\frac{I_x^i}{I_x}\right)^{x}\left(\frac{I_y^i}{I_y}\right)^{y}\left(\frac{I_z^i}{I_z}\right)^{z}\right]^{\frac{1}{2}} \qquad (4.1)$$

where m_1, m_2, etc. are the masses of individual atoms in sets of equivalent nuclei.

M is the total mass of the molecule.

α, β etc. are the number of vibrations contributed by each set of atoms to the symmetry type considered.

t is the number of translations of the symmetry type considered.

I is a moment of inertia and x, y and z = 1 or 0 depending on whether or not rotation about that axis is of the symmetry type considered.

The superscript i designates an isotopically substituted molecule.

The observed and calculated Teller-Redlich product rule ratios are given below. The moments of inertia for the various isotopic species of methylamine were calculated using computer program GCCC (chapter 5).

Molecule	Species	Calculated	Observed
CH_3ND_2/NH_2	A'	0.406	0.436
CH_3ND_2/NH_2	A''	0.444	0.495
CH_3NHD/NH_2	--	0.427	0.491
CH_3ND_2/NHD	--	0.423	0.440

From the argon matrix spectra of both the infrared and Raman, the fundamental frequencies of CH_3NH_2 and CH_3ND_2 are known with reasonable confidence and agreement between the observed and calculated product rule ratios is good.

The differences between the observed and calculated values are small and are in the direction expected as a consequence of

anharmonicity (since $v_i \approx w_i$ the observed values are higher).

In the case of the CH_3NHD molecule, the NHD scissors is unobserved, the value used is calculated from the other isotopic species scissoring frequencies using the sum rule. The torsion for the CH_3NHD molecule is also estimated using the same method. The agreement between the observed and calculated product rule ratios is reasonable in view of these approximations.

Table 4.6

Comparison of the gas and matrix methylamine fundamentals

Sym.	Mode	CH_3NH_2				
		Gas	Argon matrix		Nitrogen matrix	
		I.R.	I.R.	Raman	I.R.	Raman
A'	NH_2 sym. stretch.	3360.0	∿3346	3352.3	∿3350	3349.2
	CH_3 asym. stretch.	2962.0	2967.1	2967.4	2963.1	2963.2
	CH_3 sym. stretch.	2820.0	2819.3	2819.0	2816.0	2815.8
	NH_2 scissors	1623.0	1623	-	1642	-
	CH_3 asym. def.	1473.6	1463.8	1465.3	1462.5	1463.2
	CH_3 sym. def.	1430.6	1449.5	1451.5	1449.6	1451.0
	CH_3 rock.	1129.8	1139.7	-	1144.0	1143
	CN stretch.	1044.1	1052.3	1053.1	1049.5	1049.5
	NH_2 wag.	780.1	796.1	-	816.0	-
A''	NH_2 asym. stretch.	3423.6	∿3410	3414.8	∿3410	3411.0
	CH_3 asym. stretch.	2895.0	2990.8	2991.0	2985.3	2985.0
	CH_3 asym. def.	1485.1	1480.8	1482.2	1480.5	1481.2
	NH_2 twist.	(1419)	∿ 972	-	-	-
	CH_3 rock.	(1195)	1117.4	-	1125.0	1121
	CH_3 torsion	263.9	-	-	-	-

Table 4.6 (contd.)

Sym.	Mode	CH_3ND_2				
		Gas	Argon matrix		Nitrogen matrix	
		I.R.	I.R.	Raman	I.R.	Raman
A'	ND_2 sym. stretch.	2479	-	2461.0	~2456	2458.1
	CH_3 asym. stretch.	2961	2966.0	2966.0	2962.4	2962.8
	CH_3 sym. stretch.	2817	2818.7	2819	2814.5	2814.7
	ND_2 scissors	1234	1203.0	~1200	1207.1	~1208
	CH_3 asym. def.	1468	1462.2	1462	1462.6	1462.8
	CH_3 sym. def.	1430	1456.0	1456	1456	1457.5
	CH_3 rock.	1117	1125.5	-	1128	-
	CN stretch.	997	1006.1	1006.0	1004.1	1005.0
	ND_2 wag.	625.4	639.0	-	653.6	654
A''	ND_2 asym. stretch.	2556	2548	2548.0	2545.8	2545.8
	CH_3 asym. stretch.	2985	2991.1	2991	2987.2	2987
	CH_3 asym. def.	(1485	1479.3	1479	1479.6	1480.5
	ND_2 twist.	(820)	~758	-	-	-
	CH_3 rock.	1187	1189	-	-	-
	CH_3 torsion	224.5	-	-	-	-

Table 4.7

Comparison of the gas and matrix CH_3NH_2, CH_3NHD and CH_3ND_2 fundamentals

ν	Mode	CH_3NH_2		CH_3NHD		CH_3ND_2	
		Gas[a]	Ar matrix	Gas[b]	Ar matrix	Gas[a]	Ar matrix
ν_1	$NH_2(NHD)ND_2$ sym. stretching	3360.0	3352.3	2506	2478	2479	2461.0
ν_2	CH_3 asym. stretching	2962.0	2967.1	(2962)	2966.5	2961	2966.0
ν_3	CH_3 sym. stretching	2820.0	2819.3	(2818)	2819.0	2817	2818.7
ν_4	$NH_2(NHD)ND_2$ scissors	1623.0	1623	1469	-	1234	1203.0
ν_5	CH_3 asym. deformation	1473.6	1463.8	(1471)	1464.3	1468	1462.2
ν_6	CH_3 sym. deformation	1430.6	1449.5	(1430)	1456	1430	1456.0
ν_7	CH_3 rocking	1129.8	1139.7	1143	1130.4	1117	1125.5
ν_8	CN stretching	1044.1	1052.3	1032	1042.0	997	1006.1
ν_9	$NH_2(NHD)ND_2$ wagging	780.1	796.1	688	702.0	625.4	639.0
ν_{10}	$NH_2(NHD)ND_2$ asym. stretching	3423.6	3414.8	3388	3376	2556	2548.0
ν_{11}	CH_3 asym. stretching	2985.0	2990.8	(2985)	2991.3	2985	2991.1
ν_{12}	CH_3 asym. deformation	1485.1	1480.8	(1485)	1484.1	(1485)	1479.3
ν_{13}	$NH_2(NHD)ND_2$ twisting	(~980)[b]	~972	878	885.7	(~820)	~758
ν_{14}	CH_3 rocking	(1195)	1117.4	(1174)	-	1187	1189
ν_{15}	CH_3 torsion	263.9	-	(244)	-	2245	-

a. Ref. 96

b. Ref. 97

4.4 Multimer band assignments

The number of possible multimer species of methylamine that could be formed due to aggregation of molecules in a matrix environment is very large. For a multimer consisting of a given number of molecular units the number of possible structures of these units may be limited by the nature of the environment itself and only the more stable multimer species will be present in significant numbers. These multimer species may be divided into two classes; open chain and cyclic.

The effects of hydrogen bonding on the N-H stretching frequency is well known. Several attempts have been made to calculate the value for the enthalpy of hydrogen bond formation but the results of the various methods used {104,105,106} are inconsistent. However, there is a certain amount of evidence that methylamine is associated even in the gas phase {105}.

The presence of bands due to multimer species, which are highly dependent on the M/A ratio, are apparent in both the infrared and Raman spectra of methylamine in argon and nitrogen.

4.4.1 NH stretching region

Due to the weakness of the NH stretch in the infrared a detailed study of the concentration dependence of this region was not possible. Tentative assignments are made in Tables 4.2, 4.3, 4.4 and 4.5. A band at $\sim$ 3305 cm^{-1} in the Raman spectra of CH_3NH_2 in a nitrogen matrix disappears rapidly with increasing M/A ratio and is reasonably assigned to a dimer absorption.

For the NH stretching region bands are still present at high M/A to much lower frequency than the monomer bands. This excludes the possibility of these being due to different sites

since the expected shift would not be so great. Since there is still dimer band present in the NH_2 wagging region even at high M/A it is concluded that these bands are due to the NH stretch of this dimer.

On deuteration a similar pattern of absorptions is observed in the infrared for both argon and nitrogen but again the bands are too broad for their concentration dependence to be studied in detail.

4.4.2 NH_2 wagging region

Fig. 4.8 shows the spectral changes that occur with increasing M/A ratio for methylamine isolated in an argon matrix and also demonstrates the effects of monomer diffusion. The highest frequency multimer bands (A) disappear very quickly with increasing M/A ratio but do not appear after the diffusion operation has been carried out. These bands could well be assigned to cyclic multimer species which although trapped on deposition would be unlikely to be formed due to diffusion of monomer species.

For the bands of region (B), only one band at 818.6 cm^{-1} remains at high M/A ratio. Since, generally, the pulse deposition technique was adopted (since it gave clearer matrices) it could be argued that this band is due to monomer diffusion caused by the possible heating effect of the pulse technique. If this is true the most likely diffusion operation during deposition would be expected to be local surface diffusion. Due to the size of the methylamine molecule it is unlikely that true diffusion will occur on carrying out an annealing operation. Surface aggregation, due to evaporation of the argon matrix, is

the most likely mechanism to produce multimer species. Since this band at 818.6 cm^{-1} is present in the S.S.O. experiments at high M/A ratio and this band does not increase appreciably after diffusion this may well be due to an associated gas phase multimer species isolated in the matrix and is most probably an open chain dimer.

Fig. 4.9 demonstrates the effect of increasing the M/A ratio on the NH_2 wagging region of methylamine isolated in a nitrogen matrix. Multimer bands to high frequency of the main monomer band disappear quickly with increasing M/A ratio which may reflect on the greater isolation capabilities of nitrogen. The band at 840.8 cm^{-1} is assigned to open chain dimer. However, the intensity of the 816 cm^{-1} band proved troublesome in studying the M/A ratio dependence of the multimer species in the spectra of methylamine. It appeared to increase its relative intensity with increasing M/A ratio compared to <u>every</u> band including other <u>monomer</u> bands. It appears that some kind of long range interaction of this mode with the nitrogen matrix was occurring. A detailed discussion of this effect is delayed until chapter 8 owing to the importance of this effect in the discussion of the quantitative results.

Fig. 4.9 shows the effect of diffusion on the spectra of matrix isolated methylamine in a nitrogen matrix. Crystalline nitrogen has two stable forms α and β with a transition temperature at 35.6 K {107}. The low temperature α form, which is the one that will be formed in this series of experiments, crystallises as f.c.c. It is not expected that methylamine monomer will diffuse through the matrix below 36 K but since appreciable evaporation of the matrix is occurring the increase

in the multimer species will again be due to surface aggregation. At temperatures above the transition temperature rearrangement of the lattice structure causes excessive dislocations allowing rapid monomer diffusion to take place.

Fig. 4.10 shows that for the same M/A ratio and amount deposited, deposition at 20 K apparently produces more multimer absorption than deposition at 4 K. This would be expected due to increased isolation efficiency at the lower temperature.

However, an interesting effect is the apparent increase in intensity of the dimer band on raising the temperature of the matrix to ≈ 20 K and then decreasing again to 4 K. As can be seen from Fig. 4.10 this effect is not completely reversible but it does take place at temperatures well below T_d. The reason for this effect is not quite clear.

4.4.3 Other modes

The CN stretching mode for methylamine exhibits a series of bands shifted to higher frequency than the monomer. The bands do not change their intensity when annealing of the matrix is carried out but do disappear from the spectra on increasing the M/A ratio. Controlled experimentation at temperatures where "diffusion" could take place does not appreciably change the appearance of the bands in either argon or nitrogen matrices although bands to higher frequency appear. (Due to high multimer species formed as a result of surface aggregation.) Thus the series of bands initially observed and present in very dilute matrices are therefore reasonably due to low multimers most probably open chain dimer.

The CH_3 stretching modes, and NH_2 bending all exhibit

Fig. 4.10 Temperature Dependence of the Bands in the NH_2 Wagging Region of Methylamine in a Nitrogen Matrix

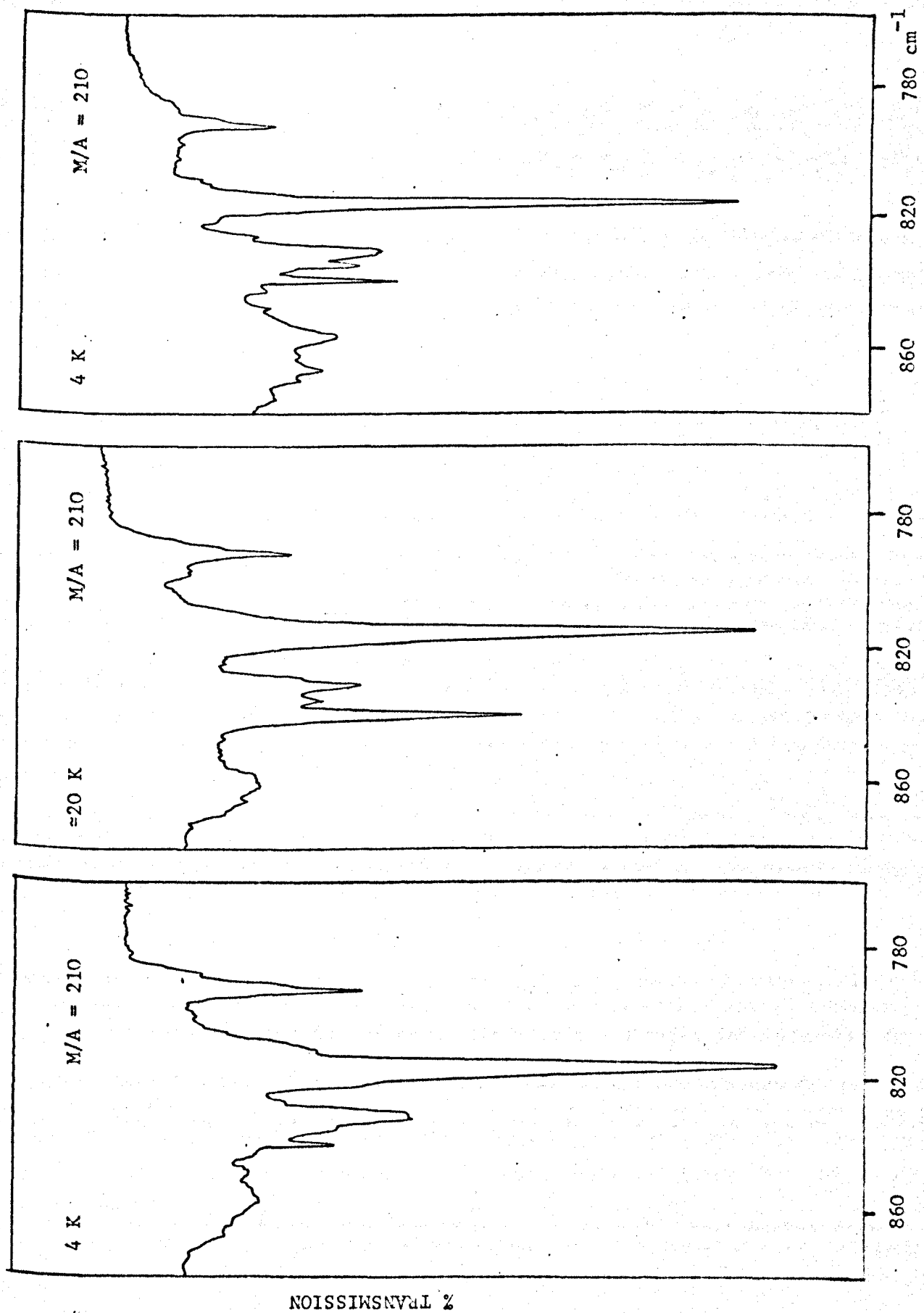

shoulders (Tables 4.2 and 4.3) which may be assigned to multimer species. Due to their close overlap with the monomer bands a detailed study of the M/A ratio dependence was not attempted. The same pattern was observed for all the isotopic species studied. The remaining CH_3 deformation modes are little affected by association effects.

4.5 Site effects

4.5.1 Methylamine in an argon matrix

This discussion of site effects will be concentrated on the NH_2 wagging region since this region appeared to be the most sensitive to the matrix environment from this respect.

At a M/A ratio of 2,000 there are five bands in the NH_2 region which appear to be due to monomer absorptions. The effect of temperature cycling was carried out to investigate the possibility of rotation of the methylamine molecule in the argon matrix. Fig. 4.11 shows the effect of temperature change of the absorptions in the NH_2 wagging region. From the results the effect of temperature change on the spectra were not reversible and excluded the possibility that methylamine is rotating and indicated the possibility of multiple trapping sites.

If the isolated molecules were indeed distributed in several alternative trapping sites or could exist in different orientations within a site without exchange between them then the environment of the matrix isolated molecules and thus the force field surrounding the molecule would be different in each case. The presence of two or more force fields will effectively modify the force constant for a particular normal vibration which would be reflected in its vibrational spectrum. It would be

Fig. 4.11 Temperature Dependence of the Bands in the NH_2 Wagging Region of Methylamine in an Argon Matrix.

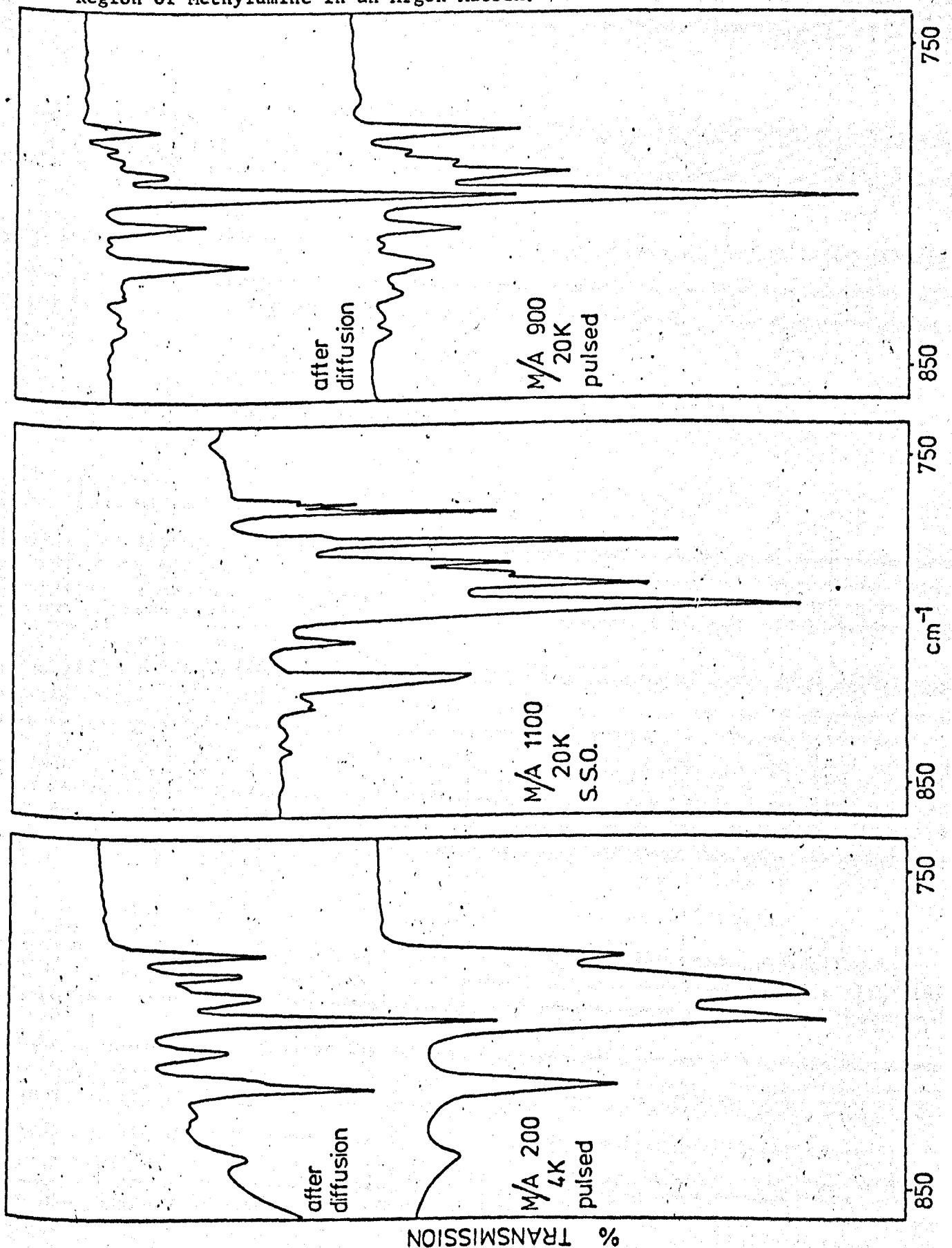

expected that these effects should be observed in all the fundamental regions. The environmental effects appear to perturb more strongly than other fundamentals although multiple monomer bands do appear in other spectral regions particularly the CN stretch.

The solid matrix formed in a typical matrix isolation experiment would be expected to be imperfect because of the nature of the deposition process (rapid condensation). It is known {108} that argon deposited at 4 K has a high density of dislocations which would tend to provide additional trapping sites. It would therefore be expected that there should be an increase in the number of trapping sites at 4 K than at 20 K and this is in fact the case. Fig. 4.11 shows the effect of deposition at 4 K and subsequent annealing and cooling to 4 K again, and also demonstrates the effect of deposition technique on the spectrum, bands at 766.8 and 764.2 cm^{-1} for the S.S.O. technique are entirely missing for the pulsed deposition experiment possibly due to the annealing effect of the latter technique.

Leach {74} discusses multiplet structure of crystalline organic solutions. Leach's argument may also be applied to matrix isolated molecules. It implies that the presence of impurities i.e. solute molecules, may induce particular and varied forms of short range or long range order in the surrounding matrix; the greater the amount of matrix host material present the greater the possibility of stabilising a particular packing structure of the matrix around the solute molecule. This effect can be seen in Fig. 4.12 by increasing the M/A ratio the relative absorption of the band at 776.2 cm^{-1} increases but this band disappears quickly when an annealing experiment is carried out

Fig. 4.12 Infrared Spectra of CH_3NH_2 in an Argon Matrix showing the M/A Ratio dependence of the Site Bands in the NH_2 Wagging Region.

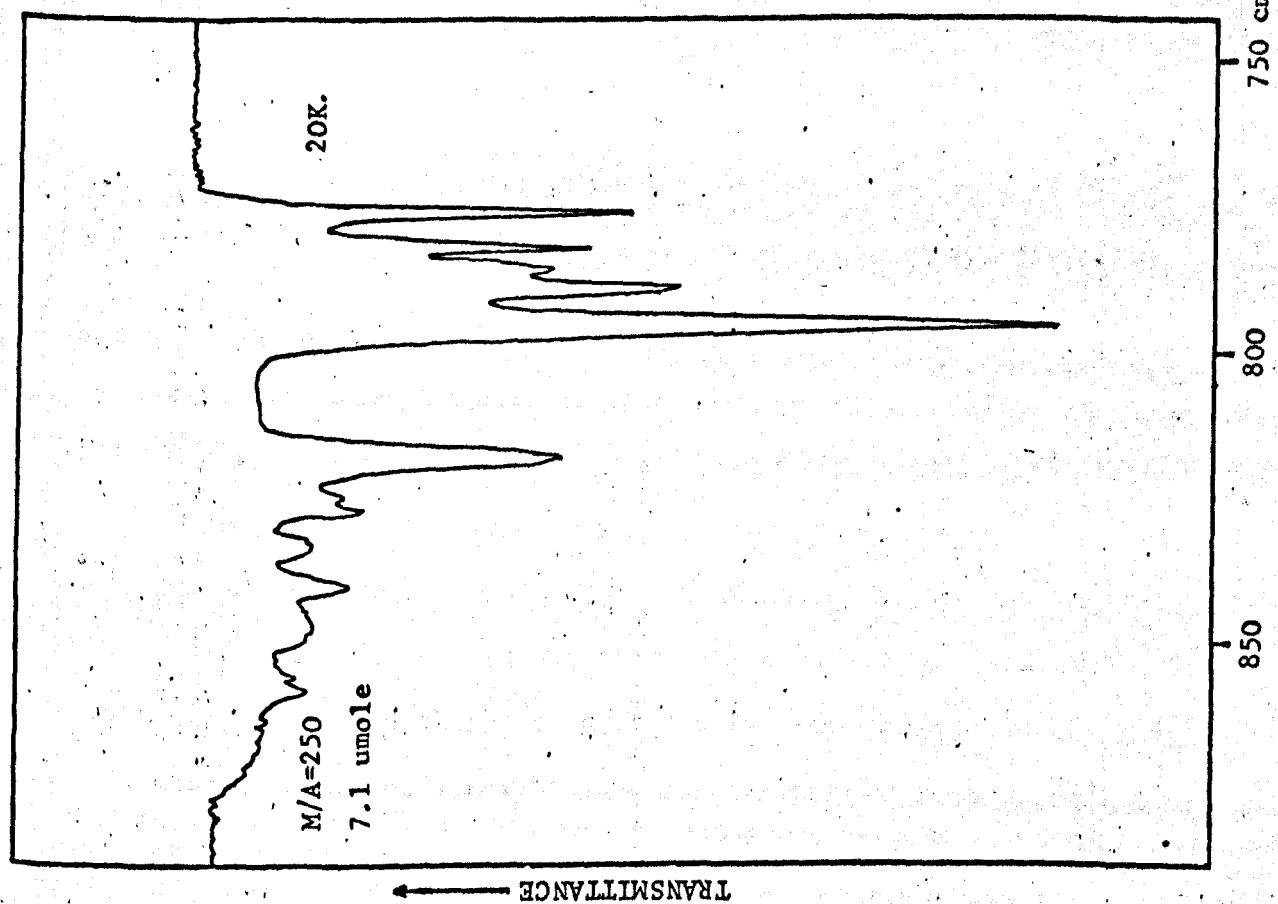

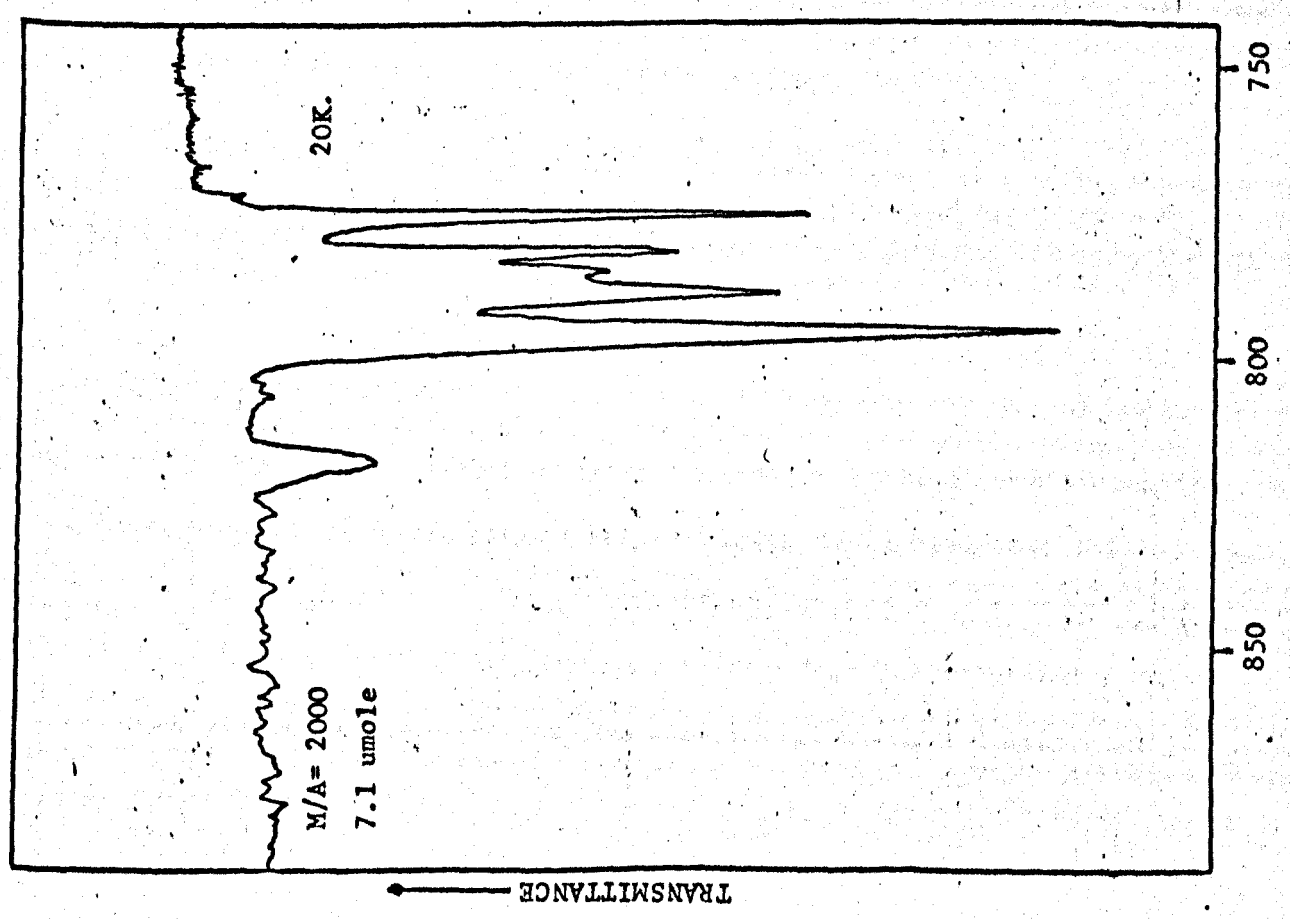

and would therefore be regarded as the least stable trapping site. The annealing of the matrix would modify the number of these multiple trapping sites and so give rise to variations in the number of multiplet structures reflected in the relative intensity of the fundamentals of the molecules isolated in them. The persistence of multiple sites after thorough annealing implies that the potential barrier to conversion of the different structures into the most stable one is very high or that the various sites have closely similar stabilities. From the spectral evidence for methylamine in argon on annealing it appears that the main monomer band does not increase its absorption and so it must be implied that none of the sites interconvert to the main monomer site but simply lose their identity as a site through aggregation.

4.6 Impurity effects on the matrix isolated spectrum of methylamine

It is well documented {109-113} that the presence of trace amounts of nitrogen impurities will be sufficient to suppress rotational features in the matrix isolated spectra of the hydrogen halides and induce bands not present in the absence of this impurity. However, water and oxygen do not appear to affect the hydrogen halide bands.

It is therefore necessary to know what effect small quantities of atmospheric or sample impurities could have upon the matrix isolated spectra of a solute molecule.

The most likely impurities to occur in the sample of methylamine are ammonia, water {113,114}, oxygen and nitrogen. No spectrum of matrix isolated methylamine was found to contain ammonia impurity. However, owing to the difficulty of efficient

drying of the methylamine several of the observed spectra did have small traces of the matrix isolated water bands. Comparison of these spectra with ones determined under similar experimental conditions but free from water impurities showed no detectable differences in the spectra except for the absence of the impurity bands.

Oxygen and nitrogen are very easily identified in an argon matrix in the Raman, having characteristic frequencies at 1552.0 cm^{-1} and 2327.2 cm^{-1} respectively. However, no matrix isolated spectra of methylamine run on the Raman equipment contained any sign of bands in these regions and it was concluded that oxygen and nitrogen impurities were absent and also that no atmospheric contamination was occurring.

The presence of oxygen and nitrogen cannot be detected in the infrared since they have no infrared active absorptions.

Only one band at 806 cm^{-1} in the NH_2 wagging region observed in the infrared spectra of CH_3NH_2 in argon was irreproducible, occasionally appearing at high M/A ratio or after a diffusion operation. This behaviour is inconsistent with either monomer or multimer species.

The effect of a 0.5% nitrogen doped argon matrix (M/A ratio = 200/1/1 $Ar/CH_3NH_2/N_2$) on the NH_2 wagging region is shown in Fig. 4.13 compared to an undoped matrix shows the appearance of a new band at 806 cm^{-1}. The general effect of nitrogen doping on the spectra gives the appearance of an undoped CH_3NH_2 matrix isolated spectra in argon except for the appearance of the impurity band at 806 cm^{-1}. The nitrogen impurity does not appear to affect the monomer bands by giving rise to additional trapping sites. Thus it is demonstrated that small quantities of

Fig. 4.13 Infrared Spectra of the NH Wagging Region of CH_3NH_2 in an Argon Matrix at 20K showing Nitrogen impurity effects.

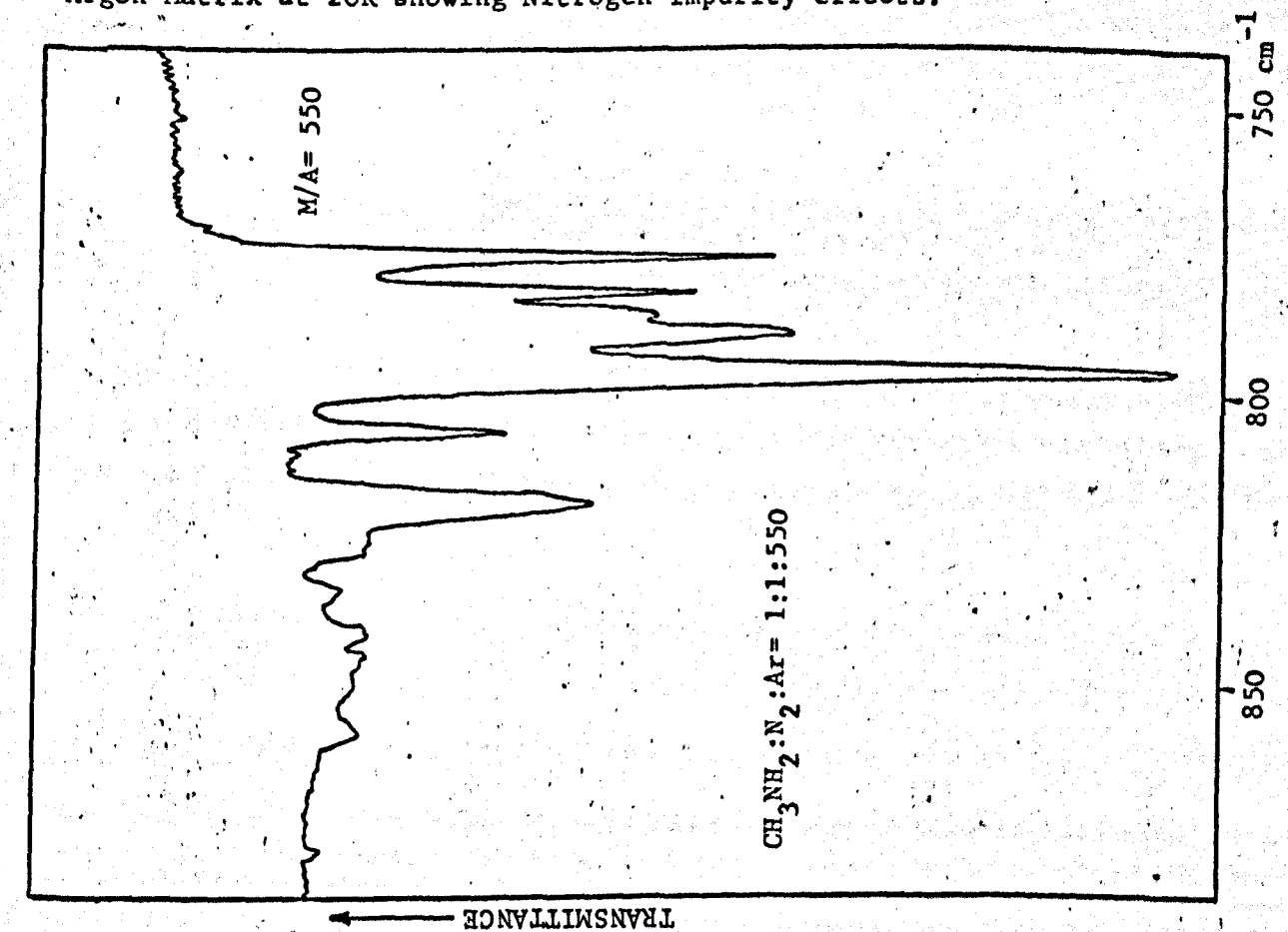

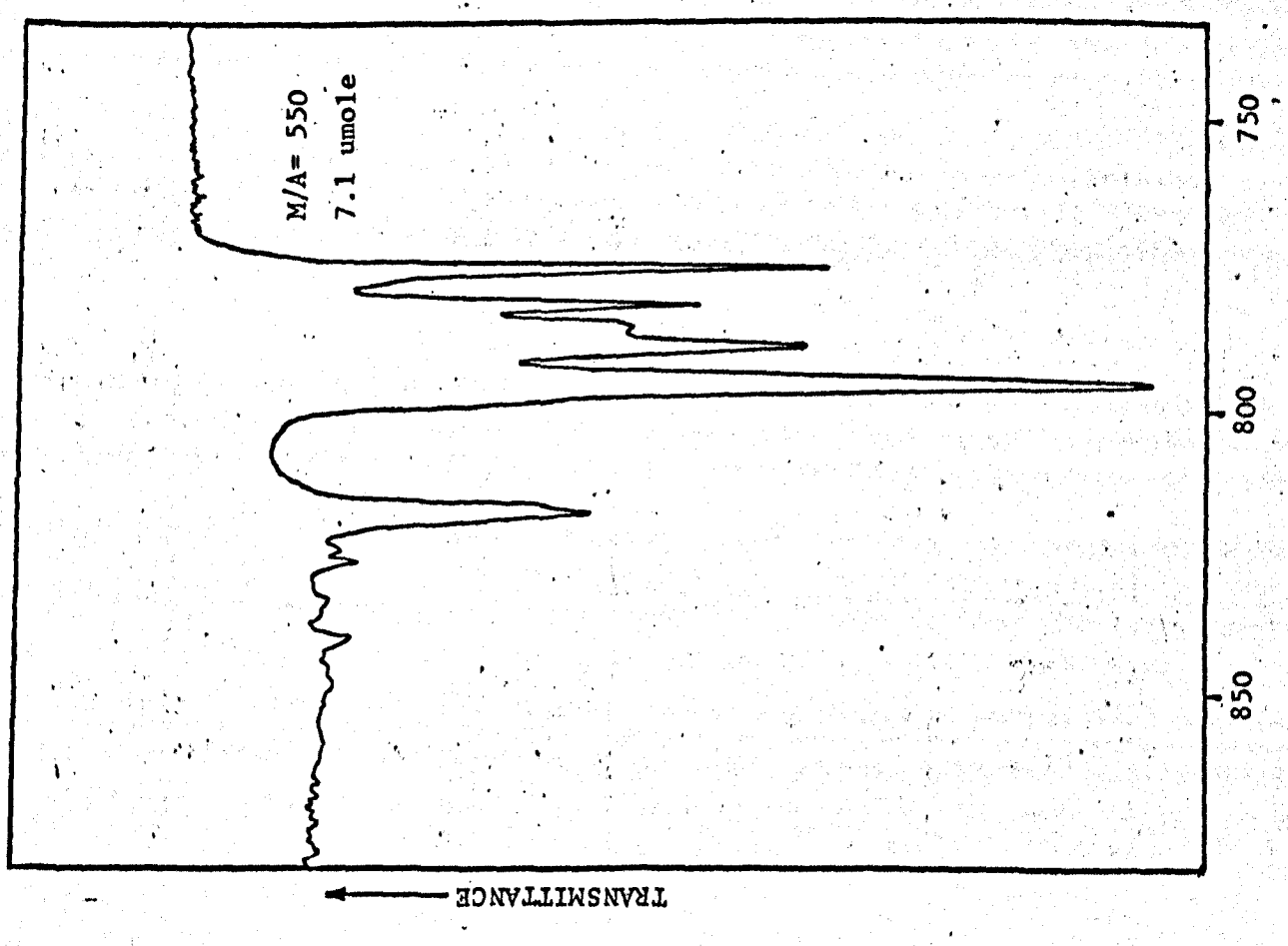

nitrogen do modify the spectrum of CH_3NH_2 in argon matrices but do not affect the monomer bands. A possible appearance of the 806 cm^{-1} band after diffusion is that redeposition of matrix gas on recooling may trap nitrogen gas not present initially on deposition.

There are two possible sources of oxygen impurity (1) from the sample and (2) from air leaks into the system. The latter can be eliminated since this would cause a nitrogen impurity at the same time which could be identified by the band at 806 cm^{-1}. The former can be eliminated because before preparation of the gaseous matrix sample mixture, the sample gas was solidified and pumped on at liquid nitrogen temperatures to $< 10^{-5}$ torr.

The vapour pressure of oxygen is greater than 10^{-5} torr at liquid nitrogen temperatures. On this basis the matrix sample will be free of oxygen impurities.

CHAPTER 5

NORMAL COORDINATE ANALYSIS OF METHYLAMINE

5.1 Introduction

The normal coordinate treatment of methylamine has been carried out by several workers {95,103,115}. However, the assignment of the NH_2 twisting mode has remained unresolved, as this is not definitely located in the gas phase spectra {96} for methylamine and its deuterated analogues. Dellepiane and Zerbi {115} carried out a normal coordinate treatment using the Urey-Bradley force field (U.B.F.F.). They calculated the NH_2 twisting frequency of CH_3NH_2, CD_3NH_2, CH_3ND_2 and CD_3ND_2 at 995, 1100, 766 and 713 cm^{-1} respectively; these values were in reasonable agreement with Crawford {103} in a previous calculation. However Hirakawa et al. {95} removed the Urey-Bradley assumption and in its place used the local symmetry field. In their calculations they were able to show that there were several sets of force constants which reproduced the other observed frequencies but gave a greatly different twisting frequency. Hirakawa et al. were also able to include the gas phase values for the frequencies of the $CH_3{}^{15}NH_2$ molecule in their data but found that although the ^{15}N isotope shifts were useful for estimating force constants which took part in the vibration of the N atom they were still unable to obtain any definite information as to the position of the twisting mode to which he gave zero weight in his calculations. They suggested the twisting frequency could be in the 1200- 1450 cm^{-1} region by a comparison with similar compounds leaving the assignment undetermined.

Wolff and Ludwig {97} presented data concerning the frequencies of the CH_3NHD molecule and in particular they assigned a band they observed at 878 cm^{-1} in the gas phase to the NHD twisting mode. They estimated (using the sum rule) the values for the twisting frequencies of CH_3NH_2 and CH_3ND_2 to be 983 cm^{-1} and 819 cm^{-1} respectively, which were in agreement with the values they previously obtained in the crystalline state {100} of 991 cm^{-1} and 824 cm^{-1} respectively.

In chapter 4 the infrared and Raman spectra of CH_3NHD was measured in argon and nitrogen matrices and an assignment made for the molecule. Bands were definitely observed at 885.7 cm^{-1} and 892.0 cm^{-1} respectively for each matrix which we assign to the NHD twisting mode. These values along with the matrix values obtained for the CH_3NH_2 and CH_3ND_2 molecule Table 4.7 were used in a normal coordinate treatment. Three assumptions were made:

1) all vibrations are assumed to be harmonic

2) the matrix environment does not appreciably perturb the molecular force constants and hence the frequencies

3) intermolecular interactions are negligible for monomer band frequencies measured at high M/A ratio.

This chapter describes a normal coordinate analysis carried out for the observed frequencies of CH_3NH_2 and CH_3ND_2 in argon matrices and then extended to the CH_3NHD molecule. It was hoped to obtain a more definite assignment in this way for the twisting mode for CH_3NH_2 and CH_3ND_2. Argon matrix (rather than nitrogen) frequencies were used since perturbations are smaller in this symmetrical matrix and thus the values obtained should approximate to the gas phase vibration.

Force constant calculations were made using the Wilson

Fig. 5.1 Coordinate System for Methylamine.

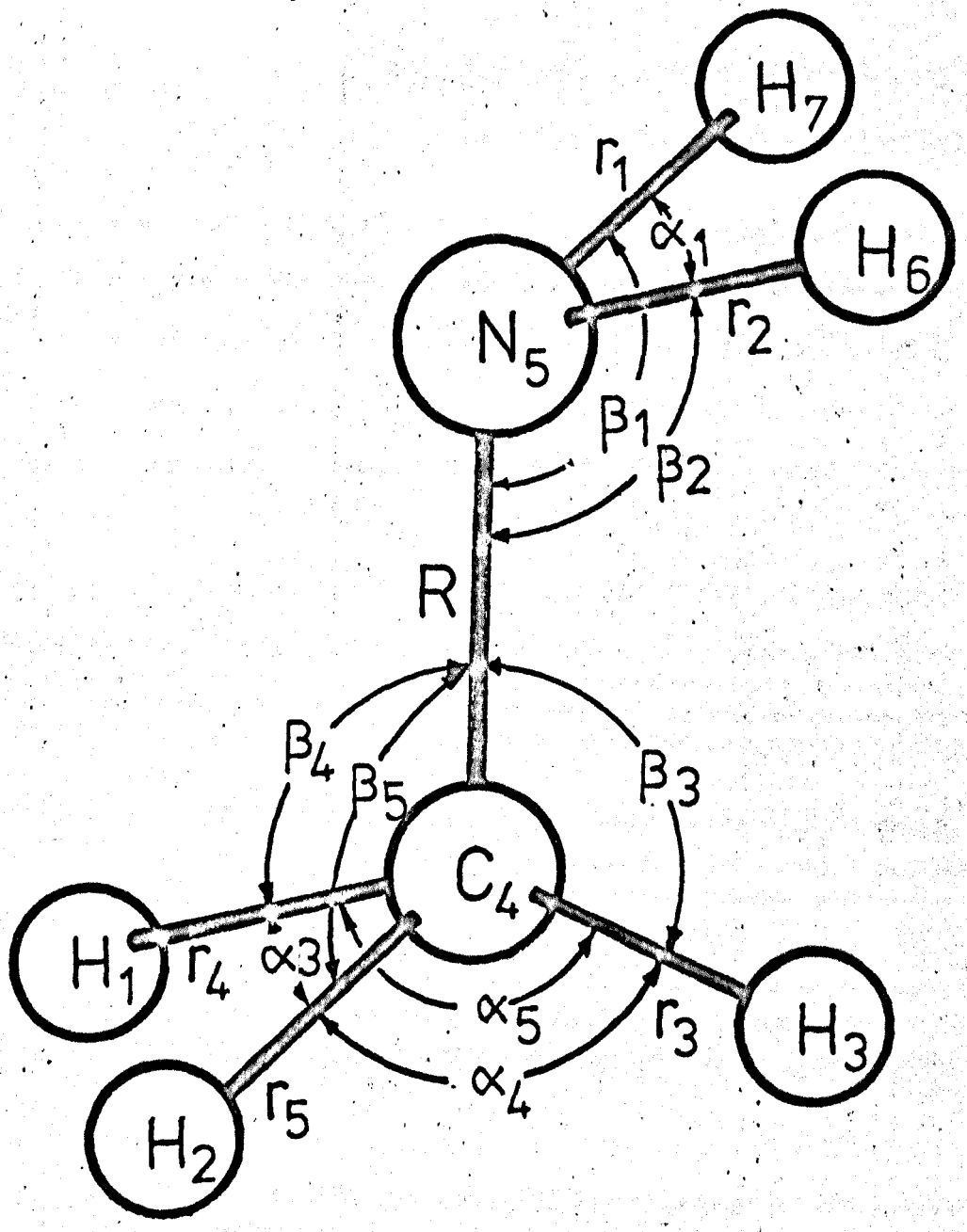

Bond Angles	Bond Lengths(Å)	Atomic Masses
$H\hat{C}H = 109^{\circ}28'$.	CH = 1·093.	H = 1·00797.
$H\hat{C}N = 109^{\circ}28'$.	CN = 1·474	C = 12·01115.
$H\hat{N}C = 112^{\circ}$.	NH = 1·014.	N = 14·0067 .
$H\hat{N}H = 105^{\circ}48'$.		

G F matrix method {116} and employed the U.B.F.F. The theoretical treatment is described below.

5.2 Theory

5.2.1 Introduction

The frequencies of a molecule which we observe in infrared or Raman spectra are determined by the kinetic and potential energies of the molecule. The potential energy is a function of the forces between the atoms constituting the molecule, while the kinetic energy is determined by the mass and coordinates of the atoms. Therefore it is possible to obtain information about the molecular field by analysing the vibrational spectra when we know the geometry of the molecule.

In diatomic molecules, the vibration of the atoms occurs along the line connecting them. For polyatomic molecules the motions of the atoms are much more complex but they can be shown to be represented as a superposition of a number of normal vibrations.

For an N atom system the position of the atoms at any instant in time may be described by their "Cartesian" displacement coordinates relative to a fixed point in space. The coordinates of an atom A are given as the components x_A, y_A and z_A, the distance of A from the origin O is given by

$$(OA)^2 = x_A^2 + y_A^2 + z_A^2 \qquad (5.1)$$

If there are N atoms, 3N coordinates are needed to describe their motion completely although only 3N - 6 (non linear molecule) coordinates will be required for describing the relative motion

of the atoms with fixed orientation of the system as a whole.

Internal coordinates may also be used in describing the relative atomic positions of the atoms e.g. changes in bond length and bond angles.

5.2.2 Potential and kinetic energy equations

The restoring forces are usually assumed proportional to the distortion of the valence bonds and angles, the proportionality constants relating the two quantities are called "force constants". The vibrational frequencies may be related to the atomic masses, molecular geometry and restoring forces using the general expression for the kinetic and potential energies of the molecule. The potential energy of a molecule referred to the equilibrium position is a function of all the coordinates involved, and provided the displacements of the atoms are small, this function may be expanded in a Taylor series as

$$V(q_1 q_2 \ldots q_{3N}) = Vo + \sum_{i}^{3N} \left(\frac{\delta V}{\delta q_i}\right)_o q_i + \frac{1}{2} \sum_{i,j}^{3N} \left(\frac{\delta^2 V}{\delta q_i \delta q_j}\right)_o q_i q_j + \ldots \quad (5.2)$$

where q_i denotes any kind of displacement coordinate. The term Vo is independent of q and can be ignored. The $\left(\frac{\delta V}{\delta q_i}\right)_o$ terms also become zero, since V must be a minimum at the equilibrium position. Terms in q^3, q^4 etc. give rise to anharmonic force constants and are neglected since these terms are small compared to q^2. The neglect of these terms is known as harmonic approximation and thus V may be represented by

$$V = \tfrac{1}{2} \sum_{i,j}^{3N} \left(\frac{\delta^2 V}{\delta q_i \delta q_j} \right)_0 q_i q_j \qquad (5.3)$$

The force constants can be defined by

$$f_{ij} = \frac{\delta^2 V}{\delta q_i \delta q_j} \qquad \text{where } f_{ij} = f_{ji}. \qquad (5.4)$$

If i and j are the same coordinate the force constant is the principal force constant. If $i \neq j$ the force constant is called an interaction force constant.

The potential energy of the molecule may be written

$$V = \tfrac{1}{2} \sum_{ij}^{3N} f_{ij} q_i q_j \qquad (5.5)$$

where the summation extends over all combinations of coordinates.

The kinetic energy may be written by expressing the displacement of each atom relative to its equilibrium position in terms of Cartesian coordinates and masses of atoms (m_N).

Thus from equation (5.1)

$$T = \tfrac{1}{2} \sum_N m_N \left[(\dot{x}_N)^2 + (\dot{y}_N)^2 + (\dot{z}_N)^2 \right] \qquad (5.6)$$

In matrix notation this equation becomes

$$2T = \dot{X}' M \dot{X} \qquad (5.7)$$

where $\dot{X}$ is a column matrix with N components, ($\dot{x}_1 \dot{y}_1 \dot{z}_1 \; \dot{x}_2 \dot{y}_2 \dot{z}_2 \; \ldots \; \ldots \; \dot{x}_N \dot{y}_N \dot{z}_N$) and M is a diagonal matrix whose elements are the masses of the atoms.

The kinetic energy, when expressed in terms of the general coordinates $q_1, q_2, \ldots\ldots, q_N$, and their time derivatives $\dot{q}_1, \dot{q}_2, \ldots\ldots, \dot{q}_N$, becomes a homogeneous quadratic function of $\dot{q}_1, \dot{q}_2, \ldots\ldots, \dot{q}_N$,

which can be written in the same form as equation (5.6) such that

$$T = \tfrac{1}{2}\sum_{ij}^{3N} a_{ij}\dot{q}_i\dot{q}_j \qquad (5.8)$$

Although the kinetic energy is more easily expressed in terms of Cartesian displacement coordinates it is more convenient to express both the kinetic and potential energies in terms of internal coordinates R.

The potential energy may thus be expressed

$$2V = (\delta^2 V/\delta R_i R_j)R_i R_j \qquad (5.9)$$

in which case the force constants may be defined by the general relationship:

$$f_{ij} = \delta^2 V/\delta R_i \delta R_j \qquad (5.10)$$

and so the potential energy expression becomes

$$2V = \sum_{ij} f_{ij} R_i R_j \qquad (5.11)$$

Here the summation is over all coordinates.

The kinetic energy may also be expressed in a similar form to equation (5.11) where

$$2T = \sum_{ij} k_{ij}\dot{R}_i\dot{R}_y \qquad (5.12)$$

where k is a function of the atomic masses of the i and j nuclei and their equilibrium configuration. Equation (5.11) may be expressed in matrix notation such that

$$2V = R'FR \qquad (5.13)$$

where F is a symmetric square matrix of the order 3N - 6 (3N - 5 for linear molecules) whose elements are the force constants. Internal coordinate displacements are given by the column matrix R and its transpose R'.

Similarly equation (5.12) is given by

$$2T = \dot{R}'K\dot{R} \tag{5.14}$$

where K is of the same order as F and whose elements are given by k_{ij}. A matrix G is defined as the inverse of K and where G is symmetric.

It is important at this point in the discussion to know the physical meaning of G.

Equation (5.8) is expressed in the form

$$T = \tfrac{1}{2}\dot{q}'Gq^{-1}\dot{q} \tag{5.15}$$

where $Gq^{-1} = \begin{matrix} a_{11} & a_{12} & \cdots\cdots \\ a_{21} & a_{22} & \cdots\cdots \\ \vdots & \vdots & \end{matrix}$ (5.16)

by definition, momentum p_i conjugate to q_i is

$$p_i = \frac{\delta T}{\delta \dot{q}_i} = a_{1i}q_i + a_{2i}q_i + \cdots\cdots \tag{5.17}$$

in matrix form this may be represented by

$$p = Gq^{-1}\dot{q} \tag{5.18}$$

therefore

$$\dot{q} = Gq^{-1}p \tag{5.19}$$

therefore

$$T = \tfrac{1}{2}p'G\dot{q}Gq^{-1}Gq\,p \tag{5.20}$$

since $Gq^{-1}Gq = E$ (5.21)

$$T = \tfrac{1}{2}p'G'qp = \tfrac{1}{2}p'Gqp \quad (5.22)$$

Accordingly equation (5.14) is expressed as

$$2T = P'GP \quad (5.23)$$

where P is momentum conjugate to R.

Therefore the G matrix is a kinetic energy matrix in the momentums which are conjugate to the coordinates.

The introduction of symmetry to normal coordinate analysis at this stage can simplify the problem by the use of group theory. Using this theory the F and G matrices are factored into blocks thereby reducing the order of the matrices.

To make use of the simplifications afforded by the use of group theory it is necessary that the 3N - 6 coordinates describing the vibrational degrees of freedom of a non-linear N atom molecule be symmetry adapted coordinates which are linear combinations of the internal coordinates. It is also convenient to construct these symmetry coordinates from equivalent internal coordinates only. The choice of the linear combinations is not arbitrary but must be made in such a way that the new symmetry coordinates transform in accordance with the character of the vibrational species concerned {121}.

The symmetry coordinates must be normalised and orthogonal.

The symmetry coordinates are of the form

$$S_j = \sum_k U_{jk}R_k \quad (5.24)$$

or in matrix notation

$$S = UR \quad (5.25)$$

$$\text{or } R = U'S \quad (5.26)$$

In equation (5.24) S_j is the j th symmetry coordinate and U_{jk} is the coefficient of the k th internal coordinate r_k. The summation is over all the equivalent internal coordinates. The elements U_{ij} of U must satisfy the relationships

$$\sum_k (U_{jk})^2 = 1 \quad \text{(normalisation)}, \tag{5.27}$$

and $$\sum_k (U_{jk} . U_{ik}) = 0 \quad \text{(orthogonality)}. \tag{5.28}$$

where i and j refer to two different symmetry coordinates which need not be in the same symmetry class.

An expression for the symmetric G and F matrix can be obtained from matrix equations (5.13), (5.14) and (5.25) combined such that

$$2V = R'FR = S'UFU'S = S'F_S S \tag{5.29}$$

where $F_S = U'FU$ (5.30)

similarly $2T = S'G_S^{-1}S$ (5.31)

where $G_S = U'G^{-1}U$ (5.32)

When the potential and kinetic energies are expressed in terms of normal coordinates Q

$$T = \tfrac{1}{2}\sum \dot{Q}_i^2 = \tfrac{1}{2}\dot{Q}'E\dot{Q} \tag{5.33}$$

$$V = \tfrac{1}{2}\sum \lambda_i Q_i^2 = \tfrac{1}{2}Q'\Lambda Q \tag{5.34}$$

We find these coordinates by solving the secular equation given in equation

$$\left| G_S F_S - \Lambda \right| L = 0 \tag{5.35}$$

Since there are no cross terms in equation (5.33) and(5.34)

application of Lagrange's equation in the form

$$\frac{\delta}{\delta t}\left(\frac{\delta T}{\delta \dot{Q}_i}\right) + \frac{\delta V}{\delta Q_i} = 0 \tag{5.36}$$

is possible, in which case

$$\ddot{Q}_i + \lambda_i Q_i = 0 \tag{5.37}$$

the solution is given as i equations of the form

$$Q_i = Q_i^o \cos((\lambda_i)^{\frac{1}{2}} t + \phi_i) \tag{5.38}$$

where Q_i^o and λ_i are properly chosen constants, t is time. The roots of these equations are

$$(\lambda_i)^{\frac{1}{2}} = (4\pi^2 \nu_i^2)^{\frac{1}{2}} \tag{5.39}$$

and the frequency $\nu_i = (\lambda_i)^{\frac{1}{2}}/2\pi$. (5.40)

By solving the secular equation (5.35) we can find the matrix L provided the determinant $G_S F_S - E\Lambda = 0$. This is in fact a transformation matrix between S and Q.

$$S = LQ \qquad \text{or} \qquad S' = Q'L' \tag{5.41}$$

The proof is as follows:

Substituting equation (5.41) into equations (5.29) and (5.31)

$$2T = \dot{S}'G_S^{-1}\dot{S} = \dot{Q}'L'G^{-1}L\dot{Q} = \dot{Q}'E\dot{Q}$$

where $L'G^{-1}L = E$ (5.42)

and $2V = S'F_S S = Q'L'F_S LQ = Q'\Lambda Q$

where $L'F_S L = \Lambda$ (5.43)

Now $L^{-1}G_s L'^{-1} = E^{-1} = E$ (5.44)

Multiplying equations (5.43) and (5.44) we obtain

$$L^{-1}G_S\tilde{L}^{-1}\tilde{L}F_SL = L^{-1}G_SF_SL = \Lambda E = \Lambda \qquad (5.45)$$

$$\therefore \quad G_SF_SL = L\Lambda \qquad (5.46)$$

This is the secular equation which we solve.

Considering again equation (5.41) in the form

$$S = LQ \qquad (5.47)$$

or $Q = L^{-1}S$

In a normal vibration in which the normal coordinate Q_N changes with frequency ν_N, all the symmetry coordinates $S_1, S_2, \ldots, S_i$ change with the same frequency but the amplitude of oscillation is different for each symmetry coordinate. The relative ratios of the amplitudes of the symmetry coordinates of a normal vibration associated with Q_N are given from equation (5.47) by

$$L_{1N} : L_{2N} : L_{3N} : \ldots\ldots\ldots L_{iN}$$

If one of these elements is relatively large compared to the others, the normal vibration is said to be predominantly due to the vibration caused by the change of this symmetry coordinate.

For the assignment of vibrational modes the potential energy distribution matrix is more convenient than the L matrix itself.

The potential energy is given by equation (5.34) as

$$V = \tfrac{1}{2}\tilde{Q}\Lambda Q$$

therefore

$$\tilde{L}FL = \Lambda \qquad (5.48)$$

If we express this equation for a single frequency ν_a the following relation is obtained.

$$\lambda_a = \sum_{ij} \tilde{L}_{ai}F_{Sij}L_{ja} = \sum_{ij} F_{Sij}L_{ia}L_{ja} \qquad (5.49)$$

This gives the potential energy distribution among the symmetry coordinates and these are given in Tables 5.8 and 5.9 for each molecule.

5.2.3 G matrix construction

The G matrix depends on the relationship between the internal coordinates expressed as a vector R and the Cartesian coordinates expressed as a vector, X.

$$R = BX \qquad \text{or} \qquad X = B^{-1}R \tag{5.50}$$

B is a rectangular matrix of order $3N.(3N - 6)$ if there are no redundancies.

From equation (5.7)

$$2T = \dot{X}'M\dot{X}$$

$$= \dot{R}'B'^{-1}MB^{-1}\dot{R} \tag{5.51}$$

Since from equation (5.29)

$$2T = \dot{R}K\dot{R} = \dot{R}G^{-1}\dot{R} \tag{5.52}$$

therefore

$$G^{-1} = B'^{-1}MB^{-1} \tag{5.53}$$

the inverse and hence the G matrix is given by

$$G = BM^{-1}B' \tag{5.54}$$

For large molecules with low symmetry calculating the G matrix is lengthy. The method used in this work developed by Decius {116} was to specify the geometry of the molecules in terms of bond lengths and angles between the bonds, and the atomic masses and calculate from these the B and M matrices. The geometry used is given in Fig. 5.1, and the G matrices derived are given in Tables 5.2, 5.3 and 5.4.

Table 5.1

Symmetry coordinates for methylamine [95]

A'

$S_1 = 1/\sqrt{2}(\Delta r_1 + \Delta r_2)$	NH_2 sym. str.
$S_2 = 1/\sqrt{3}(\Delta r_3 + \Delta r_4 + \Delta r_5)$	CH_3 sym. str.
$S_3 = 1/\sqrt{6}(2\Delta r_3 - \Delta r_4 - \Delta r_5)$	CH_3 deg. str.
$S_4 = \Delta R$	CN str.
$S_5 = 1/\sqrt{6}(2\Delta\alpha_1 - \Delta\beta_1 - \Delta\beta_2)$	NH_2 scissor.
$S_6 = 1/\sqrt{3}(\Delta\alpha_1 + \Delta\beta_1 + \Delta\beta_2)$	NH_2 wag.
$S_7 = 1/\sqrt{6}(2\Delta\alpha_3 - \Delta\alpha_4 - \Delta\alpha_5)$	CH_3 deg. def.
$S_8 = 1/\sqrt{6}(\Delta\alpha_3 + \Delta\alpha_4 + \Delta\alpha_5 - \Delta\beta_3 - \Delta\beta_4 - \Delta\beta_5)$	CH_3 sym. def.
$S_9 = 1/\sqrt{6}(2\Delta\beta_3 - \Delta\beta_4 - \Delta\beta_5)$	CH_3 deg. rock.
$S_{10} = 1/\sqrt{6}(\Delta\alpha_3 + \Delta\alpha_4 + \Delta\alpha_5 + \Delta\beta_3 + \Delta\beta_4 + \Delta\beta_5) = 0$	Redundant

---

A"

$S_1 = 1/\sqrt{2}(\Delta r_1 - \Delta r_2)$	NH_2 antisym. str.
$S_2 = 1/\sqrt{2}(\Delta r_4 - \Delta r_5)$	CH_3 deg. str.
$S_3 = 1/\sqrt{2}(\Delta\beta_1 - \Delta\beta_2)$	NH_2 twist.
$S_4 = 1/\sqrt{2}(\Delta\alpha_4 - \Delta\alpha_5)$	CH_3 deg. def.
$S_5 = 1/\sqrt{2}(\Delta\beta_4 - \Delta\beta_5)$	CH_3 deg. rock.
$S_6 = \Delta\theta$	torsion.

5.2.4 F matrix construction

The F matrix may be written by assuming a suitable starting set of force constants and these will depend on the type of field to be used. There are several of these, the most common being the generalised valence force field (G.V.F.F.) which consists of stretching and bending force constants as well as the interaction force constants between them. However, the number of independent force constants usually exceeds the number of vibrational frequencies from which these force constants can be calculated directly. One method used to overcome this difficulty is to calculate the vibrational frequencies of isotopic molecules assuming the force constants are unaffected by the isotopic change but that G and Λ(observed) change. This is satisfactory for small molecules but as the molecules become more complex the number of interaction force constants in the G.V.F.F. becomes too large to allow reliable evaluation.

Too many parameters in the potential function may to some extent be overcome by taking only selected cross terms such as in the case of the Urey-Bradley force field (U.B.F.F.) {117,118}. In this field <u>all</u> the interaction force constants are introduced through the repulsive force between non-bonded atoms. The latter represent Van der Waals interactions.

The number of force constants in the U.B.F.F. is generally much smaller than for other fields but has the advantage that the force constants have a clearer physical meaning and are often transferable from one molecule to another {119,120}.

The potential field may be represented generally by

$$V = \sum_i \left[\tfrac{1}{2}K_i(\Delta r_i)^2 + K'_i r_i(\Delta r_i)\right] + \sum_i \left[\tfrac{1}{2}H_i r_{i\alpha}^2(\Delta\alpha_i)^2 + H'_i r_{i\alpha}^2(\Delta_{\alpha i})\right] + \sum_i \left[\tfrac{1}{2}F_i(\Delta q_i)^2 + F'_i q_i(\Delta q_i)\right] \qquad (5.55)$$

Δr_i, $\Delta\alpha_i$ and Δq_i are the changes in the bond lengths, bond angles, and distances between non-bonded atoms respectively. The symbols r_i, $r_{i\alpha}$ and q_i are the values of the distances at the equilibrium position and are inserted to make the force constants dimensionally similar and K_i, K_i', H_i, H_i', F_i and F_i' represent the stretching, bending, and repulsive force constants respectively. Furthermore through the relation

$$q_{ij}^2 = r_i^2 + r_j^2 - 2r_i r_j \cos \alpha_{ij} \qquad (5.56)$$

the terms of Δq_{ij} can be represented by Δr_i, Δr_j and $\Delta\alpha_{ij}$. The linear constants K′ and H′ disappear as these are the first order terms leaving K, H, F and F′. Although U.B.F.F. has four distinct types of force constants, F′ is usually taken as -0.1 F, with the assumption that the repulsive energy between non-bonded atoms is proportional to $1/r^9$. Thus only K, H and F are needed to construct the F matrix.

The force field in this work is derived from equation (5.55). Numerical calculations were made on a CDC 7600 computer by use of programs GCCC, BGLZ and LSMB {122} written by T. Shimanouchi and converted by Dr. S. Suzuki. The programs are based on general methods as in ref. 121. The adjustment of the force constants were made according to the least square method by use of the equation

$$J'WJ\,\Delta f = J'W\Delta\lambda \qquad (5.57)$$

where W is a weight matrix

$\Delta\lambda$ is a vector whose elements are $\lambda_{k\ \text{obs.}} - \lambda_{k\ \text{calc.}}$

Δf is also a vector whose elements are $f - f^o$ where f^o is the set of force constants to be refined and f is the refined

set of force constants.

J is know as the Jacobian matrix; its elements are given by

$$J_{ij} = \Delta\lambda_i/\Delta f_j$$

The elements of the Jacobian matrix are used to refine the force constants. Since the initial force constants are usually only approximate values, the corrected force constants may still deviate from the true values and the perturbations must be repeated using the revised force field. The cycle is repeated until the calculated frequencies converge to the observed frequency parameters within a set limit.

5.3 Results and discussion

The molecule CH_3NH_2 (Fig. 5.1) considered for the force constant analysis belongs to the point group Cs. This molecule has 15 fundamental vibrational modes of which 9 are of the A′ species and 6 of the A″ species. The internal coordinates chosen for the molecule are the changes in the bond lengths r_i and R, and bond angles, α_i and β_i.

A suitable set of orthonormal symmetry coordinates {95} which can be interpreted by reference to Fig. 5.1 are given in Table 5.1 along with their approximate descriptions.

The numerical values for G_{ij} elements of CH_3NH_2, CH_3ND_2 and CH_3NHD for each symmetric block calculated by equation (5.5) are given in Tables 5.2, 5.3 and 5.4.

There were 26 frequencies assigned with reasonable confidence for the CH_3NH_2 and CH_3ND_2 molecules in the argon matrix, plus two tentatively assigned frequencies. The remaining (torsional) frequencies were not observed therefore the gas phase

Table 5.2
Numerical values of the G_s matrix for CH_3NH_2

SYMMETRIZED G MATRIX
PROBLEM NO. 1
ISOTOPE NO. 1 SYM. BLOCK NO. 1

ROW 1	1.042818	0.000000	0.000000	-.037823	-.086034	-.043410	0.000000	.000000	.038892	-.000000
ROW 2	0.000000	1.019845	-.000000	-.048068	.000000	-.000000	-.000000	-.101563	.000000	-.000000
ROW 3	0.000000	-.000000	1.103101	.000000	-.026626	.037655	.143631	-.000000	-.115787	.000000
ROW 4	-.037823	-.048068	.000000	.154650	.111328	-.034351	-.000000	.175912	.000000	.000000
ROW 5	-.086034	.000000	-.026626	.111328	2.513235	.198994	-.034451	.000000	-.006516	-.000000
ROW 6	-.043410	-.000000	.037655	-.034351	.198994	.739244	.048721	-.000000	-.117354	.000000
ROW 7	0.000000	-.000000	.143631	-.000000	-.034451	048721	2.261959	.000000	.265409	.000000
ROW 8	.000000	-.101563	-.000000	.175912	.000000	-.000000	.000000	2.032580	.000000	.000001
ROW 9	.038892	.000000	-.115787	.000000	-.006516	-.117354	.265409	.000000	1.000509	-.000000
ROW 10	-.000000	-.000000	.000000	.000000	-.000000	.000000	.000000	.000001	-.000000	.000000

SYMMETRIZED G MATRIX
PROBLEM NO. 1
ISOTOPE NO. 1 SYM. BLOCK NO. 2

ROW 1	1.084156	0.000000	-.104046	0.000000	.067363	.054227
ROW 2	0.000000	1.103101	.079878	.143631	-.115787	-.013175
ROW 3	-.104046	.079878	1.139954	.103353	-.159447	-.070766
ROW 4	0.000000	.143631	.103353	2.261958	.265410	-.017047
ROW 5	.067363	-.115787	-.159447	.265410	1.000509	.053421
ROW 6	.054227	-.013175	-.070766	-.017047	.053421	.906110

Table 5.3

Numerical values of the G_s matrix for CH_3ND_2

SYMMETRIZED G MATRIX
PROBLEM NO. 1
ISOTOPE NO. 2 SYM. BLOCK NO. 1

ROW 1	.547250	0.000000	0.000000	-.037823	-.086034	-.043410	0.000000	.000000	.038892	-.000000
ROW 2	0.000000	1.019865	-.000000	-.048068	.000000	-.000000	-.000000	-.101563	.000000	-.000000
ROW 3	0.000000	-.000000	1.103101	.000000	-.026626	.037655	.143631	-.000000	-.115787	.000000
ROW 4	-.037823	-.048068	.000000	.154650	.111328	-.034351	-.000000	.175912	.000000	.000000
ROW 5	-.086034	.000000	-.026626	.111328	1.359147	.095456	-.034451	.000000	-.006516	-.000000
ROW 6	-.043410	-.000000	.037655	-.034351	.095456	.446795	.048721	-.000000	-.117354	.000000
ROW 7	0.000000	-.000000	.143631	-.000000	-.034451	.048721	2.261959	.000000	.265409	.000000
ROW 8	.000000	-.101563	-.000000	.175912	.000000	-.000000	.000000	2.032580	.000000	.000001
ROW 9	.038892	.000000	-.115787	.000000	-.006516	-.117354	.265409	.000000	1.000509	-.000000
ROW 10	-.000000	-.000000	.000000	.000000	-.000000	.000000	.000000	.000001	-.000000	.000000

SYMMETRIZED G MATRIX
PROBLEM NO. 1
ISOTOPE NO. 2 SYM. BLOCK NO. 2

ROW 1	.588588	0.000000	-.104046	0.000000	.067363	.054227
ROW 2	0.000000	1.103101	.079878	.143631	-.115787	-.013175
ROW 3	-.104046	.079878	.657975	.103353	-.159447	-.070766
ROW 4	0.000000	.143631	.103353	2.261958	.265410	-.017047
ROW 5	.067363	-.115787	-.159447	.265410	1.000509	.053421
ROW 6	.054227	-.013175	-.070766	-.017047	.053421	.625791

Table 5.4

Numerical values of the G_s matrix for CH_3NHD

SYMMETRIZED G MATRIX
PROBLEM NO. 1
ISOTOPE NO. 3 SYM. BLOCK NO. 1

ROW 1	.795034	0.000000	0.000000	-.037823	-.086034	-.043410	0.000000	.000000	.038892	-.000000
	-.247784	0.000000	-.000000	0.000000	.000170	.000000				
ROW 2	0.000000	1.019845	-.000000	-.048068	.000000	-.000000	-.000000	-.101563	.000000	-.000000
	0.000000	.000000	.000000	.000000	-.000000	-.000000				
ROW 3	0.000000	-.000000	1.103101	.000000	-.026626	.037655	.143631	-.000000	-.115787	.000000
	0.000000	.000000	-.000349	.000000	-.000000	.000058				
ROW 4	-.037823	-.048068	.000000	.154650	.111328	-.034351	-.000000	.175912	.000000	.000000
	0.000000	.000000	0.000000	.000000	-.000000	.000000				
ROW 5	-.086034	.000000	-.026626	.111328	1.935691	.147225	-.034451	.000000	-.006516	-.000000
	-.000000	-.000116	.290599	-.000150	-.000028	-.178029				
ROW 6	-.043410	-.000000	.037655	-.034351	.147225	.592820	.048721	-.000000	-.117354	.000000
	-.000000	.000164	-.089666	.000213	-.000512	-.125886				
ROW 7	0.000000	-.000000	.143631	-.000000	-.034451	.048721	2.261959	.000000	.265409	.000000
	0.000000	.000000	-.000451	.000001	-.000000	.000075				
ROW 8	.000000	-.101563	-.000000	.175912	.000000	-.000000	.000000	2.032580	.000000	.000001
	-.000000	.000000	.000000	.000000	-.000001	-.000000				
ROW 9	.038892	.000000	-.115787	.000000	-.006516	-.117354	.265409	.000000	1.000509	-.000000
	-.000294	-.000000	.000696	-.000000	-.000000	-.000233				
ROW 10	-.000000	-.000000	.000000	.000000	-.000000	.000000	.000000	.000001	-.000000	.000000
	.000000	-.000000	-.000000	-.000000	.000000	.000000				
ROW 11	-.247784	0.000000	0.000000	0.000000	-.000000	-.000000	0.000000	-.000000	-.000294	.000000
	.836372	0.000000	-.104046	0.000000	.067363	.054227				
ROW 12	0.000000	.000000	.000000	.000000	-.000116	.000164	.000000	.000000	-.000000	-.000000
	0.000000	1.103101	.079878	.143631	-.115787	-.013175				
ROW 13	-.000000	.000000	-.000349	0.000000	.290599	-.089666	-.000451	.000000	.000696	-.000000
	-.104046	.079878	.898965	.103353	-.159447	-.070766				
ROW 14	0.000000	.000000	.000000	.000000	-.000150	.000213	.000001	.000000	-.000000	-.000000
	0.000000	.143631	.103353	2.261958	.265410	-.017047				
ROW 15	.000170	-.000000	-.000000	-.000000	-.000028	-.000512	-.000000	-.000001	-.000000	.000000
	.067363	-.115787	-.159447	.265410	1.000509	.053421				
ROW 16	.000000	-.000000	.000058	.000000	-.178029	-.125886	.000075	-.000000	-.000233	.000000
	.054227	-.013175	-.070766	-.017047	.053421	.765955				

Table 5.5

Numerical values of the F matrix for CH_3NH_2

F MATRIX
MOLECULE NO. 1 ISOTOPE NO. 1 SYM. BLOCK NO. 1

ROW 1	6.40043	0.00000	0.00000	.62593	.03818	.34827	0.00000	0.00000	0.00000	0.00000
ROW 2	0.00000	4.61935	0.00000	.63427	0.00000	0.00000	0.00000	-.04086	0.00000	.30318
ROW 3	0.00000	0.00000	4.75166	0.00000	0.00000	0.00000	-.09274	0.00000	.24327	0.00000
ROW 4	.62593	.63427	0.00000	5.12163	-.28841	.40788	0.00000	-.38364	0.00000	.38364
ROW 5	.03818	0.00000	0.00000	-.28841	.64367	-.17612	0.00000	0.00000	0.00000	0.00000
ROW 6	.34827	0.00000	0.00000	.40788	-.17612	.61644	0.00000	0.00000	0.00000	0.00000
ROW 7	0.00000	0.00000	-.09274	0.00000	0.00000	0.00000	.47271	0.00000	.04090	0.00000
ROW 8	0.00000	-.04086	0.00000	-.38364	0.00000	0.00000	0.00000	.64512	0.00000	-.23231
ROW 9	0.00000	0.00000	.24327	0.00000	0.00000	0.00000	.04090	0.00000	.93732	0.00000
ROW 10	0.00000	.30318	0.00000	.38364	0.00000	0.00000	0.00000	-.23231	0.00000	.45963

F MATRIX
MOLECULE NO. 1 ISOTOPE NO. 1 SYM. BLOCK NO. 2

ROW 1	6.37021	0.00000	.26232	0.00000	0.00000	0.00000
ROW 2	0.00000	4.82426	0.00000	-.09274	.24327	0.00000
ROW 3	.26232	0.00000	.58295	0.00000	0.00000	0.00000
ROW 4	0.00000	-.09274	0.00000	.57883	-.07849	0.00000
ROW 5	0.00000	.24327	0.00000	-.07849	.86212	0.00000
ROW 6	0.00000	0.00000	0.00000	0.00000	0.00000	.04806

Table 5.6

Numerical values of the F matrix for CH_3ND_2

F MATRIX
MOLECULE NO. 1 ISOTOPE NO. 2 SYM. BLOCK NO. 1

ROW 1	6.61915	0.00000	0.00000	.62593	.03818	.34827	0.00000	0.00000	0.00000	0.00000
ROW 2	0.00000	4.61935	0.00000	.63427	0.00000	0.00000	0.00000	-.04086	0.00000	.30318
ROW 3	0.00000	0.00000	4.75166	0.00000	0.00000	0.00000	-.09274	0.00000	.24327	0.00000
ROW 4	.62593	.63427	0.00000	5.12163	-.28841	.40788	0.00000	-.38364	0.00000	.38364
ROW 5	.03818	0.00000	0.00000	-.28841	.64367	-.17612	0.00000	0.00000	0.00000	0.00000
ROW 6	.34827	0.00000	0.00000	.40788	-.17612	.65850	0.00000	0.00000	0.00000	0.00000
ROW 7	0.00000	0.00000	-.09274	0.00000	0.00000	0.00000	.47271	0.00000	.04890	0.00000
ROW 8	0.00000	-.04086	0.00000	-.38364	0.00000	0.00000	0.00000	.64512	0.00000	-.23231
ROW 9	0.00000	0.00000	.24327	0.00000	0.00000	0.00000	.04890	0.00000	.93732	0.00000
ROW 10	0.00000	.30318	0.00000	.38364	0.00000	0.00000	0.00000	-.23231	0.00000	.45963

F MATRIX
MOLECULE NO. 1 ISOTOPE NO. 2 SYM. BLOCK NO. 2

ROW 1	6.55599	0.00000	.26232	0.00000	0.00000	0.00000
ROW 2	0.00000	4.82426	0.00000	-.09274	.24327	0.00000
ROW 3	.26232	0.00000	.58295	0.00000	0.00000	0.00000
ROW 4	0.00000	-.09274	0.00000	.57883	-.07849	0.00000
ROW 5	0.00000	.24327	0.00000	-.07849	.86212	0.00000
ROW 6	0.00000	0.00000	0.00000	0.00000	0.00000	.04890

Table 5.7

Numerical values of the F matrix for CH_3NHD

F MATRIX
MOLECULE NO. 1 ISOTOPE NO. 3 SYM. BLOCK NO. 1

ROW 1	6.42849	0.00000	0.00000	.64904	.03258	.35618	0.00000	0.00000	0.00000	0.00000
	.05169	0.00000	0.00000	0.00000	0.00000	0.00000				
ROW 2	0.00000	4.61906	0.00000	.64810	0.00000	0.00000	0.00000	-.04461	0.00000	.30693
	0.00000	0.00000	0.00000	0.00000	0.00000	0.00000				
ROW 3	0.00000	0.00000	4.75206	0.00000	0.00000	0.00000	-.09274	0.00000	.24857	0.00000
	0.00000	0.00000	0.00000	0.00000	0.00000	0.00000				
ROW 4	.64904	.64810	0.00000	5.11636	-.29907	.42294	0.00000	-.39201	0.00000	.39201
	0.00000	0.00000	0.00000	0.00000	0.00000	0.00000				
ROW 5	.03258	0.00000	0.00000	-.29907	.65651	-.21364	0.00000	0.00000	0.00000	0.00000
	0.00000	0.00000	0.00000	0.00000	0.00000	0.00000				
ROW 6	.35618	0.00000	0.00000	.42294	-.21364	.65343	0.00000	0.00000	0.00000	0.00000
	0.00000	0.00000	0.00000	0.00000	0.00000	0.00000				
ROW 7	0.00000	0.00000	-.09274	0.00000	0.00000	0.00000	.47271	0.00000	.04090	0.00000
	0.00000	0.00000	0.00000	0.00000	0.00000	0.00000				
ROW 8	0.00000	-.04461	0.00000	-.39201	0.00000	0.00000	0.00000	.64875	0.00000	-.23593
	0.00000	0.00000	0.00000	0.00000	0.00000	0.00000				
ROW 9	0.00000	0.00000	.24857	0.00000	0.00000	0.00000	.04090	0.00000	.94458	0.00000
	0.00000	0.00000	0.00000	0.00000	0.00000	0.00000				
ROW 10	0.00000	.30693	0.00000	.39201	0.00000	0.00000	0.00000	-.23593	0.00000	.50415
	0.00000	0.00000	0.00000	0.00000	0.00000	0.00000				
ROW 11	.05169	0.00000	0.00000	0.00000	0.00000	0.00000	0.00000	0.00000	0.00000	0.00000
	6.38250	0.00000	.27200	0.00000	0.00000	0.00000				
ROW 12	0.00000	0.00000	0.00000	0.00000	0.00000	0.00000	0.00000	0.00000	0.00000	0.00000
	0.00000	4.82611	0.00000	-.09274	.24857	0.00000				
ROW 13	0.00000	0.00000	0.00000	0.00000	0.00000	0.00000	0.00000	0.00000	0.00000	0.00000
	.27200	0.00000	.63923	0.00000	0.00000	0.00000				
ROW 14	0.00000	0.00000	0.00000	0.00000	0.00000	0.00000	0.00000	0.00000	0.00000	0.00000
	0.00000	-.09274	0.00000	.56685	-.07849	0.00000				
ROW 15	0.00000	0.00000	0.00000	0.00000	0.00000	0.00000	0.00000	0.00000	0.00000	0.00000
	0.00000	.24857	0.00000	-.07849	.86952	0.00000				
ROW 16	0.00000	0.00000	0.00000	0.00000	0.00000	0.00000	0.00000	0.00000	0.00000	0.00000
	0.00000	0.00000	0.00000	0.00000	0.00000	.04800				

Table 5.8

Potential energy distribution for the frequencies of CH_3NH_2

POTENTIAL ENERGY DISTRIBUTION
MOLECULE NO. 1 ISOTOPE NO. 1 SYM. BLOCK NO. 1

	FREQUENCIES	3352.312	2966.509	2818.629	1620.972	1463.403	1449.904	1135.983	1047.752	796.227	0.000
S 1	NH S STR	100.46	.02	.07	.01	.00	.17	.15	.81	2.73	0.00
S 2	CH3 SSTR	.04	.00	100.37	.11	.00	.10	.02	1.14	.09	0.00
S 3	CH3 DSTR	.01	100.95	.00	.02	.09	.00	.65	.03	.08	0.00
S 4	CN STR	.05	.00	.13	.61	.18	8.23	1.46	98.39	5.72	0.00
S 5	NH2 SCSR	.04	.02	.01	99.30	.02	3.57	.86	.17	6.41	0.00
S 6	NH2 WAG	.00	.01	.00	.00	.19	.02	4.73	.00	111.44	0.00
S 7	CH3 DDEF	.00	.16	.00	.17	58.18	1.53	38.68	.99	.97	0.00
S 8	CH3 SDEF	.01	.00	.23	2.11	2.55	99.43	.09	.30	.32	0.00
S 9	CH3 DRCK	.02	.11	.00	.01	33.72	.60	61.86	1.93	3.39	0.00
S10	REDUNDNT	0.00	0.00	0.00	0.00	0.00	0.00	0.00	0.00	0.00	0.00

POTENTIAL ENERGY DISTRIBUTION
MOLECULE NO. 1 ISOTOPE NO. 1 SYM. BLOCK NO. 2

	FREQUENCIES	3414.800	2990.845	1480.294	1214.934	996.419	270.378
S 1	NH A STR	100.36	.04	.01	.11	1.35	.00
S 2	CH3 DSTR	.02	100.84	.02	.38	.37	.00
S 3	NH2 TWST	.03	.07	.44	21.13	80.19	.03
S 4	CH3 DDEF	.00	.23	99.77	.34	1.10	.00
S 5	CH3 DRCK	.06	.11	4.30	78.62	19.49	.01
S 6	TORSION	.00	.00	.00	.03	.01	99.96

Table 5.9

Potential energy distribution for the frequencies of CH_3ND_2

POTENTIAL ENERGY DISTRIBUTION
MOLECULE NO. 1 ISOTOPE NO. 2 SYM. BLOCK NO. 1

	FREQUENCIES	2956.590	2819.374	2460.995	1462.860	1455.658	1205.462	1129.219	1010.940	638.831	0.000
S 1	ND S STR	.01	.12	101.06	.02	.20	.01	.01	.27	2.36	0.00
S 2	CH3 SSTR	.00	100.22	.20	.00	.16	.29	.05	.89	.04	0.00
S 3	CH3 DSTR	100.95	.00	.02	.09	.00	.01	.67	.03	.06	0.00
S 4	CN STR	.00	.12	.26	.14	6.13	20.43	3.92	81.22	2.23	0.00
S 5	ND2 SCSR	.01	.01	.22	.02	.36	87.32	4.81	10.06	7.00	0.00
S 6	ND2 WAG	.01	.00	.02	.13	.01	.29	2.20	.37	112.05	0.00
S 7	CH3 DDEF	.16	.00	.00	58.61	1.58	1.72	37.57	.70	.52	0.00
S 8	CH3 SDEF	.00	.24	.01	2.31	100.99	.74	.02	.46	.25	0.00
S 9	CH3 DROK	.11	.00	.10	33.55	.55	3.68	60.65	1.08	2.11	0.00
S10	REDUNDNT	0.00	0.00	0.00	0.00	0.00	0.00	0.00	0.00	0.00	0.00

POTENTIAL ENERGY DISTRIBUTION
MOLECULE NO. 1 ISOTOPE NO. 2 SYM. BLOCK NO. 2

	FREQUENCIES	2991.055	2548.000	1479.805	1188.999	758.002	223.508
S 1	ND A STR	.02	100.75	.01	.07	.96	.01
S 2	CH3 DSTR	100.83	.04	.02	.55	.19	.00
S 3	ND2 TWST	.06	.21	.22	5.38	95.89	.08
S 4	CH3 DDEF	.23	.00	99.91	.81	.49	.00
S 5	CH3 DROK	.10	.26	4.47	92.85	4.91	.01
S 6	TORSION	.00	.01	.00	.02	.06	99.91

Table 5.10

Observed and calculated frequencies for CH_3NH_2, CH_3NHD and CH_3ND_2

ν*	Mode	CH_3NH_2			CH_3NHD			CH_3ND_2		
		Obs. (cm^{-1})	Calc. (cm^{-1})	Δν%	Obs. (cm^{-1})	Calc. (cm^{-1})	Δν%	Obs. (cm^{-1})	Calc. (cm^{-1})	Δν%
ν_1	NH_2 sym. stretch.	3352.3	3352.3	0.0	3376.0	3376.0	0.0	2461.0	2461.0	0.0
ν_2	CH_3 asym. stretch.	2967.1	2966.5	0.0	2966.5	2966.5	0.0	2966.0	2966.6	0.0
ν_3	CH_3 sym. stretch.	2819.3	2818.6	0.0	2819.0	2819.0	0.0	2818.7	2819.4	0.0
ν_4	NH_2 scissors	1623.0	1621.0	0.0	(1469.0)	1490.2	-1.4	1203.0	1205.5	-0.2
ν_5	CH_3 asym. def.	1463.0	1463.2	0.0	1464.3	1464.5	0.0	1462.2	1462.9	0.0
ν_6	CH_3 sym. def.	1449.5	1449.9	0.0	1456.0	1435.0	1.4	1456.0	1455.7	0.0
ν_7	CH_3 rock.	1139.7	1136.0	0.3	1174.0	1201.9	-2.4	1125.5	1129.2	-0.3
ν_8	CN stretch.	1052.3	1047.8	0.4	1042.0	1044.7	-0.2	1006.1	1010.9	-0.5
ν_9	NH_2 wagging	796.1	796.2	0.0	702.0	708.6	-0.9	639.0	638.8	0.0
ν_{10}	NH_2 asym. stretch.	3414.8	3414.8	0.0	2478.0	2478.0	0.0	2548.0	2548.0	0.0
ν_{11}	CH_3 asym. stretch.	2990.8	2990.8	0.0	2991.3	2991.3	0.0	2991.1	2991.1	0.0
ν_{12}	CH_3 asym. def.	1480.8	1480.3	0.0	1484.1	1465.0	1.3	1479.3	1479.8	0.0
ν_{13}	NH_2 twist.	(972.0)	996.4	-2.5	885.7	885.8	0.0	758.0	758.0	0.0
ν_{14}	CH_3 rock.	(1117.4)	1214.9	-8.7	1130.4	1135.2	-0.4	1189.0	1189.0	0.0
ν_{15}	CH_3 torsion	(263.9)	270.4	-2.5	(244)	241.1	1.2	(224.5)	223.5	0.4

* the order of the frequencies is the same as in reference 95

values were used for these frequencies. This vibration is not expected to mix with the others, as can be seen from the potential energy distributions in Tables 5.8 and 5.9 calculated from equation 5.49.

The initial set of force constants, which were taken from reference 95, were iterated until a reasonable fit of the calculated to the observed frequencies was obtained. The final F matrices for CH_3NH_2 and CH_3ND_2 are given in Tables 5.5 and 5.6. The observed and calculated frequencies for the two molecules are given in Table 5.10. The degree of mixing of symmetry coordinates (shown in Tables 5.8 and 5.9) was not regarded as serious indicating that the symmetry coordinates used (Table 5.1) were good descriptions of the normal coordinates.

The G_s matrix was calculated for the CH_3NHD molecule (Table 5.4) and using the F matrix obtained from the previous calculation of the CH_3NH_2 and CH_3ND_2 molecules, a set of frequencies was calculated. These are given in Table 5.10.

It is a general convention to use empirically different force constants for NH and ND stretching vibrations as the anharmonicity for these vibrations is large. In order to obtain a reasonable fit for methylamine it was necessary to use different values for the NH_2 and ND_2 wagging (and the NHD wagging) vibrations {95}. This is reasonable as the amplitudes of these vibrations, which correspond to the "umbrella" motion of the ammonia molecule, are large compared with other frequencies. This is the reason why the F matrices are slightly different for each isotopic species.

One further point which must be made is that as the CH_3NHD molecule has no symmetry, the G matrix cannot be factored into

blocks. However the local symmetry of the CH_3 group remains the same so although the molecule has no overall symmetry, for the convenience of the calculation and transferability of the force field, the same symmetry coordinates as for the Cs symmetry are used.

The results of the calculation indicate that with a definite assignment for the NHD twist at 885.7 cm^{-1} the corresponding values for the NH_2 and ND_2 twisting motions must be around 996 cm^{-1} and 758 cm^{-1} respectively. This result is in agreement with the tentative assignment made in chapter 4 from the observed spectra of CH_3NH_2 and CH_3ND_2 at 972 cm^{-1} and 758 cm^{-1}. The assignment of the CH_3A'' rock at 1189 cm^{-1} for CH_3ND_2 is confirmed by the calculations, but the CH_3NH_2 mode cannot correspond with the band observed at 1117 cm^{-1} in the argon matrix. It must occur at about 1200 cm^{-1}, but no absorption was observed at this frequency in the matrix.

CHAPTER 6

ETHYLAMINE IN ARGON AND NITROGEN MATRICES

6.1 Introduction

Wolff and Ludwig {97,100,102} have studied the infrared and Raman spectra of gaseous ethylamine and its deuterated analogue ($C_2H_5ND_2$). They present an approximate assignment for the bands they observe and in particular they observe splitting of the CCN symmetric stretching vibration which they attribute to rotational isomerism around the C-N bond. Two conformers of the ethylamine molecule may exist, with the NH_2 group trans (I) or gauche (II) with respect to the methyl group. Ethylamine in the trans configuration belongs to the point group Cs and of the 24 fundamental vibrations , 14 are of the A' species and 10 are of the A" species. In the gauche conformation there is no element of symmetry.

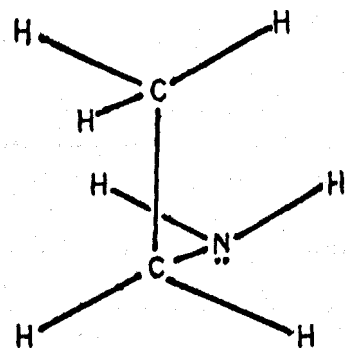

trans-form (I)

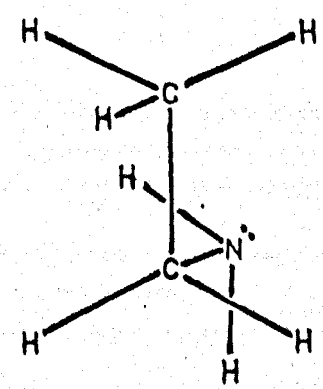

gauche-form (II)

Fig. 6.1

Experimentation carried out for ethylamine

I N F R A R E D

Molecule	Matrix	M/A	Technique	Temperature (K)	Amount of sample deposited (μmol)
$C_2H_5NH_2$	Nitrogen	100	S.S.O.	20	30.0
"	"	1010	"	"	12.0
"	"	1000	"	"	12.6
"	"	100	P.M.I.	"	35.9
"	"	100	"	"	8.7
"	"	100	"	"	17.9
"	"	220	"	"	13.8
"	"	500	"	"	14.9
"	"	1000	"	"	6.0
"	Argon	106	S.S.O.	20	54.0
"	"	995	"	"	20.7
"	"	1000	"	"	18.6

R A M A N

$C_2H_5NH_2$	Nitrogen	100	P.M.I.	20	80.0
"	Argon	100	"	"	60.0

Fig. 6.1 Infrared and Raman Spectra of the NH_2 Stretching Region of $C_2H_5NH_2$ in an Argon Matrix deposited and recorded at 20K.

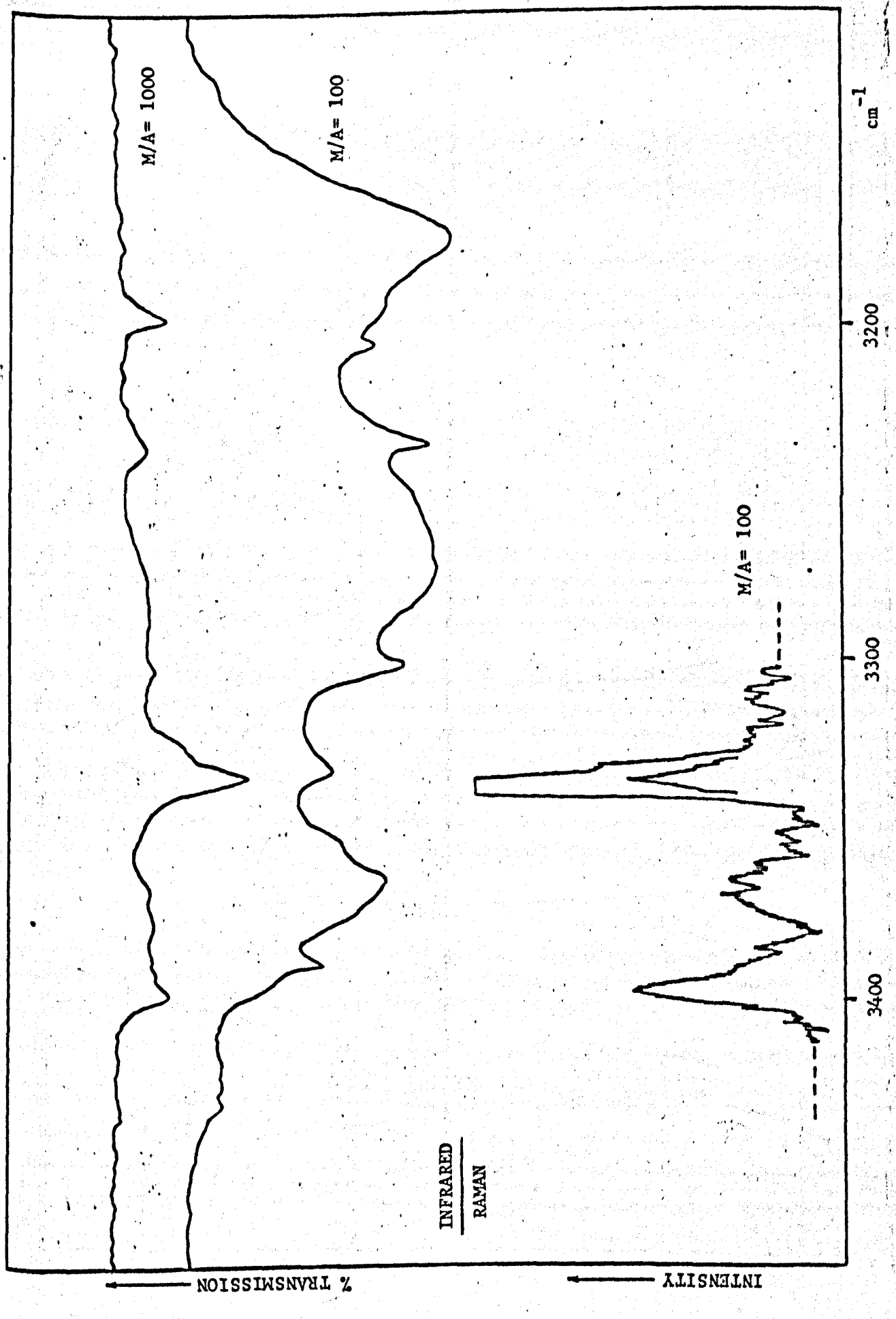

Fig. 6.2 Infrared and Raman Spectra of the CH_3 Stretching Region of $C_2H_5NH_2$ in an Argon Matrix deposited and recorded at 20K.

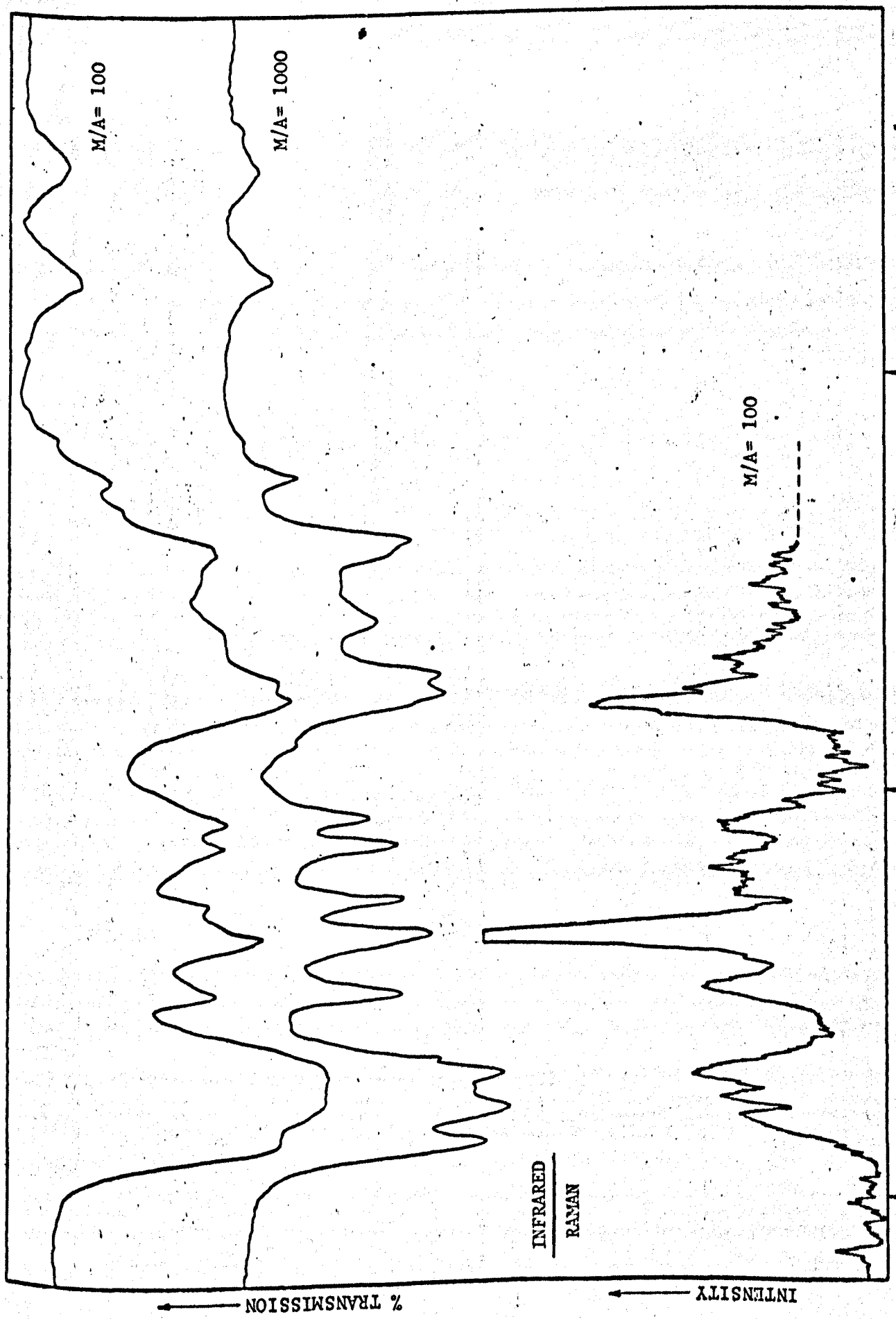

Fig. 6.3 Infrared and Raman Spectra of the CH_3 Deformation, CH_2 Rocking and CH_2 Twisting Regions for $C_2H_5NH_2$ in an Argon Matrix recorded at 20K.

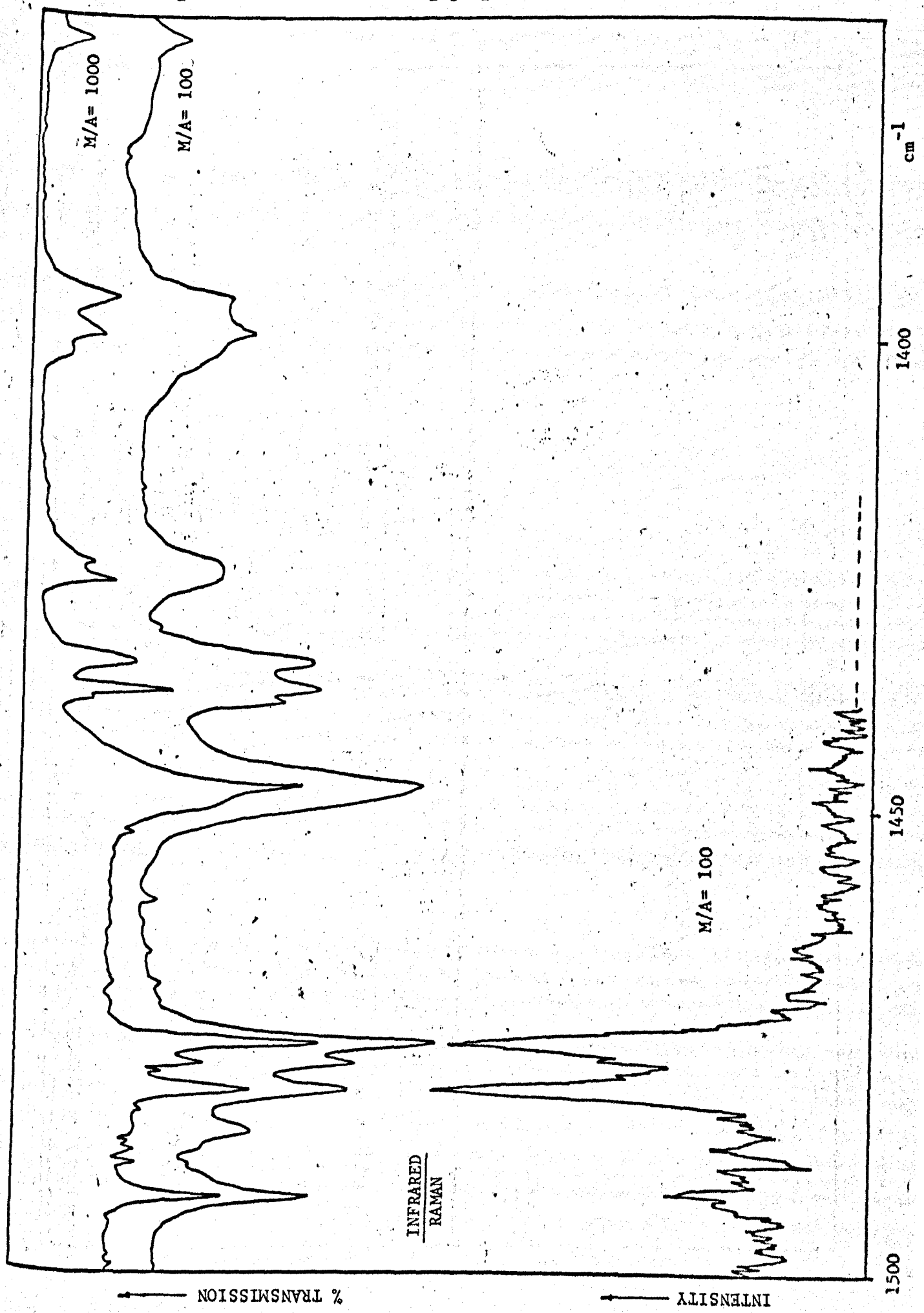

Fig. 6.4 Infrared and Raman Spectra of the CH_3 Rocking and the CCN Asymmetric Stretching Regions for $C_2H_5NH_2$ in an Argon Matrix at 20K.

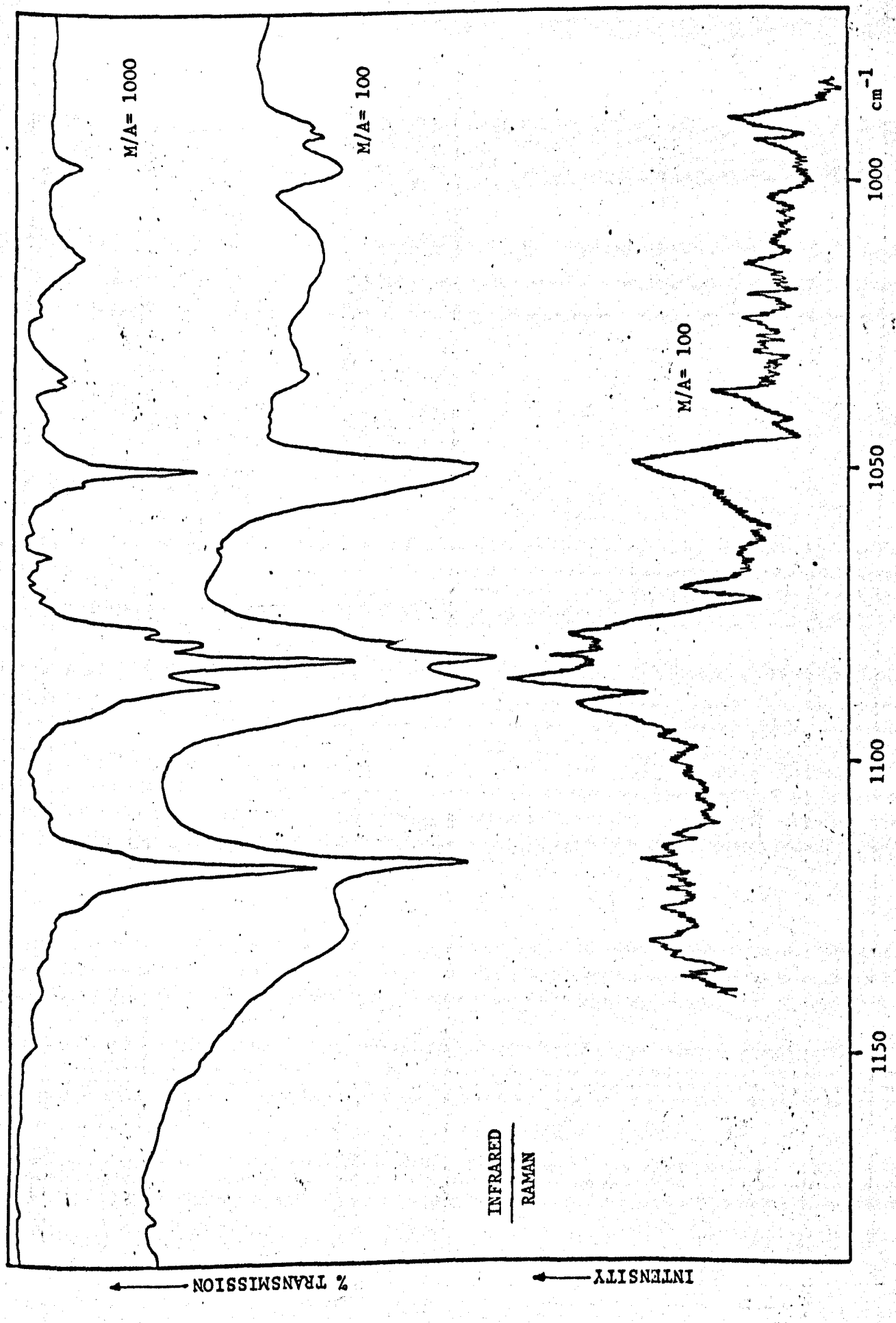

Fig. 6.5 Infrared Spectra of the CH_2 Rocking, NH_2 Twisting, CCN Symmetric Stretching and NH_2 Wagging Regions for $C_2H_5NH_2$.

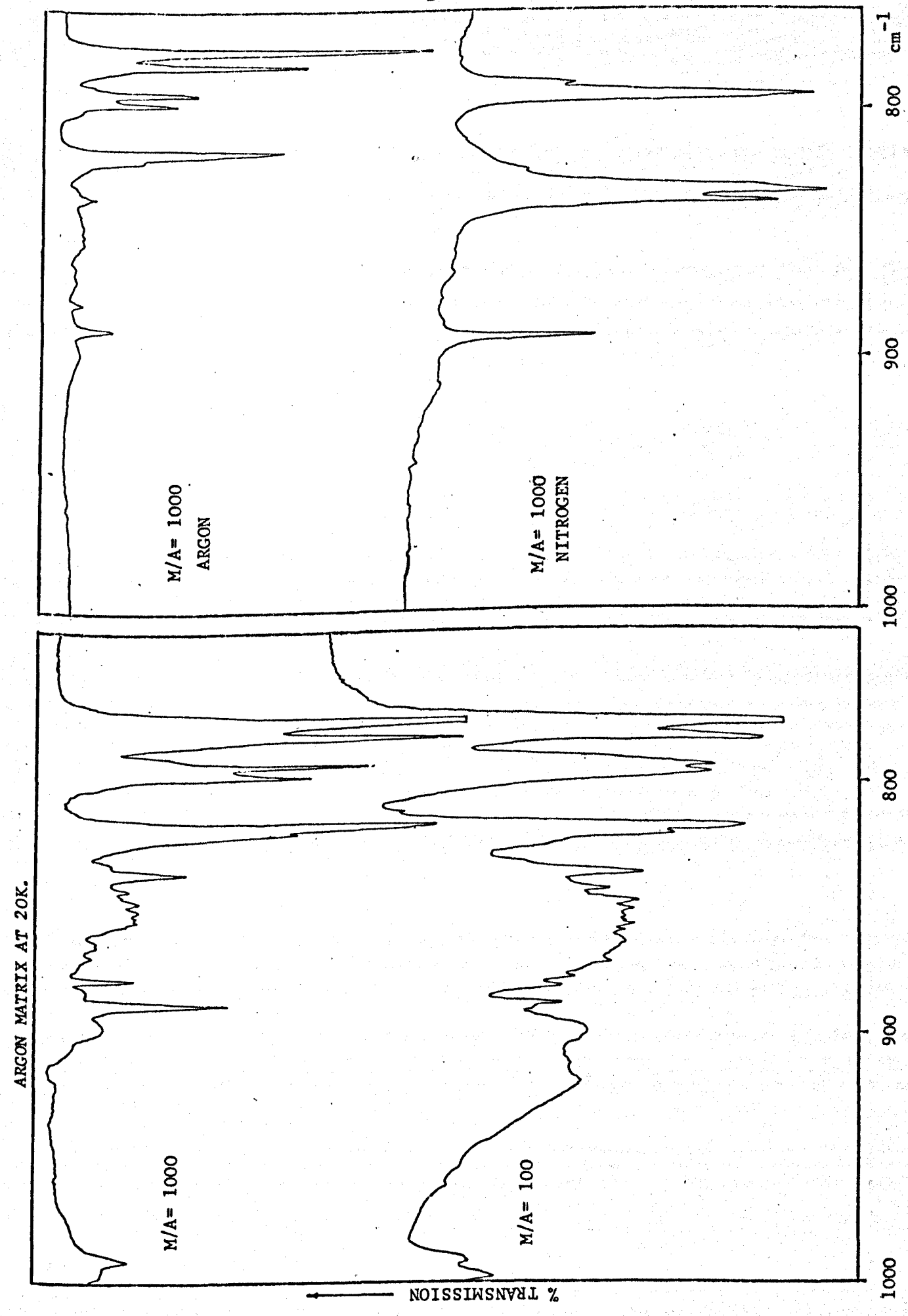

Fig. 6.6 Infrared and Raman Spectra of the CCN Symmetric Stretching Region for $C_2H_5NH_2$ in Argon and Nitrogen Matrices at 20 K

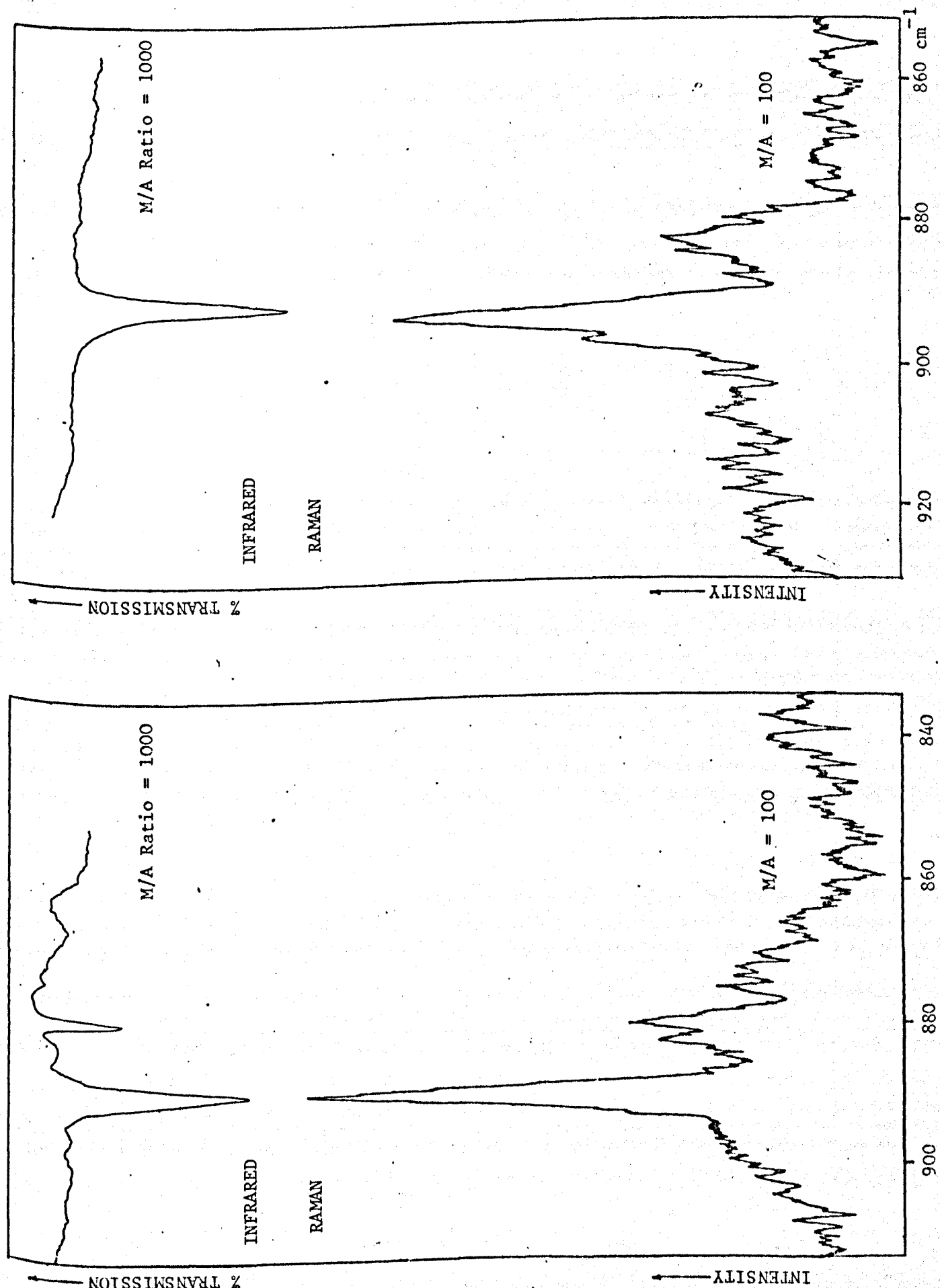

Table 6.2

Infrared and Raman bands observed for $C_2H_5NH_2$ in an argon matrix

Frequency cm^{-1}		Species	Assignment
Infrared	Raman		
∿3435	-	multimer	
∿3398	3402.6	MONOMER	NH_2 asym. stretching (A")
∿3390	-	multimer	
∿3364	-	multimer	
∿3334	3334.9	MONOMER	NH_2 sym. stretching (A')
-	∿3330	multimer	
3300.5	-	multimer	
∿3274	-	multimer	
3236	-	Monomer	2 x 1620.6 = 3241.2 (A')
3207.5	-	multimer	
3196	-	-	1620.6 + 1374.5 = 2995.1 (A')
∿3172	-	-	
2986.2	2986	MONOMER	CH_3 asym. stretching (A')
2978.0	2976.0	MONOMER	CH_3 asym. stretching (A")
2972.8	2972	multimer	
2969.0	2969	MONOMER	CH_2 asym. stretching (A")
2965.3	2960.0	monomer or multimer	2 x 1483.5 = 2967.0 (A')
2948.6	2948.5	Monomer	1460.4 + 1374.5 = 2834.9 (A')
2934.0	2934.5	MONOMER	CH_3 sym. stretching (A')
2925.8	2923.7	Monomer	2 x 1460.4 = 2920.8 (A')
2912.4	-	Monomer	1460.4 + 1451.2 = 2911.6 (A")
2905.8	2907.2	Monomer	2 x 1451.2 = 2902.4 (A')
2888.1	-	monomer	1394.6 + 1374.5 = 2769.1 (A')
2879	-	multimer	
2876.0	2877.0	MONOMER	CH_2 sym. stretching (A')
2871.2	-	monomer	second site
2858.8	-	monomer	
2842.1	-	multimer	
2839.8	-	Monomer	1483.5 + 1374.5 = 2858.0 (A')
2823.8	-	Monomer	1394.5 + 1460 = 2854.9 (A')

Table 6.2 (contd.)

Frequency cm^{-1}		Species	Assignment
Infrared	Raman		
2814.8	-	multimer	
2775	-	Monomer	2 x 1394.6 = 2789.2 (A')
2748	-	Monomer	1394.6 + 1374.5 = 2769.1 (A')
2724	∿2722	Monomer	2 x 1374.5 = 2749.0 (A')
2714	2712.3	multimer	
∿1646	-	multimer	
∿1636	-	dimer	
1620.6	-	MONOMER	NH_2 scissors (A')
1483.5	1483.6	MONOMER	CH_2 deformation (A')
1481.3	-	multimer	
1476	1478.5	multimer	
1473	1473.8	multimer	
1469.3	-	multimer	
1460.4	1461.8	MONOMER	CH_3 asym. deformation (A')
1456.3	1455.2	multimer	
1454.3	-	multimer	
1451.2	1451.6	MONOMER	CH_3 asym. deformation (A")
1436	-	multimer	
1418.8	-	multimer	
1398	-	multimer	
1394.6	∿1400	MONOMER	CH_3 sym. deformation (A')
1376.5	-	multimer	
1374.5	-	MONOMER	CH_2 rocking (A')
1368.6	-	multimer	
1351.3	-	?	impurity
1347.8	-	?	
1303	-	multimer	
1298	-	MONOMER	CH_2 twisting (A")
1290	-	multimer	
∿1235	-	multimer	
∿1128	-	multimer	
∿1118	1118.6	MONOMER	CH_3 rocking (A')
∿1115	-	multimer	

Table 6.2 (contd.)

Frequency cm^{-1}		Species	Assignment
Infrared	Raman		
1086.1	1088	multimer	
1082.2	1082.0	MONOMER	CCN asym. stretching (A')
1080.0	-	multimer	
1076.7	-		
1064	-		
1052.0	-		
1049.3	1050.8	MONOMER	CH_3 rocking A"
1034.6	1039	monomer	site band
1032.7	-	multimer	
~1013	-	multimer	
~ 998	-	multimer	
991.7	991	MONOMER	NH_2 twisting A"
989.8	-	multimer	
~ 921	-		
~ 900	-		
889.1	889.6	MONOMER	CCN sym stretching (A') — trans
878.8	880.4	MONOMER	CCN sym stretching (A') — gauche
~ 854	-	multimer	
842	-		
835.7	-		
~ 820	-		
817.0	-	MONOMER	CH_2 rocking (A")
797.6	-	Monomer	second site — NH_2 wagging (gauche)
(795.4)	-		CH_3NH_2 — NH_2 wagging (gauche)
793.2	-	MONOMER	
~ 790	-	monomer ?	
782.0	-	Monomer	NH_2 wagging (trans) (A')
776.2	-	MONOMER	
410.0	-	MONOMER	CCN bending (A')
~ 349	-	dimer	

Table 6.3

Infrared and Raman bands observed for $C_2H_5NH_2$ in a nitrogen matrix

Frequency cm^{-1}		Species	Assignment
Infrared	Raman		
∿3399	∿3399	MONOMER	NH_2 asym. stretching (A")
∿3392	-	multimer	
∿3368	3341.2	MONOMER	NH_2 sym. stretching (A')
∿3308	-	multimer	
∿3275	-	Monomer	2 x 1640 = 3280 (A')
3210	-	multimer	
2985.5	2984.2	MONOMER	CH_3 asym. stretching (A')
2979.5	2978	MONOMER	CH_3 asym. stretching (A")
2976.0	-	multimer	
2970.5	2970.4	MONOMER	CH_2 asym. stretching (A")
2966.9	-	Monomer	2 x 1485.6 = 2971.2 (A')
∿2957	-	multimer	
2947.3	2948.0	Monomer	1462.8 + 1396.0 = 2858.8
∿2937	-	multimer	
2933.5	2934.5	MONOMER	CH_3 sym. stretching (A')
2924.9	-	Monomer	2 x 1462.8 = 2925.6 A'
2917.1	2918.8	Monomer	1462.8 + 1451.4 = 2914.2 (A")
2908.5	2908	Monomer	2 x 1451.4 = 2902.8 (A')
2895.3	-	Monomer	1403.2 + 1396.0 = 2799.0 (A')
2878.6	2878	MONOMER	CH_2 sym. stretching (A')
2874.6	-	multimer	
2868.2	2867.8		
∿2857	-	multimer	
2852.6	2850	Monomer	1485.6 + 1396.0 = 2881.6 (A')
∿2843	-	multimer	
2830.3	-	multimer	
2823.1	-	Monomer	1403.2 + 1462.8 = 2866.0 (A')
2816.3	-	multimer	
2786.8	-	multimer	
2779.0	-	Monomer	2 x 1403.2 = 2806.4 (A')

Table 6.3 (contd.)

Frequency cm^{-1}		Species	Assignment
Infrared	Raman		
∿1640	-	MONOMER	NH_2 scissors (A')
1485.6	∿1486	MONOMER	CH_2 deformation (A')
1481.5	-	multimer	
1462.8	1462.5	MONOMER	CH_3 asym. deformation (A')
	1458	multimer	
1451.4	1452.5	MONOMER	CH_3 asym. deformation (A")
1403.2	-	MONOMER	CH_3 sym. deformation (A')
1396.0	∿1391	MONOMER	CH_2 rocking (A')
1387.2	-	multimer	
1378.5	-		
1375.0	-		
1365.2	-		
1303.0	∿1311	MONOMER	CH_2 twisting (A")
1238.0	1239.2	multimer	
-	1226.5		
1143.7	-		
1127.0	1126.5		
1123.2	∿1124	MONOMER	CH_3 rocking (A')
-	∿1092	multimer	
1086.9	1086.9	MONOMER	CCN asym. stretching (A')
1056.7	1053.2	MONOMER	CH_3 rocking(A")
1050.3	-	multimer	
∿1043.5	-	multimer	
997.0	-	MONOMER	NH_2 twisting (A")
∿ 935	-	multimer	
∿ 911	-		
-	895.8		
890.8	892.4	MONOMER	CCN sym. stretching (A') (trans)
-	881.5	multimer	

Table 6.3 (contd.)

Frequency cm^{-1}		Species	Assignment
Infrared	Raman		
879.0	-	multimer	
~ 870	-		
864.0	-		
858.0	-		
849.0	-	dimer	
845.0	-	dimer	
836.8	-	monomer	site band
832.3	-	MONOMER	CH_2 rocking (A")
~ 824	-	multimer	
(816)	-		CH_3NH_2 impurity
802	-	multimer	
795.0	-	Monomer	
793.2	-	MONOMER	NH_2 wagging (A') (trans)
~ 791	-	multimer	
788.8	-	multimer	
417.0	-	MONOMER	CCN bending (A')
413.0	-	monomer	site band

Table 6.4

Comparison of the gas and matrix fundamentals of ethylamine in the infrared and Raman

Sym.	Mode	Gas	Argon matrix		Nitrogen matrix	
		IR/R	Infrared	Raman	Infrared	Raman
A'	NH_2 sym. stretch.	3345	∿3334	3334.9	-	3341.2
	CH_3 asym. stretch.	2978	2986.2	2986	2985.5	2984.2
	CH_3 sym. stretch.	2936	2934.0	2934.5	2933.5	2934.5
	CH_2 sym. stretch.	2897	2876.0	2877.0	2878.6	2878
	NH_2 scissors	1622	1620.6	-	1640	-
	CH_2 def.	1480	1483.5	1483.6	1485.6	1486
	CH_3 asym. def.	1460	1460.4	1461.8	1462.8	1462.5
	CH_3 sym. def.	1400	1394.6	∿1400	1403.2	-
	CH_2 rock.	1381	1374.5	-	1396.0	∿1391
	CH_3 rock.	1118	∿1118	1118.6	1123.2	∿1124
	CCN asym. stretch.	1088	1082.2	1082.0	1086.9	1086.9
	CCN sym. stretch.	893 883	889.1(T) 878.8(G)	889.6(T) 880.4(G)	890.8(T)	892.4(T)
	NH_2 wag.	775	793.2(G) 776.2(T)	- -	793.2(T)	-
	CCN bend.	408	410.0	-	417.0	-
A''	NH_2 asym. stretch.	3411	∿3398	3402.6	∿3399	∿3399
	CH_3 asym. stretch.	2978	2978.0	2976.0	2979.5	2978
	CH_2 asym. stretch.	-	2969.0	2969	2970.5	2970.4
	CH_3 asym. def.	1460	1451.2	1451.6	1451.4	1452.5
	CH_2 twist.	1297	1298.0	-	1303.0	∿1311
	CH_3 rock.	1055	1049.3	1050.8	1056.7	1053.2
	NH_2 twist	993	991.7	991	997.0	-
	CH_2 rock.	-	817.0	-	832.3	-
	CH_3 torsion	-	-	-	-	-
	NH_2 torsion	-	-	-	-	-

T = Trans

G = Gauche

A complete spectral assignment has not previously been attempted and this work was undertaken to fill in the gaps in the assignments and also as a precursor for the quantitative experimentation of chapter 8. All matrix samples were deposited at 20 K. Experimentation carried out on ethylamine is given in Table 6.1.

6.2 Monomer assignments

6.2.1 NH_2 stretching region

The monomer absorptions in the NH stretching region of ethylamine in the infrared are weak in both argon and nitrogen. The bands in argon at high M/A ratio do display asymmetry but it is difficult to conclude whether this is due to the conformers isolated in the matrix or the presence of monomer ethylamine in alternative trapping sites. The Raman bands are much stronger, the frequencies of the NH stretches being easily identified for both argon and nitrogen matrices (Fig. 6.1) and are given in Tables 6.2 and 6.3. The NH_2 symmetric stretch for the argon matrix displays a shoulder to lower frequency of the main monomer band at $\sim$ 3330 cm^{-1} at 1.5 cm^{-1} resolution but at the M/A ratio studied is most likely due to multimer.

6.2.2 CH stretching region

The spectra of ethylamine in the CH stretching region are complex for both matrices in the infrared and Raman (Fig. 6.2). In this region there are five fundamentals, three due to the methyl group and two due to the methylene group. By comparison with the gas spectrum, the Raman matrix spectra and their M/A ratio dependence, the bands at 2986.2, 2978.0 and 2934.0 cm^{-1}

are assigned to the monomer CH_3 stretching fundamentals and the bands at 2969.0 and 2876.0 in the infrared in an argon matrix are assigned to the monomer CH_2 stretching fundamentals. The CH_3 and CH_2 symmetric stretches are readily identified since they are intense in the Raman spectra. The remaining monomer absorptions are bands due to combinations and overtones of the CH deformation region. Tentative assignments for argon and nitrogen are given in Tables 6.2 and 6.3 respectively along with the corresponding Raman frequencies.

6.2.3 NH_2 scissors

The NH_2 scissors region is weak and in a region of strong atmospheric absorptions. Only one band at 1620.6 cm^{-1} and 1640 cm^{-1} in argon and nitrogen matrices respectively is present at high dilution and assigned to this fundamental.

6.2.4 CH deformation region

The CH deformation region of ethylamine (Fig. 6.3) is very similar to that of ethanol {34}. There are four CH deformations in this region; one due to the methylene group and three due to the methyl group. The former fundamental is located at 1483.5 cm^{-1} and 1485.6 cm^{-1} in argon and nitrogen respectively.

The remaining deformations are located at 1460.4, 1451.2 and 1394.6 cm^{-1} in an argon matrix and at 1462.8, 1451.4 and 1403.2 cm^{-1} in a nitrogen matrix. The bands for the argon matrix at 1460.4 cm^{-1} and 1451.2 cm^{-1} are assigned to the A' and A" asymmetric deformation respectively and the band at 1394.6 cm^{-1} is assigned to the symmetric deformation, the corresponding bands appear for the nitrogen matrix and are given

in Table 6.3.

6.2.5 Other CH_2 and CH_3 modes

The three remaining CH_2 modes are the CH_2 rocking A' and A", and the CH_2 twisting A", Figs. 6.4 and 6.5. The CH_2 A' rocking is located at 1374.5 cm^{-1} and the CH_2 A" rocking is at 817 cm^{-1} for an argon matrix. For nitrogen these modes are at 1396.0 cm^{-1} although the CH_2 A" rocking mode is split at 836.8 and 832.3 cm^{-1} most probably due to site effects. There are two CH_3 rocking modes which are at 1118 cm^{-1} and 1123.2 cm^{-1} for the A' mode in argon and nitrogen respectively and 1049.3 cm^{-1} and 1056.7 cm^{-1} for the A" mode in argon and nitrogen respectively, in the infrared. The CH_2 A" twisting is identified in the infrared at 1298.0 cm^{-1} and 1303 cm^{-1} in argon and nitrogen matrices, it is weak in the Raman and only observable in a nitrogen matrix at $\sim$1311 cm^{-1}.

6.2.6 Skeletal vibrations (CCN stretching and CCN bending)

The CCN stretches are easily identified in argon and nitrogen matrices in both the infrared and Raman results (Fig. 6.6). The CCN asymmetric stretch A' is at 1082.2 cm^{-1} and 1086.9 cm^{-1} for argon and nitrogen matrices for both the infrared and Raman. The CCN symmetric stretch in argon is a doublet which can be assigned to the two conformers, the band at 889.1 cm^{-1} being assigned to the trans and lower frequency component at 878.8 cm^{-1} being assigned to the gauche conformer in the infrared results. However, in nitrogen only one band is observed being at 890.8 cm^{-1} and is presumably the trans conformer. The Raman results agree for ethylamine in an argon matrix but conflict with the infrared results for nitrogen. The CCN symmetric stretch appears to be

a doublet, as for the argon matrix. However, due to the weakness of the Raman effect it was necessary to work at higher M/A ratios than in the infrared and it may well be that the lower frequency component of the doublet in the Raman results for nitrogen may coincide with a multimer band of the CCN symmetric stretch. The same argument can of course be applied for the Raman spectra doublet of ethylamine in an argon matrix. The infrared results imply that the ratio of the trans:gauche for the nitrogen matrix is much higher than in the argon matrix.

6.2.7 NH_2 wagging region

Two groups of bands are observed in argon which must be assigned to monomer ethylamine. The bands at 776.2 and 782.0 cm^{-1}, are assigned to the trans conformer and the bands at 793.2 cm^{-1} and 797.6 cm^{-1} to the gauche conformer (Fig. 6.5). The splitting is explained as being due to ethylamine existing in alternative trapping sites. Temperature cycling does not affect the relative intensity of the two bands due to the trans conformer but does cause changes in the intensities of the gauche bands. However these changes are reversible. Since ethylamine must be regarded as being too large to be rotating some kind of site effect is occurring on temperature cycling which appears to affect the gauche conformer (the least stable) more than the trans conformer.

For nitrogen (Fig. 6.5), only one group of bands can be assigned to the NH_2 wagging mode of ethylamine and this must be due to the trans conformer, it being the more stable form at 20 K. Shoulders appear on the main monomer band (793.2 cm^{-1}) at high M/A ratio indicating the presence of alternative trapping sites. Owing to the sensitivity of this mode to the matrix environment

they are more apparent here than in the other regions. Assignments for this region for both matrices in the infrared and Raman are given in Tables 6.2 and 6.3.

6.2.8 Torsional modes

No bands were found for the torsions in either nitrogen or argon in the infrared for the experimental frequency range (down to 250 cm^{-1}) and no bands were observable in the Raman spectra.

The monomer frequencies for ethylamine in argon and nitrogen matrices in the infrared and Raman are summarised in Table 6.4 along with their approximate descriptions.

6.3 Multimer assignments

6.3.1 Introduction

There is a certain amount of evidence {105} to suppose that ethylamine is associated in the gas phase as in the case of methylamine (see chapter 4) in which case the most likely associated species would be open chain dimer.

6.3.2 NH_2 stretching region

Multimer species of ethylamine are weak in the infrared and large amounts of matrix material had to be deposited to obtain a spectra so their concentration dependence was difficult to study in detail. Tentative assignments are given in Tables 6.2 and 6.3. Only two multimer bands at 3236 cm^{-1} and 3207.5 cm^{-1} in the argon matrix are present at high M/A ratio indicating that the extent of hydrogen bonding in dilute matrices is limited. These are most probably due to open chain dimer. Similar bands are observed for the nitrogen matrix.

6.3.3 NH_2 wagging region

Several bands here are concentration dependent but this region is complicated by the presence of multimer species of the CH_2 A" rocking vibration (Fig. 6.5). However, a band at 835.7 cm^{-1} in argon and 845.0 cm^{-1} in nitrogen in the infrared is most probably due to open chain dimer since it is still present at high M/A ratios. Bands to higher frequency at $\sim$ 850 cm^{-1} in both matrices which would imply that they are due to higher multimers formed as a result of diffusion along dislocation sites during the annealing process. No bands were observed in this region in the Raman.

6.3.4 Other modes

There is evidence of multimer species present in the NH_2 scissors region. The band at $\sim$ 1636 cm^{-1} and $\sim$ 1650 cm^{-1} in argon and nitrogen is assigned to the open chain dimer of ethylamine. The CH stretching region exhibits shoulders to lower frequency than the monomer bands but these disappear quickly as the M/A ratio is increased. Likewise bands in the CH_3 deformation and CH_2 rocking regions have shoulders all of which are due to the multimer species. The CH_3 A" rock has a broad shoulder to higher frequency at $\sim$ 1123 cm^{-1}. This is too high for a multimer band of the CCN asymmetric stretch and so is assigned to the multimer of the CH_3 A" rock. The CH_3 A' rock is broad at low M/A ratio but sharpens at high M/A ratio with a multimer shoulder at 1052.0 cm^{-1}. A band at 1086.1 cm^{-1} changes its relative intensity with increasing M/A ratio but is still present at high M/A ratio and is assigned to the open chain dimer species.

6.4 Conclusion

Several anomalies have arisen as a result of the matrix isolated spectra of ethylamine. If Wolff's gas phase assignment for the CCN symmetric stretch is correct, his Raman results indicate the presence of the two conformers in the gas phase and also in the liquid at 153 K. It would also be expected that a splitting of the NH_2 symmetric stretch should also be observed, since in the gauche conformation the NH_2 group will interact with the methylene group in this conformation, but no splitting is reported in this work. The gas phase Raman spectrum of ethylamine was reinvestigated and the NH_2 symmetric stretch examined at 0.6 cm^{-1} resolution (C.A.T.): no splitting was observed. The Raman matrix results for this region also showed no splitting of the strong NH_2 symmetric stretch of ethylamine in argon at the highest resolution achievable for the conditions (1.5 cm^{-1}).

The CCN symmetric stretch in the infrared results (Fig. 6.6) indicate clearly that this fundamental is a doublet in argon but a singlet in nitrogen. The doublet being assigned to the presence of the two conformers. The Raman results for nitrogen conflict with the evidence for the results in the infrared. However, this additional band observed, not present for the infrared results at high M/A ratio, could be due to the presence of multimer species.

The strongest evidence is supplied in favour of the two conformers by the NH_2 wagging region. Only one group of bands can be reasonably assigned to the NH_2 wagging mode in nitrogen whereas for argon two groups of bands appear being assigned to the two conformers.

Although complications arise in this region for the argon matrix due to the presence of multiple trapping sites (which are apparently reversibly temperature sensitive), the evidence on the whole is in favour of the presence of the two conformers.

Since the gaseous mixture is deposited and condensed very rapidly, it is reasonable to suppose that the relative intensities at the highest M/A ratio reflect the proportions of the two conformers in the gas phase at room temperature. This would appear to be the case. The ratio of trans:gauche in the gas phase Raman is 2.7:1 {102}. The value for argon for the relative optical densities of the two conformers is 2.6:1.

Silvi et al {123} undertook a study of allyl fluoride, allyl alcohol and allyl amine isolated in argon and nitrogen matrices. They observed both isomers for allyl fluoride in argon and nitrogen. However, for allyl alcohol and allyl amine only one conformer is present in argon whereas the results for nitrogen show the presence of both conformers. Annealing experiments indicated a temperature dependence of the bands suggesting that interconversion was occurring.

The conclusion from these results would therefore be that the shape of the argon site is such as to allow the correct equilibrium of the two conformers to be attained at the temperature of deposition i.e. one conformation predominant at 20 K. However for the nitrogen matrix the barrier to interconversion at 20 K is too high and only at elevated matrix temperatures is there sufficient energy to allow interconversion to take place.

In the light of the above discussion the result for ethylamine, which indicates the opposite effect, is rather surprising. Further investigation would be advantageous, a study of $C_2H_5ND_2$

should help to resolve the problem, but from the evidence of this work it is felt that the above tentative conclusions are reasonable.

CHAPTER 7

AMMONIA IN ARGON AND NITROGEN MATRICES

7.1 Introduction

Over the past 18 years several authors {58,59,62,64,124, 125} have reported examinations of ammonia isolated in both argon and nitrogen matrices. The investigations have been only in the infrared and have been primarily concerned with the ν_2 (umbrella motion) region where the reasons for the fine structure observed have been disputed for both matrices.

The examination of ammonia in solid matrices is of interest firstly because the small size of the ammonia molecule may permit the possibility of rotation and inversion taking place in the matrix site and secondly at low M/A ratios the hydrogen bonding of the multimers of ammonia may be useful in distinguishing the different types of multimer species present in the matrix.

Becker and Pimentel {124} first examined ammonia suspended in argon, xenon and nitrogen. This work was repeated by Milligan et al {59} for ammonia isolated in argon and nitrogen matrices from which they concluded that rotation and inversion of ammonia was occurring in both matrices due to the temperature dependence of the fine structure they observed for the ν_2 region. However the interpretation was contradicted by Pimentel et al {125} for the nitrogen matrix. From their diffusion and temperature dependence experiments they could assign only one band in the ν_2 region at 970 cm^{-1} to monomeric ammonia, which implied that the matrix site in nitrogen effectively restricts the motional

freedom of the trapped ammonia molecules. They did not negate the interpretation of Milligan for ammonia in an argon matrix.

Hopkins et al {58} studied the time dependence of the lines they observed for ammonia in an argon matrix to investigate the possibility of nuclear spin conversion affecting the population of the energy levels and hence the intensity of the lines. However from the lack of time dependence they concluded that most of the fine structure was not due to rotation and certainly that nuclear spin conversion was slow below 20 K. This conclusion was supported from their results by the lack of temperature dependence of the lines in question. They offered the fact that the population of the J = 2 level at 4.2 K would be low regardless of whether nuclear spin conversion was taking place and hence the line that Milligan {59} assigned to R (2) should have been much smaller.

Abouaf-Marguin et al analysed the molecule under the D_3 rotational subgroup. They presented the allowed transitions {62} from $\nu_2 = 0$ to $\nu_2 = 1$ for the first rotational levels. They were able to conclude that if deposition of the ammonia/argon gas mixture is fast enough no spin conversion can take place. therefore the E symmetry level, $1^{\pm}$, will be appreciably populated even at 4 K. However they were able to show that spin conversion could take place if deposition was slow, borne out by the reduction of the number of observed lines.

More recently Cugley and Pullin {64} took the argument of nuclear spin conversion still further by presenting computed relative intensities of vibration-rotation transitions as a function of temperature for (a) no spin conversion model and (b) total spin conversion model. They were able to show that,

from their temperature dependent results for the monomer bands in the ν_2 region, the no spin conversion model closely resembles the experimental results. As a check the relative intensities of the vibration-rotation transitions as a function of temperature were computed (Fig. 7.1) and were in agreement with Cugley and Pullin's graphs {64}.

The observed temperature dependence of these lines correlates reasonably well with that predicted. However the stretching modes are weak in the infrared, and the degenerate bending mode ν_4 lies in the water bending absorption region, so these bands have not been studied in any detail.

Pimentel et al {125} reported a study of the hydrogen-bonding of ammonia in a nitrogen matrix and concluded that the dimer bands they observed were most probably due to an open chain structure. However, Rosengren and Pimentel {126} reported a triplet $^{14}N/^{15}N$ splitting pattern for the 986 cm^{-1} (ν_2) dimer band of ammonia in the nitrogen matrix which would be consistent with a cyclic dimer structure.

In a nitrogen matrix there is a second band at 1004 cm^{-1} apparently due to dimer whereas for ammonia in an argon matrix there is only one band that could be assigned to dimer at 1000 cm^{-1}.

It was therefore felt advantageous to extend the work to the Raman in the stretching region where the symmetric stretch ν_1 is expected to be strong and hence confirm or reject the idea of rotation of ammonia in the argon matrix since the Raman rotational transitions will be different to the infrared {127}. It was also hoped to obtain additional information as to the structure of the dimers observed in both matrices.

The experimentation carried out in both the infrared and

Fig. 7.1 Predicted temperature dependence of ν_2 rotational lines in infrared spectrum of ammonia.

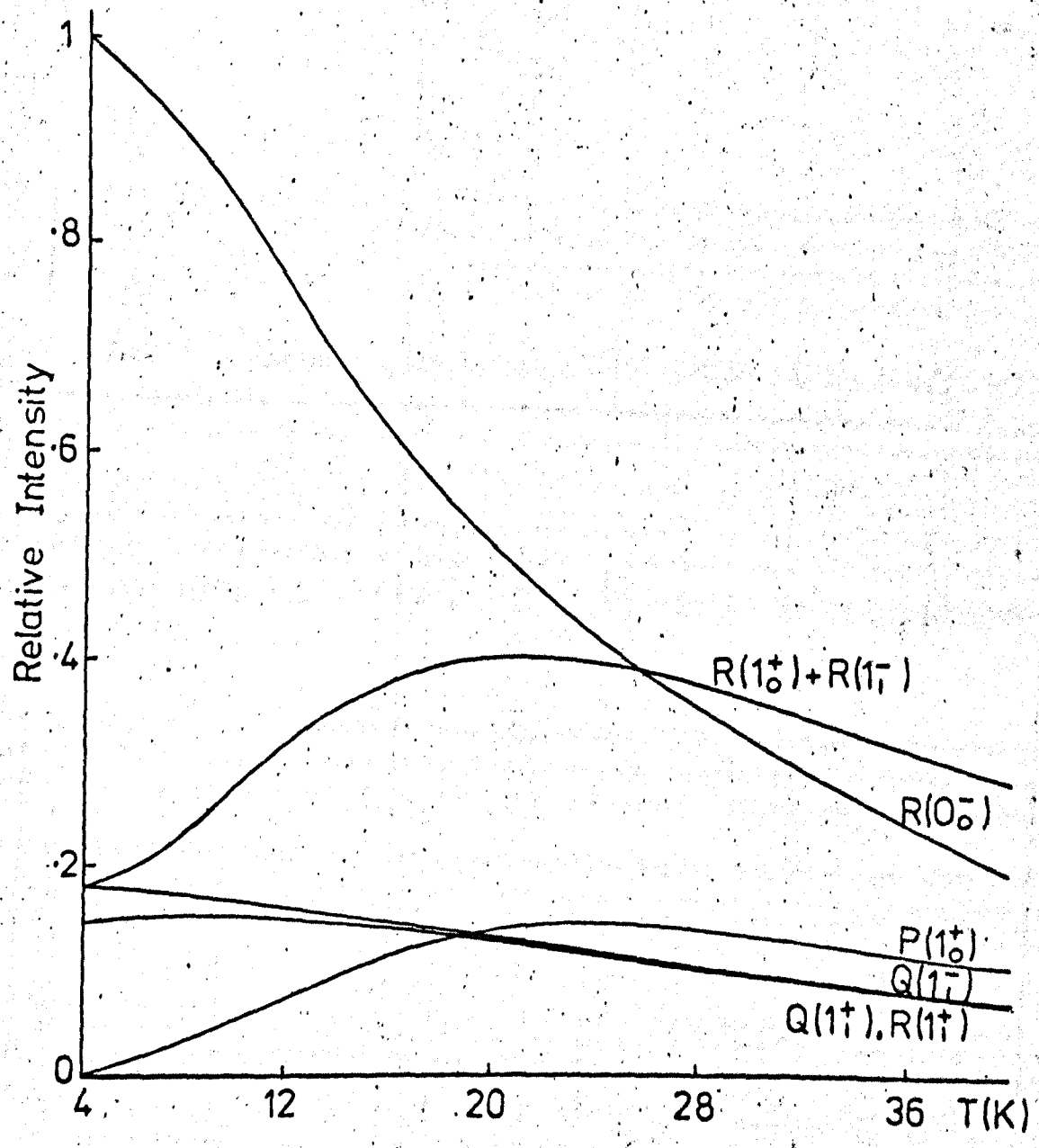

Table 7.1

Experimentation carried out for ammonia

I N F R A R E D

Molecule	Matrix	M/A	Technique	Temperature (K)	Amount of sample deposited (μmol)
NH_3	Nitrogen	980	S.S.O.	20	20.0
"	"	55	P.M.I.	"	29.0
"	"	110	"	"	37.4
"	"	530	"	"	13.0
"	"	990	"	"	5.0
"	Argon	1028	S.S.O.	"	68.0
"	"	1910	"	"	9.9
"	"	110	P.M.I.	"	16.3
"	"	210	"	"	9.9
"	"	350	"	"	8.9
"	"	760	"	"	6.6
"	"	980	"	"	9.3
"	"	1530	"	"	5.8
NH_3/H_2O	Argon	350	"	20	8.5

R A M A N

NH_3	Argon	52	P.M.I.	16	101
"	"	99	"	20	101
"	"	100	"	"	60
"	"	100	"	"	81
"	"	100	"	"	99
"	"	100	"	"	105
"	"	100	"	"	110
"	"	100	"	17	90
"	"	100	"	"	100
"	"	110	"	16	99
"	"	190	"	"	61
"	"	460	"	"	40
"	Nitrogen	52	"	17	100
"	"	105	"	16	98

Fig. 7.2 Comparison of the Observed and Predicted Infrared and Raman Spectra of the ν_1/ν_3 Region of NH_3 in Argon at 20K.

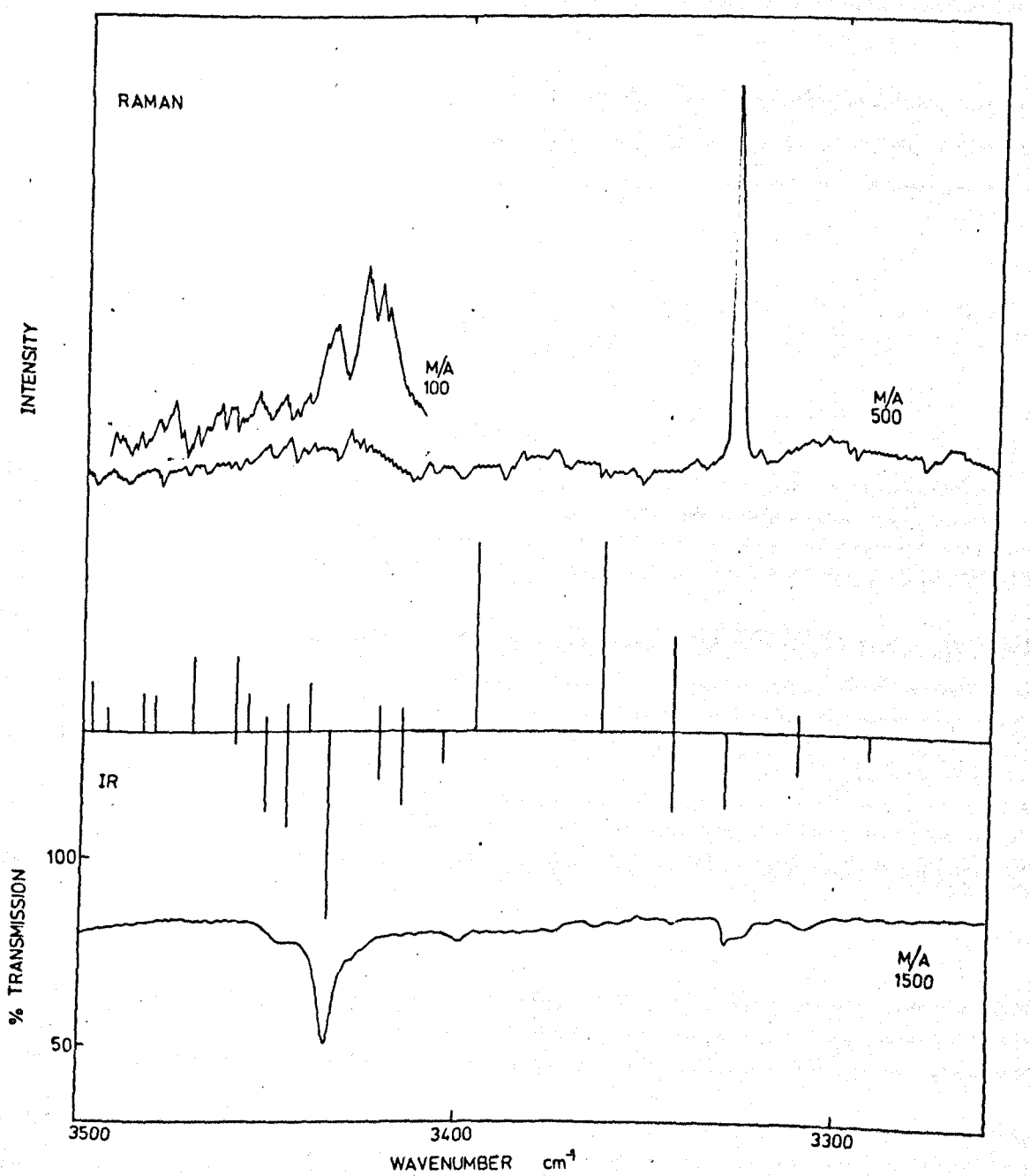

Fig. 7.3 Infrared and Raman Spectra of the ν_1/ν_3 Region of NH_3 in an Argon Matrix at 20K, showing diffusion effects.

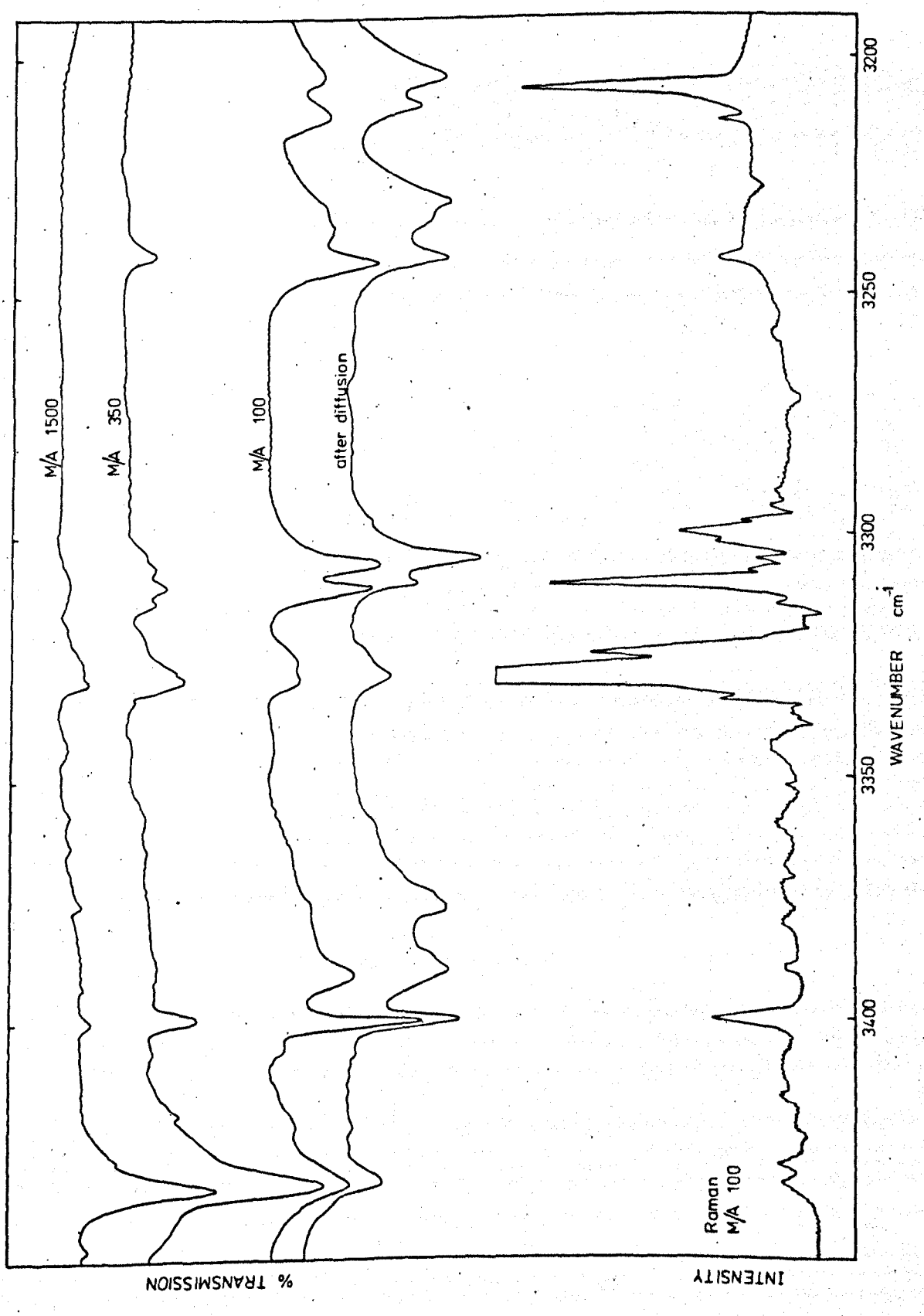

Fig. 7.4 Comparison of the Observed and Predicted Infrared Spectra of the ν_2 Region of NH_3 in Argon at 20K.

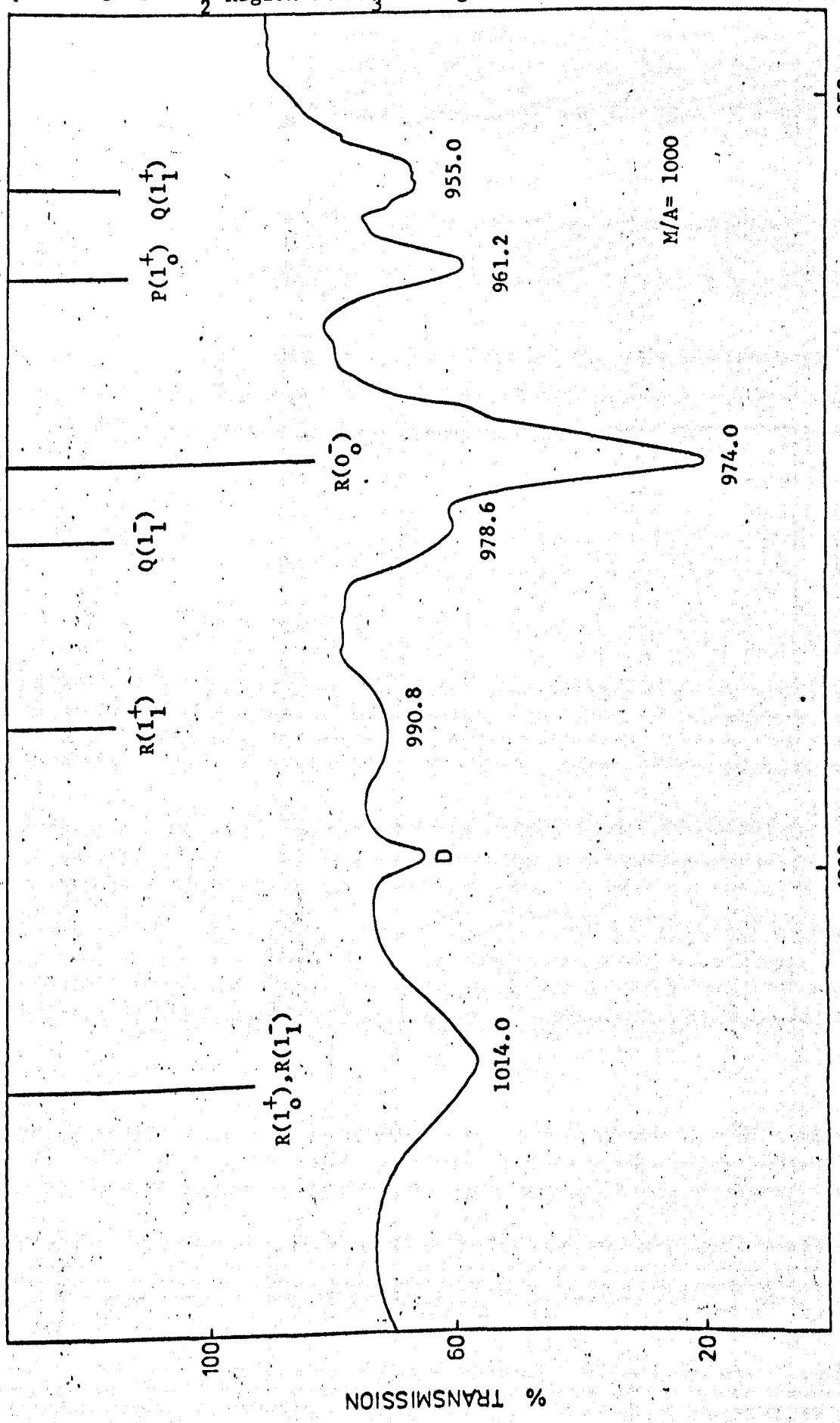

Fig. 7.5 Infrared Spectra of the ν_2 Region of NH_3 in Argon at 20K.

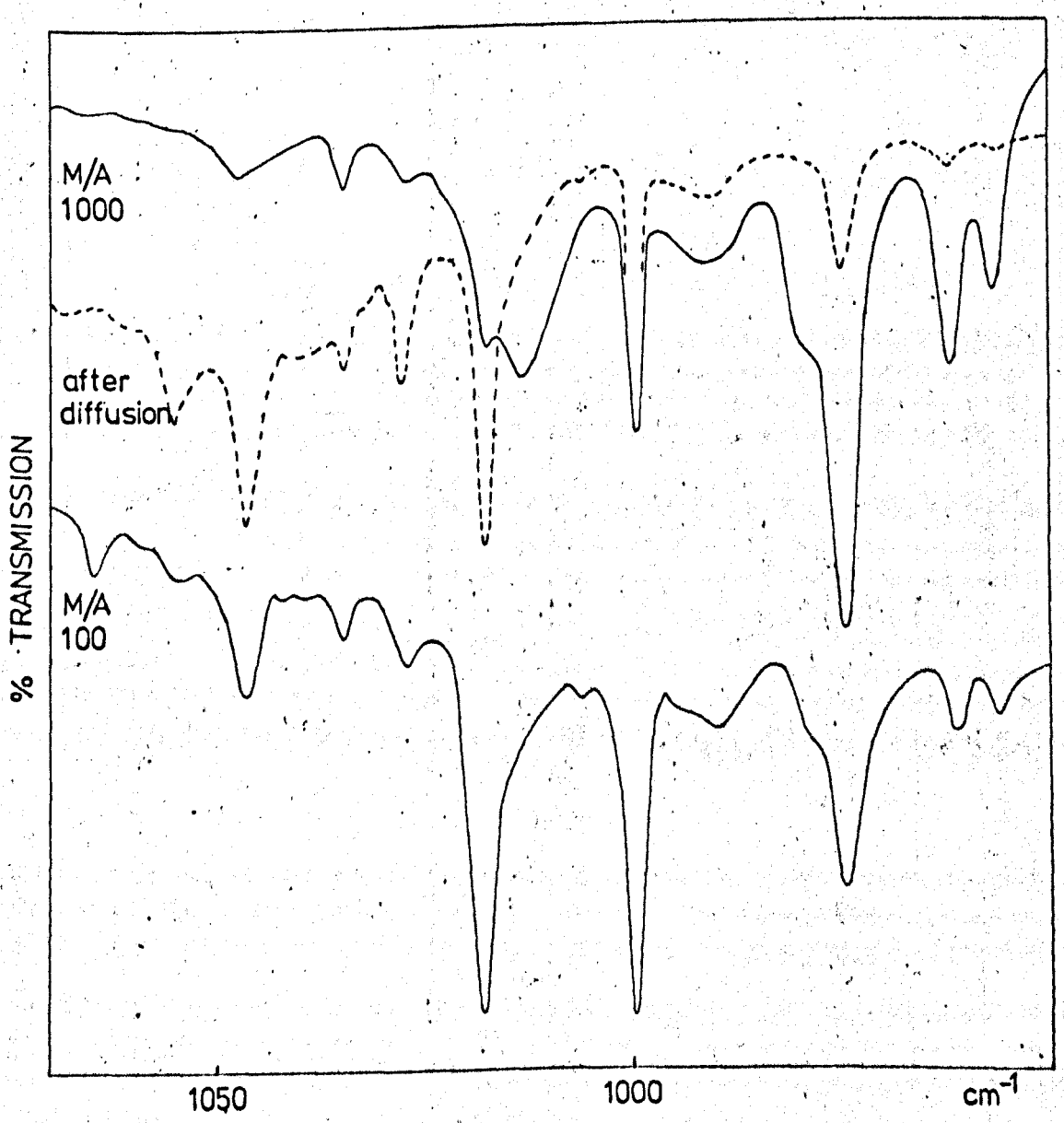

Fig. 7.6 Infrared and Raman Spectra of the ν_1/ν_3 Region of NH_3 in a Nitrogen Matrix at 20 K, showing diffusion effects

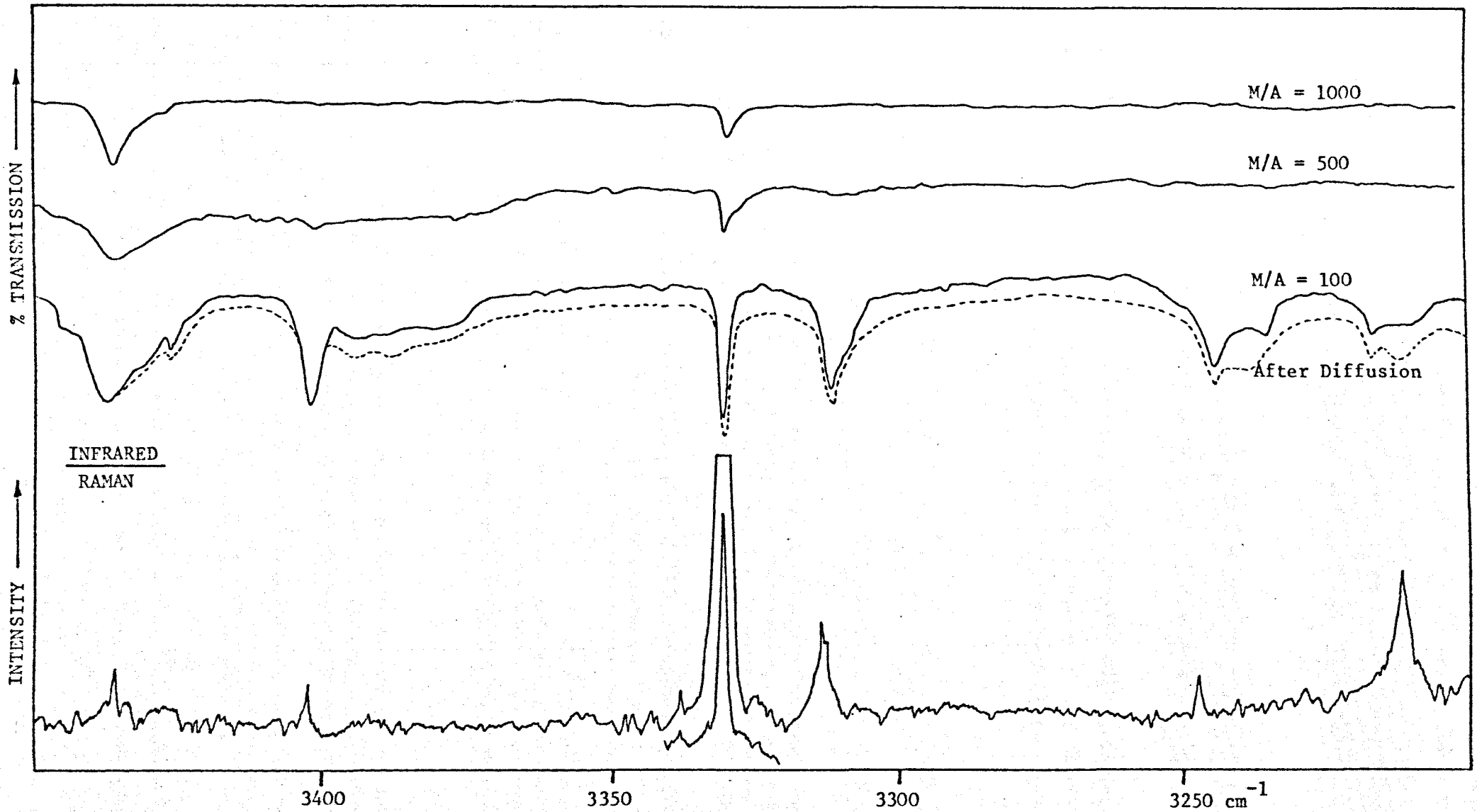

Fig. 7.7 M/A Ratio dependence of the Bands in the ν_2 Region for NH_3 in a Nitrogen Matrix deposited and recorded at 20K.

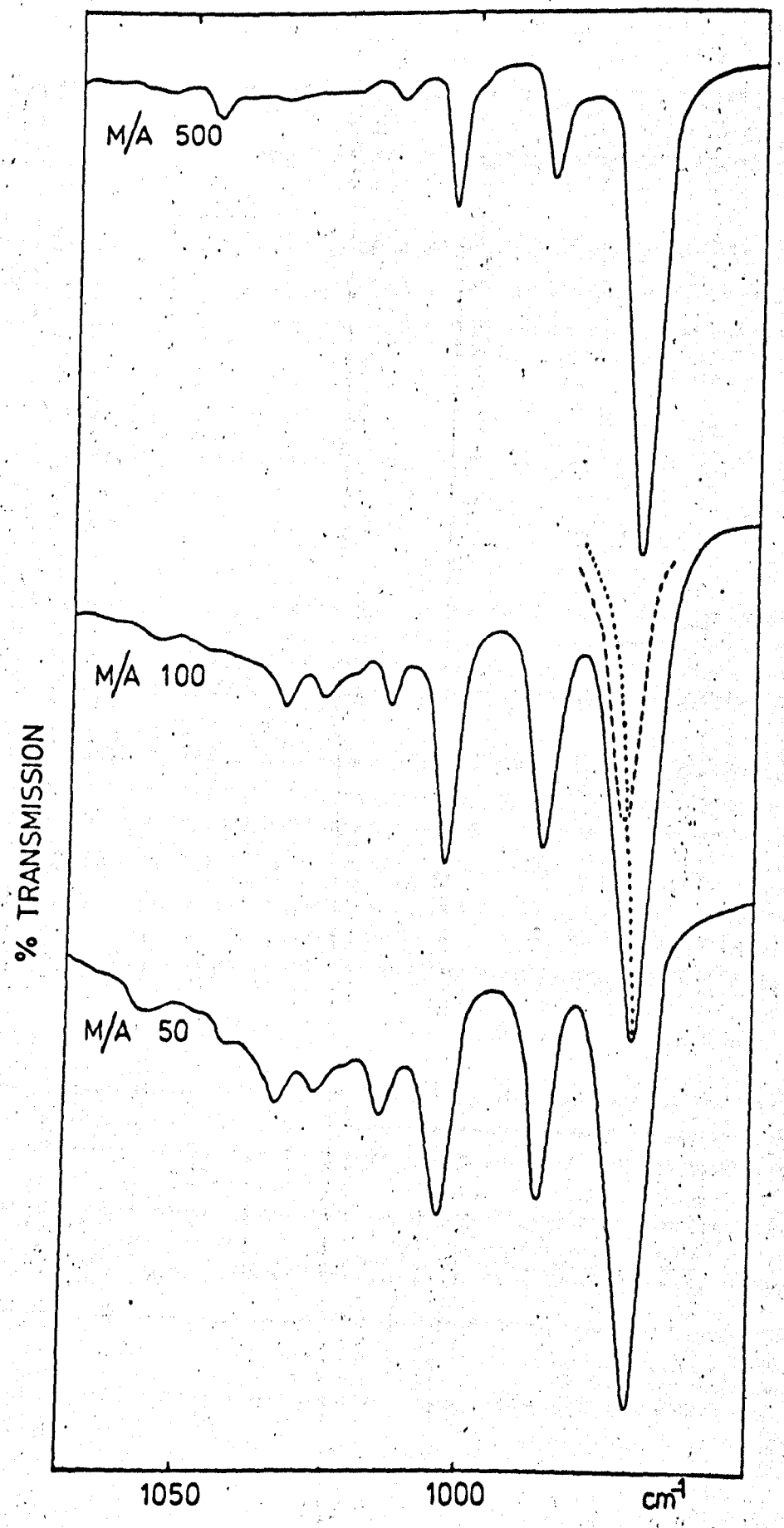

Table 7.2

Infrared and Raman bands observed for ammonia in an argon matrix

Frequency cm^{-1}		Species	Assignment
Infrared	Raman		
3446.6	-	?	
3434.8	3434.3	MONOMER	NH_3 asym. stretching (E)
3429	3429	o.c. dimer	
3421	3424.4	trimer	
3404	-	tetramer	
3400.0	3400.3	o.c. dimer	NH_2 asym. stretching
3389.8	-	trimer	
3376.0	-	tetramer	
∿3360	3351	multimer	
3344	3338.6	?	
3328.8	3327.6	MONOMER	NH_3 sym. stretching (A_1)
3325	3324.6	o.c. dimer	
3309.8	3310.5	o.c. dimer	NH_2 sym. stretching
3304.0	3301.6	trimer	
∿3296	3294	tetramer	
3241	3242	o.c. dimer	NH stretching
∿3235	3231.4	trimer	
3228	3327.6	tetramer	
3210	3213.0	trimer	
-	3206.6	MONOMER	2 ν_4 in Fermi Resonance with ν_1
3202	-	tetramer	NH stretching
1654	-	multimer	NH bending
1643.2	-	o.c. dimer	
1638.4	-	MONOMER	NH_3 asym. bending (E)
1635	-	?	
1620	-	monomer	second site monomer

Table 7.2 (contd.)

Frequency cm^{-1}		Species	Assingment
Infrared	Raman		
1089.0	-	multimer	
1065.0	-	multimer	
1055.0	-	tetramer	
1046.6	∿1050	tetramer	
∿1041	1041		
(1035.0)	-		H_2O/NH_3 dimer
1027.5	1027.5	trimer	
1017.8	-	trimer	NH_3 sym. bending (monomer) or
1014.0	-	MONOMER	NH bending (multimer)
999.7	1002.4	o.c. dimer	
990.8	-	MONOMER	
∿(989)	-	cyclic dimer	
978.6	-	MONOMER	
974.0	-	MONOMER and o.c. dimer	
961.2	-	MONOMER	
955.0	-	MONOMER	
-	222.3	o.c. dimer	N - H ••• N stretch
-	105.0	o.c. dimer	NH_3 rocks
-	∿ 60	o.c. dimer	torsion

Table 7.3

Infrared and Raman bands observed for ammonia in a nitrogen matrix

Frequency cm^{-1}		Species	Assignment
Infrared	Raman		
3446.8	3443.5	?	
3438.3	3438.8	MONOMER	NH_3 asym. stretching (E)
3426.8	-	o.c. dimer	
3402.3	3402.1	o.c. dimer	NH_2 asym. stretching
3394	-	trimer	
3389	-	tetramer	
3380	-	multimer	
3329.5	3330.4	MONOMER	NH_3 sym. stretching (A_1)
-	3327.5	o.c. dimer	
3310.7	3312.7	o.c. dimer	NH_2 sym. stretching
3308.0	3310.2	trimer ?	
3250	3249.2	trimer or cyclic dimer	
3243	3242.2	o.c. dimer	NH stretching
3234	-	trimer	
∿3215	3212.0	MONOMER	2 ν_4 in Fermi Resonance with ν_1
3210	3209.4	trimer	NH stretching
-	3200.6	multimer	
1668	∿1659	multimer	NH bending
1647	-	multimer	
1638	-	dimer	
1630	-	MONOMER	NH_3 asym. bending (E)
1619.0	-	monomer	second site monomer
1616	-	multimer	
1143	-	Monomer	ν_2 + ?
∿1056	-	tetramer	H_2O/NH_3 dimer
(1045)	-		
1042	-	tetramer	
1033	-	tetramer	
1026	-	trimer	
1014.5	-	trimer	NH_3 sym. bending (monomer) or NH bending (multimer)
1004.0	-	o.c. dimer	
986.0	-	cyclic dimer	
(972)	-	o.c. dimer	
969.8	-	MONOMER	

Raman for ammonia isolated in argon or nitrogen matrices along with the temperature of deposition is given in Table 7.1.

7.2 Monomer assignments

The NH stretching region (Figs. 7.2,7.3 and 7.6) is complicated by multimer absorptions in both argon and nitrogen at low M/A ratios. However at high M/A ratios the number of bands in this region decreases and from the M/A ratio dependence and comparison of both the infrared and Raman spectra it is clear that the very high intensity Raman band at 3327.6 cm^{-1} (argon) or 3330.4 cm^{-1} (nitrogen) is the NH symmetric stretch ν_1 corresponding to the weaker absorptions in the infrared at 3328.8 cm^{-1} and 3329.5 cm^{-1} in argon and nitrogen respectively. A band is also observed at 3206.6 cm^{-1} in the Raman spectra due to 2 ν_4 intensified by interaction with ν_1.

The NH antisymmetric stretching vibration ν_3 is more easily observable in the infrared at 3434.8 cm^{-1} and 3438.3 cm^{-1} in argon and nitrogen respectively. This region in the Raman is very weak and only observable at low M/A ratios where it is complicated by the presence of close lying multimer bands. The corresponding monomer ν_3 bands of the Raman results are assigned at 3434.3 cm^{-1} and 3438.3 cm^{-1} for argon and nitrogen matrices respectively.

The degenerate bending ν_4 is difficult to analyse since it lies in the water bending region in the infrared and is too weak to be observable in the Raman. However, bands at 1638.4 cm^{-1} and 1630.0 cm^{-1} in argon and nitrogen respectively are assigned to this mode. In both matrices a "second site" monomer absorption is observed at 1620.0 cm^{-1}.

For the symmetric bending region ν_2 (Figs. 7.5 and 7.7) only one band in nitrogen at 969.8 cm^{-1} is present at high M/A ratio and is assigned to this mode. However six bands at 1014.0, 990.8, 978.6, 974.0. 961.2 and 955.0 cm^{-1} are still present at high M/A ratio in the argon spectra and it must be concluded that they are all due to monomeric ammonia. No monomer bands were observable in the ν_2 region at any M/A ratio in the Raman results.

A band at 1143 cm^{-1} in the infrared in nitrogen present at high M/A ratio is also assigned to monomeric ammonia although it is not observed in the infrared for an argon matrix and it is not observable in the Raman for either matrix. This has been assigned to a combination of ν_2 with a librational mode of the ammonia in the nitrogen matrix {125}.

7.2.1 Discussion of ammonia in an argon matrix

The symmetric stretching mode ν_1 (which has the same symmetry A_1 as the symmetric bending mode ν_2) is extremely strong in the Raman spectra for ammonia isolated in the argon matrix. Spectra have been observed at M/A ratios as high as 500 where bands due to multimer species are negligible. The observed Raman spectrum is compared with that predicted on the rotational model previously used to fit the infrared data in Fig. 7.2 and it can be clearly seen that there is no agreement between the observed and predicted spectra. Only one band due to monomer is observed in the Raman for this mode even at the maximum sensitivity available. This frequency is coincident with the infrared results for the ν_1 mode in argon.

For ammonia to be rotating in the argon matrix, theory

predicts the strongest Raman band will be S(0) and the strongest infrared band to be R(0). It would also mean that the pure rotational transitions (observed in the gas phase using a mercury arc source){128} should also be observable in the low frequency region of the Raman spectra.

From the coincidence of the infrared and Raman bands for the ν_1 vibration and the lack of pure rotational transitions in the Raman spectra it must be concluded that ammonia is not rotating in the matrix. The presence of the apparent rotational lines in the infrared of the ν_2 region is confusing.

Attempts were made to observe bands in the ν_2 region in the Raman spectra to provide further information but despite repeated experimentation which included "C.A.T.ting" the region over 30 hour periods to build up the signal to noise ratio, no bands were observable.

In an attempt to explain the discrepancy between the infrared ν_2 results and the Raman ν_1 results the possibility was considered that although ammonia may not be rotating it may be undergoing some other motional activity within the matrix, such as a reorientation of the molecule within the site which would lead to a similar potential barrier to that of inversion

Miller and Decius {73} have set out a formal group theoretical approach to this type of problem and this was applied to ammonia (C_{3v}) in a substitutional site (Oh) in an argon matrix. An outline of the important points of the theory are given below along with the solution to the above problem.

7.2.2 Theoretical considerations

The approach to the problem uses the methods of group theory developed by Longuet-Higgins {129} and utilises the fact that the Hamiltonian is invariant to interchanges of the position and spins of any set of identical nuclei, an inversion of the positions of all particles in the centre of mass, and the product of such a permutation and an inversion. Let P stand for a permutation, E for the identity, E* for an inversion of all particles, and P* for the product PE* = E*P.

For a molecule isolated in a matrix not all the operations are feasible. This method will be used to determine which operations are feasible and which are not. The symmetry group for the problem then, is the set of all feasible operations. However, before continuing there are several definitions which need to be mentioned.

A permutation or permutation-inversion for a rigid molecule is equivalent to a point group operation on the internal coordinates followed by a bodily rotation of the molecule about an axis through the centre of the mass. This can be represented as $P(r) = Q(r_e - R\rho)$ (7.1)

where R is a point group operation, Q is a rotation, r_e is the 3n dimensional vector describing the equilibrium positions of the atoms, ρ is the corresponding displacement vector, and $r = r_e + \rho$. Once the 1 to 1 mapping between P and R is established it can be shown that the group {R} is isomorphic to the group {P}. The operation R for each P and P* will determine the symmetry of translation and rotation and therefore μ and α.

The group Q is important in classifying the rotational states since it consists of bodily rotations of the molecules.

The group Q is isomorphic to the permutation group unless the molecule possesses a centre of symmetry in which case {Q} is isomorphic to the subgroup of {P} which is just the permutations. Therefore for any group {P} the symmetry of μ and α can be found from {R} and the transformation of the rotational coordinates can be found from {Q}.

For a molecule isolated in a matrix site let us assume that the guest molecule has the symmetry of the point group $\overline{M}$ and it occupies a substitutional site in the host matrix which has the symmetry of the point group S.

Operations in $\overline{M}$ are related to the crystal and space-fixed axes. The point groups $\overline{M}$ and S can be divided into the rotational subgroup of permutations plus the set of permutation inversions. These are denoted as follows:

$$\overline{M} = \overline{M}(P) + \overline{M}(P^*) \qquad \text{and} \qquad S = S(P) + S(P^*) \quad (7.2)$$

If $\overline{M}$ or S is a rotational group then there are no operations of the type P*.

The elements of a group which are appropriate for a guest molecule in a host crystal consist of products of operations in S(P) with operations in $\overline{M}(P)$ and operations in S(P*) with operations in $\overline{M}(P)$. The symmetry of the vibrational, rotational and nuclear spin states can therefore be determined from the combined group. As the movement of the molecule may be expected to be restricted by the host molecules interest is centred on the rotational states and multiplet structure near the high barrier limits, where the motion may be regarded as librational but with the splittings being due to tunnelling between equivalent potential minima. Correlation methods {116} can be employed to aid the

solution of the group theoretical analysis and will enable the description of the splittings of states near the librational limit for any assumed orientation of the molecule at its potential minima with respect to rotation. From the symmetry of the dipole and polarizability tensors, selection rules can be applied to predict the infrared and Raman spectra.

The appropriate group will depend on the freedom of the molecule to rotate with respect to the crystal. The largest possible group is the combination of all operations of S(P) with $\overline{M}(P)$ and all combinations of S(P*) with $\overline{M}(P^*)$. This group will be denoted by $G = (S.\overline{M})$. Some operations in G become less feasible (physically) as the barrier to rotation increases and at the high barrier or librator limit, rotation of the molecule with respect to the crystal is not feasible. The problem necessitates the correlation between the free rotation group G and the high barrier subgroup $\overline{\overline{H}}$, the motional energy levels will then be given as a function of the barrier height. Whether S or $\overline{M}$ is a rotational group or not determines how the group G is formed. For example, if both S and $\overline{M}$ are rotational groups then the order of G is given by $g = s.m$, where g, s and m represent the order of their respective groups, since all combinations are allowed. If either S or $\overline{M}$ is not a rotational group, then $g = \frac{1}{2}s.m$ since combinations of P's with P*'s are not allowed.

At the limit of no rotation the appropriate subgroup of $\overline{\overline{H}}$ is isomorphic ($\cong$) to the highest common subgroup of S and $\overline{M}$ if the molecule is orientated to the crystal in the highest symmetry possible.

An operation in $\overline{\overline{H}}$ consists of the product of an operation in S with an operation in $\overline{M}$ so that there is no rotation of the

molecule relative to the crystal when the molecule is at an equilibrium position.

The librational states in $\bar{\bar{H}}$ have a degeneracy which is increased by the factor g/h (h is the order of $\bar{\bar{H}}$) and this factor is also the number of equivalent minima in the potential with respect to rotation. In certain cases there may be significant groups which lie in between the limits for G and $\bar{\bar{H}}$ as a result of the fact that some relative rotations may be feasible but not all. In this case the group would be a subgroup of $G = (S,\bar{M})$ but the problem would be essentially no different than that for G and $\bar{\bar{H}}$.

7.2.3 Application of the theory to a $\overline{C_{3v}}$ molecule in an Oh field.

We are now in a position to solve this problem with the aid of the above group theory.

For this problem $\bar{M} = \overline{C_{3v}}$ and S = Oh. Since neither S nor $\bar{M}$ is a rotational group but S is a direct product group (with {E,i})

$$S = S(P) \times \{E,i\} \qquad (7.3)$$

whereas $\bar{M}$ is not a direct product group, then G will be the direct product:

$$G = {}'S'(P) \times {}'\bar{M}' \qquad (7.4)$$

where $'S'(P) \cong S$ and $'\bar{M}' \cong \bar{M}$.

This amounts to saying that operations in $'S'(P)$ are products of $\bar{E}$ in $\bar{M}$ with an operation in S(P), operations in $'\bar{M}'(P)$ are products of E in S with an operation in $\bar{M}(P)$, and operations in $'\bar{M}'(P^*)$ are products of i in S with an operation in $M(P^*)$. The character table can now be found from those of $\bar{M}$ and S(P), and the symmetry species are products of those in $\bar{M}$ and S(P).

It follows that from equation 7.4

$$G = \text{'O' x '}\overline{C_{3v}}\text{'} \qquad (7.5)$$

The {Q}group for O is O and the {Q}group for C_{3v} is D_3 {73}.

Therefore the group for the rotational problem is

$$G = O \times D_3 \qquad (7.6$$

This group is given in Fig. 7.8.

A C_{3v} molecule such as NH_3 in an Oh field may have a potential minimum if the H atoms point toward the corners of the cube, i.e. aligned along a C_3 axis of the cube. This is the position that ammonia is thought to occupy in the Oh substitutional site of an argon matrix, in which case the greatest common subgroup for Oh and C_{3v} is C_{3v}. So at the librator limit it is assumed that $\bar{\bar{H}} = C_{3v}$, where the order (h) of $\bar{\bar{H}} = 6$.

The character table and correlation between G and $\bar{\bar{H}}$ is given in Fig. 7.8.

It is seen that $\bar{\bar{H}} = \{E\bar{E}, C_3\bar{C}_3, C_2'\bar{C}_2\}$ since it is clear that $E\bar{E}$, $C_3\bar{C}_3$, and $C_2'\bar{C}_2$ are the only products from $G = (Oh, \overline{C_{3v}})$ which leave the molecule unchanged with respect to rotation relative to the crystal.

Since neither S or $\bar{M}$ is a rotational group the order (g) of G is given by

$$g = \tfrac{1}{2}s.m$$
$$= \tfrac{1}{2}.48.6$$
$$= 144$$

Therefore the librational states in $\bar{\bar{H}}$ have a degeneracy increased by a factor of g/h = 144/6 = 24. This is in fact the case as seen from Fig. 7.8.

Fig. 7.8

Character table for $(Oh, \overline{C_{3v}})$ and correlation to the group $\overline{\overline{C_{3v}}}$

	$\overline{1E}$	$\overline{8C_3}$	$\overline{3C_2}$	$\overline{6C_4}$	$\overline{6C'_2}$	$\overline{2EC_3}$	$\overline{16C_3C_3}$	$\overline{6C_2C_3}$	$\overline{12C_4C_3}$	$\overline{12C'_2C_3}$	$\overline{3EC_2}$	$\overline{24C_3C_2}$	$\overline{9C_2C_2}$	$\overline{18C_4C_2}$	$\overline{18C'_2C_2}$	$H = C_{3v}$
$A_1\overline{A}_1$	1	1	1	1	1	1	1	1	1	1	1	1	1	1	1	A_1
$A_1\overline{A}_2$	1	1	1	1	1	1	1	1	1	1	-1	-1	-1	-1	-1	A_2
$A_1\overline{E}$	2	2	2	2	2	-1	-1	-1	-1	-1	0	0	0	0	0	E
$A_2\overline{A}_1$	1	1	1	-1	-1	1	1	1	-1	-1	1	1	1	-1	-1	A_2
$A_2\overline{A}_2$	1	1	1	-1	-1	1	1	1	-1	-1	-1	-1	-1	1	1	A_1
$A_2\overline{E}$	2	2	2	-2	-2	-1	-1	-1	1	1	0	0	0	0	0	E
$E\ \overline{A}_1$	2	-1	2	0	0	2	-1	2	0	0	2	-1	2	0	0	E
$E\ \overline{A}_2$	2	-1	2	0	0	2	-1	2	0	0	-2	1	-2	0	0	E
$E\ \overline{E}$	4	-2	4	0	0	-2	1	-2	0	0	0	0	0	0	0	$A_1 + A_2 + E$
$F_1\overline{A}_1$	3	0	-1	1	-1	3	0	-1	1	-1	3	0	-1	1	-1	$A_2 + E$
$F_1\overline{A}_2$	3	0	-1	1	-1	3	0	-1	1	-1	-3	0	1	-1	1	$A_1 + E$
$F_1\overline{E}$	6	0	-2	2	-2	-3	0	1	-1	1	0	0	0	0	0	$A_1 + A_2 + 2E$
$F_2\overline{A}_1$	3	0	-1	-1	1	3	0	-1	-1	1	3	0	-1	-1	1	$A_1 + E$
$F_2\overline{A}_2$	3	0	-1	-1	1	3	0	-1	-1	1	-3	0	1	1	-1	$A_2 + E$
$F_2\overline{E}$	6	0	-2	-2	2	-3	0	1	1	-1	0	0	0	0	0	$A_1 + A_2 + 2E$

Fig. 7.9 Multiplication Table for the group $G=(O_h, \overline{C_{3v}})$.

	$A_1\bar{A}_1$	$A_1\bar{A}_2$	$A_1\bar{E}$	$A_2\bar{A}_1$	$A_2\bar{A}_2$	$A_2\bar{E}$	$E\bar{A}_1$	$E\bar{A}_2$	$E\bar{E}$	$F_1\bar{A}_1$	$F_1\bar{A}_2$	$F_1\bar{E}$	$F_2\bar{A}_1$	$F_2\bar{A}_2$	$F_2\bar{E}$
$A_1\bar{A}_1$	$A_1\bar{A}_1$	$A_1\bar{A}_2$	$A_1\bar{E}$	$A_2\bar{A}_1$	$A_2\bar{A}_2$	$A_2\bar{E}$	$E\bar{A}_1$	$E\bar{A}_2$	$E\bar{E}$	$F_1\bar{A}_1$	$F_1\bar{A}_2$	$F_1\bar{E}$	$F_2\bar{A}_1$	$F_2\bar{A}_2$	$F_2\bar{E}$
$A_1\bar{A}_2$	$A_1\bar{A}_2$	$A_1\bar{A}_1$	$A_1\bar{E}$	$A_2\bar{A}_2$	$A_2\bar{A}_1$	$A_2\bar{E}$	$E\bar{A}_2$	$E\bar{A}_1$	$E\bar{E}$	$F_1\bar{A}_2$	$F_1\bar{A}_1$	$F_1\bar{E}$	$F_2\bar{A}_2$	$F_2\bar{A}_1$	$F_2\bar{E}$
$A_1\bar{E}$	$A_1\bar{E}$	$A_1\bar{E}$	$A_1\bar{A}_1 + A_1\bar{A}_2 + A_1\bar{E}$	$A_2\bar{E}$	$A_2\bar{E}$	$A_2\bar{A}_1 + A_2\bar{A}_2 + A_2\bar{E}$	$E\bar{E}$	$E\bar{E}$	$E\bar{A}_1 + E\bar{A}_2 + E\bar{E}$	$F_1\bar{E}$	$F_1\bar{E}$	$F_1\bar{A}_1 + F_1\bar{A}_2 + F_1\bar{E}$	$F_2\bar{E}$	$F_2\bar{E}$	$F_2\bar{A}_1 + F_2\bar{A}_2 + F_2\bar{E}$
$A_2\bar{A}_1$	$A_2\bar{A}_1$	$A_2\bar{A}_2$	$A_2\bar{E}$	$A_1\bar{A}_1$	$A_1\bar{A}_2$	$A_1\bar{E}$	$E\bar{A}_1$	$E\bar{A}_2$	$E\bar{E}$	$F_2\bar{A}_1$	$F_2\bar{A}_2$	$F_2\bar{E}$	$F_1\bar{A}_1$	$F_1\bar{A}_2$	$F_1\bar{E}$
$A_2\bar{A}_2$	$A_2\bar{A}_2$	$A_2\bar{A}_1$	$A_2\bar{E}$	$A_1\bar{A}_2$	$A_1\bar{A}_1$	$A_1\bar{E}$	$E\bar{A}_2$	$E\bar{A}_1$	$E\bar{E}$	$F_2\bar{A}_2$	$F_2\bar{A}_1$	$F_2\bar{E}$	$F_1\bar{A}_2$	$F_1\bar{A}_1$	$F_1\bar{E}$
$A_2\bar{E}$	$A_2\bar{E}$	$A_2\bar{E}$	$A_2\bar{A}_1 + A_2\bar{A}_2 + A_2\bar{E}$	$A_1\bar{E}$	$A_1\bar{E}$	$A_1\bar{A}_1 + A_1\bar{A}_2 + A_1\bar{E}$	$E\bar{E}$	$E\bar{E}$	$E\bar{A}_1 + E\bar{A}_2 + E\bar{E}$	$F_2\bar{E}$	$F_2\bar{E}$	$F_2\bar{A}_1 + F_2\bar{A}_2 + F_2\bar{E}$	$F_1\bar{E}$	$F_1\bar{E}$	$F_1\bar{A}_1 + F_1\bar{A}_2 + F_1\bar{E}$
$E\bar{A}_1$	$E\bar{A}_1$	$E\bar{A}_2$	$E\bar{E}$	$E\bar{A}_1$	$E\bar{A}_2$	$E\bar{E}$	$A_1\bar{A}_1 + A_2\bar{A}_1 + E\bar{A}_1$	$A_1\bar{A}_2 + A_2\bar{A}_2 + E\bar{A}_2$	$A_1\bar{E} + A_2\bar{E} + E\bar{E}$	$F_1\bar{A}_1 + F_2\bar{A}_1$	$F_1\bar{A}_2 + F_2\bar{A}_2$	$F_1\bar{E} + F_2\bar{E}$	$F_1\bar{A}_1 + F_2\bar{A}_1$	$F_1\bar{A}_2 + F_2\bar{A}_2$	$F_1\bar{E} + F_2\bar{E}$
$E\bar{A}_2$	$E\bar{A}_2$	$E\bar{A}_1$	$E\bar{E}$	$E\bar{A}_2$	$E\bar{A}_1$	$E\bar{E}$	$A_1\bar{A}_2 + A_2\bar{A}_2 + E\bar{A}_2$	$A_1\bar{A}_1 + A_2\bar{A}_1 + E\bar{A}_1$	$A_1\bar{E} + A_2\bar{E} + E\bar{E}$	$F_1\bar{A}_2 + F_2\bar{A}_2$	$F_1\bar{A}_1 + F_2\bar{A}_1$	$F_1\bar{E} + F_2\bar{E}$	$F_1\bar{A}_2 + F_2\bar{A}_2$	$F_1\bar{A}_1 + F_2\bar{A}_1$	$F_1\bar{E} + F_2\bar{E}$
$E\bar{E}$	$E\bar{E}$	$E\bar{E}$	$E\bar{A}_1 + E\bar{A}_2 + E\bar{E}$	$E\bar{E}$	$E\bar{E}$	$E\bar{A}_1 + E\bar{A}_2 + E\bar{E}$	$A_1\bar{E} + A_2\bar{E} + E\bar{E}$	$A_1\bar{E} + A_2\bar{E} + E\bar{E}$	All combinations of E's & A's	$F_1\bar{E} + F_2\bar{E}$	$F_1\bar{E} + F_2\bar{E}$	$F_1\bar{A}_1 + F_1\bar{A}_2 + F_1\bar{E} + F_2\bar{A}_1 + F_2\bar{A}_2 + F_2\bar{E}$	$F_1\bar{E} + F_2\bar{E}$	$F_1\bar{E} + F_2\bar{E}$	$F_1\bar{A}_1 + F_1\bar{A}_2 + F_1\bar{E} + F_2\bar{A}_1 + F_2\bar{A}_2 + F_2\bar{E}$
$F_1\bar{A}_1$	$F_1\bar{A}_1$	$F_1\bar{A}_2$	$F_1\bar{E}$	$F_2\bar{A}_1$	$F_2\bar{A}_2$	$F_2\bar{E}$	$F_1\bar{A}_1 + F_2\bar{A}_1$	$F_1\bar{A}_2 + F_2\bar{A}_2$	$F_1\bar{E} + F_2\bar{E}$	$A_1\bar{A}_1 + E\bar{A}_1 + F_1\bar{A}_1 + F_2\bar{A}_1$	$A_1\bar{A}_2 + E\bar{A}_2 + F_1\bar{A}_2 + F_2\bar{A}_2$	$A_1\bar{E} + E\bar{E} + F_1\bar{E} + F_2\bar{E}$	$A_2\bar{A}_1 + E\bar{A}_1 + F_1\bar{A}_1 + F_2\bar{A}_1$	$A_2\bar{A}_2 + E\bar{A}_2 + F_1\bar{A}_2 + F_2\bar{A}_2$	$A_2\bar{E} + E\bar{E} + F_1\bar{E} + F_2\bar{E}$
$F_1\bar{A}_2$	$F_1\bar{A}_2$	$F_1\bar{A}_1$	$F_1\bar{E}$	$F_2\bar{A}_2$	$F_2\bar{A}_1$	$F_2\bar{E}$	$F_1\bar{A}_2 + F_2\bar{A}_2$	$F_1\bar{A}_1 + F_2\bar{A}_1$	$F_1\bar{E} + F_2\bar{E}$	$A_1\bar{A}_2 + E\bar{A}_2 + F_1\bar{A}_2 + F_2\bar{A}_2$	$A_1\bar{A}_1 + E\bar{A}_1 + F_1\bar{A}_1 + F_2\bar{A}_1$	$A_1\bar{E} + E\bar{E} + F_1\bar{E} + F_2\bar{E}$	$A_2\bar{A}_2 + E\bar{A}_2 + F_1\bar{A}_2 + F_2\bar{A}_2$	$A_2\bar{A}_1 + E\bar{A}_1 + F_1\bar{A}_1 + F_2\bar{A}_1$	$A_2\bar{E} + E\bar{E} + F_1\bar{E} + F_2\bar{E}$
$F_1\bar{E}$	$F_1\bar{E}$	$F_1\bar{E}$	$F_1\bar{A}_1 + F_1\bar{A}_2 + F_1\bar{E}$	$F_2\bar{E}$	$F_2\bar{E}$	$F_2\bar{A}_1 + F_2\bar{A}_2 + F_2\bar{E}$	$F_1\bar{E} + F_2\bar{E}$	$F_1\bar{E} + F_2\bar{E}$	$F_1\bar{A}_1 + F_1\bar{A}_2 + F_1\bar{E} + F_2\bar{A}_1 + F_2\bar{A}_2 + F_2\bar{E}$	$A_1\bar{E} + E\bar{E} + F_1\bar{E} + F_2\bar{E}$	$A_1\bar{E} + E\bar{E} + F_1\bar{E} + F_2\bar{E}$	All except $(A_1\bar{A}_1 + A_1\bar{A}_2 + A_1\bar{E})$	$A_2\bar{E} + E\bar{E} + F_1\bar{E} + F_2\bar{E}$	$A_2\bar{E} + E\bar{E} + F_1\bar{E} + F_2\bar{E}$	All except $(A_1\bar{A}_1 + A_1\bar{A}_2 + A_1\bar{E})$
$F_2\bar{A}_1$	$F_2\bar{A}_1$	$F_2\bar{A}_2$	$F_2\bar{E}$	$F_1\bar{A}_1$	$F_1\bar{A}_2$	$F_1\bar{E}$	$F_1\bar{A}_1 + F_2\bar{A}_1$	$F_1\bar{A}_2 + F_2\bar{A}_2$	$F_1\bar{E} + F_2\bar{E}$	$A_2\bar{A}_1 + E\bar{A}_1 + F_1\bar{A}_1 + F_2\bar{A}_1$	$A_2\bar{A}_2 + E\bar{A}_2 + F_1\bar{A}_2 + F_2\bar{A}_2$	$A_2\bar{E} + E\bar{E} + F_1\bar{E} + F_2\bar{E}$	$A_1\bar{A}_1 + E\bar{A}_1 + F_1\bar{A}_1 + F_2\bar{A}_1$	$A_1\bar{A}_2 + E\bar{A}_2 + F_1\bar{A}_2 + F_2\bar{A}_2$	$A_1\bar{E} + E\bar{E} + F_1\bar{E} + F_2\bar{E}$
$F_2\bar{A}_2$	$F_2\bar{A}_2$	$F_2\bar{A}_1$	$F_2\bar{E}$	$F_1\bar{A}_2$	$F_1\bar{A}_1$	$F_1\bar{E}$	$F_1\bar{A}_2 + F_2\bar{A}_2$	$F_1\bar{A}_1 + F_2\bar{A}_1$	$F_1\bar{E} + F_2\bar{E}$	$A_2\bar{A}_2 + E\bar{A}_2 + F_1\bar{A}_2 + F_2\bar{A}_2$	$A_2\bar{A}_1 + E\bar{A}_1 + F_1\bar{A}_1 + F_2\bar{A}_1$	$A_2\bar{E} + E\bar{E} + F_1\bar{E} + F_2\bar{E}$	$A_1\bar{A}_2 + E\bar{A}_2 + F_1\bar{A}_2 + F_2\bar{A}_2$	$A_1\bar{A}_1 + E\bar{A}_1 + F_1\bar{A}_1 + F_2\bar{A}_1$	$A_1\bar{E} + E\bar{E} + F_1\bar{E} + F_2\bar{E}$
$F_2\bar{E}$	$F_2\bar{E}$	$F_2\bar{E}$	$F_2\bar{A}_1 + F_2\bar{A}_2 + F_2\bar{E}$	$F_1\bar{E}$	$F_1\bar{E}$	$F_1\bar{A}_1 + F_1\bar{A}_2 + F_1\bar{E}$	$F_1\bar{E} + F_2\bar{E}$	$F_1\bar{E} + F_2\bar{E}$	$F_1\bar{A}_1 + F_1\bar{A}_2 + F_1\bar{E} + F_2\bar{A}_1 + F_2\bar{A}_2 + F_2\bar{E}$	$A_2\bar{E} + E\bar{E} + F_1\bar{E} + F_2\bar{E}$	$A_2\bar{E} + E\bar{E} + F_1\bar{E} + F_2\bar{E}$	All except $(A_1\bar{A}_1 + A_1\bar{A}_2 + A_2\bar{E})$	$A_1\bar{E} + E\bar{E} + F_1\bar{E} + F_2\bar{E}$	$A_1\bar{E} + E\bar{E} + F_1\bar{E} + F_2\bar{E}$	All except $(A_2\bar{A}_1 + A_2\bar{A}_2 + A_2\bar{E})$

The first excited librator states in $\overline{C}_{3v}$ are of symmetry $A_1 + E$ but before the number of transitions from the A_1 level can be worked out, the selection rules for the various types of transitions that are possible must be found.

Since neither S nor $\overline{M}$ is a rotational group but S is a direct product group all the molecular symmetries have their usual symmetry species from M, including the electric tensors in internal coordinates, multiplied by the totally symmetric species from S(P). Therefore in internal axes the symmetry of μ is $A_1\overline{A}_1 + A_1\overline{E}$ and the symmetry of α is $A_1\overline{A}_1 + A_1\overline{E}$.

The symmetry species for a quantity in external axes has the symmetry species in S(P), times either the totally symmetric species or antisymmetric species from $\overline{M}$ ($= C_{3v}$) depending on whether the symmetry species in S was symmetric or antisymmetric to the operation involved in the direct product (i or h). Since S ($= Oh$) contains i then μ(external) has the antisymmetric species in $\overline{M}$; this is because μ is ungerade and α is gerade with respect to i.

Therefore in external axes the symmetry of μ is $F_1\overline{A}_2$ and the symmetry of α is $A_1\overline{A}_1 + E\overline{A}_1 + F_2\overline{A}_1$.

Before discussing the possible types of transitions involved it is important to distinguish between two classes of transitions involving the librational modes. In the first category the librational quantum number (which becomes an oscillator quantum number in the high barrier limit), does not change, but a transition between levels for a single librational state split by tunnelling occurs. These can be regarded as tunnelling transitions, but they will be described here conveniently as "orientation transitions".

In the second category there are changes in the librational quantum numbers: These will be described simply as "librational" transitions. Thus we may speak about pure orientation, pure libration, vibration-orientation, or vibration-libration transitions, reserving the latter two terms for cases in which an internal vibration undergoes a transition simultaneously with changes in the "rotational states".

We must first consider the librational transitions from the $n = 0$ (A_1) level to the $n = 1$ ($A_1 + E$) level in both the infrared and Raman. The correlation in G as seen from Fig. 7.8 is

$$A_1 = A_1\bar{A}_1 + A_2\bar{A}_2 + E\bar{E} + F_1\bar{A}_2 + F_1\bar{E} + F_2\bar{A}_1 + F_2\bar{E}$$

$$E = A_1\bar{E} + A_2\bar{E} + E\bar{A}_1 + E\bar{A}_2 + E\bar{E} + F_1\bar{A}_1 + F_1\bar{A}_2 + 2F_1\bar{E} + F_2\bar{A}_1 + F_2\bar{A}_2 + 2F_2\bar{E}$$

The allowed infrared and Raman librational or orientation transitions are determined by the selection rules in external axes.

i.e. $\Gamma(\mu) = F_1\bar{A}_2$

and $\Gamma(\alpha) = A_1\bar{A}_1 + E\bar{A}_1 + F_2\bar{A}_1$

If the product of the transition contains one of the irreducible representations for the infrared and Raman given above then that transition will be allowed.

The nuclear spin wave function for ammonia ($I_H = \frac{1}{2}$) is $4A_1\bar{A}_1 + 2A_1\bar{E}$ {130}. The overall wavefunction must be $\Gamma\bar{A}_2$ (as H is a fermion) where $\Gamma = A_1, A_2, E, F_1$ or F_2.

Assuming the vibronic symmetry is $\bar{A}_1$, it follows that for $I_H = \frac{1}{2}$ only $\Gamma\bar{A}_2$ or $\Gamma\bar{E}$ librational states can exist.

Fig. 7.10

Vibration-libration transitions in the infrared and Raman for the n = 0 to n = 1 librational mode

(a) INFRARED

A_1 —— A_1 transition

$A_1\bar{A}_1 \longrightarrow F_1\bar{A}_2$

$A_2\bar{A}_2 \longrightarrow F_2\bar{A}_1$

$E\bar{E} \longrightarrow F_1\bar{E}, F_2\bar{E}$

$F_1\bar{A}_2 \longrightarrow A_1\bar{A}_1, F_2\bar{A}_1$

$F_1\bar{E} \longrightarrow E\bar{E}, F_1\bar{E}, F_2\bar{E}$

$F_2\bar{A}_1 \longrightarrow A_2\bar{A}_2, F_1\bar{E}$

$F_2\bar{E} \longrightarrow E\bar{E}, F_1\bar{E}, F_2\bar{E}$

A_1 —— E transition

$A_1\bar{A}_1 \longrightarrow F_1\bar{A}_2$

$A_2\bar{A}_2 \longrightarrow F_2\bar{A}_1$

$E\bar{E} \longrightarrow F_1\bar{E}, F_2\bar{E}$

$F_1\bar{A}_2 \longrightarrow E\bar{A}_1, F_1\bar{A}_1, F_2\bar{A}_1$

$F_1\bar{E} \longrightarrow A_1\bar{E}, E\bar{E}, 2F_1\bar{E}, 2F_2\bar{E}$

$F_2\bar{A}_1 \longrightarrow E\bar{A}_2, F_1\bar{A}_2, F_2\bar{A}_2$

$F_2\bar{E} \longrightarrow A_2\bar{E}, E\bar{E}, 2F_1\bar{E}, 2F_2\bar{E}$

Fig. 7.10

(b) RAMAN

A_1 —— E transition

$A_1\bar{A}_1 \longrightarrow A_1\bar{A}_1,\ F_2\bar{A}_1$

$A_2\bar{A}_2 \longrightarrow A_2\bar{A}_2,\ F_1\bar{A}_2$

$E\bar{E} \longrightarrow 2E\bar{E},\ F_1\bar{E},\ F_2\bar{E}$

$F_1\bar{A}_2 \longrightarrow A_2\bar{A}_2,\ F_1\bar{A}_2,\ F_1\bar{E}$

$F_1\bar{E} \longrightarrow E\bar{E},\ 3F_1\bar{E},\ 2F_2\bar{E}$

$F_2\bar{A}_1 \longrightarrow A_1\bar{A}_1,\ F_2\bar{A}_1,\ F_2\bar{E}$

$F_2\bar{E} \longrightarrow E\bar{E},\ 2F_1\bar{E},\ 3F_2\bar{E}$

A_1 —— E transition

$A_1\bar{A}_1 \longrightarrow E\bar{A}_1,\ F_2\bar{A}_1$

$A_2\bar{A}_2 \longrightarrow E\bar{A}_2,\ F_1\bar{A}_2$

$E\bar{E} \longrightarrow 2E\bar{E},\ A_1\bar{E},\ A_2\bar{E},\ F_1\bar{E},\ F_2\bar{E}$

$F_1\bar{A}_2 \longrightarrow 2F_1\bar{A}_2,\ F_2\bar{A}_2$

$F_1\bar{E} \longrightarrow E\bar{E},\ 3F_1\bar{E},\ 2F_2\bar{E}$

$F_2\bar{A}_1 \longrightarrow 2F_2\bar{A}_1,\ F_1\bar{A}_1$

$F_2\bar{E} \longrightarrow E\bar{E},\ 2F_1\bar{E},\ 3F_2\bar{E}$

Fig. 7.11

Vibration-orientation transitions in the infrared and Raman

(a) INFRARED

For an $A_1\bar{A}_1$ vibration

Selection rule is $A_1A_1 \times \Gamma(\mu)(\text{ext}) = F_1\bar{A}_2$

$A_2\bar{A}_2 \longrightarrow F_2\bar{A}_1$

$E\bar{E} \longrightarrow F_1\bar{E}, F_2\bar{E}$

$F_1\bar{A}_2 \longrightarrow A_1\bar{A}_1$

$F_1\bar{E} \longrightarrow E\bar{E}, F_2\bar{E}$

$F_2\bar{E} \longrightarrow E\bar{E}, F_1\bar{E}$

For an $A_1\bar{E}$ vibration

Selection rule is $A_1\bar{E} \times \Gamma(\mu)(\text{ext}) = F_1\bar{E}$

$A_2\bar{A}_2 \longrightarrow F_2\bar{E}$

$E\bar{E} \longrightarrow F_1\bar{A}_2, F_1\bar{E}, F_2\bar{E}, F_2\bar{A}_1$

$F_1\bar{A}_2 \longrightarrow E\bar{E}, F_1\bar{E}, F_2\bar{E}$

$F_1\bar{E} \longrightarrow F_1\bar{A}_2, F_1\bar{E}, F_2\bar{E}, F_2\bar{A}_1, A_1\bar{A}_1$

$F_2\bar{E} \longrightarrow F_1\bar{A}_2, F_1\bar{E}, F_2\bar{E}, F_2\bar{A}_1, A_2\bar{A}_2$

Fig. 7.11

(b) RAMAN

For an $A_1\bar{A}_1$ vibration

Selection rule is $A_1\bar{A}_1 \times \Gamma(\alpha)(\text{ext}) = A_1\bar{A}_1 + E\bar{A}_1 + F_2\bar{A}_1$

$A_2\bar{A}_2 \longrightarrow F_1\bar{A}_2$

$E\bar{E} \longrightarrow F_1\bar{E}, F_2\bar{E}$

$F_1\bar{A}_2 \longrightarrow A_2\bar{A}_2$

$F_1\bar{E} \longrightarrow E\bar{E}, F_2\bar{E}$

$F_2\bar{E} \longrightarrow E\bar{E}, F_1\bar{E}$

For an $A_1\bar{E}$ vibration

Selection rule is $A_1\bar{E} \times \Gamma(\mu)(\text{ext}) = A_1\bar{E} + E\bar{E} + F_2\bar{E}$

$A_2\bar{A}_2 \longrightarrow E\bar{E}, F_1\bar{E}$

$E\bar{E} \longrightarrow F_1\bar{A}_2, F_2\bar{A}_1, F_1\bar{E}, F_2\bar{E}$

$F_1\bar{A}_2 \longrightarrow 3F_1\bar{E}, 2F_2\bar{E}, E\bar{E}$

$F_1\bar{E} \longrightarrow A_2\bar{A}_2, F_1\bar{A}_2, F_2\bar{A}_1, F_1\bar{E}, F_2\bar{E}$

$F_2\bar{E} \longrightarrow A_1\bar{A}_1, F_1\bar{A}_2, F_2\bar{A}_1, F_1\bar{E}, F_2\bar{E}$

The vibrational activity in the infrared and Raman effect follows the selection rules of the internal axes. The overall transitions are governed by the selection rules in the external axes and some vibration-orientation or vibration-libration transitions may be formally allowed. From the symmetry of μ and α in internal axes $A_1\bar{A}_1$ and $A_1\bar{E}$ vibrations are allowed in the infrared and Raman.

The selection rule for vibration-orientation or vibration-libration is given by $\Gamma(\mu)(\text{int}) \times \Gamma(\mu)(\text{ext})$. For an $A_1\bar{A}_1$ vibration in the infrared this is $\Gamma(\mu) = F_1\bar{A}_2$ and for an $A_1\bar{E}$ vibration the selection rule is $\Gamma(\mu) = F_1\bar{E}$.

In the Raman the selection rule for vibration-orientation or vibration-libration is $\Gamma(\alpha)(\text{int}) \times \Gamma(\alpha)(\text{ext})$ so for an $A_1\bar{A}_1$ vibration this is $\Gamma(\alpha) = A_1\bar{A}_1 + E\bar{A}_1 + F_2\bar{A}_1$ and for an $A_1\bar{E}$ vibration it is $\Gamma(\alpha) = A_1\bar{E} + E\bar{E} + F_2\bar{E}$.

It must be noted that a transition to the same internal level is only allowed if all the selection rules are included in the product.

Using these selection rules vibration-libration and vibration-orientation transitions in the infrared and Raman can be obtained with the aid of the multiplication table given in Fig. 7.9. These are given in Figs. 7.10 and 7.11.

7.2.4 Conclusions

There are three types of motion (apart from vibration) that ammonia might be undergoing in the substitutional site of the argon matrix.

1) Rotation (and inversion) — low barrier.

2) Libration-Orientation — medium barrier.

3) Libration — high barrier.

The rotational possibility has already been discussed in detail in 7.2.1 above, the main points in the argument against rotation taking place being the coincidence of the infrared and Raman bands of the ν_1 symmetric stretch and the lack of pure rotational transitions in the Raman.

Orientation may be interpreted physically as a movement of the molecule within the matrix site through successive potential minima (24 altogether). This should therefore result in fine structure being observed on the vibrational bands provided the splitting is large enough. The size of the splitting would depend on the potential barrier. Vibration-libration transitions should also be observable, in principle. In the high barrier limit libration is the only possible motion. No librational transitions were observed in the low frequency region, and the fine structure of the ν_2 vibration in the infrared spectrum is too complex to be explained on a purely librational model - which predicts only a $\nu_2 + \nu_{lib}$ band.

From Fig. 7.11 it can be seen that for an $A_1\bar{A}_1$ vibration the vibration-orientation transitions in the infrared approximate to those in the Raman. Since there is obvious structure in the ν_2 region in the infrared for the argon matrix and coincidence between the infrared and Raman for ν_1, the vibration-orientation model fits the results reasonably if one assumes that these "tunnelling" transitions will cause appreciable splitting on ν_2 and not on ν_1. It also has to be assumed that the vibration-libration transitions are too weak to be observed. The first assumption is not too unreasonable since for inversion"tunnelling" transitions which occur in the gas phase spectrum of ammonia the

splitting of ν_2 is much greater than that for ν_1. Since the vibration-libration transitions will also have a complex structure the resulting broad absorptions may be too weak to observe. Verification or contradiction of the hypothesis that the structure of the ν_2 absorption in the infrared is due to vibration-orientation can only be achieved by obtaining a spectrum of the ν_2 region in the Raman, which is not possible with the present equipment.

7.3 Multimer assignments

From the M/A dependence and controlled diffusion experiments for ammonia in argon and nitrogen matrices many bands due to multimer species have been identified in this work. Assignments are given in Tables 7.2 and 7.3.

Fig. 7.3 demonstrates the effect of changing the M/A ratio of ammonia in an argon matrix on the NH stretching region and also the effects of the diffusion operation.

7.3.1 NH antisymmetric stretching (E)

In the NH antisymmetric stretching ν_3 region there are several bands displaying different M/A ratio dependence in the infrared relative to the monomer band at 3434.8 cm^{-1}. This band is asymmetric at low M/A ratio having a shoulder at 3429 cm^{-1} whose closeness to the monomer band would imply that it is due to an open chain dimer. This dimer also has an absorption at 3400.0 cm^{-1}, trimer and tetramer absorbing to lower frequency at 3389.8 cm^{-1} and 3376.0 cm^{-1} respectively. The latter two bands are the first to disappear on increasing the M/A ratio but always increase their intensity after a diffusion experiment relative to the dimer band at 3400.0 cm^{-1}. A similar pattern of bands is

observed in this region for ammonia isolated in a nitrogen matrix (Fig. 7.6), but there is much less trimer and tetramer present for the same M/A ratio. (This would reflect on the greater isolating efficiency of nitrogen.)

7.3.2 NH symmetric stretching (A_1)

For the NH symmetric stretching ν_1 region again multimer species absorb here to a lower frequency than the weak monomer band at 3328 cm^{-1} for the argon matrix. This band has a shoulder at 3325 cm^{-1} which is resolved in the Raman spectra at 3324.6 cm^{-1} and is reasonably assigned to open chain dimer along with the band at 3309.8 cm^{-1}. The band at 3304.0 cm^{-1} parallels intensity changes with the band at 3389.8 cm^{-1} and is assigned to trimer. It is very weak in the Raman spectra at 3301.6 cm^{-1}.

7.3.3 N — H (... N) stretching

The previous discussion of the NH stretches were of multimer bands arising from the NH stretches of the free NH_3 and NH_2 groups of the multimer species. However several bands are also observed at low M/A ratio due to the NH stretches of the NH bond of the ammonia molecules directly involved in the formation of the hydrogen bond of the multimer species. The latter are found in the 3250-3200 cm^{-1} region and their intensity changes parallel bands in the ν_1 and ν_3 regions. On the basis of the M/A ratio dependence and diffusion experiments for the argon matrix a band at 3241 cm^{-1} is assigned to dimer and bands at $\sim$3235 cm^{-1} and 3210.0 cm^{-1} are assigned to trimers. A band at 3202 cm^{-1} is due to tetramer. The trimer and tetramer bands are observable (but weak) in the Raman results for argon.

A similar pattern of bands occurs for the nitrogen matrix in the infrared and Raman but there is less trimer and tetramer compared to the dimer bands. Diffusion experiments were carried out for the nitrogen matrix results.

7.3.4 NH antisymmetric bending (E)

The NH antisymmetric bending ν_4 region was not studied in great detail in the infrared for either matrix due to its lying in a region of atmospheric absorption. However, tentative assignments have been made for both matrices and are given in Tables 7.2 and 7.3. No bands were observable for the argon matrix in the Raman, and only one band at 1659 cm^{-1} was observable in the Raman for the nitrogen matrix. This band was weak and only observable at low M/A ratio and is presumably due to multimer species.

7.3.5 NH symmetric bending A_1

Fig. 7.5 shows the effect of the M/A ratio dependence and diffusion experiment on the bands of the NH symmetric bending ν_2 region in an argon matrix. There is a certain amount of overlap occurring between monomer and multimer species, which makes identification of the multimer species difficult.

The bands at 1027.5 cm^{-1} and 1017.8 cm^{-1} are assigned to trimer bands whereas the band at 999.7 cm^{-1} is assigned to a dimer species. This is because the trimer bands disappear from the spectra more quickly on increasing the M/A ratio and increase their intensity on carrying out a diffusion experiment at the expense of the band at 999.7 cm^{-1} and the monomer bands. This is presumably as a direct result of diffusion

of monomer to join up with dimer. Bands to higher frequency are assigned to high multimer. Tentative assignments for these bands are given in Table 7.2.

In addition, from the relative intensities of the monomer bands in the argon matrix before and after the diffusion operation there appears to be a multimer band lying under the monomer band at 974 cm^{-1}. This multimer band is extremely close to the monomer band frequency which would imply that it has an open chain structure, most probably open chain dimer.

There are fewer bands in the ν_2 region for ammonia isolated in a nitrogen matrix (Fig. 7.7) but all display M/A ratio dependence relative to the monomer band at 969.8 cm^{-1}. The bands at 1026 and 1014.5 cm^{-1} are assigned to trimer (corresponding to the trimer bands of argon at 1027.5 cm^{-1} and 1017.8 cm^{-1}) and disappear relative to the dimer band at 1004.0 cm^{-1} in nitrogen (corresponding to the dimer band at 999.7 cm^{-1} for argon) as the M/A ratio is increased. There is however an additional band at 986.0 cm^{-1} for the nitrogen matrix results which at first sight appears to behave similarly to the band at 1004.0 cm^{-1} assigned to open chain dimer. However this band, if present in the argon results, must be considerably weaker. From the results of diffusion experiments it may well be under the monomer band at 990.8 cm^{-1}. The second band due to open chain dimer lies close to the monomer band (see below) thus the band at 986.0 cm^{-1} is due to a different dimer species of which a cyclic structure is the most likely.

For the nitrogen matrix the monomer band at 969.8 cm^{-1} is highly asymmetric at low M/A ratio implying that there is another band overlapping but not resolved. By the use of a curve analysis

technique (Fig. 7.7), the band is estimated to have a frequency of $\sim$ 972 cm^{-1}. Its close proximity to the monomer band implies that it is due to open chain dimer corresponding to the band at 974 cm^{-1} for the argon matrix.

7.3.6 Hydrogen bond vibrational modes

The Raman spectra of ammonia in an argon matrix at low M/A ratios show the presence of three bands at 222.3, 105.2 and $\sim$ 61 cm^{-1}. These bands were observed for different Raman laser excitation frequencies so are not due to laser lines. Since they are only present at low M/A ratios they are believed to be due to the ammonia open chain dimer, which is the most prominent multimer species at these M/A ratios. The 222.3 cm^{-1} band is assigned to the hydrogen bond stretching mode and the bands at 102.5 and 61 cm^{-1} to deformation modes.

7.3.7 Impurity bands

Cugley and Pullin {64} reported anomalous bands for ammonia isolated in an argon matrix which they suspected of being due to oxygen and nitrogen impurities in the argon. By doping the argon with oxygen or nitrogen they were able to show that the bands they observed at 968 cm^{-1} and 972 cm^{-1} were due to oxygen and nitrogen impurities respectively. In this work only one spectrum contained a shoulder at 972 cm^{-1} due to nitrogen impurities, the other spectra were free of these impurity bands.

Only one band in the infrared spectra of ammonia in argon was irreproducible and this was the band at 1035.0 cm^{-1}. This was suspected to be due to water impurity in the ammonia sample giving rise to an ammonia-water mixed dimer.

Fig. 7.12 Infrared Spectra of the ν_2 Region of NH_3 in an Argon Matrix at 20 K showing Water impurity effects

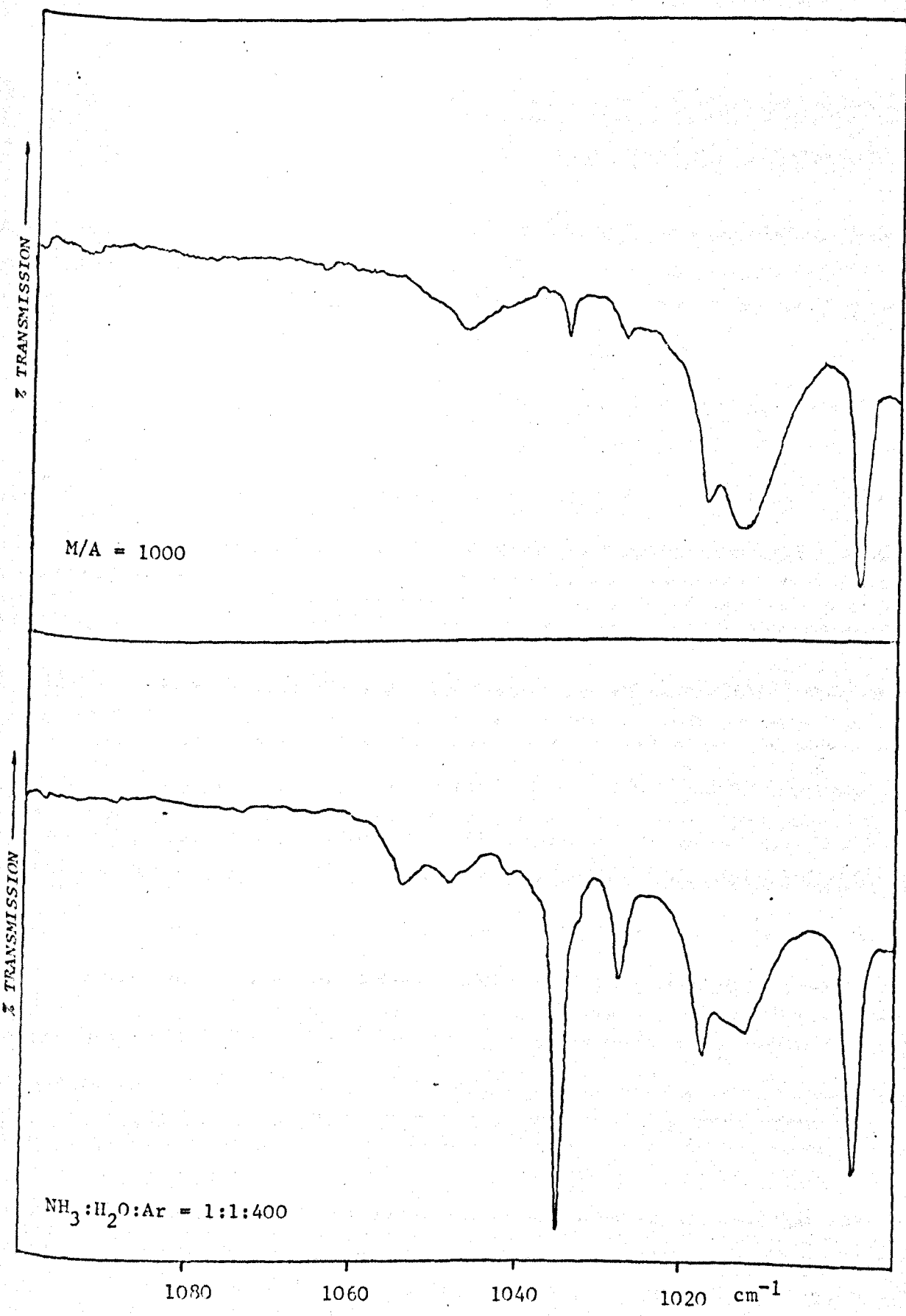

To confirm this an experiment was made using a 1:1 NH_3/H_2O mixture. Fig. 7.12 shows the effect of this mixture compared to an undoped sample. Clearly the band at 1035 cm^{-1} is due to ammonia complexing with the water to form a mixed dimer. Abouaf-Marquin reported a similar impurity band for ammonia isolated in a neon matrix {62}.

7.3.8 Conclusions

Fig. 7.13 shows the two possible types of dimer that can be formed; the open chain structure (C_s) and the cyclic structure (C_{2h}).

The bands observed for the dimers in argon include bands at frequencies close to those of the monomer bands which strongly suggest an open chain structure.

A normal coordinate analysis has been carried out by Dr S. Suzuki for the open chain dimer in argon {131}. The calculated frequencies are given in Table 7.4 and are in good agreement with those observed. The force field obtained was applied to calculate the frequencies of the cyclic dimers and the results suggest that the stretching region dimer bands for this structure would be close to the open chain structure dimer bands. The cyclic dimer band of the ν_2 region of ammonia in a nitrogen matrix is observed at 986 cm^{-1} and corresponds to a very weak band at ~990 cm^{-1} in the argon matrix. It is also observed that the dimer absorptions in the nitrogen matrix for the stretching region at low M/A ratios are rather broader than their argon matrix counterparts which would suggest that the conclusion from the normal coordinate analysis is reasonable.

It appears therefore that in nitrogen both types of dimer

Fig. 7.13 Open Chain and Cyclic Ammonia Dimer Structures.

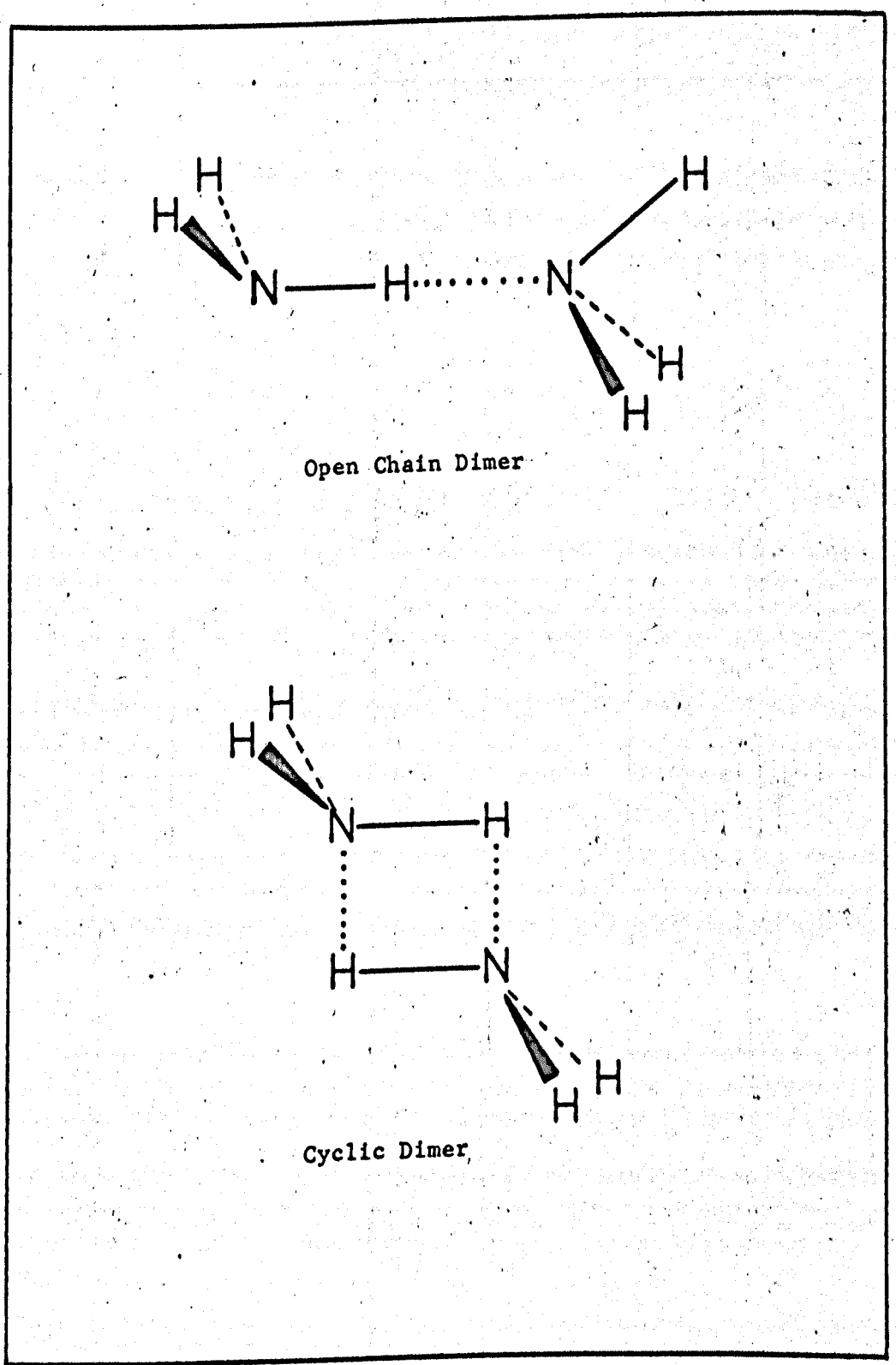

Table 7.4

Ammonia open chain dimer frequencies

Approximate description	Obs.	Calc.
NH_3 degen. stretch A', A"	3428	3432
NH_2 asym. stretch A"	3400	3402
NH_3 sym. stretch A'	3325	3326
NH_2 sym. stretch A'	3310	3310
NH stretch A'	3241	3240
NH_2 twist A"	1643	1645
NH_2 scissors A'		1640
NH_3 degen. deformation A', A"	(1638)	1638
NH_2 wag A'	1000	1013
NH_3 sym. deformation A'	(974)	975
N ... H stretch A'	223	223
NH_3 rock A', A"	105	103
torsion A"	60	60

exist but for argon the dimer is predominantly open chain. This may be explained as being due to the differences in the nature of the trapping sites. For nitrogen the site would have a cylindrical shape which may be better suited for accommodating the cyclic structure rather than the more spherical argon trapping site.

CHAPTER 8

QUANTITATIVE STUDIES OF AMINES IN ARGON AND NITROGEN MATRICES

8.1 Introduction

Odour pollution is a regular accompaniment of industrialization though until recently it has received less publicity than many other forms of pollution. Monitoring of atmospheric pollutants today is aimed toward systematically collecting and evaluating aerometric and related data to provide information concerning pollutant concentrations in ambient air, emissions from polluting sources and meteorological conditions. These monitoring activities are important from a legalistic point of view in order to produce usable information which when collected and structured may be presented for application to problem solving efforts by the researcher, the pollution control official, the industrialist and the concerned community.

Although the concentration of malodorous substances in waste gases is very low, even minute concentrations may cause considerable annoyance to the community and hence controlling such odours is a complex and often frustrating problem.

Odour is a physiological response of the individual. In all cases, the odorant will be in the vapour state or have an appreciable vapour pressure at ambient temperatures in order to have been detected. The olefactory detection threshold in humans is very low e.g. 10^8 to 10^9 molecules of odorant in the nose is sufficient for detection {131} (1 μ mol of ethyl mercaptan contains approximately 10^{17} molecules). Instruments which measure the physical or chemical characteristics of a malodorous gas

cannot be used to measure odour - only the amount of odorous substance present. It may be argued therefore that, to date, the only reliable and accurate instruments for measuring odour are the olefactory cells in human nasal tissue.

Odour thresholds for pure compounds vary widely as can be seen from Table 8.1 showing threshold values for a few familiar materials {132}.

Techniques for sampling and analysing malodorous gases are inherently difficult and require high sensitivity of equipment because these gases are only present in small quantities of the order 1 ppm - 1 ppb. The development of gas chromatography utilising sensitive detectors, such as the flame ionization detector, has increased the possibilities of determination of trace quantities of such gases and much pioneering work has already met with success {133-136}. However, separation of the pollutants is often complicated by the presence of constituents which the detecting system was not designed to analyse. One method of overcoming this problem is to design a sampling system to remove particular types of pollutants from the atmosphere i.e. sulphides, amines, mercaptans or olefins etc. which could then be analysed on chromatographic equipment with columns specifically suited for that type of pollutant {136}. In the case of the amines two problems arise.

(i) When dealing with basic nitrogen-containing compounds such as the primary amines, there is a "peak tailing effect" due to the adsorption of the sample on the chromatographic support and leads to the formation of asymmetric peaks making proper quantitative evaluation of the separated compounds difficult. Several workers {137-140} have tried to overcome this

Table 8.1

Odour Thresholds in Air (PPM Volume) {132}

Compound	ppm	Compound	ppm
Acetic acid	1.0	Butyric acid	0.001
Acetone	100	Carbon disulphide	0.21
Methylamine	0.021	Dimethyl sulphide	0.001
Diemthylamine	0.047	Ethyl mercaptan	0.001
Trimethylamine	0.00021	Methyl mercaptan	0.0021
Ammonia	46.8	Nitrobenzene	0.047
Benzene	4.68	Sulphur dioxide	0.47

problem by developing columns which have "anti-tailing" agent treated supports and found them satisfactory for their requirements.

(ii) The lower aliphatic amines have similar retention times and serious overlap of the peaks occurs making quantitative analysis difficult.

Secondary and tertiary amines present less peak tailing effects and so the discussion following will be centred on the primary amines which appear to cause the most trouble, namely ammonia, methylamine and ethylamine.

8.2 Development of technique

The use of matrix isolation as a research tool in the quantitative analysis of gaseous mixtures has already been applied by Rochkind {6,36,38,39,141}. He successfully applied it to the analysis of hydrocarbon mixtures {6} and deuterated ethylenes using a modified matrix isolation technique known as Pulsed Matrix Isolation. It retains the main characteristics of conventional matrix isolation technique but replaces the slow continuous condensation by a controlled pulse deposition process. Nitrogen was chosen as the matrix diluent gas which avoided the possibility of complicated rotational structure for small molecules, since no molecule is known to rotate in a nitrogen matrix. Rochkind diluted his sample gases to a pressure of approximately 700 torr with nitrogen, and used a pulse volume of 16 mls and reported {36} that pulses of this size, condensed onto a cooled window at 20 K, gave transparent, low scattering matrices. More recently Perutz and Turner {142} have shown that the technique may be adopted for other matrix gases and they put forward many advantages over the more conventional S.S.O. technique. It was also found

during experimentation that P.M.I. tends to give better matrices than S.S.O.

Application of the technique to quantitative analysis depends upon the application of the Beer-Lambert law to the matrix isolated molecules absorption bands. The accepted law requires that:

$$\text{Absorbance} = \log\left(\frac{I_o}{I}\right) = \alpha.c.l.$$

where

I_o = incident radiation intensity

I = transmittance at peak frequency

α = absorption coefficient for the transition

c = the concentration of the absorbing species

l = the path length.

Hence cl for matrix purposes equals the number of absorbing molecules trapped in the matrix through which the incident radiation from the spectrometer can pass. However, the actual number of micromoles deposited will depend on the geometry of the apparatus and on the sticking coefficient of the substance under the conditions used. Thus the amount actually condensed will be effected by several factors; these will be the rate at which the material is deposited, the temperature of the support window, the distance of the injection needle from the window and the rate at which uncondensed sample is pumped out of the cell, thought to be negligible because of the efficiency of cryopumping.

However, providing experimental conditions are kept constant, results should be reproducible on a particular piece of equipment.

As already mentioned in chapter 2 the existing system proved inadequate for the quantitative analysis of the amines

for the following reasons;

(i) The S.S.O. equipment required relatively large amounts of sample to keep the flow rate approximately constant.

(ii) The small changes in pressure of the storage bulb during calibration experiments for the amine samples were difficult to measure accurately with the mercury manometer.

(iii) The amines themselves became adsorbed into the Apiezon "N" grease of the vacuum taps which meant that a certain unknown quantity of amine was being removed from the sample mixture bulbs and this was obviously undesirable.

The resultant Beer's law plots when using the S.S.O. technique were unsatisfactory when quantitative estimates of the amines were made, being non reproducible from experiment to experiment. To overcome these problems, a new sample preparation and deposition system was built on similar lines to Rochkind's system already mentioned. A pulsed matrix isolation system was built in which all the taps were of the greaseless type (Young's p.t.f.e.) and the mercury manometer was replaced by a pressure transducer (the calibration of which is given in chapter 2, Fig. 2.6). The main storage bulb was only 500 mls and the total volume of the sampling system necessary for deposition was one tenth of that of the S.S.O. system.

Once the sample had been made up at an M/A ratio of 100 with nitrogen, deposition was carried out by pressurising the measured volume and allowing this volume to condense on the cooled CsI window of the cell at 20 K. The pressure of each pulse was measured by means of the pressure transducer. The actual micromoles of sample of each pulse was calculated using the following relationship:

Number of μ moles per pulse = $(16.036.V_m.P_m)/(T_m.MA)$

where V_m = measured volume

P_m = pressure of gas mixture

T_m = temperature of gas (room temperature)

MA = M/A ratio.

Rochkind had shown that good matrix spectra could be obtained by depositing the gas phase mixtures by this method. Using hydrocarbons in nitrogen at M/A ratio of 100 and pulse pressure of 700 torr, he obtained sharp infrared spectra which obeyed Beer's law (i.e. peak intensity was proportional to the amount of hydrocarbons deposited). However he did not report on the degree of isolation achieved and it was felt that in the case of amines that investigation of this point was necessary.

Pulse pressures of 700-100 torr were used and it was found that between 400 torr and 100 torr no appreciable difference in isolation was observable at M/A ratio 100. Also at high pulse pressures tailing of the Beer's law graph was experienced, which was believed to be occurring due to excessive annealing of the matrix. As the matrix layer built up the heat of condensation of successive pulses had to be removed through this layer whose thermal conductivity was not as good as that of the CsI window, hence excessive annealing occurred. However, with pulse pressures below 400 torr tailing of the Beer's law graph did not occur even for considerable thicknesses of matrix.

The angle at which the gas sample was deposited onto the cooled window was varied. No difference was observed between 45° and 90° but deposition normal to the window was adopted. The following conditions were adherred to during the quantitative experimentation.

(i) A deposition temperature of 20 K.

(ii) Initial pulse size of approximately 400 torr.

(iii) Pulsing at one minute intervals.

(iv) The injection needle was placed just outside the radiation shield which had been modified to allow maximum transmission of energy through the CsI deposition window. Using this method good Beer's law plots were obtained (Fig. 8.1).

8.3 Results

Experimentation was carried out initially using methylamine as the sample gas to test the reproducibility of the technique.

An M/A ratio of 100 was used with nitrogen as the matrix gas. Pulsing was carried out as previously described and the spectrum run over the strongest absorbing region (at 816 cm^{-1}) between each pulse. A calibration graph was drawn of micromoles deposited against peak height absorbance. The experiment was repeated and using the previous calibration graph to calculate amount deposited from peak height absorbance, the error of estimated and calculated was ±3% (Fig. 8.2).

Calibration experiments for ammonia, methylamine and ethylamine were carried out for all the strong bands in the spectrum of each isolated molecule (Figs. 8.3(a) - 8.3(c)). Good Beer's law plots were obtained in each case. Once the calibration graphs had been made for each molecule, mixtures of the amines were made up with an overall M/A ratio of 100. Hence with a known ratio of methylamine/ethylamine in nitrogen an experiment was carried out to estimate the amount of the two molecules present by the P.M.I. technique using the calibration graphs of each molecule.

Fig. 8.1 Beer's Law Graph for some Bands in the Spectrum of Methylamine in a Nitrogen Matrix at 20 K

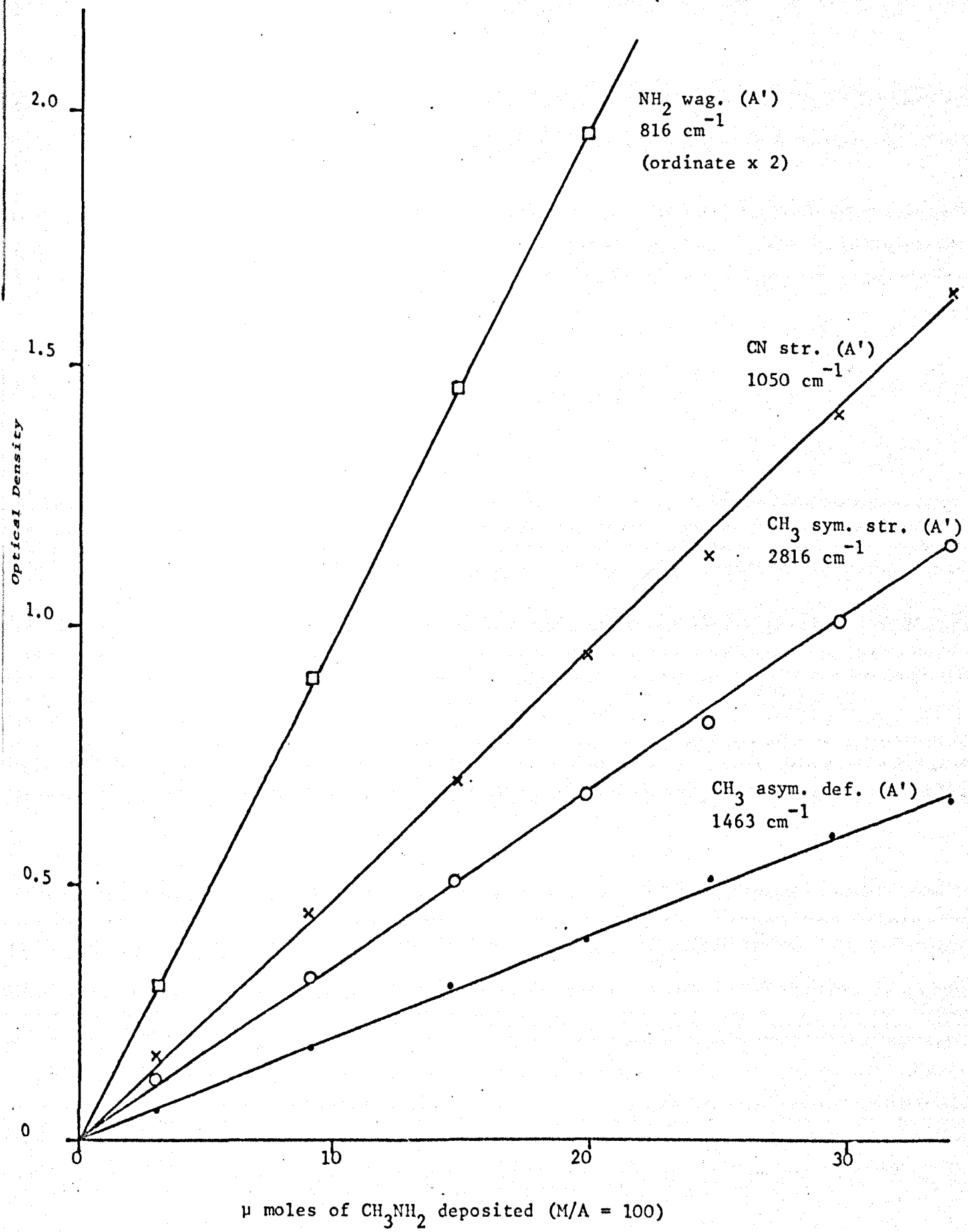

Fig. 8.2 Graph of Optical Density of the NH_2 Wagging Mode at at 816 cm^{-1} versus μ moles of Methylamine deposited at 20 K

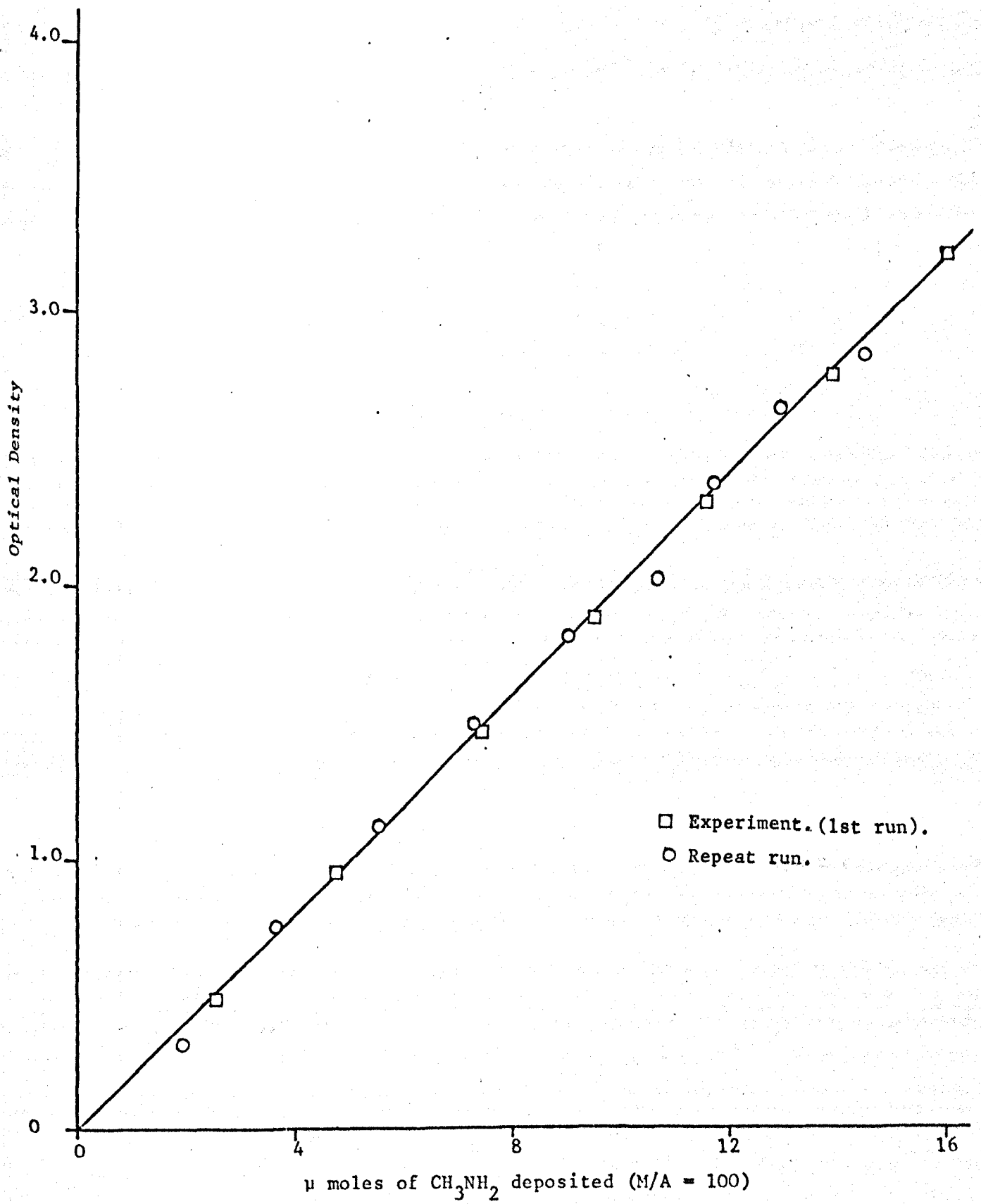

Fig. 8.3 (a) Calibration Graphs for Ammonia in Nitrogen at 20 K

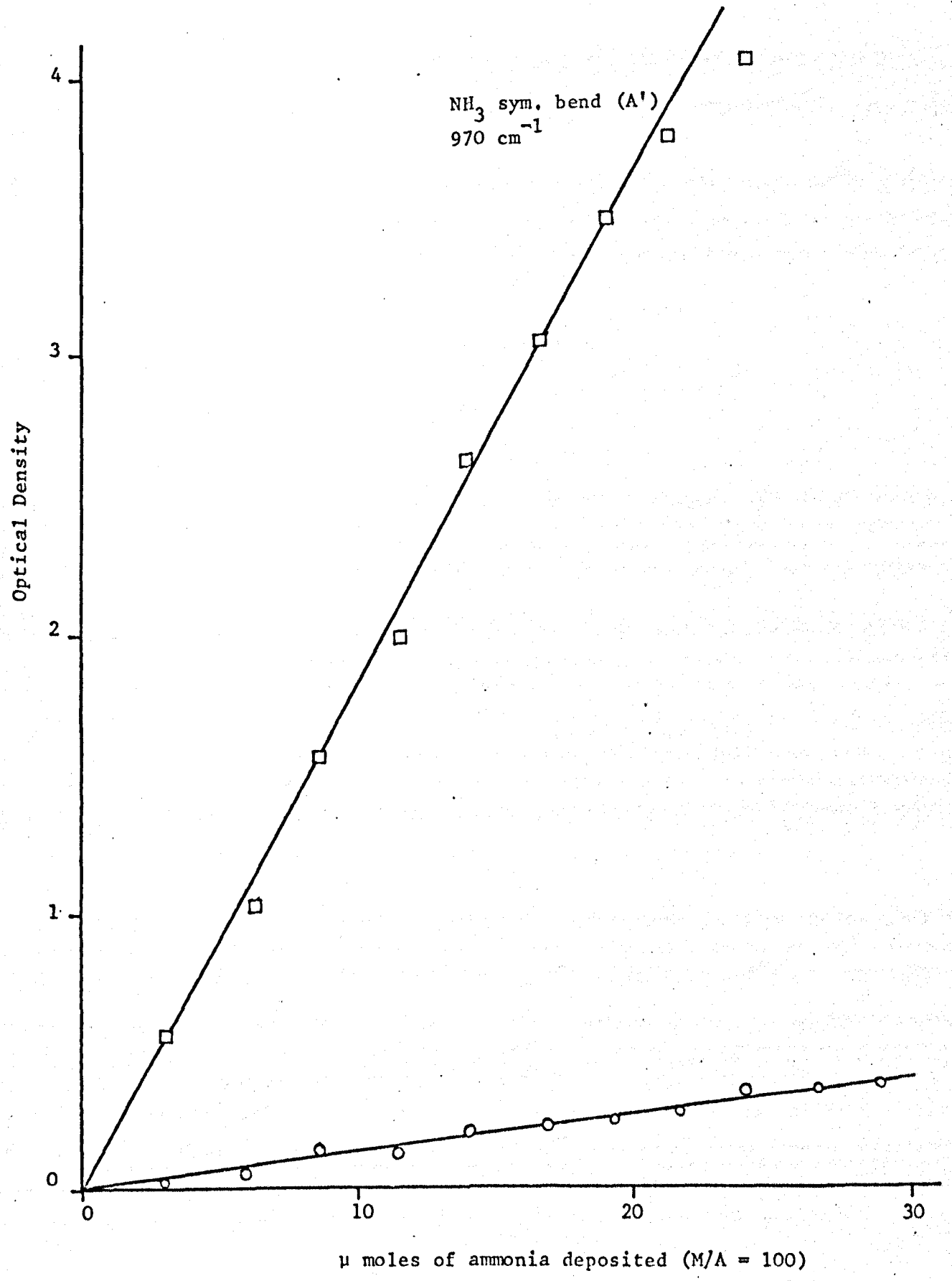

Fig. 8.3 (b) Calibration Graphs for Methylamine in NItrogen at 20 K

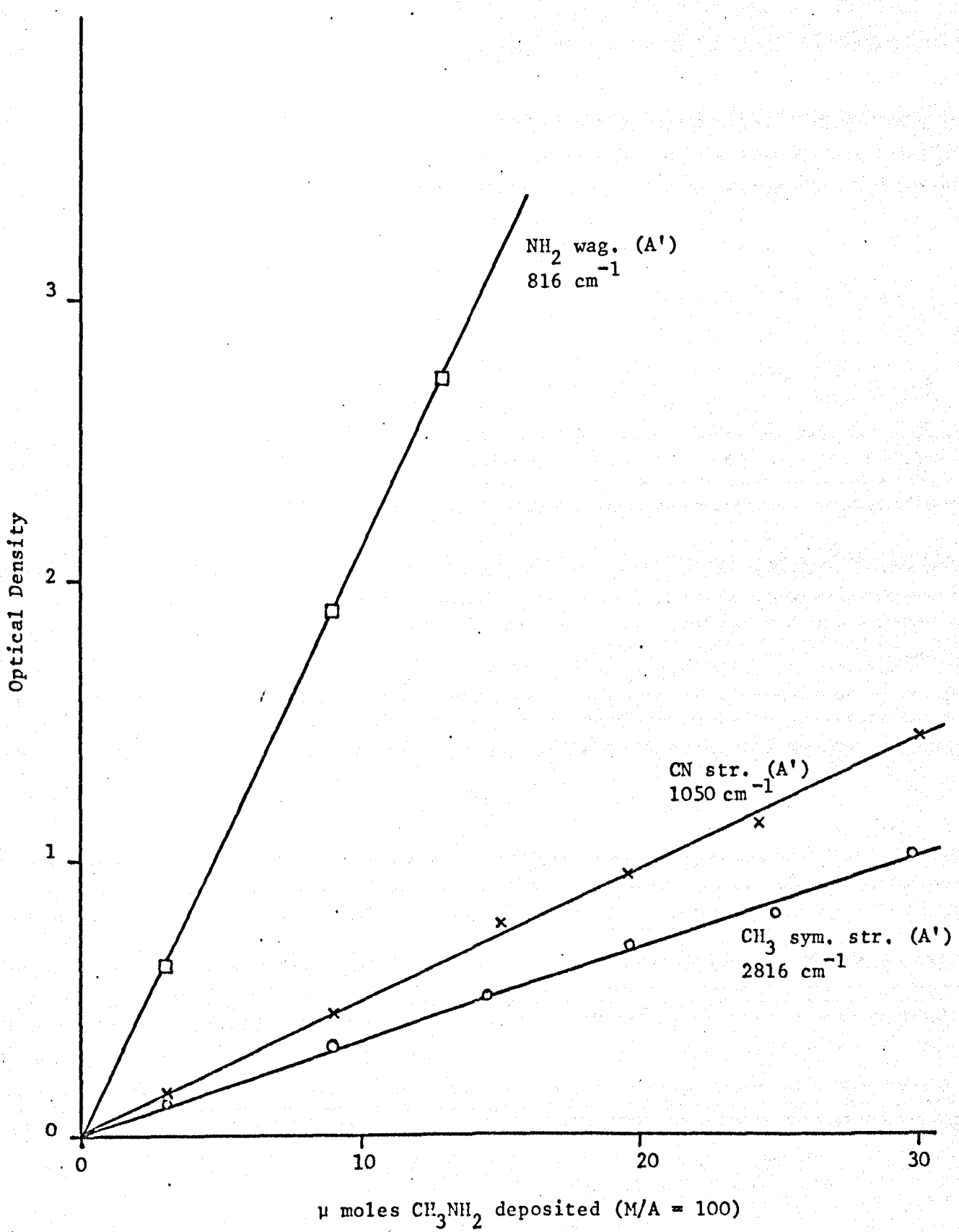

Fig. 8.3 (c) Calibration Graphs for Ethylamine in Nitrogen at 20 K

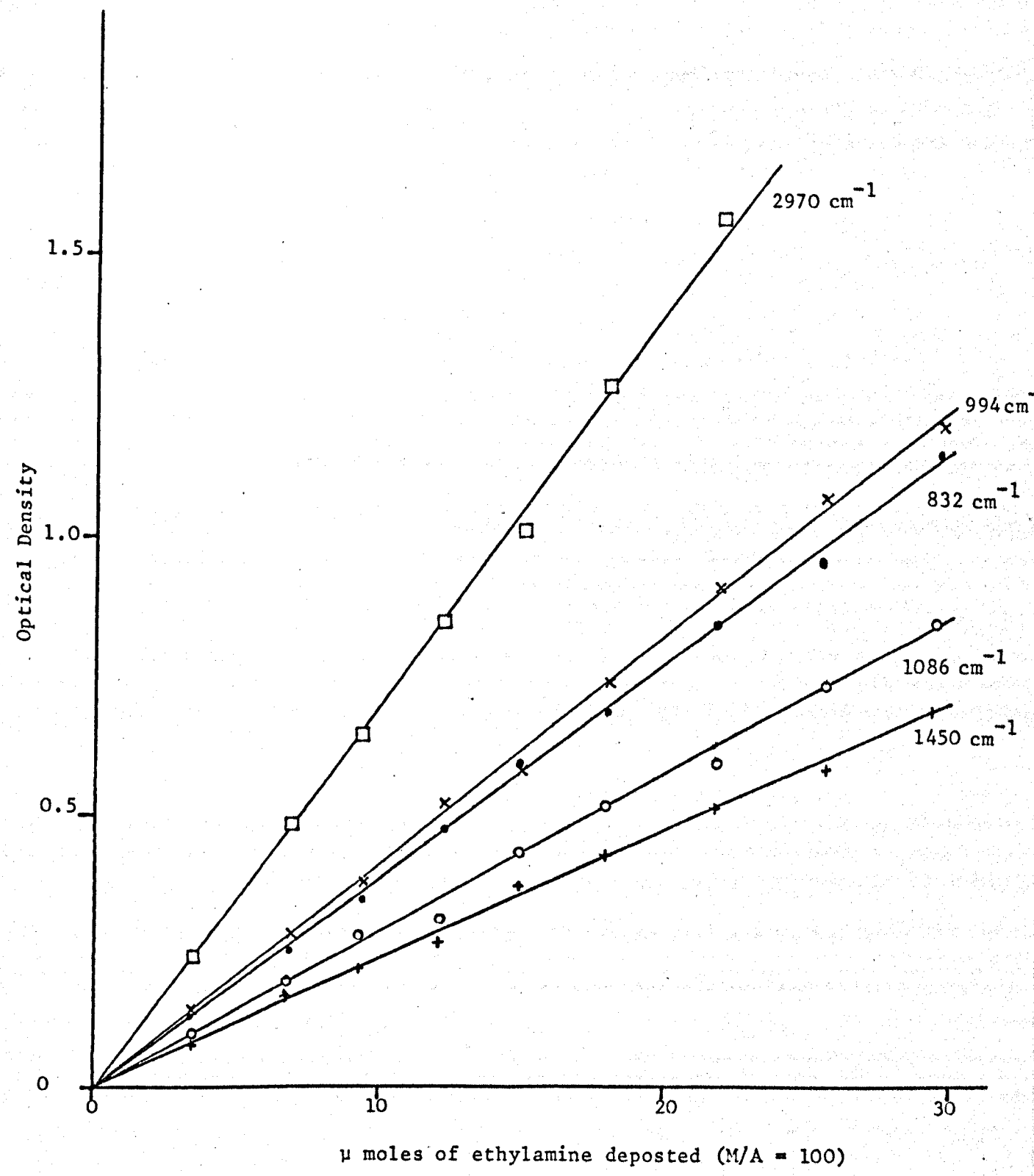

From the results it was immediately apparent that although the correct amount of ethylamine could be estimated from its calibration graph, there appeared to be less methylamine than calculated for the pulse size. This result was confirmed for several other experiments using fresh samples of methylamine/ethylamine mixtures at overall M/A ratios of 100 in nitrogen.

Since the frequency of the calibration band for methylamine did not shift it is unlikely that hydrogen bonding between ethylamine and methylamine affected the intensity of the methylamine calibration band and not the frequency. However ethylamine might affect the spectrum of the methylamine molecule by distortion of the matrix.

A series of experiments were carried out to investigate the effect of changing the M/A ratio on the monomer bands of methylamine, ethylamine and ammonia (chapters 4, 6 and 7).

Theoretically the relative intensities of all the monomer bands for a particular molecule isolated in a site in a matrix should remain the same no matter what M/A ratio is used.

Figs. 8.4, 8.5 and 8.6 show the results of these experiments. The intensity of the strongest monomer band at 816 cm^{-1} for a nitrogen matrix (corresponding to the NH_2 wagging vibration) relative to other monomer bands appears to be extremely M/A dependent, while other monomer bands studied for methylamine behave normally. Fig. 8.7 demonstrates that the calibration plot of a "normal" monomer band of methylamine is independent of the matrix ratios. No similar effect for the monomer bands ofammonia or ethylamine was found on changing the M/A ratio.

These experiments were repeated for an argon matrix (chapters 4, 6 and 7) but no effect similar to that in the

Fig. 8.4 Plot of Relative Optical Density of some Monomer Bands of Methylamine in Nitrogen at 20K versus M/A Ratio

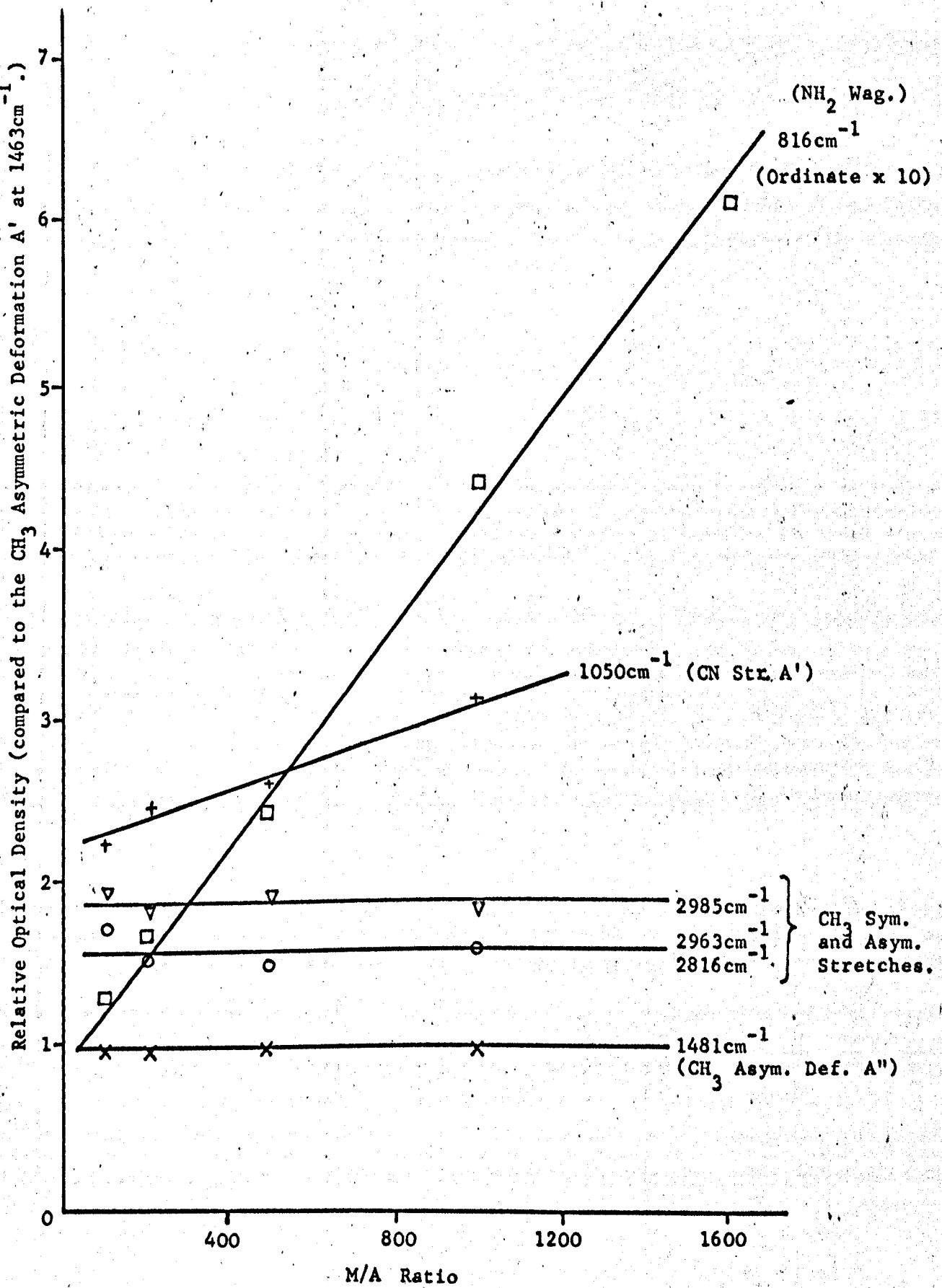

Fig. 8.5 Plot of Relative Optical Density of some Monomer Bands of Ethylamine in Nitrogen versus M/A ratio

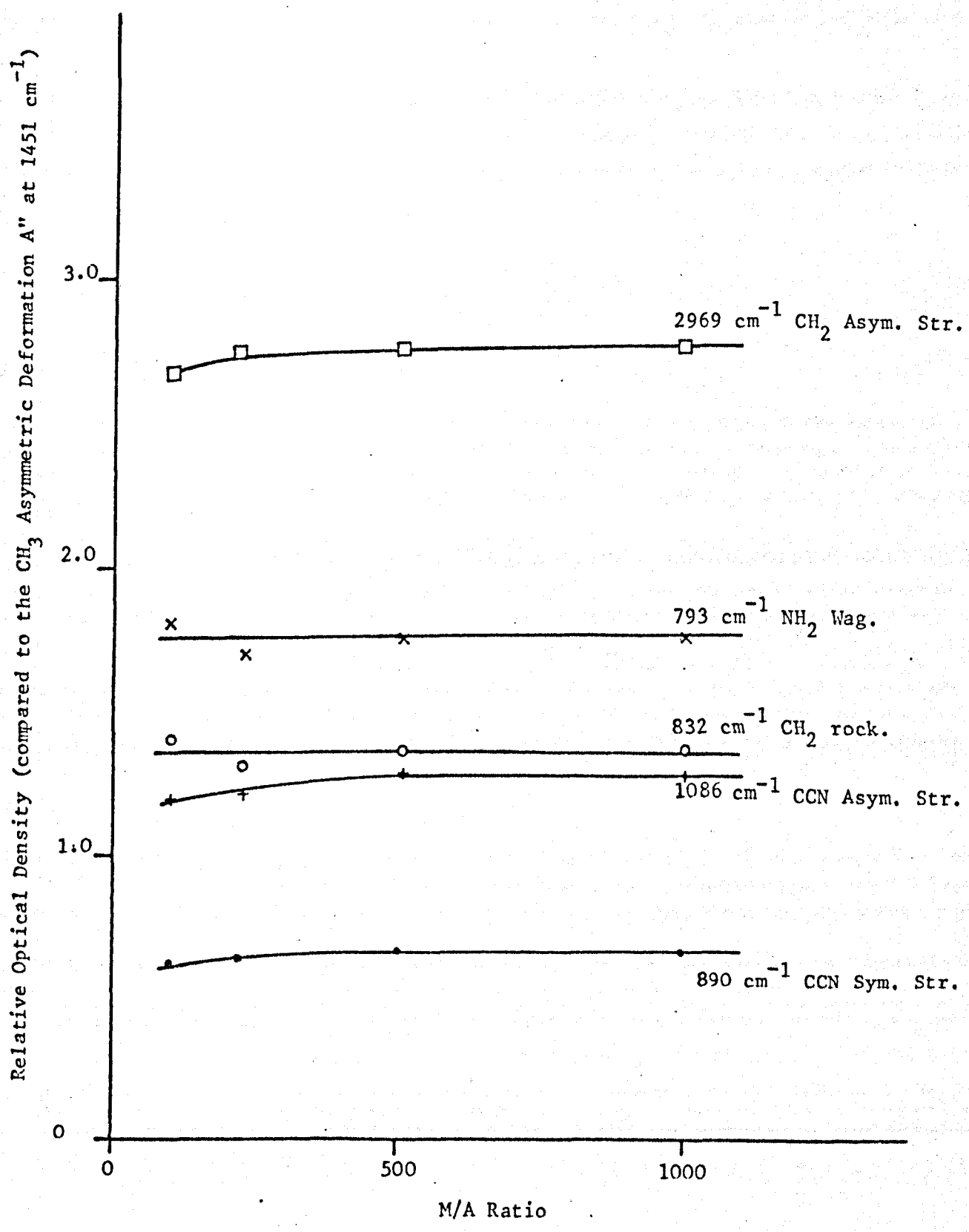

Fig. 8.6 Plot of Relative Optical Density of some Monomer bands of Ammonia in Nitrogen versus M/A ratio

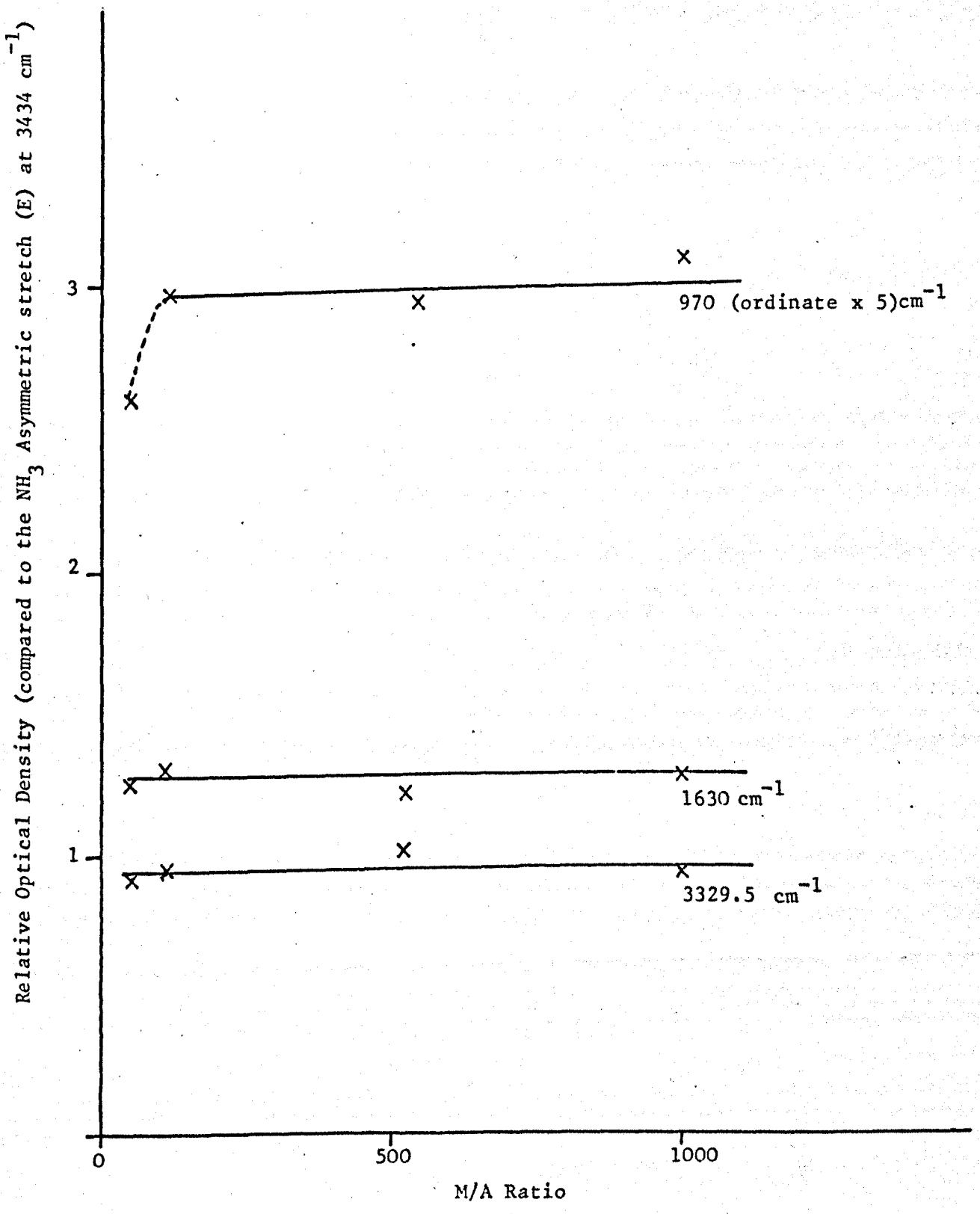

Fig. 8.7 Plot of Optical Density versus μ mols of Methylamine Deposited

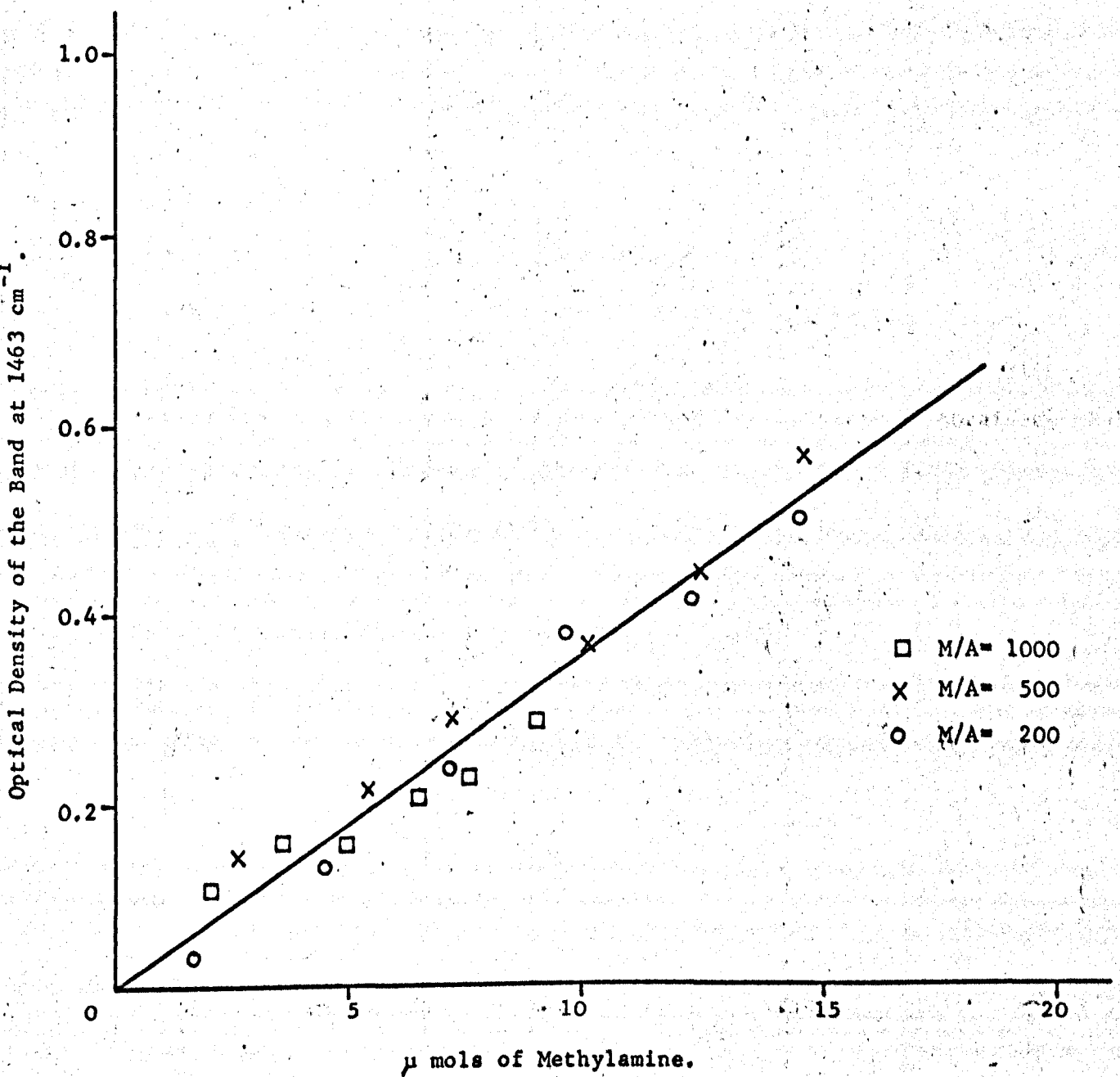

nitrogen matrix was observed. Fig. 8.8 shows the comparison of nitrogen results with those of argon for methylamine.

It would appear that some kind of interaction of the methylamine molecule in the nitrogen matrix is affecting the intensity of the NH_2 wagging mode without causing a shift in frequency.

As a check, instead of using peak height absorbance as a measure of intensity, the area of absorbance under the M/A ratio dependent band for methylamine (816 cm^{-1}) was measured. Since datalogging facilities were available it was a straight-forward matter to obtain a tape output of the region of interest and integrate the separate bands by using program COL 1B.

Although absolute intensities of the isolated bands could not be measured, Fig. 8.9 clearly shows that both integrated and peak height absorbance show that intensification of the 816 cm^{-1} band is occurring as the M/A ratio is increased.

There seems therefore some kind of interaction which is occurring between methylamine and the nitrogen molecules increasing the intensity of the NH_2 wagging vibration without shifting the frequency. Unfortunately, no bands were observable in the Raman for this region and no apparent increase in intensity of the Raman bands for the NH_2 stretching vibration was observable over the range of M/A ratios studied.

An increase in intensity of the NH_2 wagging vibration necessarily implies a corresponding increase in the change of dipole moment with the appropriate normal coordinate. It is surprising that such a large change can occur without any apparent effect on the frequency of this mode or on the intensities of other modes associated with the NH_2 group.

Fig. 8.8 Comparison of the M/A Dependence of the NH_2 Wagging Mode for Methylamine in Argon and Nitrogen matrices

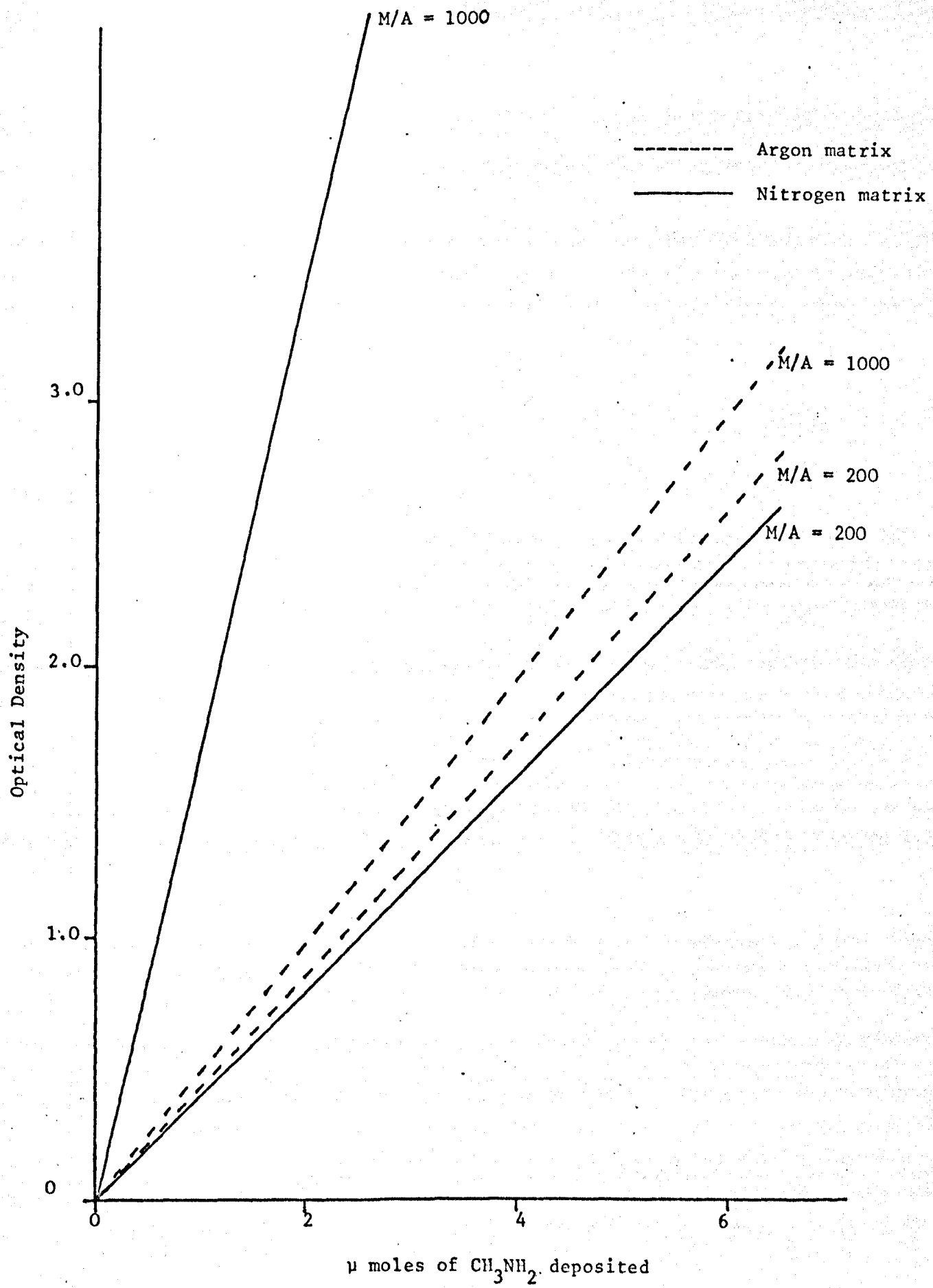

Fig. 8.9 Comparison of Integrated and Peak Height Absorbance for the Band at 816 cm^{-1} for Methylamine in Nitrogen at 20 K

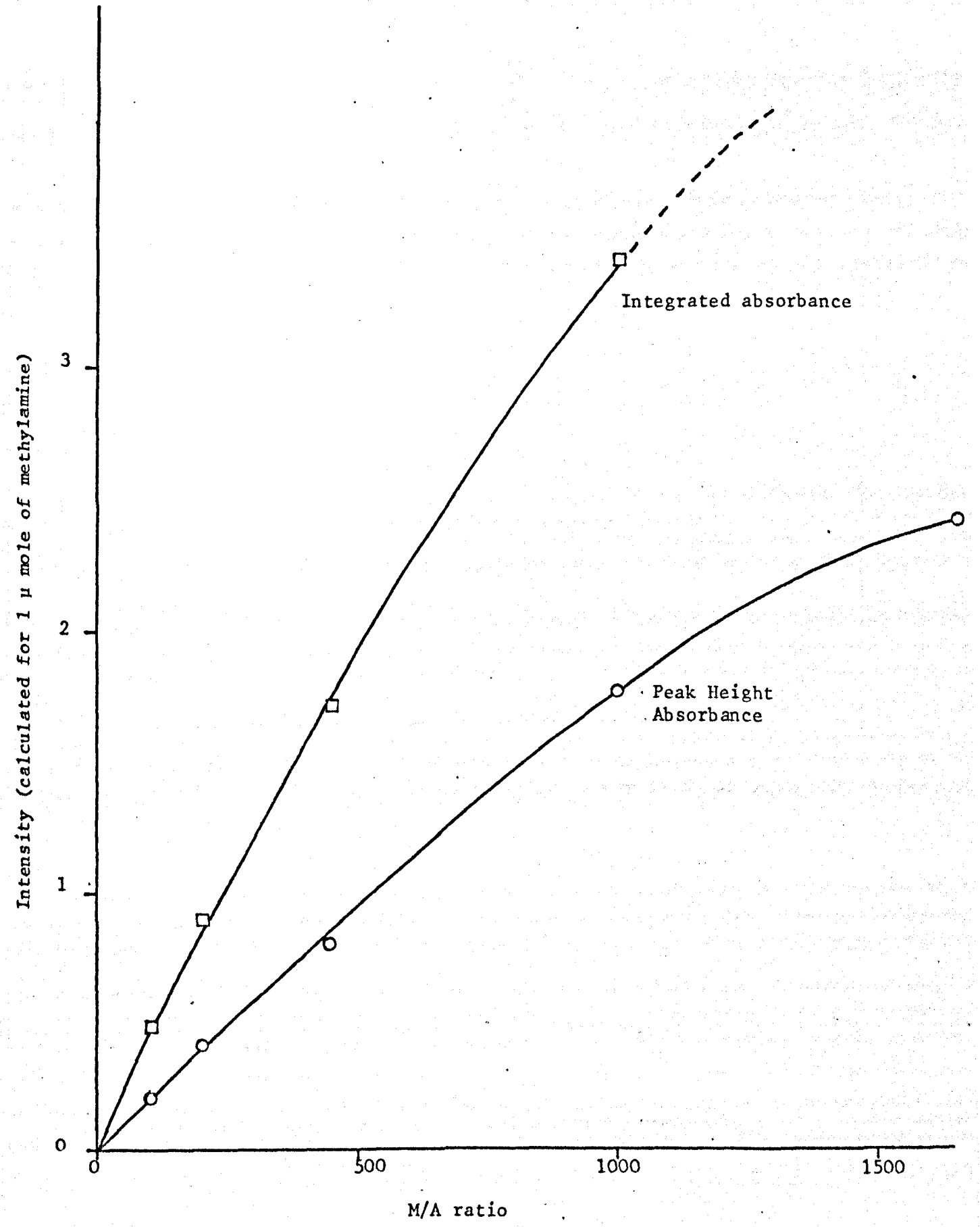

Fig. 8.10 Infrared Spectra of a Mixture of Ammonia, Methylamine and Ethylamine in Nitrogen at 20 K compared to the corresponding gas-liquid Chromatographic Analysis

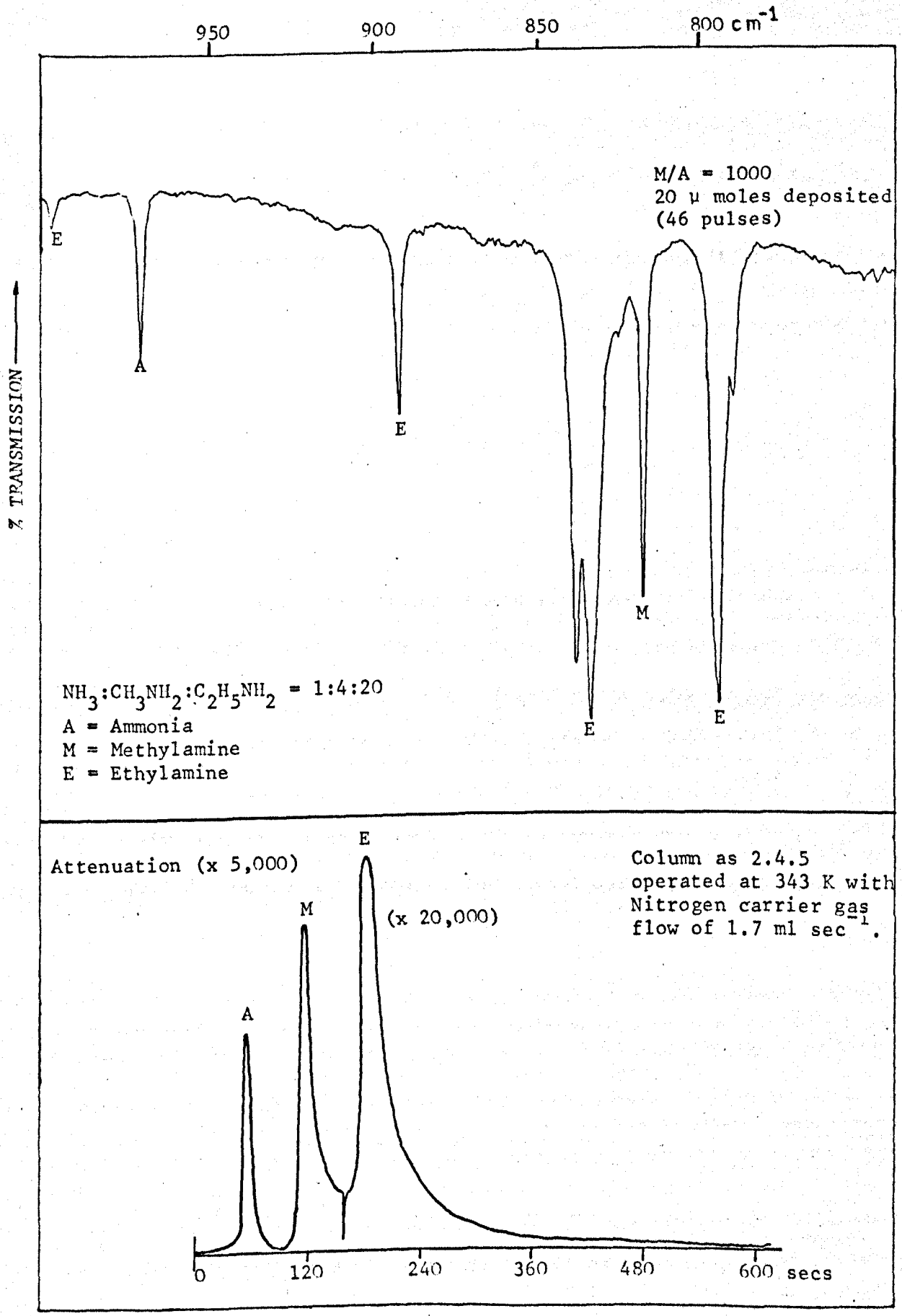

For methylamine in nitrogen the intensity increase for the monomer band associated with the NH_2 wagging mode as a function of M/A ratio cannot be directly associated with adjacent guest interactions (i.e. ammonia, methylamine, ethylamine interactions) since this effect would be expected to perturb the frequency or cause splitting of the band and this is not observed. It is thought that the effect of M/A ratio changes is to vary the degree of distortion of the nitrogen lattice and hence the interactions between the nitrogen molecules and the methylamine molecule. Further investigation of this phenomena was not undertaken since no theoretical considerations for the effect could be applied.

8.4 Conclusion

The pulse deposition method for analysis of primary amines is satisfactory for vibrational transitions of monomer species which are not affected by the degree of dilution or by intermolecular interactions. Unfortunately these transitions may not be best suited to quantitative studies since they may not give the strongest bands. Nitrogen gives better isolation and avoids the complications of rotational and multiple site splitting of the bands of the amines.

Comparison of the observed intensities of the bands in the spectrum with calibration sensitivities for the particular bands enabled estimates to be made of the concentrations of the identified components of a mixture of the amines studied. Using this method, comparison of the monomer bands which were not affected by the M/A ratio in nitrogen allowed in the case of the methylamine/ethylamine mixtures, the number of μmoles deposited for each molecule

to be estimated to within ±5% using the appropriate calibration graphs.

Qualitative analysis of a gaseous mixture of amines can be carried out by comparison of the P.M.I. spectrum of the mixture with those of the suspected components. On this argument the P.M.I. technique has obvious applications as a supplement to gas chromatography since the three amines in this work have similar retention times and only one peak is available for identification whereas several absorptions occur in the nitrogen matrix for each molecule. Fig. 8.10 demonstrates the qualitative use of the P.M.I. technique. A spectrum of a mixture of ammonia, methylamine and ethylamine in nitrogen at M/A ratio of 1000 at 20 K is compared to the corresponding gas-liquid chromatographic analysis.

APPENDIX 1

Surface pretreatment prior to "Araldite" bonding

The Araldite resins adhere firmly to most materials and bonds of considerable strength may be obtained solely after the removal of grease and surface deposits.

(a) Glass and metal surfaces

The surfaces to be bonded are degreased with acetone roughened with emery cloth and washed again with acetone.

(b) Polytetrafluoroethylene tubing

The surface to bonded is degreased with acetone and allowed to dry. The tubing is then dipped into "Bond Aid" etchant for 30 secs (preferably under an atmosphere of nitrogen to avoid unnecessary oxidation of the etchant). After this time, the tubing is removed and washed with ethanol, to remove any traces of the etchant. The tubing is then washed in acetone and allowed to dry.

The premixed Araldite resins may now be applied to the surfaces. The Araldite usually cures in 24 hours forming excellent vacuum tight bonds.

APPENDIX 2

Specifications for the Type 4-366 General Purpose Pressure Transducer.

Input Parameters	High Pressure Range	Low Pressure Range
Pressure Ranges	lbf/in² (p.s.i.) 0–75 to 0–10,000 Standard Ranges are: 0–75, 100, 150, 250, 500, 1,000, 1,500, 2,500, 3,500, 5,000 and 10,000 **Absolute and Sealed Gauge**	lbf/in² (p.s.i.) 0–10 to 0–50 Standard Ranges are: 0–10, 15, 25, 50 **Absolute and Vented Gauge**
Pressure Limits	Two times rated pressure when applied for 3 minutes shall not cause a zero set to exceed 0.5% F.R.O.	
Pressure Media	Armco 17–4PH stainless steel	Armco 17–4PH and 15–7MO stainless steels
Rated Electrical Excitation	10 V. D.C. or A.C. r.m.s. carrier frequency 0–20,000 Hz	
Maximum Electrical Excitation	12 V. D.C. or A.C. r.m.s. without damage	
Impedance	350Ω nominal, 330Ω minimum	
Output		
Full Range Output	40 mV+20% –10% open circuit at rated excitation and +25°C	
Residual Unbalance	Within ±5% of F.R.O. at zero pressure and +25°C	
Natural Frequency (Mechanical)	Above 15,000 Hz	Above 10,000 Hz
Impedance	350Ω ±10% at 25°C	
Resolution	Infinite	
Non-Linearity & Hysteresis	Combined effects of non-linearity and hysteresis shall not exceed ±0.5% F.R.O.	Combined effects of non-linearity and hysteresis shall not exceed ±1.0% F.R.O.
Environmental		
Compensated Temperature Range	0 to 120°C	
Operational Temperature Range	–54°C to +120°C	
Thermal Zero Shift	Within 0.035% F.R.O./°C over compensated temperature range	Within 0.050% F.R.O./°C over compensated temperature range
Thermal Sensitivity Shift	Within 0.035% F.R.O./°C over compensated temperature range	Within 0.050% F.R.O./°C over compensated temperature range
Steady Acceleration	At 100g the response will not exceed 0.02% F.R.O./g.	At 100g the response will not exceed 0.05% F.R.O./g.
Linear Vibration	At 35g sinusoidal vibration from 5 to 2,000 Hz (limited by half-inch double amplitude) the response is less than 0.06% F.R.O./g.	At 35g sinusoidal vibration from 5 to 2,000 Hz (limited by half-inch double amplitude) the response is less than 0.08% F.R.O./g.
Altitude	Ambient pressures of 2× F.R., or 180 p.s.i., whichever is less, will not damage the transducer	Ambient pressures of 2× F.R. will not damage the transducer
Humidity	100% Relative Humidity	Absolute units 100%; vented gauge units also 100% if cable end is protected from moisture.
Mechanical Shock	1,000g half sine wave pulse for a duration of one millisecond will not damage the transducer.	
Physical		
Electrical Connection	Integral sealed cable assembly in standard lengths of 1m or 3m. Other lengths to special order. Maximum continuous operating temperature 100°C.	
Insulation Resistance	500 MΩ minimum at 85 V. D.C. over compensated temperature range.	
Weight	142 gms, with 1m cable assembly.	

APPENDIX 3

CALC 1B

This program calculates the amount of matrix sample deposited from the Raman pulse matrix isolation sampling system.

Input parameters:

1) Number of pulses required.
2) Initial pressure in the sample bulb (torr).
3) Temperature (K).
4) M/A ratio used.
5) Volume of bulb (mls).
6) Volume of "measured volume" (mls).

Output:

The program calculates the amount of sample deposited after each pulse, and the total amount deposited.

```
CALC1B;
"BEGIN"
"INTEGER" I;
"REAL" X,XX,K,MA,N,P,T,V1,V2;
"PRINT"
'N    P      TEMP   M/A    V1     V2'L'';
"READ" N,P,T,MA,V1,V2;
"BEGIN"
"ARRAY" A,B[1:N];
XX:=A[1]:=B[1]:=1; X:=V1/(V1+V2); K:=(235.54*P)/(T*MA);
"PRINT" ''L2'   TORR.    UM.   TOT UM.'L'';
"FOR" I:=2 "STEP" 1"UNTIL" N "DO"
"BEGIN"
        XX:=XX*X;
      B[I]:=XX;
      A[I]:=XX+A[I-1];
"END";
"FOR" I:=1 "STEP" 1 "UNTIL" N "DO"
"PRINT" SAMELINE,ALIGNED(3,2),P*B[I],ALIGNED(2,3),K*B[I],K*A[I],''L'';
"END";
"END"
```

APPENDIX 4

Procedure decode (Wnum, Trans)

Each data word from the DDR-1C consists of:

(i) A coded wavenumber value.

(ii) A coded transmission value.

(i) Decoding of the wavenumber value depends on which range of the spectrometer is in operation. The computer decides in which range the point lies and decodes it accordingly.

(ii) The transmission scale is linear over a smaller range than the scale on the spectrometer, the computer decodes the transmission value to correspond with the reading on the chart paper.

A procedure for decoding the data words from the DDR-1C in the Elliot 903 computer is given below.

```
"PROCEDURE" DECODE(WNUM,TRANS);
"REAL" WNUM,TRANS;
"BEGIN"
     "REAL" R,S,TT;
      "SWITCH"ZZ:=OUT;
      "IF" WNUM "LE" 99800 "AND" WNUM "GE" 78000 "THEN"
      "BEGIN"
            TT:=5000;S:=99752;R:=0.142857143;
            "GOTO" OUT;
      "END";
      "IF" WNUM "LE" 75000 "AND" WNUM "GE" 52000 "THEN"
      "BEGIN"
            TT:=2500;S:=74552;R:=0.071428571;
            "GOTO" OUT;
      "END";
      "IF" WNUM "LE" 50000 "AND" WNUM "GE" 28000 "THEN"
     "BEGIN"
           TT:=1000;S:=49352;R:=0.028571429;
           "GOTO" OUT;
      "END";
      "IF" WNUM "LE" 25000 "AND" WNUM "GE" 3000 "THEN"
      "BEGIN"
           TT:=500;S:=24152;R:=0.014285714;
           "GOTO" OUT;
     "END";
OUT:
      WNUM:=TT-((S-WNUM)*R);
      TRANS:=(TRANS-35)/9.3;
     "END";
```

APPENDIX 5

SRCH 2A

Input parameters

1) Number of bands to be searched.
2) Number of points to be scanned (usually 10-20 is sufficient).
3) Wavenumber limit of the band search (usually 2 cm^{-1}).
4) If plot of scanned points required then 1 otherwise 2.
5) Approximate wavenumber value of the band centres to be searched in descending magnitude.

Output

1) Prints the search values (cm^{-1}) and the band centres found (cm^{-1}).
2) Plot of scanned points if required in (4).

```
SRCH 2A;
"BEGIN"
"REAL" MAX,MIC,MIN,SET,D,WW,TT;
"INTEGER" I,J,NUM,X,STOP,PRINT;
"COMMENT" DECLARATION OF DECODE;
"PROCEDURE" DECODE(WNUM,TRANS);
"REAL" WNUM,TRANS;
"BEGIN"
      "REAL" R,S,TT;
      "SWITCH"ZZ:=OUT;
      "IF" WNUM "LE" 99800 "AND" WNUM "GE" 78000 "THEN"
      "BEGIN"
            TT:=5000;S:=99752;R:=0.142857143;
            "GOTO" OUT;
      "END";
      "IF" WNUM "LE" 75000 "AND" WNUM "GE" 52000 "THEN"
      "BEGIN"
            TT:=2500;S:=74552;R:=0.071428571;
            "GOTO" OUT;
      "END";
      "IF" WNUM "LE" 50000 "AND" WNUM "GE" 28000 "THEN"
      "BEGIN"
           TT:=1000;S:=49352;R:=0.028571429;
           "GOTO" OUT;
      "END";
      "IF" WNUM "LE" 25000 "AND" WNUM "GE" 3000 "THEN"
      "BEGIN"
           TT:=500;S:=24152;R:=0.014285714;
           "GOTO" OUT;
      "END";
OUT:
      WNUM:=TT-((S-WNUM)*R);
      TRANS:=(TRANS-35)/9.3;
      "END";
"SWITCH" Z:=L0,L,LL,LLL;
        "READ" NUM,X,SET,PRINT;
"BEGIN"
"ARRAY" W,T[1:X],S[1:NUM];
        "FOR" I:=1 "STEP" 1 "UNTIL" NUM "DO" "READ" S[I];
        STOP:=NUM; NUM:=1;
L:
        "READ" WW,TT;
        DECODE(WW,TT);
        "IF" ABS(WW-S[NUM])>2*SET "THEN" "GOTO" L;
        "FOR"  I:=1 "STEP" 1 "UNTIL" X "DO" "BEGIN"
                                          "READ" WW,TT;
                                          DECODE(WW,TT);
                                          W[I]:=WW; T[I]:=TT;
                                          "END";
```

```
LO:
        "FOR" I:=1 "STEP" 1 "UNTIL" X-1 "DO" "BEGIN"
                                                W[I]:=W[I+1];
                                                T[I]:=T[I+1];
                                            "END";
        "READ" WW,TT;
        DECODE(WW,TT);
        "IF" ABS(WW-S[NUM])>2*SET "THEN" "GOTO" L;
        W[X]:=WW; T[X]:=TT;
        "IF"  ABS(S[NUM]-W[X"DIV"2])<SET
        "THEN" I:=6 "ELSE"
        "BEGIN"
              "IF" (S[NUM]-W[X"DIV"2])>SET "THEN" "BEGIN"
              "PRINT" ''L2'NO BAND FOUND,SET VALUE EXCEEDED
FOR BAND SEARCH VALUE OF',SAMELINE,FREEPOINT(6),S[NUM],
'WAVENUMBER.'L2'';
             "GOTO" LLL;
        "END";
        "GOTO" LO;
        "END";
LL:
        "IF" I=X-5 "THEN" "GOTO" LO;
        "IF" T[I]<T[I+2] "AND" T[I]<T[I+3] "AND" T[I]<T[I+4]
        "AND" T[I]<T[I+5] "AND"  T[I]<T[I-2] "AND" T[I]<T[I-3]
        "AND" T[I]<T[I-4] "AND"  T[I]<T[I-5]
        "THEN" "BEGIN"
                    MAX:=1000; MIN:=0;
                    "FOR" J:=1 "STEP" 1 "UNTIL" X "DO"
              "BEGIN"
                    "IF" T[J]<MAX "THEN"    "BEGIN"
                                                MAX:=T[J];
                                                MIC:=W[J];
                                            "END";
                    "IF" T[J]>MIN "THEN" MIN:=T[J];
              "END";
        "PRINT" ''L2'BAND AT',SAMELINE,FREEPOINT(6),MIC,'WAVENUMBER.
SEARCH VALUE ='',SAMELINE,FREEPOINT(6),S[NUM],'WAVENUMBER.';
        "IF" PRINT=1 "THEN" "FOR" I:=1 "STEP" 1 "UNTIL" X "DO"
              "BEGIN"
              D:=ENTIER(((T[I]-MAX)*62/(MIN-MAX))+0.5);
              "PRINT" FREEPOINT(6),W[I];
              "FOR" J:=1 "STEP" 1 "UNTIL" D "DO" "PRINT" ''B160'';
              "PRINT" '*';
              "END";
              "END"
        "ELSE" "BEGIN"
                    I:=I+1;
                    "GOTO" LL;
              "END";
LLL:
        NUM:=NUM+1;
        STOP:=STOP-1;
        "IF" STOP>0 "THEN" "GOTO" LO;
        "END";
"END"
```

APPENDIX 6

COL 1B

Input parameters

1) Maximum number of points to be integrated (<400).
2) 2 times the number of pairs of wavenumber values for each integration.
3) If smoothing required for
   (a) The band points then 1 otherwise 0.
   (b) The baseline points then 1 otherwise 0.
4) If repeat of (3) required then 1 otherwise 0.
5) If dummy baseline required then 1 otherwise 0. If (5) is 1 then input required baseline transmission value.
6) Wavenumber limits for each integration.
7) Band points terminated by -1000.
8) If (5) is 0 then input baseline points terminated by -1000.
9) If (4) is 1 then repeat (3) and (4) inputs only.
10) If (5) is 1 then input baseline transmission value for next integration.
11) If (5) is 0 then (7) to (11).

The program working is governed by the initial parameters, these can be altered after each set of conditions has been carried out.

The program calculates the integrated absorptions between the wavenumber limits specified for separated matrix bands.

```
COL 1B;
"BEGIN"
"INTEGER" I,N,X,NUM,CHECK,RP1,SMA,SMAA,SMB,SMBB,STOP,SET;
"REAL" B,H,W,1,INTEG,MAX,MIC,BASE,BL;
"SWITCH" Z:=L2,L3,L4,L5,LL5,L6,FINISH;
"COMMENT" DECLARATIONS OF PROCEDURES NOW FOLLOWS;
"PROCEDURE" DECODE(WNUM,TRANS);
"REAL" WNUM,TRANS;
"BEGIN"
      "REAL" R,S,TT;
      "SWITCH"ZZ:=OUT;
      "IF" WNUM "LE" 99800 "AND" WNUM "GE" 78000 "THEN"
      "BEGIN"
            TT:=5000;S:=99752;R:=0.142857143;
            "GOTO" OUT;
      "END";
      "IF" WNUM "LE" 75000 "AND" WNUM "GE" 52000 "THEN"
      "BEGIN"
            TT:=2500;S:=74552;R:=0.071428571;
            "GOTO" OUT;
      "END";
      "IF" WNUM "LE" 50000 "AND" WNUM "GE" 28000 "THEN"
      "BEGIN"
           TT:=1000;S:=49352;R:=0.028571429;
           "GOTO" OUT;
      "END";
      "IF" WNUM "LE" 25000 "AND" WNUM "GE" 3000 "THEN"
      "BEGIN"
           TT:=500;S:=2415R;R:=0.014285714;
           "GOTO" OUT;
      "END";
OUT:
      WNUM:=TT-((S-WNUM)*R);
      TRANS:=(TRANS-35)/9.3;
      "END";
"PROCEDURE" SMOOTH(NC,A);
"VALUE" NC; "INTEGER" NC; "ARRAY" A;
"BEGIN"
"INTEGER" I,J,N,Q;  "REAL"SUM;  "ARRAY" INT,T[1:11];
"SWITCH"ZZZ:=L1,FIN;
"FOR" I:=1 "STEP" 1 "UNTIL" 10 "DO" T[I]:=A[I];
Q:=429;
INT[Q]:=INT[11]:=-36;
INT[2]:=INT[10]:=9;
INT[3]:=INT[9]:=44;
INT[4]:=INT[8]:=69;
INT[5]:=INT[7]:=84;
INT[6]:=89;
N:=5; J:=11;
```

```
L1:
T[11]:=A[J];
N:=N+1; SUM:=0.0;
"FOR" I:=1 "STEP" 1 "UNTIL" 11 "DO"
SUM:=INT[I]*T[I]+SUM;
A[J-5]:=T[6]:=SUM/Q;
"IF" N=NC-5 "THEN" "GOTO" FIN;
"FOR" I:=1 "STEP" 1 "UNTIL" 10 "DO" T[I]:=T[I+1];
J:=J+1;
"GOTO" L1;
FIN:
"END";
"PROCEDURE" TRANSPOSE(NC,A,B);
"VALUE" NC; "INTEGER" NC; "ARRAY" A,B;
"BEGIN"
"INTEGER" I,X; "REAL" MA,MB,F,G,AA;
MA:=(A[NC]-A[1])/(NC-1);
MB:=(B[NC]-B[1])/(NC-1);
X:=-1; AA:=A[1];
"FOR" I:=1 "STEP" 1 "UNTIL" NC "DO"
"BEGIN"
        X:=X+1;
        F:=MA*X+AA;
        G:=MB*X+B[1];
    A[I]:=G+(A[I]-F);
"END";
"END";
"PROCEDURE" INTEGRATE(K,L,J,A,B);
"VALUE" L,J; "INTEGER" J; "REAL" K,L; "ARRAY" A,B;
"BEGIN"
"INTEGER" I,M; "REAL" SUM;
SUM:=LN(A[1]/B[1])-LN(A[J]/B[J]);
  M:=J-1;
"FOR" I:=2 "STEP" 2 "UNTIL" M "DO"
SUM:=SUM+4*LN(A[I]/B[I])+2*LN(A[I+1]/B[I+1]);
  K:=SUM*L/3.0;
"END";
"PROCEDURE" SEARCH(N,A,B,C,X,Y,Z);
"VALUE" N; "INTEGER" N; "REAL"X,Y,Z; "ARRAY" A,B,C;
"BEGIN"
"INTEGER" J;
X:=1000;
"FOR" J:=1 "STEP" 1 "UNTIL" N "DO"
"BEGIN"
"IF" A[J]<X "THEN" "BEGIN"
          X:=A[J];
          Y:=B[J];
          Z:=C[J];
          "END";
"END";
"END";
"READ" N,X,SMA,SMB,RPT,SET;
"IF" SET=1 "THEN" "READ" BL;
STOP:=RPT; SMAA:=SMA; SMBB:=SMB;
"BEGIN"
"ARRAY" AW,AT,BT[1:N],S[1:X];
"FOR" I:=1 "STEP" 1 "UNTIL" X "DO" "READ" S[I];
N:=NUM:=1; CHECK:=1;
```

```
L2:
        "READ" W,T;
        DECODE(W,T);
        "IF" W>S[NUM] "THEN" "GOTO" L2;
        AW[N]:=W;
        AT[N]:=T;
L3:
        "READ"W,T;
        DECODE(W,T);
        "IF" W "GE" S[NUM+1] "THEN" "BEGIN"
        N:=N+1;
        AW[N]:=W;
        AT[N]:=T;
        "GOTO" L3;
        "END"
"ELSE"  "BEGIN"
        "IF" (N "DIV" 2)*2=N "THEN" "BEGIN"
        N:=N+1;
        AW[N]:=W; AT[N]:=T;
        "END";
        "END";
        "IF" SET=1 "THEN" "BEGIN"
        "FOR" I:=1 "STEP" 1 "UNTIL" N "DO" BT[I]:=BL;
        H:=(AW[1]-AW[N])/(N-1);
        "GOTO" LL5;
        "END";
L4:
        "READ" B;
        "IF" B=-1000 "THEN" "GOTO" L5 "ELSE" "GOTO" L4;
L5:
        "READ" W,T;
        DECODE(W,T);
        "IF" W>S[NUM] "THEN" "GOTO" L5;
        "FOR" I:=1 "STEP" 1 "UNTIL" N "DO"
        "BEGIN"
        "READ" W,T;
        DECODE(W,T);
        BT[I]:=T;
        "END";
        H:=(AW[1]-AW[N])/(N-1);
LL5:
        "IF" CHECK>1 "AND" RPT=1 "THEN" "READ" SMA,SMB,RPT;
        "IF" SMA=1 "THEN" "BEGIN"
        SMOOTH(N,AT);
        "PRINT" ''L1'BAND POINTS SMOOTHED.';
        "END" "ELSE" "PRINT" ''L1'BAND POINTS UNSMOOTHED.';
        "IF" SMB=1 "THEN" "BEGIN"
        SMOOTH(N,BT);
        "PRINT" ''L1'BASELINE POINTS SMOOTHED.';
      "END" "ELSE" "PRINT" ''L1'BASELINE POINTS UNSMOOTHED.';
        "IF" SET=1 "THEN" "PRINT" ''L1'TRANSPOSITION NOT REQUIRED.'
        "ELSE" "BEGIN"
        TRANSPOSE(N,BT,AT);
        SEARCH(N,AT,AW,BT,MAX,MIC,BASE);
        "PRINT" ''L1'TRANSPOSITION OF BASELINE POINTS.';
        "END";
```

```
INTEGRATE(INTEG,H,N,B1,A1);
"PRINT" ''L1'INTERVAL BETWEEN POINTS=',SAMELINE,FREEPOINT(6),H,
 ''L1'START OF INTEGRATION=',SAMELINE,FREEPOINT(6),AW[1],'CM-1
   END OF INTEGRATION=',SAMELINE,FREEPOINT(6),AW[N],'CM-1
NUMBER OF POINTS TO BE INTEGRATED=',SAMELINE,N,'
INTEGRATED PEAK ABSORPTION FROM',SAMELINE,FREEPOINT(6),AW[1],
'CM-1 TO ',SAMELINE,FREEPOINT(6),AW[N],'CM-1=',SAMELINE,
FREEPOINT(6),INTEG;
        "IF" SET "NE" 1 "THEN"
"PRINT" ''L1'BAND AT',SAMELINE,FREEPOINT(6),MIC,
'WAVENUMBER.
PEAK HEIGHT ABSORPTION AT',SAMELINE,FREEPOINT(6),MIC,'CM-1=',
LN(BASE/MAX),''L2'';
        CHECK:=CHECK+1;
        "IF" RPT=1 "THEN" "GOTO" LL5;
L6:
        "READ" B;
        "IF" B=-1000 "THEN" NUM:=NUM+2 "ELSE" "GOTO" L6;
        "IF" NUM>X "THEN" "GOTO" FINISH;
        "FOR" I:=1 "STEP" 1 "UNTIL" N "DO"
        BT[N]:=AW[N]:=AT[N]:=0.0;
        "IF" SET=1 "THEN" "READ" BL;
        CHECK:=1; RPT:=STOP; N:=1; SMA:=SMAA; SMB:=SMBB;
        "GOTO" L2;
        "END";
FINISH:
        "END"
```

REFERENCES

1. G. N. Lewis, D. Lipkin and T. T. Magel, J. Amer. Chem. Soc., 63, 3005, (1941).
2. G. N. Lewis and D. Lipkin, J. Amer. Chem. Soc., 64, 2801, (1942).
3. I. Norman and G. Porter, Nature, Lond., 174, 508, (1954).
4. E. Whittle, D. A. Dows and G. C. Pimentel, J. Chem. Phys., 22, 1943, (1954).
5. E. D. Becker and G. C. Pimentel, J. Chem. Phys., 25, 224, (1956).
6. M. M. Rochkind, Analyt. Chem., 39, 567, (1967).
7. M. Krietmann and D. Barnett, J. Chem. Phys., 43, 364, (1965).
8. D. E. Milligan and M. E. Jacox, J. Chem. Phys., 51, 277, (1969).
9. Formation and Trapping of Free Radicals, eds. A. M. Bass and H. P. Broida, Academic Press, New York, (1960).
10. B. Meyer, Low Temperature Spectroscopy, American Elsevier, New York, (1971).
11. Vibrational Spectroscopy of Trapped Species, ed. H. E. Hallam, John Wiley, (1973).
12. A. Snelson, J. Phys. Chem., 74, 537, (1970).
13. J. H. Current and J. K. Burdett, J. Phys. Chem., 73, 3505, (1969).
14. H. W. Brown and G. C. Pimentel, J. Chem. Phys., 29, 883, (1958).
15. G. E. Ewing, W. E. Thompson and G. C. Pimentel, J. Chem. Phys., 32, 927, (1960).
16. D. E. Milligan and M. E. Jacox, J. Chem. Phys., 41, 3032, (1964).

17. J. F. Ogilvie, Spectrochim. Acta, 23A, 737, (1967).

18. D. E. Milligan and M. E. Jacox, J. Chem. Phys., 38, 2627, (1963).

19. W. L. S. Andrews and G.C. Pimentel, J. Chem. Phys., 44, 2361, (1966).

20. A. Snelson, J. Phys. Chem., 74, 537, (1972).

21. L. Andrews, J. Chem. Phys., 48, 972, (1968).

22. L. Andrews, J. Chem. Phys., 57, 51, (1972).

23. L. Andrews and J. J. Raymond, J. Chem. Phys., 55, 3081, (1971).

24. H. E. Hallam, Ann. Reports (A), 67, 117, (1970).

25. L. Andrews and T. G. Carver, J. Chem. Phys., 49, 896, (1968).

26. J. S. Shirk and A. M. Bass, J. Chem. Phys., 49, 5156, (1968).

27. D. E. Milligan and M. E. Jacox, J. Chem. Phys., 51, 1952, (1969).

28. M. J. Linevsky, J. Chem. Phys., 34, 587, (1961).

29. M. J. Linevsky, J. Chem. Phys., 38, 658, (1963).

30. A. Snelson and K. S. Pitzer, J. Phys. Chem., 67, 882, (1963).

31. A. Loewenschuss, A. Ron and O. Schnepp, J. Chem. Phys., 49 272, (1968).

32. A. Loewenschuss, A. Ron and O. Schnepp, J. Chem. Phys., 50, 2502, (1969).

33. R. A. Frey, R. D. Werder and H. H. Gunthard, J. Mol. Spectroscopy, 35, 260, (1970).

34. A. J. Barnes and H. E. Hallam, Trans. Faraday Soc., 66, 1932, (1970).

35. A. J. Barnes, H. E. Hallam and J. D. R. Howells, J. Chem. Soc. Faraday II, 68, 737, (1972).

36. M. M. Rochkind, Spectrochim. Acta, 27A, 547, (1971).

37. M. M. Rochkind, Environ. Sci. Technol., 1, 434, (1967).

38. M. M. Rochkind, Science, 160, 196, (1968).

39. M. M. Rochkind, Analyt. Chem., 40, 762, (1968).

40. W. West and R. T. Edwards, J. Chem. Phys., 5, 14, (1937).

41. E. Bauer and M. Magat, J. Phys. Radium, 9, 319, (1938); Physica, 5, 718, (1938).

42. A. D. Buckingham, Proc. Roy. Soc., A248, 169, (1958); ibid., A255, 32, (1960); Trans Faraday Soc., 56, 753, (1960).

43. J. G. David and H. E. Hallam, Spectrochim. Acta, 23A, 593, (1967).

44. H. Friedmann and S. Kimel, J. Chem. Phys., 41, 2552, (1964); ibid., 43, 3925, (1965); ibid., 44, 4359, (1966); ibid., 47, 3589, (1967).

45. J. O. Hirschfelder, C. F. Curtiss and R. B. Bird, Molecular Theory of Gases and Liquids, Wiley, New York, (1954).

46. D. C. McKean, Spectrochim. Acta., 23A, 2405, (1967).

47. D. E. Mann, N. Acquista and D. White, J. Chem. Phys., 44, 3453, (1966).

48. M. J. Linevsky, J. Chem. Phys., 34, 587, (1961).

49. A. J. Barnes, H. E. Hallam and G. F. Scrimshaw, Trans, Faraday Soc., 65, 3159, (1969).

50. J. B. Davies and H. E. Hallam, Trans. Faraday Soc., 67, 3176, (1971).

51. G. C. Pimentel and S. W. Charles, Pure Appl. Chem., 7, 111, (1963).

52. M. T. Bowers, G. I. Kerley and W. H. Flygare, J. Chem. Phys., 45, 3399, (1966).

53. A. J. Barnes, H. E. Hallam and G. F. Scrimshaw, Trans. Faraday Soc., 65, 3127, 3150, (1969) and references therein.

54. K. B. Harvey and H. F. Shurvell, J. Mol. Spectroscopy, 25, 120, (1968).

55. J. A. Glasel, J. Chem. Phys., 33, 252, (1960).

56. A. J. Tursi and E. R. Nixon, J. Chem. Phy., 30, 1521, (1970).

57. E. Catalano and D. E. Milligan, J. Chem. Phys., 30, 45, (1959).

58. H. P. Hopkins, jr., R. F. Curl, jr., and K. S. Pitzer, J. Chem. Phys., 48, 2959, (1968).

59. D. E. Milligan, R. M. Hexter and K. Dressler, J. Chem. Phys., 34, 1009, (1961).

60. R. E. Meredith, Ph.D. Thesis, University of Michigan, (1963).

61. J. F. Hanlan, Ph.D. Thesis, University of California, (1961).

62. L. Abouaf-Marguin, H. Dubost and F. Legay, Chem. Phys. Letters, 7, 61, (1970).

63. L. Abouaf-Marguin and H. Dubost, Chem. Phys. Letters, 15, 445, (1972).

64. J. A. Cugley and A. D. E. Pullin, Chem. Phys. Letters, 17, 406, (1972).

65. J. A. Cugley and A. D. E. Pullin, Spectrochim. Acta, 29A, 1665, (1973).

66. D. E. Milligan and M. E. Jacox, J. Chem. Phys., 43, 4487, (1965).

67. J. E. Williams and J. N. Murrell, J. Amer. Chem. Soc., 93, 7149, (1971).

68. J. M. Allavena, R. Rysnik, D. White, V. Calder and D. E. Mann, J. Chem. Phys., 50, 3399, (1969).

69. D. Cabana, G. B. Savitsky and D. F. Hornig, J. Chem. Phys., 39, 2942, (1963).

70. E. D. Sprague and F. Williams, J. Chem. Phys., 54, 5425, (1971).

71. R. L. Armstrong, J. Chem. Phys., 39, 2263, (1963).

72. H. F. King and D. F. Hornig, J. Chem. Phys., 44, 4520, (1966).

73. R. E. Miller and J. C. Decius, J. Chem. Phys., 59, 4871, (1973), and references therein.

74. S. Leach, Pure Appl. Chem., 27, 457, (1971).

75. Tables of Wave-numbers for the Calibration of Infrared Spectrometers, Butterworths, London, (1961).

76. A. Cabana, A. Anderson and R. Savoie, J. Chem. Phys., 42, 1122, (1965).

77. E. Nixon, Raman Newsletter, (1969).

78. I. R. Beattie and R. Collis, J. Chem. Soc., (A), 2960, (1969).

79. J. S. Shirk and H. H. Claassen, J. Chem. Phys., 54, 3237, (1971).

80. J. W. Nibler and D. A. Coe, J. Chem. Phys. 55, 5133, (1971).

81. H. Huber, G. A. Ozin and A. Vander Voet, Nature, 232, 166, (1971).

82. G. A. Ozin and A. Vander Voet, J. Chem. Phys., 56, 4768, (1972).

83. H. Huber, E. P. KÜndig, M. Moskovits and G. A. Ozin, J. Amer. Chem., 95, 332, (1973).

84. D. Boal, G. Briggs, H. Huber, G. A. Ozin, E. A. Robinson and A. Vander Voet, Nature, 231, 174, (1971).

85. M. Lesiecki, J. W. Nibler and C. W. DeKock, J. Chem. Phys., 57, 1352, (1972).

86. J. H. Darling and J. S. Ogden, Inorg. Chem. 11, 666, (1972).

87. R. R. Smardzewski and L. Andrews, J. Chem. Phys., 57, 1327, (1972); L. Andrews and A. Hatzenbuhler, ibid., 57, 51, (1972).

88. L. Andrews and A. Hatzenbuhler, J. Chem. Phys., 56, 3398, (1972).

89. J. K. Burdett and J. J. Turner, J. Chem. Soc., D, 885, (1971).

90. J. E. Cahill and G. E. Leroi, J. Chem. Phys., 51, 1324, (1969).

91. J. A. Koringstein, Introduction to the theory of the Raman effect, Reidel, (1972).

92. J. E. F. Jenkins, Ph.D. Thesis, University of Salford, (1970).

93. D. A. Hatzenbuhler, R. R. Smardzewski and L. Andrews, 26, 479, (1972).

94. J. R. Durig, S. F. Bush and F. G. Baglin, J. Chem. Phys., 49, 2106, (1968).

95. A. Y. Hirakawa, M. Tsuboi and T. Shimanouchi, J. Chem. Phys., 57, 1236, (1972).

96. A. P. Gray and R. C. Lord, J. Chem. Phys., 26, 690, (1957).

97. H. Wolff and H. Ludwig, J. Chem. Phys., 56, 5278, (1972).

98. H. Wolff and D. Staschewski, Z. Electrochem., 65, 840, (1961).

99. H. Wolff and D. Staschewski, Ber. Bunsenges. Physik. Chem., 68, 135, (1964).

100. H. Wolff and H. Ludwig, Ber. Bunsenges. Physik. Chem., 70, 474, (1966); 71, 1107, (1967).

101. H. Wolff, J. Chem. Phys., 52, 2800, (1970).

102. H. Wolff and H. Ludwig, Ber. Bunsenges. Physik. Chem., 68, 143, (1964).

103. E. L. Wu, G. Zerbi, S. Califano and B. Crawford, J. Chem. Phys., 35, 2060, (1961).

104. J. D. Lambert, G. A. H. Roberts, J. S. Rowlinson and V. J. Wilkinson, Proc. Roy. Soc. (London), 196A, 113, (1949).

105. J. D. Lambert and E. D. T. Strong, Proc. Roy. Soc. (London), 200A, 566, (1950).

106. J. G. Aston, C. W. Siller and G. H. Messerly, J. Amer. Chem. Soc., 59, 1743, (1937).

107. W. F. Giauque and J. O. Clayton, J. Amer. Chem. Soc., 55, 4875, (1933).

108. A. Cabana, A. Anderson and R. Savoie, J. Chem. Phys., 42, 1122, (1965).

109. D. E. Mann, N. Acquista and D. White, J. Chem. Phys., 44, 3453, (1966).

110. M. T. Bowers and W. H. Flygare, J. Chem. Phys., 44, 1389, (1966).

111. L. F. Keyser and G. W. Robinson, J. Chem. Phys., 44, 3225, (1966).

112. A. J. Barnes, H. E. Hallam and G. F. Scrimshaw, Trans. Faraday Soc., 65, 3159, (1969).

113. E. Catalano and D. E. Milligan, J. Chem. Phys., 30, 45, (1959).

114. A. J. Tursi and E. R. Nixon, J. Chem. Phys., 52, 1521, (1970).

115. G. Dellepiane and G. Zerbi, J. Chem. Phys., 48, 3573, (1968).

116. E. B. Wilson, J. C. Decius and P. C. Cross, Molecular Vibrations, McGraw-Hill, New York, (1955).

117. T. Shimanouchi, J. Chem. Phys., 25, 660, (1956).

118. H. C. Urey and C. A. Bradley, Phys. Rev., 38, 1969, (1931).

119. J. Overend and J. R. Scherer, J. Chem. Phys, 32, 1289, 1296, 1720, (1960); 33, 446, (1960); 34, 547, (1961); 36, 3308, (1962).

120. T. Shimanouchi, Pure Appl. Chem., 7, 131, (1963).

121. P. Gans, Vibrating Molecules, Chapman and Hall, (1971).

122. T. Shimanouchi, Computer Programs for Normal Coordinate Treatment of Polyatomic Molecules, (1968).

123. B. Silvi, F. Froment, J. Corset and J. P. Perchard, Chem. Phys. Letters, 18, 561, (1973).

124. E. D. Becker and G. C. Pimentel, J. Chem. Phys., 25, 224, (1956).

125. G. C. Pimentel, M. O. Bulanin and M. Van Thiel, J. Chem. Phys., 36, 500, (1962).

126. K. Rosengren and G. C. Pimentel, J. Chem. Phys., 43, 507, (1965).

127. G. Hertzberg, Molecular Spectra and Molecular Structure, Volume II, Infrared and Raman Spectra of Polyatomic Molecules, D. Van Nostrand Co., New York, (1945).

128. C. M. Lewis and W. V. Houston, Phys. Rev., 44, 903, (1933).

129. H. C. Longuet-Higgins, Mol. Phys.,6, 445, (1963).

130. E. B. Wilson, J. Chem. Phys., 3, 276, (1935).

130a S. Suzuki, unpublished work.

131. A. L. Moncrieff, The Chemical Senses, Chapter 4, Wiley, (1946).

132. J. F. Bryd and A. H. Phelps, Jr., Odour and Its Measurements, Chapter 23 in A. C. Stern, Air Pollution, Volume 2, Academic Press, (1968).

133. D. F. Adams, R. K. Koppe and W. M. Tuttle, J. Air Pollut. Control Ass., 5, 31, (1965).

134. G. C. Cave, Tappi, 46, 1, (1963).

135. M. Feldstein, S. Balestrieri and D. A. Levaggi, J. Air Pollut. Control Ass., 15, 215, (1965).

136. T. Okita, Atmos. Environ. 4, 93, (1970).

137. Y. L. Sze, M. L. Borke and D. M. Ottenstein, Anal. Chem., 35, 240, (1963).

138. J. R. Lindsay Smith and D. J. Waddington, Anal. Chem., 40, 522, (1968).

139. J. R. Lindsay Smith and D. J. Waddington, J. Chromatog., 42, 183, (1969).

140. W. Biernacki, J. Chromatog., 50, 135, (1970).

141. M. M. Rochkind, Appl. Spectroscopy, 22, 313, (1968).

142. R. N. Perutz and J. J. Turner, J. Chem. Soc. Faraday Trans. II, 69, 452, (1973).